Design of a 3D Printed Bicycle Helmet Using Fused Deposition Modeling

Final Design Report
MECH 4860

Prepared For:

Client: Precision ADM

Advisor: Dr. Paul Labossiere

Submission Date: December 7, 2015

Team 17

Véronique Cormier

Samuel Friesen

Ryan Olson

Carl To

PRECISION ADM
ADVANCED DIGITAL MANUFACTURING

Executive Summary

Team 17 from MECH 4860 was tasked with designing a 3D printed bicycle helmet with an internal lattice structure that absorbs impacts. The goal was to produce a helmet design that is printed from one continuous material using fused deposition modeling (FDM). The helmet was to be designed as a general purpose road helmet.

Precision ADM required the following deliverables: CAD models of the helmet's design, which can be fully printed as a prototype, finite element analysis (FEA) of the helmet's impact absorption capabilities, computational fluid dynamics (CFD) analysis of the helmet's aerodynamic performance, and a complete budget for the helmet. The helmet was required to cost less than $1500 to produce.

The team began with generating concepts for the internal lattice structure and overall helmet geometry that were screened and scored to obtain the final concepts. CAD models were developed to facilitate the FEA and CFD analysis. Dynamic, non-linear impact analysis was performed using ABAQUS/CAE to design the internal lattice structure to meet the CPSC standard for bicycle helmets. Star CCM+ was used to perform CFD analysis to evaluate the helmet's drag and ventilation performance.

The final helmet design is comprised of three swept segments containing an optimized lattice structure. To accommodate printing requirements, drain holes were implemented into the exterior shell of the helmet to ensure that the support structures can be dissolved after printing. The helmet is designed to be printed in polycarbonate (PC) and the final weight of helmet is 779 g. For the final product, the price of the helmet was estimated to be between $1380.27 and $1500.27.

The impact FEA determined that the maximum deceleration of the head is 297 g's in a 6.2 m/s impact on a flat surface, which is below the maximum value specified in the CPSC standard. From the CFD, the helmet has a drag coefficient of 0.4644 at a pitch angle of 45° and wind velocity of 30 km/h. The average velocity of the airflow through the vents is 22.469 km/h at a wind speed of 30 km/h and pitch angle of 45°.

Table of Contents

List of Figures

List of Tables

1.0 Introduction

Precision Advanced Digital Manufacturing (ADM) is a newly formed company that specializes in metal and polymer additive manufacturing. The company consists of engineers and technologists that focus on producing parts for medical and aerospace applications. 3D printing has the benefits of design flexibility and reduced manufacturing time. Precision ADM recognizes the benefits of 3D printing, and is exploring the feasibility of utilizing fused deposition modelling (FDM) as a printing method to manufacture bicycle helmets.

Bicycle helmets provide the wearer head protection in accidents that may occur, but also act as a thermal insulator on the rider's head. Therefore, ventilation is an important aspect of the helmet to ensure the comfort of the cyclist. A bicycle helmet should also be designed to minimize aerodynamic drag. Engineers and manufacturers are looking to develop new technology to improve bicycle helmet performance for both the average consumer and the performance athlete.

In 2014, Precision ADM proposed the idea of a polymer 3D printed bicycle helmet. A team of Biosystems engineering students, *Team Helmet*, researched and manufactured a custom fitted 3D printed helmet within the team's project timeline. The helmet was composed of three layers: the outer shell, impact absorption layer, and inner skull cap. *Team Helmet* was unsuccessful in designing the helmet as a single 3D printed part. Instead, the inner impact absorption layer was filled with expanded polystyrene (EPS) and the shell of the helmet was 3D printed in acrylonitrile butadiene styrene (ABS). The inner skull cap was designed using 3D scans of a member of *Team Helmet's* head [1]. The prototype of the bicycle helmet by *Team Helmet* is shown in Figure 1.

Figure 1: 3D Printed prototyped designed by Team Helmet [2].

Our team has been tasked with redesigning the helmet to be entirely 3D printed. The design of the helmet will focus on the design and analysis of the impact absorption structure and on aerodynamics to optimize performance. A cost analysis of the helmet will be included as well.

1.1 Project Objective

The objective of the project is to design a 3D printed bicycle helmet that will be capable of protecting the wearer's head in the event of an impact. The helmet will be printed in a uniform material, which will include the inner and outer shells as well as the impact absorption lattice substructure. To verify the design of the helmet, computational structural and aerodynamic analysis will be performed on the helmet.

At the end of the project timeline, our team expects to have a bicycle helmet design that fulfills the needs outlined by the client as listed below:

i) The helmet will be made of a continuous 3D printed material by fused deposition modeling (FDM)

ii) Impact analysis using finite element analysis (FEA) will be performed to verify that the helmet will meet the necessary safety standards

iii) The aerodynamic performance of the helmet will be verified with computational fluid dynamics (CFD)

iv) The ventilation of the helmet will be optimized while reducing aerodynamic drag

v) The helmet will have a broad fit range for multiple users

vi) The helmet will meet the budget set by the client

vii) The helmet will be designed as a general-purpose road helmet

The following deliverables will be provided to the client:

i) CAD models of the helmet design
ii) Fully printed prototype of the helmet design manufactured by Precision ADM
iii) CFD analysis of the helmet aerodynamic performance
iv) Finite element analysis of the helmet impact performance
v) Budget of the project

The following items will not be included:

i) Location of straps and retention method
ii) The location of padding inside the helmet
iii) 3D scan data for individual wearers for the design of inner skull cap

1.2 Target Specifications

The target specifications provide the team with quantifiable goals that the final design must meet or surpass. In order to define target specifications, the team has established the client's needs and ranked them according to importance to the project. Next, metrics have been defined based on the needs. The metrics provide a means of quantifying and measuring the client's needs. Ideal values and marginal values have been assigned to the metrics, as to provide a benchmark that the design will be measured against. Finally, the constraints and limitations of the project have been determined.

1.2.1 Client Needs

A set of client needs have been defined for the 3D printed bicycle helmet. Some of the established needs were directly stated by Precision ADM, while others are inherent needs of a bicycle helmet. TABLE I lists the needs for the bicycle helmet design, and assigns each need an impact score out of 5 based on its priority, 5 being the highest priority. Needs that received a high importance score are critical to the client and scope of the project. Needs with lower importance scores are still vital for a bicycle helmet, but are not as critical to the scope of this project. Following TABLE I are the justifications for the assigned importance of each need.

TABLE I: PRIORITIZED CLIENT NEEDS

#		Need	Importance
N1	The helmet	is entirely 3D printed	5
N2	The helmet	prevents head injury	5
N3	The helmet	provides ventilation to the head	4
N4	The helmet	can withstand environmental conditions	4
N5	The helmet	does not obstruct vision	4
N6	The helmet	is aerodynamic	3
N7	The helmet	is visually appealing	3
N8	The helmet	is lightweight	3
N9	The helmet	is affordable to manufacture	2
N10	The helmet	is comfortable	1

Need #1: The helmet is entirely 3D printed

The bicycle helmet must be entirely 3D printed as a single, continuous piece. Precision ADM would like to prove the feasibility of 3D printing the entire helmet structure. Thus, this need is the main goal of the project and as result, received an impact score of 5.

Need #2: The helmet prevents head injury

The primary function of a bicycle helmet is to prevent head injury in the event of an impact. Therefore, this need received an importance score of 5 as the project cannot be considered a success without meeting this objective.

Need #3: The helmet provides ventilation to the head

Precision ADM requires aerodynamic analysis of the bicycle helmet as part of the project scope. The helmet must provide ventilation to the head, so that the wearer will not overheat after extended periods of biking or in hot temperatures. Ventilation also has an impact on aerodynamic performance [3]. As a result, this need has been given an importance score of 4.

Need #4: The helmet can withstand environmental conditions

Different environmental conditions, such as extreme heat, cold, or moisture, must not affect the helmet's ability to protect the head in an impact. Therefore, to ensure the helmet remains capable of protecting the wearer in any set of conditions, the environmental conditions must be considered as a need. As a result, this need has been given an importance score of 4.

Need #5: The helmet does not obstruct vision

The 3D printed bicycle helmet must be designed in such a way that it does not obstruct the view of the wearer. Any obstruction of view could be a safety concern when riding a bicycle. This need has been given an importance score of 4.

Need #6: The helmet is aerodynamic

Biking is a physical activity that is heavily affected by wind and biking speed, as a result it is important to consider aerodynamic drag when designing a bicycle helmet. The client did not specify a market for the helmet; however, the 3D printed bicycle helmet should be designed to minimize aerodynamic drag in order to be a realistic design. As a result, this need has been given an importance score of 3 because it is important to consider, but not as crucial as providing ventilation or ensuring the helmet is safe.

Need #7: The helmet is visually appealing

Precision ADM would like the helmet to be visually appealing. The 3D printed bicycle helmet will be a good example of the potential of 3D printing parts that are both functional and aesthetically pleasing due to the flexibility of 3D printed part design. Therefore, this need has been given an importance score of 3.

Need #8: The helmet is lightweight.

Precision ADM would like the helmet to achieve a weight similar to or better than competitor helmets in order to be relatively lightweight. Since the helmet could potentially be worn for long periods of time, the helmet should be lightweight to reduce wearer fatigue. This need has been given an importance score of 3.

Need #9: The helmet is affordable to manufacture

Manufacturing costs must be considered to ensure the helmet can be sold at a competitive price point. Material costs are relatively low, but the cost of printing the helmet is largely dependent on the printing hours and the part complexity. However, for the scope of this project, the importance of low cost does not outweigh the importance of achieving a safe and durable helmet. Therefore, this need has been given an importance score of 2.

Need #10: The helmet is comfortable

Since a bicycle helmet is worn on the head, it is important that the helmet is comfortable. However, the project is concentrated on designing the impact attenuation structure to protect the wearer, so the need of comfort has been given a low importance score of 1. Nevertheless, the comfort of the helmet will still be considered to ensure the design can fit properly on the wearer's head.

1.2.2 Metrics

The technical specifications for the 3D printed helmet consist of a metric and a value. The metrics help establish the degree to which each specification meets the established needs of the client. Each metric has a marginal and ideal value with defined units. The ideal value represents the best case scenario for that metric, whereas the marginal value is an acceptable value for the same metric. In the cases where a metric is defined by a standard, the marginal value is the value specified by the standard. The ideal value improves upon the standard value by a certain percentage. In the cases where the metric is defined by competitor benchmarking, the marginal value is the average value of the competitor helmets and the ideal value is the best competitor value. TABLE II lists every metric, the corresponding need, the metric's units and the importance score.

TABLE II: PRELIMINARY MARGINAL AND IDEAL METRIC VALUES

Metric #	Need #	Metric	Importance	Units	Marginal Value	Ideal Value
M1	N1	Helmet is fully 3D printed	5	Yes/No	Yes	Yes
M2	N2,N4[1,3]	Impact deceleration at 6.2 m/s	5	G-Force	<300	<280
M3	N2,N4[2,3]	Impact deceleration at 4.8 m/s	5	G-Force	<300	<280
M4	N3,N10	Head temperature at 30 km/h wind speed	4	Celsius	<29.08	<25.5
M5	N5	Unobstructed field of view	4	degrees	>105	>115
M6	N6	Drag coefficient	3	non dimensional	<0.269	<0.232
M7	N7	Helmet aesthetics	3	subjective	>4	>7
M8	N8	Weight	3	grams	<251.5	<175
M9	N9	Cost	2	$ (CDN)	1100 to 1500	<1100
M10	N10	Fits wearers head	1	subjective	>1	3
M11	N10	No pressure points	1	subjective	>1	3

[1] Conditions based on a flat anvil impact in the CPSC Standard

[2] Conditions based on a hemispherical anvil and curbstone anvil impact in the CPSC Standard

[3] The helmet’s ability to withstand different environmental conditions is verified by conditioning helmets in various environments and performing standard impact testing

Metric #1: Helmet is fully 3D printed

This metric can be defined with a yes or no value. By designing the helmet as a single, continuous 3D printed part that includes the inner shell, impact attenuation layer and outer shell, this metric can be confirmed, which will meet Need #1 of the client.

Metric #2 and Metric #3: Impact deceleration at 6.2 m/s and 4.8 m/s

The 3D printed bicycle helmet's ability to prevent head injury can be defined by the deceleration rate of the head during impact. The lower the deceleration is, the more energy is being absorbed by the crushing of the impact attenuation structure inside the helmet. If more energy is absorbed by the helmet, less energy will be absorbed into the head, and as a result, the safer the head will be from injury. Safety standards for bicycle helmets use the deceleration upon impact of a certain energy level or speed as a basis for their testing criteria [4] [5]. Therefore, the testing guidelines established in the standards can be used as a baseline for the analysis of the 3D printed bicycle helmet.

The US Consumer Product Safety Commission (CPSC) is the most common standard for certifying bicycle helmets in North America [5].The CPSC has become the accepted benchmark for bicycle helmet testing in Canada due to the larger North American market it caters to. In the CPSC standard, the helmet is secured to a headform, which is mounted on a free-fall, guide-wire apparatus. The headform and support assembly must have a combined mass of 5.0±0.1 kg, which excludes the helmet. A linear accelerometer is placed at the center of gravity of the test headform to measure the deceleration. The center of impact can be anywhere on or above the test line provided that it is 120 mm from any prior impact site measured along the helmet surface. In the CPSC Standard, the helmet deceleration must be below 300 g's during an impact at a velocity of 6.2 m/s ±3% [5]. Complying with this standard will ensure that the 3D printed helmet is meeting Need #2.

The CPSC standard also has environmental conditioning requirements where the helmet is conditioned in different environments for at least 4 hours before impact testing. The various conditioning environments are shown in TABLE III. By meeting this standard, the 3D printed helmet will meet Need #4.

TABLE III: CPSC HELMET CONDITIONING [5]

Environment	# of Helmets	Temperature (°C)	Length of time (hrs)
Ambient	2	17 to 27	≥4
Hot	2	47 to 53	≥4
Cold	2	-13 to -17	≥4
Water	2	17 to 27	≥4

TABLE IV shows the full test schedule for every conditioned helmet including the maximum peak deceleration for each impact.

TABLE IV: CPSC TEST SCHEDULE [5]

Test Helmet #	Environment	Anvil*	# of Impacts	Impact Velocity (m/s)	Drop Height (m)	Input Energy (J)	Max Peak Deceleration (G-Force)
1	Ambient	Flat	2	6.2±3%	1.96	96	300
		Hem	2	4.8±3%	1.17	57	300
2	High Temperature	Flat	2	6.2±3%	1.96	96	300
		Hem	2	4.8±3%	1.17	57	300
3	Low Temperature	Flat	2	6.2±3%	1.96	96	300
		Hem	2	4.8±3%	1.17	57	300
4	Water	Flat	2	6.2±3%	1.96	96	300
		Hem	2	4.8±3%	1.17	57	300
5	Ambient	Curb	1	4.8±3%	1.17	57	300
6	Low Temperature	Curb	1	4.8±3%	1.17	57	300
7	High Temperature	Curb	1	4.8±3%	1.17	57	300
8	Water	Curb	1	4.8±3%	1.17	57	300

*hem – hemisphere, curb – curbstone

Metric #4: Head temperature at 30 km/h wind speed

The temperature of the cyclist's head will be a function of the quality of ventilation in the helmet. Improving the ventilation through various means will decrease the temperature of the head. Therefore, the head temperature will provide an effective metric for Need #3. The temperature of the head also has an impact on the comfort of the bicycle helmet wearer. As a result, the head temperature is also a factor in meeting Need #10.

A study by RMIT University in Melbourne, Australia was used as the basis for assigning marginal and ideal values to this metric. In the study, five helmets were tested in a wind tunnel to assess their thermal and aerodynamic efficiency [6]. The helmets were attached to a heated mannequin outfitted with nine thermocouples. The helmet was positioned at a 0° yaw angle and a 45° pitch, which is a practical biking position. The mannequin head was set to 56 °C at a wind speed of 0 km/h. The wind speed was increased from 30 km/h to 70 km/h in 10 km/h increments. The greatest variation between head temperatures for the different helmets was observed at 30 km/h, thus this speed was used as the basis for this metric.

TABLE V summarizes the head temperature data for the five helmets tested in the study as well as the average and minimum head temperatures, which were used as the basis for the marginal and ideal metric values.

TABLE V: RMIT UNIVERSITY HEAD TEMPERATURE DATA [6]

Helmet	Head Temp at 30 km/h
Prowell F22- Raptor	28.6
LG Rocket	32.4
Giro Advantage	31
Giro Ionos	25.5
Giro Atmos	27.9
AVERAGE	29.08
MINIMUM	25.5

Metric #5: Unobstructed field of view

The CPSC Standard tests the field of view of a helmet [5]. The guidelines for this standard can be used as a metric to validate the corresponding need. As required by the CPSC standard, a 105° field of view from the vertical centerline in either direction is required at all times. In no way can the helmet obstruct the wearer's field of view [5]. The marginal value for this metric is greater than 105°. The ideal value for this metric is greater than 115°. Complying with this standard will ensure that Need #5 is met.

Metric #6: Drag coefficient

The drag coefficient of an object is a non-dimensional value that can be used to quantify the drag of an object in a fluid, which in this case is air. The drag coefficient for the 3D printed bicycle helmet will be an effective metric for Need #6. The smaller the drag coefficient is, the less drag force a cyclist will experience due to the helmet while riding a bike.

The study by RMIT University also measured the drag coefficient for every helmet in the study. The drag coefficients for the helmets at a 0° yaw angle and a 45° pitch angle are presented in TABLE VI [6]. The average drag coefficient is the marginal metric value and the minimum drag coefficient is the ideal metric value.

TABLE VI: RMIT UNIVERSITY DRAG COEFFICIENT DATA [6]

Helmet	Drag Coefficient
Prowell F22- Raptor	0.285
LG Rocket	0.274
Giro Advantage	0.232
Giro Ionos	0.278
Giro Atmos	0.277
AVERAGE	0.269
MINIMUM	0.232

Metric #7: Helmet Aesthetics

The aesthetics of the helmet is a subjective metric; however a value for the metric can be obtained by creating a scoring system. The aesthetic appearance of the helmet can be compared to other helmets on the market. A focus group can be used to obtain a value for this metric and confirm that Need #7 is being met. The helmet aesthetics can be ranked on a 0 to 10 subjective scale in a double blind experiment. A helmet with a score of zero is extremely visually unappealing. A helmet with a score of 5 is average looking, and a helmet with a score of 10 is extremely visually appealing. The marginal value is a score greater than 4 and the ideal value is a score greater than 7.

Metric #8: Weight

The weight of the 3D printed helmet can be measured to determine whether Need #8 is being met. The value of the metric can be defined by benchmarking competitor helmet weights. To assign marginal and ideal values to this metric, six higher-end helmets with varying prices were selected for the competitor analysis. The average weight of the six helmets was used as the marginal metric value and the lightest weight was used as the ideal metric value. TABLE VII shows the competitor helmet weights.

TABLE VII: COMPETITOR WEIGHT COMPARISONS [7]

Helmet	Weight (g)
Giro Synthe Helmet	250
Bell Star Pro	280
Bell Array	340
Limar Ultralight	175
Lazer Z1	220
POC Octal	244
AVERAGE	251.5
MINIMUM	175

Metric #9: Cost

The manufacturing cost for one helmet includes the cost of materials and the total cost of running the 3D printer to produce the helmet. This metric can confirm Need #9 is being met. Precision ADM provided an expected range of $1000 to $1500 for the helmet manufacturing costs, which is largely due to printing time. The marginal metric value is a cost range from $1100 to $1500. The ideal metric value is a cost less than $1100.

Metric #10: Fits wearer's head

How the helmet fits on the wearers head is another subjective metric. This metric can be evaluated by asking a focus group how well the helmet fits compared to other helmets in a double blind experiment. To keep the experiment unbiased, the participants in the experiment must have the same approximate head size corresponding to the general size of the helmet. The score that the helmet receives in the experiment will be a metric to confirm Need #10 is being met. The degree to which the helmet fits the wearer's head can be ranked on a 0 to 3 subjective scale. A score of 0 is a helmet that is extremely loose or so tight that it won't fit on the rider's head. A score of 1 is a helmet that is fairly loose or tight. A score of 2 is a helmet that is slightly loose or tight and a score of 3 is a helmet with a perfect fit. The marginal value is a score greater than 1 and the ideal value is a score of 3.

Metric #11: No pressure points

The presence of pressure points is the final subjective metric. The wearer of the 3D printed helmet should not feel any increased pressure points anywhere along the surface of their head that is in contact with the helmet. The same method for evaluating Metric #11 can be used to evaluate this metric. The score that the helmet receives in the experiment will be another metric for confirming Need #10 is being met. The amount and severity of pressure points in the helmet can be ranked on a 0 to 3 subjective scale. A score of 0 is a helmet that results in extreme discomfort due to pressure points. A score of 3 is a helmet with no discomfort due to pressure points. The marginal value is score greater than 1 and the ideal value is a score of 3.

1.3 Constraints and Limitations

After gathering more information from Precision ADM regarding the needs of the project, a list of constraints and limitations was formed. The TABLE XIII summarizes the constraints and the aspects of those constraints that was faced throughout the project.

TABLE VIII: LIST OF CONSTRAINTS

#	Constraints	Values
1	Material Selection	ABS-M30, ABS-M30i, ASA, ABS ESD7, NYLON 12, PC, PC ISO, ULTEM 9085
2	Number of Materials Used	1 material
3	Project Time	September 16 to December 7 (84 days)
4	Print Lead Time	2 weeks
5	Cost of Manufacturing	$1,500
6	Volume of Build Envelope	16 x 14 x 16 in.
7	Printing Resolution	0.013 in, 0.010 in, 0.007in, 0.005 in, (Dependent on material selection)
8	Layer Orientation	XZ vs. ZX fibre orientation
9	Fill Method	Cross-hatch, Hexagonal, Custom
10	Meets CPSC and CSA Standards	Environment, Construction, Impact Energy, Material, Vision Impairment

Constraint #1: Material Selection

Material selection for the cycling helmet is restricted to what can be provided through Stratasys. Stratasys is a company that specializes in additive manufacturing methods and looks to incorporate these methods in many different industries. Stratasys is able to provide 13 different variations of printing material, ranging from multiple ABS plastics, polycarbonates, and ULTEM thermoplastics.

Precision ADM will be using the Fortus 400mc 3D printer, which has 10 compatible materials [8]. Mechanical, thermal, electrical, and other material properties are provided for each thermoplastic. The properties are from material testing performed by Stratasys on 3D printed specimens. In order to perform FEA on lattice structures, the mechanical properties of the materials being considered are required. Stratasys has performed ASTM D638 tensile testing on 3D printed dog bones specimens, as well ASTM D790 flexural testing on every available material. Stratasys has also performed ASTM D695 compressive testing on some materials. Five of the available materials have tensile, flexural, and compressive testing performed on 3D printed specimens with two different print orientations. Test properties are given for both orientations. Figure 2 illustrates the two different printing orientations.

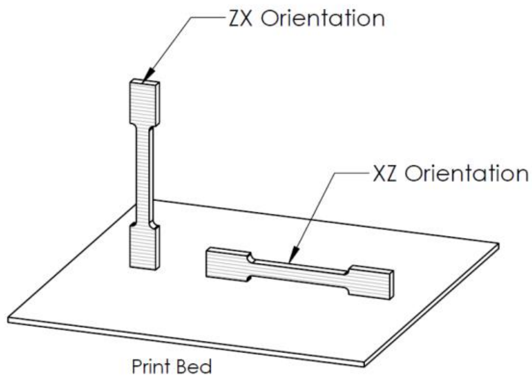

Figure 2: Stratasys test specimen print orientations [7].

TABLE IX shows the published mechanical properties for the materials where orientation is not specified.

TABLE IX: STRATASYS MATERIAL PROPERTIES WITH UNSPECIFIED PRINT ORIENTATION [8]

Property	ABSi	ABS ESD7	ABS-M30i	PC ISO	PPSF/PPSU
Tensile Strength (MPa)	37	36	36	57	55
Tensile Modulus (MPa)	1920	2400	2400	2000	2100
Tensile Elongation (%)	4.4	3	4	4	3
Flexural Strength (MPa)	62	61	61	90	110
Flexural Modulus (MPa)	1920	2400	2300	2100	2200

TABLE X shows the published mechanical properties for materials printed in both the XZ and ZX orientations.

TABLE X: STRATASYS MATERIAL PROPERTIES FOR MULTIPLE PRINT ORIENTATIONS [8]

Property	ABS-M30		ASA		PC		NYLON 12		ULTEM 9085	
Plane	**XZ**	**ZX**	**XZ**	**ZX**	**XZ**	**ZX**	**XZ**	**ZX**	**XZ**	**ZX**
Tensile Strength, Yield (MPa)	31	26	29	27	40	30	32	28	47	33
Tensile Strength, Ultimate (MPa)	32	28	33	30	57	42	46	38.5	69	42
Tensile Modulus (MPa)	2230	2180	2010	1950	1944	1958	1282	1138	2150	2270
Tensile Elongation at Break (%)	7	2	9	3	4.8	2.5	30	5.4	5.8	2.2
Tensile Elongation at Yield (%)	2	1	2	2	2.2	2	2.4	2.7	2.2	1.7
Flexural Strength (MPa)	60	48	60	48	89	68	67	61	112	68
Flexural Modulus (MPa)	2060	1760	1870	1630	2006	1800	1276	1180	2300	2050
Flexural Strain at Break (3.5%)	4	3.5	No Break	4	No Break	4	No Break	>10	No Break	3.7
Compressive Strength, Yield (MPa)	No Data	No Data	No Data	No Data	69	64	51	55	100	87
Compressive Strength, Ultimate (MPa)	No Data	No Data	No Data	No Data	193	65	167	6	181	90
Compressive Modulus (MPa)	No Data	No Data	No Data	No Data	7564	1565	5033	1069	7012	1731

Other material properties that will be required for the design and analysis of the bike helmet are listed in TABLE XI. The densities are provided by Stratasys, and Poisson’s ratio comes from various literature sources. The Poisson’s ratio for ASA and PPSF/PPSU was not available.

TABLE XI: GENERAL MATERIAL PROPERTIES [7] [14] [15]

Material	Density (kg/m3)	Poisson's Ratio
ABSi	1080	0.35
ABS ESD7	1040	0.35
ABS-M30	1040	0.35
ABS-M30i	1040	0.35
ASA	1050	-
PC ISO	1200	0.37
PC	1200	0.37
NYLON 12	1000	0.408
ULTEM 9085	1340	0.44
PPSF/PPSU	1280	-

Constraint #2: Number of Materials Used

Precision ADM has specified that the helmet must be printed from one continuous material. In general, current helmets are made from two shells with an expandable foam between the shells acting as the impact attenuation structure. Instead, Precision ADM is looking to print all aspects of the helmet structure without post manufacturing assembly. This requires the impact attenuation structure, inner shell, and outer shell to be printed as one continuous material.

Constraint #3: Project Time

Project time is a constraint that is enforced by the MECH 4860 Engineering Design course timeline. The team's project schedule is developed in accordance with the MECH 4860 deadlines. Consequently the timeline falls between the days of September 24th, 2015 to December 9th, 2015.

Constraint #4: Lead Time

Precision ADM specified a maximum lead time of two weeks for printing an item. The lead time is dependent on the complexity of the part. The schedule for printing by Precision ADM prioritizes paying customers, which will potentially increase the lead time for us. Since there is no way to predict how many projects Precision ADM will be receiving, a maximum lead time of two weeks has been assumed for any printed part or prototype.

Constraint #5: Cost of Manufacturing

A budget of $1000 to $1500 has been set by Precision ADM. The approximate value of the Biosystems group's helmet was $1000, however the previous helmet did not have a printed internal structure. Additional printing will be necessary to create the internal structure, which leads to higher labour costs. Therefore Precision ADM has provided larger budget.

Constraint #6: Volume of Build Envelope

Each 3D printer has a set build envelope which defines the maximum dimensions of a single printed object. The upgraded configuration of the Fortus 400mc that will be used has a build envelope of 16 x 14 x 16 inches [9]. Consequently, any single part that is being manufactured must fit within this volume in its printing orientation. In other words, no single dimension can exceed the boundaries defined by the build envelope.

Constraint #7: Printing Resolution

The Fortus 400mc is capable of printing in four different resolutions or in order words, strand thicknesses. These four strand thicknesses are 0.013 in, 0.010 in, 0.007 in, and 0.005 in. The finer the strand thickness, the higher the resolution of the part. Furthermore, with a finer strand thickness, the volume fraction of the polymer will be greater, resulting in a part that will act more like a uniform material. Regardless, there will be a certain amount of voids induced based on the strand thickness used. Material selection will be closely related to the printing resolution since only some materials can be printed in all strand thicknesses. TABLE XV outlines the available strand thicknesses for all of the material choices.

TABLE XII: AVAILABLE MATERIALS AND STRAND THICKNESS [7]

Layer Size	ABSi	ABS ESD7	ABS-M30	ABS-M30i	ASA	PC ISO	PC	NYLON 12	ULTEM 9085	PPSF/ PPSU
0.013 in	●		●	●	●	●	●	●	●	●
0.010 in	●	●	●	●	●	●	●	●	●	●
0.007 in	●	●	●	●	●	●	●	●		
0.005 in	●		●	●	●					

Constraint #8: Layer Orientation

The layer orientation and fibre orientation will have a large effect on the helmet's directional strength. The printer will always lay strands in the flat horizontal plane (XY plane) in either the X or Y direction [10]. The layered style of printing and the orientation of the strands within each layer results in anisotropic behaviours. As a result, depending on the defined print orientation of the cycling helmet, the direction of the material strands will affect the helmet's strength in different directions.

Constraint #9: Fill Method

In addition to the machine's volumetric limitations, the machine has pre-set fill methods. For example, if a part's external geometry has been fully defined, there are optional volume "fill" methods that can be selected to automatically fill the interior of the part. The two fill methods that can be selected are a cross hatch pattern and a hexagonal pattern. Both methods have a light, medium, and heavy fill density option. Alternatively, a custom fill method can be used. This would require fully defining every aspect of the cycling helmet including external and internal geometry and densities. Each fill method and density combination would produce different strength and impact characteristics. If a more intensive and customized approach is required, a custom fill method may be developed.

Constraint #10: Meets CPSC standards

For the 3D printed cycling helmet to be proven a feasible product, it must pass all pertaining aspects of CPSC standard. The testing procedures from those standards include passing the required impact energy test when subjected to both hot, cold, and ambient temperatures. The details of these test were discussed earlier in 1.2.2 Metrics. In the case of helmet construction, the outer surface must be smooth and there cannot be any ridged protrusions on the inner surface.

The material choice will also be constrained by its ability to withstand aging and normal use when exposed to the sun, extreme temperature ranges and rain. CSA standards do not specifically state the type of material required, but rather that the material properties must not significantly change when exposed to environmental conditions. The material choice must also ensure that it does not cause skin irritation upon contact [4].

Vision impairment is also a constraint that will be encountered during the design of the helmet. CPSC standards require that the helmet must allow for 105 degrees of peripheral vision from the center line at all times [5]. This will contribute to the design of the shape of the helmet.

1.4 Helmet Design Plan

A structured approach has been used to develop the design of the 3D printed bicycle helmet. The design of the bicycle helmet went through a series of distinct stages beginning with the project definition stage, followed by concept development, and finally the detailed design stage. Each stage had multiple steps that progressed the helmet design from the initial concept to the final design. The design of the helmet began with developing the lattice design, followed by the general geometry of the helmet. The final lattice design was then implemented into the helmet. Finally, aerodynamic analysis was performed to determine the optimum ventilation geometry and evaluate the aerodynamic performance of the helmet. Figure 3 shows the chronological design process the team followed beginning with the project definition and ending with the final design.

.

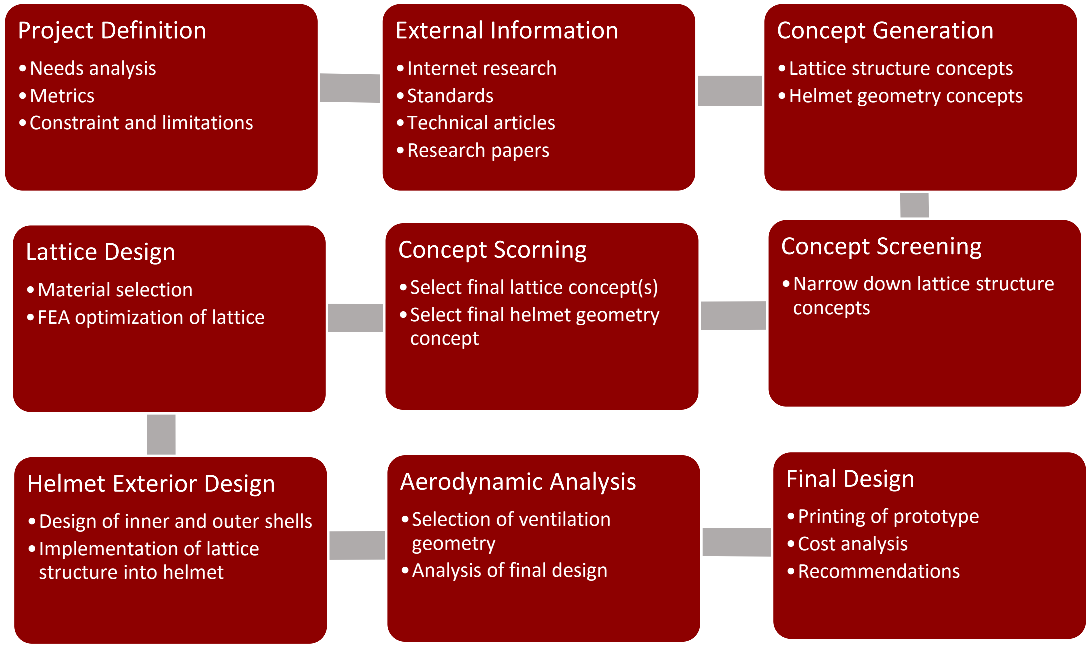

Figure 3: Helmet design flow chart.

The results from the external research can be found in Appendix A. A visual representation of the relationships between the client needs, metrics and benchmarking known as a House of Quality can be found in Appendix B. The project time line spanned from September 24th to December 9th, and a detailed work breakdown structure and Gantt chart can be found in Appendix C.

2.0 Internal Concept Generation

The team used systematic methods such as individual concept generation, collective brainstorming and the SCAMPER method for internal concept generation to develop viable concepts for the helmet design. These concept generation methods led to a set of potential designs for the two main subsections of the bicycle helmet: the impact absorption layer and the outer shell geometry.

2.1 Concept Generation for Lattice Structures

TABLE XIII outlines all of the initial lattice structure concepts that were evaluated throughout the screening phase. Each concept has its own unique characteristics with respect to its design and function.

TABLE XIII: LATTICE STRUCTURE CONCEPTS

#	Description	Visual
1	"Offset Boxes" • Square or rectangular lattice with offset spacing • Designed to absorb impact energy through bending of horizontal members and bucking of vertical members	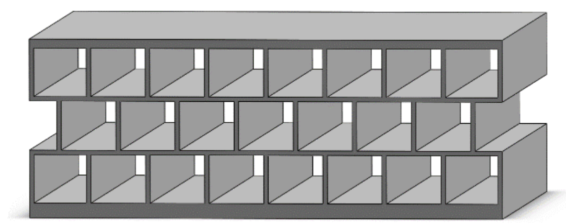
2	"Aligned Boxes" • Square or rectangular lattice with aligned spacing • Stiffer alternative to concept 1	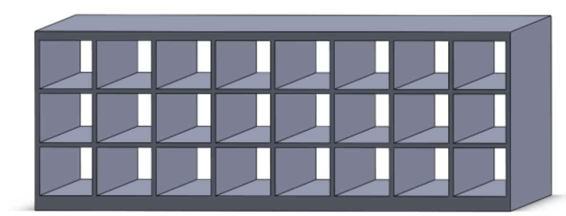
3	"Offset Triangles" • Triangular lattice where six members meet at single node • Alternatively, horizontal members could be removed to form a diamond lattice	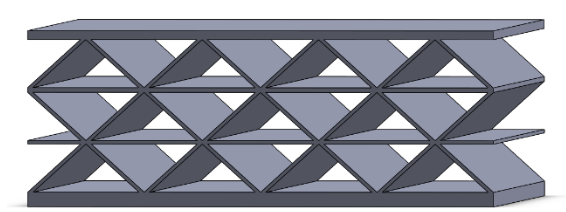

#	Description	Visual
4	"Aligned Triangles" • Vertically aligned triangles designed to put horizontal members in bending to absorb impact energy	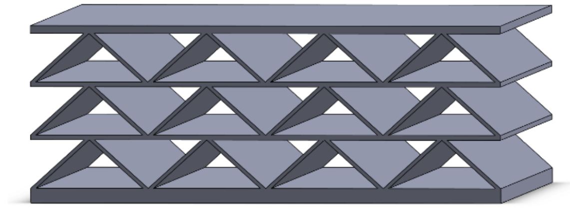
5	"Offset Circles" • Circular lattice with offset spacing designed to minimize material between adjacent circles	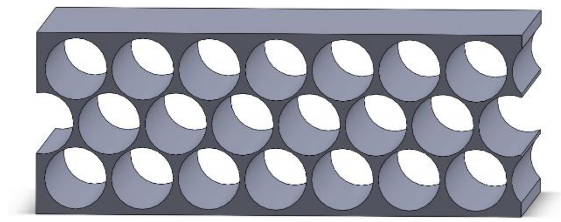
6	"Aligned Circles" • Circular lattice with aligned spacing	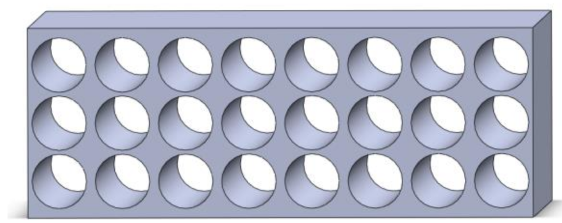
7	"Aligned Hexagons" • Hexagon style lattice that is aligned vertically and horizontally	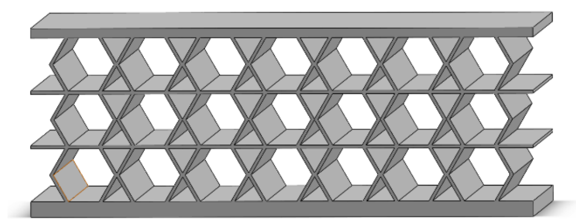
8	"Spaced Hexagons" • Hexagon lattice where each column of hexagons are spaced apart • Designed to induce predictable buckling during impact	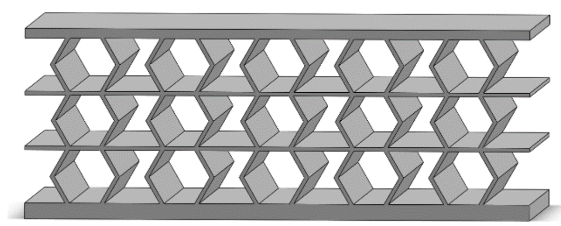

#	Description	Visual
9	"Honeycomb" • Hexagons arranged in a honeycomb style lattice	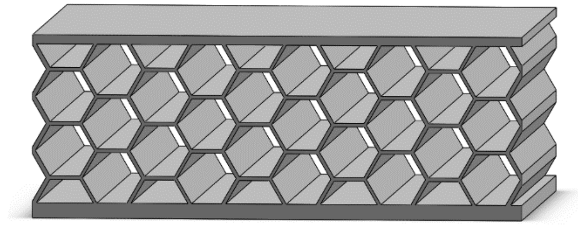
10	• "Octet Truss" • • Figure 4 shows a unit cell of the octet truss. 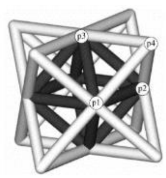 **Figure 4: Octet truss [18].**	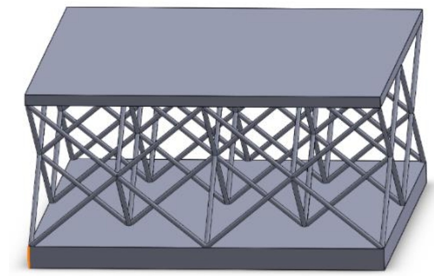
11	"3D Kagome Structure" • Three cylindrical members cross each other at a midpoint at set angles to produce a triangular hour glass shape. • 3D truss system provides even distribution of energy	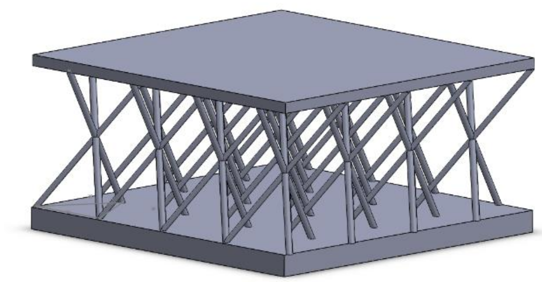
12	"Cubic Nodal Lattice" • Six cylindrical members meet at a single node to form cubic shapes	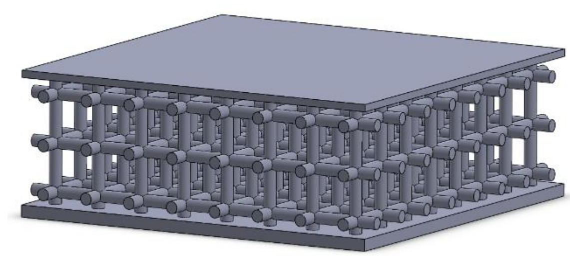

#	Description	Visual
13	"Pillars" • Layers separated by pillar structures arranged in an offset formation to induce bending in the horizontal layers	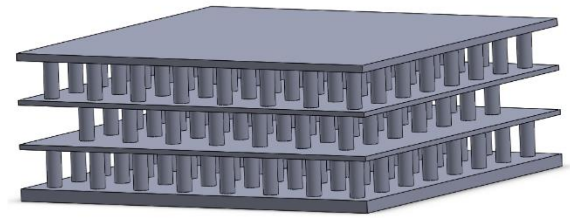
14	"Lateral Voids" • Horizontal internal cut-outs designed to deflect into each other upon impact	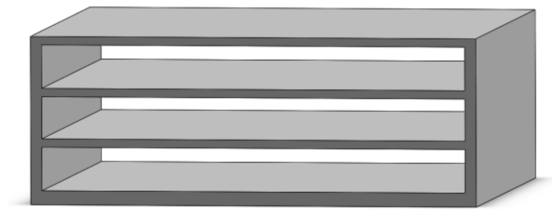
15	"Asterisk Lattice" • Triangular lattice designed to deflect into vertical members	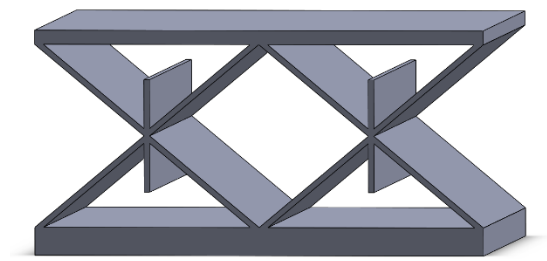
16	"Sparse Fill" [11] • A fill option available on Stratasys Fortus 3D printers • Applies material filament called rasters in a grid pattern • Rasters are applied in a single direction per layer	No image available; pre-set option for available 3D printer.
17	"Sparse Double Dense Fill" [11] • A fill option available on Stratasys Fortus 3D printers • Rasters are applied in crosshatch pattern on every layer for added strength	No image available; pre-set option for available 3D printer.

2.2 Concept Generation for Helmet Geometry

TABLE XIV outlines all of the initial helmet outer shell concepts that will be evaluated in the next screening phase after the final lattice structure is selected. Each concept has its own unique characteristics with respect to its design and function.

TABLE XIV: HELMET OUTER SHELL CONCEPTS

#	Descriptions	Visuals
1	"Sectioned Helmet with Gap Vents" • Based on traditional bicycle helmet design	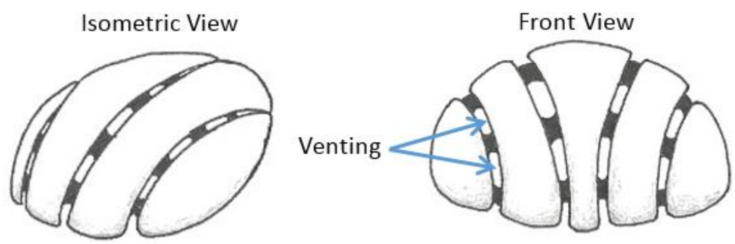
`2	"Built-in Vent Tubes" • Vented tubes would be integrated into the helmet • Inlet at the front would ventilate the head, and an outlet would be located at the back of the helmet.	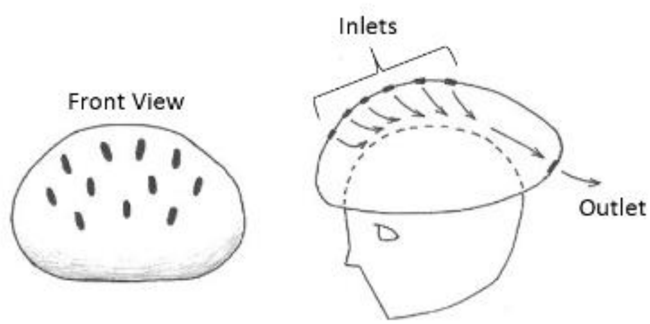 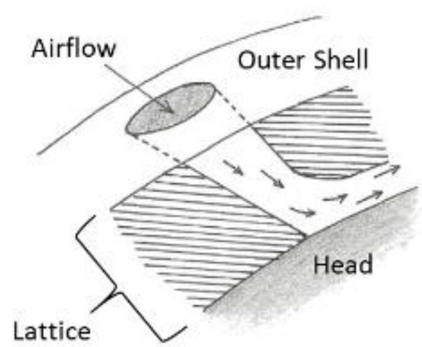

<table>
<tr><th>#</th><th>Descriptions</th><th>Visuals</th></tr>
<tr><td>3</td><td>“Integrated Vent Design”
Air would flow from outer vents and flow into inner channels that would aid in the cooling of the rider’s head.</td><td>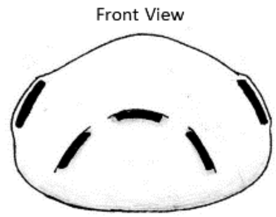

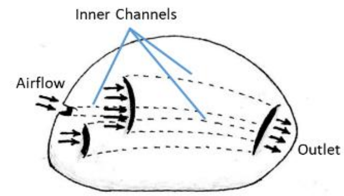
</td></tr>
<tr><td>4</td><td>“Modular Bicycle Helmet”
Helmet would be composed of smaller pieces that are assembled afterwards
This design fails to meet the need of printing the helmet as a single piece
The advantage is that the orientation of parts on the print bed could be optimized
Could be necessary if the internal lattice geometry proves difficult to print due to support material requirements</td><td>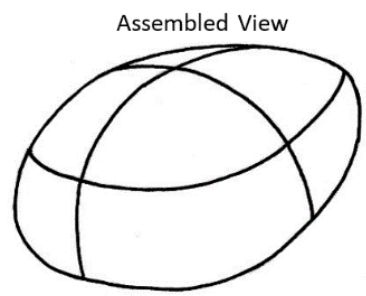

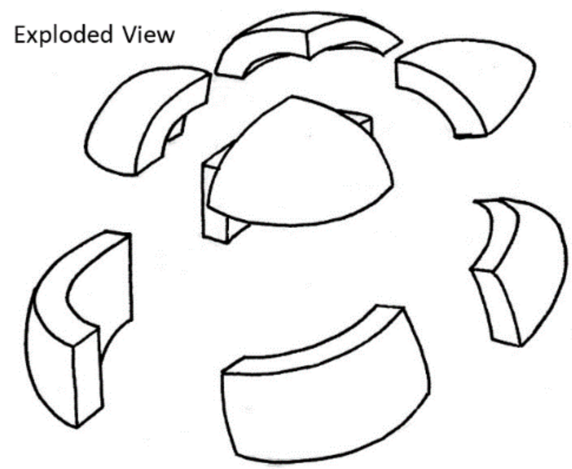
</td></tr>
<tr><td>5</td><td>“Multi-Vent Spine Helmet”
Vents are aligned behind each other, and airflow would traverse along the “spine” of vents</td><td>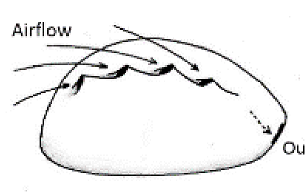

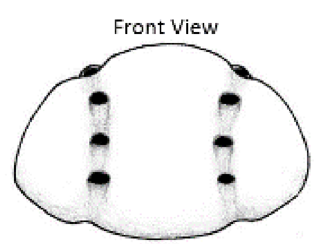
</td></tr>
</table>

3.0 Concept Selection

The selection process consists of two stages, the screening and the scoring. The screening stage involves narrowing down a large subset of concepts, to a smaller set. This smaller set is then thoroughly analyzed to decide upon a final concept. The selection process is performed for the lattice structure and the helmet geometry.

3.1 Concept Screening for Lattice Structure

The screening phase was used to evaluate the proposed lattice structure concepts. It is important to note that the overall helmet outer shell concepts were not evaluated during the screening phase. The lattice design influences the overall helmet design, and therefore the lattice structure must be established first. This section of the report explains in detail aspects of the criteria, as well as the process used to screen the concepts. Each concept was given a score based on how well it met the criteria, which led to the ranking of the concepts. To conclude the screening phase, the five top ranking concepts were retained for further investigation.

3.1.1 Lattice Screening Criteria

The set of criteria that was used to evaluate each lattice structure consisted of simplicity, and the lattice’s ability to absorb energy.

Simplicity

Lattice simplicity is a major factor in the feasibility of implementing the concept into the helmet. The lattice complexity varies with orientations and styles of lattice geometry. For example, whether the lattice is 2-dimensional or 3-dimensional, as well as whether the lattice is swept parallel along the surface of the helmet, or extruded perpendicular to the surface of the helmet will affect the level of complexity. In addition, the orientation of the lattice will affect the ability to model the helmet in CAD software. Developing an accurate model is crucial to ensure the validity of our FEA results. Selecting a complex lattice would potentially add complications when modeling the helmet. A complex lattice could also increase computation times and in turn, affect simulation results. Simplicity is evaluated on a scale of 1 to 5. A value of 1 will represent a complicated lattice and a value of 5 will be a simple lattice design.

Ability to Absorb Energy

The ability of a lattice to absorb energy through deflection is an important aspect when considering concepts. A lattice that is able to absorb an impact and dissipate energy efficiently is ideal. As defined by the CSA standards, no significant portion of the helmet can break off during an impact. If a part were to break off, it could pose a further risk of injury to the user. Due to the requirements defined by the standard, a lattice that is able to absorb an impact with the least amount of fracture is ideal, and therefore will be considered a 5. A lattice that will absorb an impact through fracture and crushing could pose a risk to the user. Structures that exhibit these kinds of features will be given a value of 1. Through the screening phase, the criteria was evaluated using basic static load simulations to predict deformation and stress distribution. Figure 5 illustrates the loads and fixtures used to evaluate each lattice with a static load scenario.

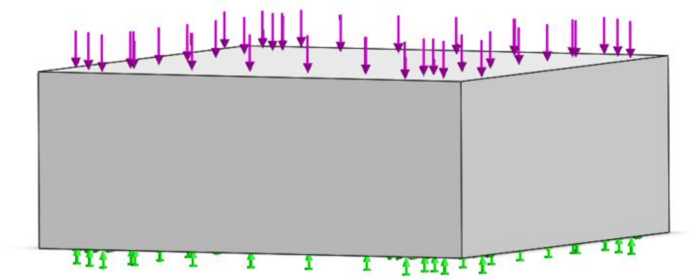

Figure 5: Loads and fixtures for static FEA in SolidWorks.

A simplified FEA model with a rectangular profile was used for the static analysis of each lattice concept in SolidWorks. The bottom face of the lattice structure was completely fixed and a 300 N distributed load was applied to the top face. Figure 5 provides a visual representation of the loads and fixtures that will be applied to the lattice structures. The green arrows represent the fixture, and the purple arrows represent the applied load. Although the numerical results of each analysis were not considered, the results were used as a visual aid in determining the lattice's ability to absorb impact energy. Both stress and displacement colour plots were produced to help visualize each concept's response to loading. However, the SolidWorks FEA does have limitations that were considered; namely, static load studies in SolidWorks do not account for buckling. Since the lattice is experiencing a compressive load, the buckling failure mode will be a factor in the lattice's ability to absorb energy. Therefore, the potential for a structure to buckle was considered, but no buckling analysis was done at this stage. The stress distribution and displacement plots for each concept can be found in Appendix D.

3.1.2 Lattice Screening Results

Each concept was evaluated by the team based on the two criteria and a total score was determined. The goal was to screen the lattice designs and determine the top five ranking concepts. TABLE XV outlines the results from the screening phase.

TABLE XV: CONCEPT SCREENING RESULTS DETAILS

Concepts	Selection Criteria		Total Score	Rank	Continue Forward with Design
	Simplicity	Energy Absorption			
1	5	4	9	1	X
2	5	1	6	6	
3	3	2	5	11	
4	4	5	9	1	X
5	4	2	6	6	
6	5	1	6	6	
7	3	3	6	6	
8	3	5	8	3	X
9	3	4	7	4	X
10	1	4	5	11	
11	1	4	5	11	
12	2	2	4	14	
13	3	4	7	4	X
14	4	2	6	6	
15	3	3	6	6	
16	4	2	6	6	
17	4	2	6	6	

X-Indicates that concept progressed forward for further analysis.

Based on the screening results, concepts 1 and 4 achieved a score of 9 out of 10, concept 8 achieved a score of 8, and concepts 9 and 13 achieved a score of 7. These five concepts showed favorable characteristics in terms of simplicity and their ability to absorb impact energy. Each concept that progressed through the screening phase will be explained in further detail. It is important to note that a sensitivity analysis will not be performed on the results as there are only two criteria that the concepts were evaluated against. With only two criteria and equal weighting, each point for the concept has a large influence on the score.

TABLE XVI: CONCEPT SCREENING RESULTS

#	Concept Name and Image	#	Concept Name and Image
1	Offset Boxes	**4**	Aligned Triangles
	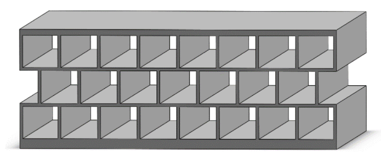		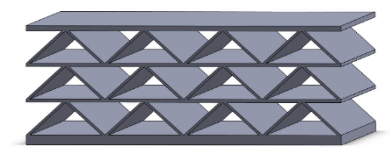
8	Spaced Hexagons	**9**	Honeycomb
	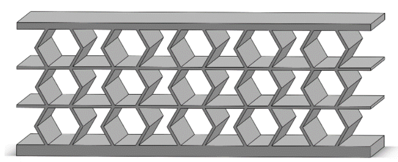		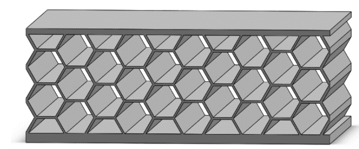
13	Pillars		
	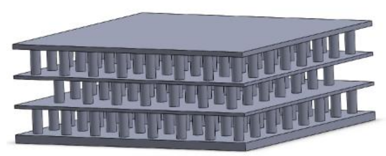		

Concept 1 – Offset Boxes:

Concept 1, the offset box style lattice, achieved a score of 5 out of 5 for simplicity. When evaluating simplicity, the feasibility to implement the lattice into a varying curved surface such as the helmet is considered. In addition, the lattice must inherently be a simple design with respect to shape and geometry. The more complicated the design, the more difficult the mesh required for impact simulations. Both parameters are considered when looking at the simplicity of the lattice structure. Concept 1 was also given a score of 4 out of 5 for its ability to absorb energy. Based on the initial analysis, there is a uniform stress distribution throughout the vertical members of the lattice. Each of the three layers show the same stress characteristics, yet the layers show a progressive displacement. Inherent in the concept, the horizontal skin layers are designed to bend as a way of absorbing energy upon impact. Concept 1 was deducted one point under energy absorption due to the structure's potential to buckle under heavy impacts. Buckling could result in a sharp deceleration whereas a more controlled deceleration is favored. Concept 1 showed many favorable characteristics and was advanced to the scoring phase.

Concept 4 – Aligned Triangles:

Concept 4 features an aligned triangular 2-dimensional cross section. This concept was given a 4 out of 5 on simplicity. This is due to its triangular cross section. The triangular cross section is still a very simple design, but in comparison with the box style cross section, it is not as versatile to implement, and Concept 4 received a lower score. After reviewing the static load testing in SolidWorks, it was apparent that the aligned triangular lattice is capable of significant energy absorption. By orientating the base of each triangle on the tip of the triangle below, the base layer of each triangle will deflect under loading. The structure is able to absorb impact energy through the bending of these layers, and therefore, this concept was given a 5 for its ability to absorb energy. Upon further development, this structure could be capable of significant energy absorption. Therefore, this concept advanced to the scoring phase.

Concept 8 – Spaced Hexagons:

Concept 8 utilizes a spaced out hexagon cross section. In theory, the spacing between the hexagons allows for predictable deflection during an impact that will absorb energy. This concept was given a 3 out of 5 for simplicity. This is due to the spacing between the hexagons, which adds complexity when modeling the lattice. This concept could be difficult to implement into the helmet's curved surface relative to the other lattice designs. Alternatively, our basic analysis showed an even stress distribution and a progressive displacement throughout the lattice under the static load. The shape of each hexagon should induce buckling in a controlled manner and produce more favorable results under a compressive load. For these reasons, concept 8 received a score of 5 out of 5 for its ability to absorb energy. This concept advanced to the scoring phase.

Concept 9 – Honeycomb:

Concept 9 uses a honeycomb style geometry. This concept was given a 3 for simplicity since it closely resembles concept 8. Modeling the lattice possess some difficulty due to the staggered orientation of the hexagons. This concept also does not have any definitive layers and therefore, restricts the ability to vary the layer thickness. Appendix D details the stress and displacement plots. The hexagon cross section allows for compression and the orientation of the pattern adds support to each honeycomb cell. Concept 9 has good stress characteristics, but does not show a very distinct displacement progression throughout the thickness of the structure. Therefore, concept 9 was given a 4 out of 5 for its ability to absorb energy and it will move on to the scoring phase.

Concept 13 – Pillars:

Concept 13 utilizes a series of vertical pillars throughout each layer of the lattice, which are divided by interior surface skins. The pillars are offset to allow for bending of the skins to absorb impact energy. This lattice required a different style of modeling due to the vertical orientation and 3-dimensional spacing, and therefore, added complexity to the process. This resulted in a score of 3 out of 5 for lattice simplicity. In the static load FEA, concept 13 provided a different set of results with respect to the other concepts. The interior layer collapsed while the upper and lower layers stayed relatively intact. Although the interior layer collapsed, the overall progression of displacement is still present. The stress plot shows that the skins between the lattice experience bending due to the offset pillars between each layer. This is beneficial to the overall impact energy absorption. As a result, concept 13 was given a 4 out of 5 for energy absorption. Concept 13 was the last design that progressed on to the scoring phase.

Excluded Concepts:

All of the other concepts that were outside of the top 5 were not included in the scoring phase. Concepts that exhibited less deflection and higher stress could potentially be too stiff to absorb a sufficient amount of energy upon impact. Concept 2, the aligned boxes, is an example of insufficient energy absorption. The aligned boxes do not utilize any sort of bending deflection to absorb energy, but rather the vertical walls of the boxes would compress and buckle. The process of buckling would absorb energy, but the initial deceleration due to impact would be greater than if the structure was designed to deform under loading. For this reason, concept 2 does not exhibit favorable characteristics in terms of energy absorption. This is a similar issue that many of the concepts that received low scores in terms of energy absorption exhibited. Additionally, concepts 10 and 11 were deemed far too complex to incorporate into a helmet. These concepts featured a 3-dimensional pyramid style lattice. Although they would likely provide good compression characteristics, they did not progress to the scoring phase due to their complexity. Favorable energy absorption characteristics can be achieved with a much more simplistic design. These trends were seen in many of the concepts and thus, allowed us to eliminate them during the screening process.

3.1.3 Concept Improvements

Each lattice concept has its own set of parameters that can be modified to further improve the design. Based on the style and shape of the lattice, different changes were made. TABLE XVII lists the possible design evolutions that pertain to each concept. Some of these evolutions were applied when performing detailed FEA to gain insight.

TABLE XVII: POTENTIAL CONCEPT MODIFICATIONS

#	Potential Modifications	Visual
1	• Adjust height and width of box dimensions for increased or decreased stiffness • Add radii on corners • Change wall thicknesses • Adjust inner or outer skin thicknesses • Vary thicknesses throughout each layer • Add cross-holes for air flow	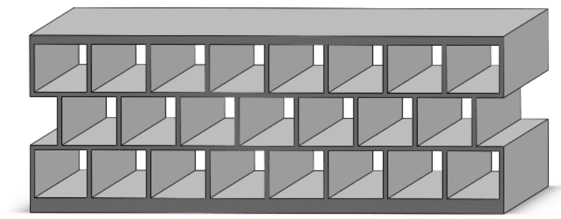
4	• Adjust angle of triangles to add or remove stiffness • Thickness of triangle walls • Thickness of horizontal layers • Add radii on corners • Orientation of triangles can be shifted • Varying thicknesses throughout each layer	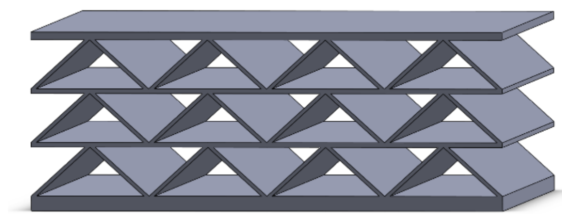
8	• Increase or decrease space between hexagons • Change wall thickness • Change layer thickness • Add curved members • Increase width of hexagons • Increase/Decrease angles inside of hexagons • Add radius to hexagon walls • Layer density of hexagons • Rotate hexagons to increase compressibility • Varying thickness throughout each layer	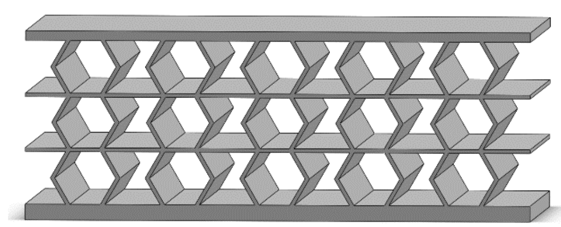

#	Potential Modifications	Visual
9	• Change wall thickness • Change layer thickness • Add curved members • Increase hexagon width • Increase/decrease angles inside of hexagons • Add radius to walls • Layer density of hexagons • Rotate hexagons to increase compressibility • Varying thickness throughout each layer	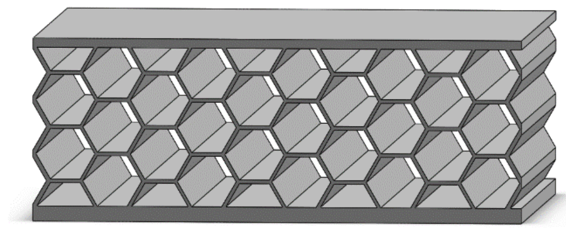
13	• Change number of layers • Change pillar diameters • Add fillets on pillars • Change spacing between pillars • Implement alternating angles • Orthogonal alternation layers • Varying thickness throughout each layer	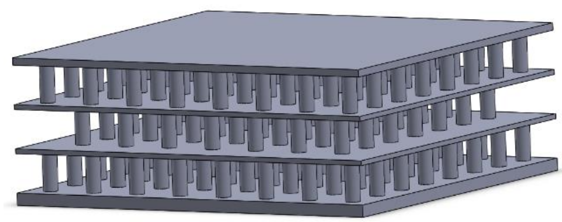

3.2 Concept Scoring for Lattice Structure

In order to select a lattice concept for the final design, the five remaining concepts were scored based on a set of established criteria. The initial list of concepts were screened using visual aids and static FEA on a basic compressive loading situation. To score the remaining concepts, dynamic impact FEA was performed on each lattice design to simulate an impact. From the results, each concept was scored by comparing the lattice's impact absorption performance.

3.2.1 Lattice Scoring Criteria

The criteria for concept scoring will be the same as the set of criteria used for the screening process. Both simplicity and ability to absorb impact energy will be evaluated. Simplicity will be judged relative to the 5 designs being evaluated, and energy absorption will utilize ABAQUS/CAE software to evaluate the lattice impact properties. These criteria will determine the concept's overall score. A criteria weighting matrix will not be used to assign weights due to the minimal criteria, and the logical order of importance for the user. This section will describe the process used to evaluate each concept against the established criteria.

Simplicity:

Simplicity was evaluated using the same approach as in the screening phase. The lattice would ideally be a simple design, while still being able to function as an impact absorbing structure. Simplicity affects the ability to implement the structure into a curved surface such as the helmet. In addition, the more complicated a lattice is, the more difficult it may be to generate a mesh for FEA. An accurate mesh is crucial to ensure accurate FEA results. Therefore, a lattice received a score of 5 for being a simple design and a 1 for being a complex design. As viewed from the customer's perspective, simplicity of the lattice design is not a major factor. Whether the lattice is extremely complex or very simple, the user will not be affected. For this reason simplicity received a lower criteria weighting with respect to energy absorption. Simplicity represented 40% of the overall final score for the concepts.

Ability to Absorb Energy:

Throughout the scoring phase, the lattice's ability to absorb energy was evaluated through impact simulations in ABAQUS/CAE software. Each test piece was standardized by weight and outer dimensions to ensure similar characteristics. Upon impact, the deceleration values between lattice structures was compared. Concepts were not evaluated against the CSA or CPSC test standard requirements; rather, the results were used to provide insight on the relative performance between each concept. For scoring, numerical values to rank each concept in terms of energy absorption was used. The concepts were rated on a scale of 1 to 5 relative to each other. Therefore, the maximum and minimum deceleration values were used to establish a range of values that correspond to each score. For example, if two concepts had very close deceleration rates, they may have still received the same score because they are evaluated based on a range of values, rather than just rank. Since the ability of the lattice to absorb energy ultimately defines the safety of the helmet, this criteria was given a heavy weight with respect to simplicity. The ability to absorb energy represented 60% of the concept's final score. This is the most critical aspect of the criteria set and therefore, it was given the most influence.

3.2.2 Lattice Concept FEA

The evaluation of the screened concepts was performed using the results of a dynamic explicit study in ABAQUS/CAE software. Solid models containing a portion of the lattice were created for each concept to test in ABAQUS. The FEA studies were designed to simulate the moment of impact for the flat anvil and hemispherical anvil tests in the CPSC Standard. The CPSC Standard is the most widely recognized bicycle helmet safety standard in North America, so it was chosen as the baseline standard. From the study results, the concepts were scored and ranked.

Set up of Concept Finite Element Analysis

In order to use FEA to compare each lattice structure, SolidWorks models of each concept were designed and imported into ABAQUS/CAE. The lattice structures were designed as a simplified FEA model with an overall rectangular profile as opposed to a radial helmet shape. Simplifying the lattice to a small rectangular profile is more efficient for preliminary analysis of the helmet internal structure. The study results still provide valuable insight into the energy absorbing capabilities of each concept. In order to properly compare each concept, the models had to have consistency in terms of dimensions and weight. The dimensions of the concept FEA models are shown in Figure 6.

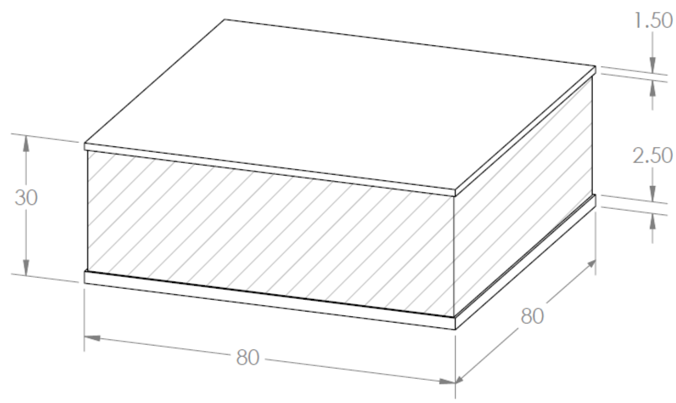

Figure 6: Concept FEA model dimensions in millimeters.

For the internal structure, each lattice was given three layers and 1 mm initial wall thickness for most members. The density of ABS-M30, 1040 kg/m^3, was selected arbitrarily to calculate the weight of each concept FEA model. The weight of each initial concept model ranged from 34 g to 64 g. In order to create consistency between the models, the wall thicknesses of each concept were varied until every concept weighed 50 g. By keeping the weight constant, the number of independent variables is reduced and the impact deceleration for each lattice design can be compared against each other.

The FEA models were imported into ABAQUS/CAE and material properties were assigned. Out of the 10 materials available for the Stratasys Fortus 400mc, only Polycarbonate (PC), NYLON 12, and Ultem 9085 have complete tensile and compressive test data. Polycarbonate was chosen as the material for the dynamic analysis. The experimental yield and ultimate stress test values was converted from nominal stress values to true stress values. The material properties for PC are shown in TABLE XVIII.

TABLE XVIII: PC MATERIAL PROPERTIES

	Property	XZ Axis	ZX Axis
General Properties	Density	1200	
	Poisson's Ratio	0.37	
Tensile Yield Properties	Tensile Modulus, (MPa)	1944	1958
	Nominal Yield Stress, (MPa)	40	30
	Nominal Yield Strain	0.022	0.02
	True Yield Stress, (MPa)	40.88	30.6
Tensile Ultimate Properties	Nominal Ultimate Stress, (MPa)	57	42
	Nominal Ultimate Strain	0.048	0.025
	True Ultimate Stress, (MPa)	59.736	43.05
Compressive Properties	Compressive Modulus, (MPa)	7564	1565
	Yield Stress, (MPa)	69	64
	Ultimate Stress, (MPa)	193	65

TABLE XVIII shows that the compressive modulus is almost four times greater than the tensile modulus in the XZ orientation. Even though the helmet will be under an overall compressive force in an impact, many members in the lattice structure will experience both tensile and compressive forces as they are put into bending. Also, if the lattice is designed in a swept conformal shape to the inner and outer surfaces of the helmet, different sections of the helmet will be printed in either the XZ or ZX orientations depending on the overall orientation of the helmet on the print bed. Therefore, for the sake of simplicity, the smallest modulus tensile modulus between the two orientations was chosen for the concept FEA.

The bicycle helmet impact tests from the CPSC standard were used as the basis for the simulated FEA impact studies. For the flat anvil test, a planar surface was fixed to the bottom surface of the lattice model. The plane was assumed to be perfectly rigid and every degree of freedom was fixed. For the hemispherical anvil test, a perfectly rigid hemispherical surface with a radius of 48 mm, as defined by the CPSC standard, was placed at the center point of the lattice model surface and fixed in every degree of freedom. The tangential contact behavior between the hemisphere surface and the bottom lattice model plane was given a friction coefficient of 0.3 [12]. This coefficient is based on a standard value for dry dynamic contact between a metal and plastic. For both anvil studies, a crushing plane was given a mass of 5 kg to simulate the headform in the CPSC Standard and was placed on the top surface of the lattice model. The plane was given an instantaneous velocity of 6.2 m/s as defined by the standard in the direction of the lattice model. This simulates the moment of impact between the anvil and bicycle helmet with 96 J of impact energy. The motion of the plane was restricted in every translational and rotational direction except in the translational direction of the lattice structure. Figure 7 shows the assemblies for the flat and hemispherical anvil studies.

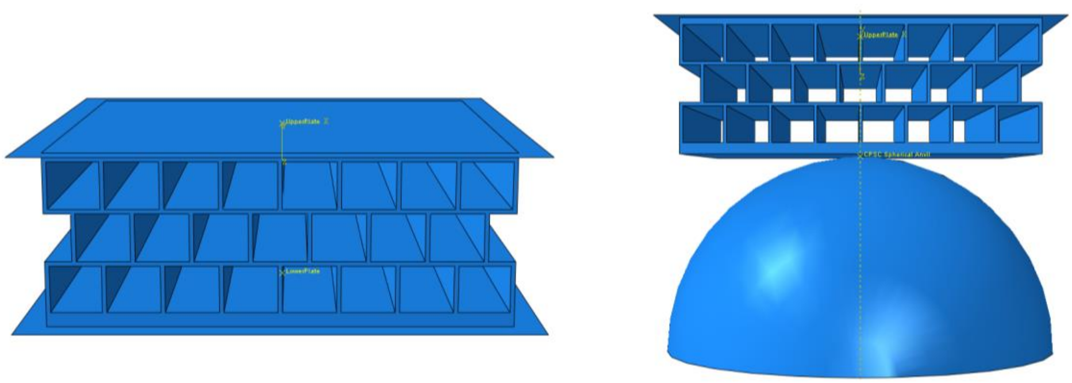

Figure 7: Flat and hemispherical anvil impact assemblies for Concept 1.

The time period for the impact step was given a length of 0.01 seconds. This was based on preliminary analysis, which showed that the length of the entire impact would occur within 0.01 seconds. ABAQUS was set to solve 40 evenly-spaced time increments between 0 and 0.01 seconds to ensure no sudden deceleration peaks were missed. To evaluate the energy absorbing ability of the lattice, the translational acceleration of the crushing plane was calculated and plotted at each time step.

For the sake of time and simplicity, tetrahedral elements were used to mesh the entire lattice FEA model for each concept. The mesh was generated automatically using ABAQUS and it was based on a specified seed size. Given the dimensions of the model, the default suggested seed size for the mesh was 0.0046 meter. The impact study was performed for Concept 1 with the 0.0046 meter seed size. Corresponding studies were performed with a 0.0023 and 0.00115 meter seed size. The resulting calculated impact decelerations for each seed size are plotted in Figure 8.

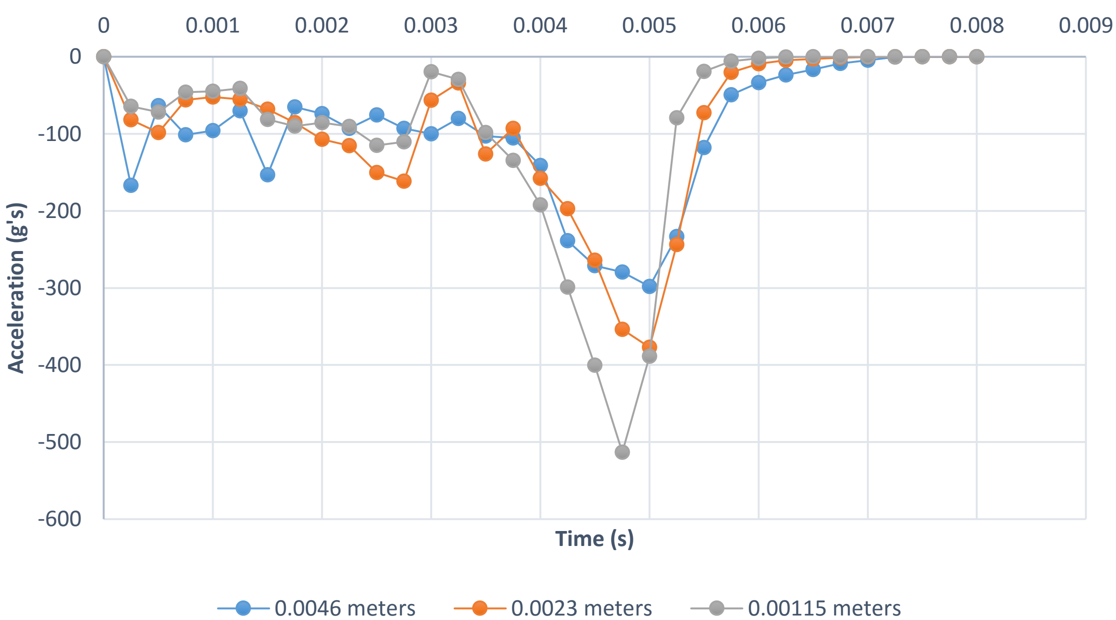

Figure 8: Concept 1 impact deceleration comparison for varying mesh seed sizes.

The 0.0046 meter seed size has fairly different results when compared to the two finer seed sizes. The 0.0023 and 0.00115 meter seed sizes show relatively similar results for each time increment except for between 0.004 seconds and 0.0055 seconds. During this interval, the lattice crushing plane is bottoming out, which results in the large deceleration spike. Even though it is not possible to state that the results are converging based on Figure 8, the 0.0023 meter results are close enough in comparison to the 0.00115 meter results to use the 0.0023 meter seed size for the rest of the concept analysis. Since this is a comparative analysis, completely accurate results are not required. Also, using the 0.0023 meter seed size drastically reduces the computing time for each study.

Since each concept impact analysis performs the calculations at the same intervals, the deceleration at every interval can be summed to compare the total impact absorption energy for each concept. It can be noted that total sum of deceleration values for the 0.0023 and 0.00115 meter seed sizes have a percent difference of 0.79%, which indicates that the results are equivalent in total energy. The tetrahedral mesh with a 0.0023 meter seed used for the concept evaluation is shown in Figure 9 for Concept 1.

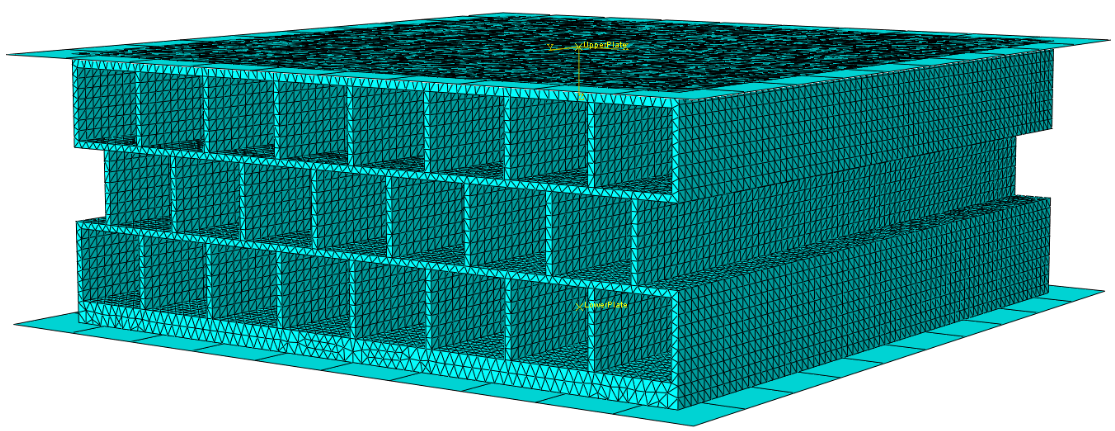

Figure 9: Generated tetrahedral solid mesh of Concept 1 with a 0.0023 meter seed size.

The lattice members in Concepts 1, 4, 8 and 9 consist of swept walls. The mesh for these members was generated easily without any partitioning of the lattice model. However, the automatic mesh generation was less ideal for the geometry in concept 13. The automatic tetrahedral mesh created a dense grouping of elements around each pillar, which drastically increased the required computing time. The pillars could also be meshed more effectively by partitioning them and generating a hexahedral solid mesh of the pillars separately from the horizontal layers. Figure 10 shows the results of the automatic tetrahedral mesh generation of Concept 13.

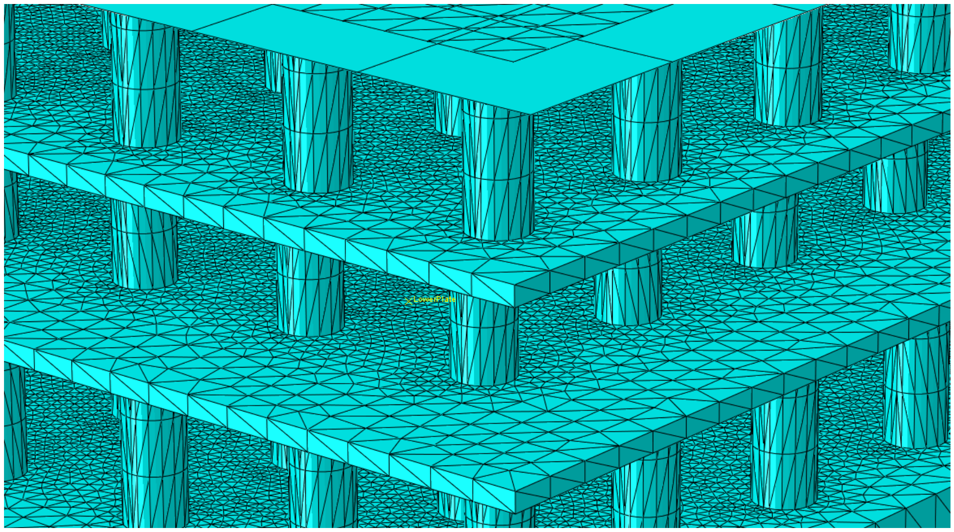

Figure 10: Generated tetrahedral solid mesh of concept 13 with a 0.0023 meter seed size.

Since simplicity of the lattice geometry is an important criteria in the concept evaluation, Concept 13 was left out of further concept analysis as it was not possible to generate an efficient mesh. The generated mesh for every concept can be seen in Appendix F.

Results of Concept Finite Element Analysis

FEA studies were performed for every screened concept using the method outlined in Section 0. The acceleration of the upper plate, which was assigned the inertial mass and velocity, was plotted at every increment of the 0.01 second impact step for each concept. The deceleration of the crushing plane over the impact duration is compared in Figure 11 and Figure 12. The overall time period was reduced to 0.007 seconds in the figures as the impact has reached its conclusion at that time.

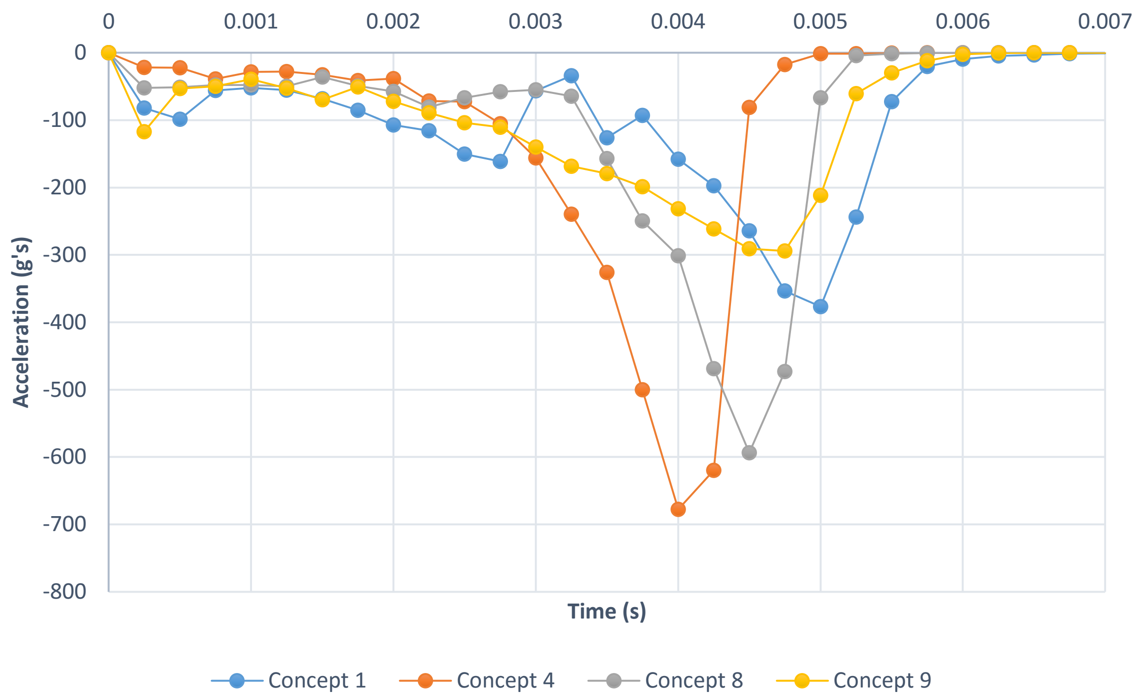

Figure 11: Concept comparison of flat anvil impact decelerations.

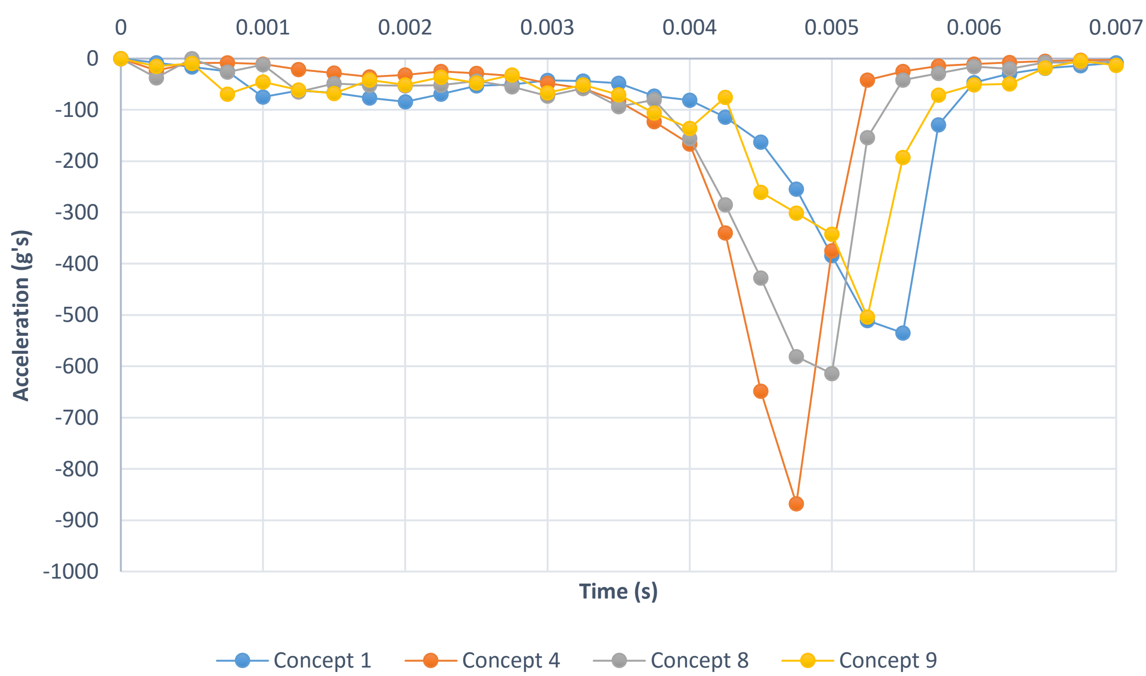

Figure 12: Concept comparisons of hemispherical anvil impact decelerations.

Figure 11 and Figure 12 show that the greatest peak deceleration for every concept occurs as the crushing plane bottoms out. The deceleration of every concept stays well below 200 g’s until the plane bottoms out for both the flat and hemispherical anvils. This suggests that every concept is not stiff enough as currently designed. However, the results do not need to be below 300 g’s, as specified by the CPSC Standard, since the purpose of the analysis is to compare each concept against each other. The final design will have increased stiffness to prevent the crushing plane from bottoming out.

The peak deceleration for every FEA concept study is shown in TABLE XIX. This data, combined with the comparison of each deceleration curve in Figure 11 and Figure 12, is used to score each concept’s ability to absorb impact energy.

TABLE XIX: PEAK DECELERATION FOR FLAT AND HEMISPHERICAL ANVIL CONCEPT FEA

Concept	Flat Anvil Peak Deceleration (g's)	Hemispherical Anvil Peak Deceleration (g's)
1	377	535
4	678	868
8	594	614
9	294	504

Figure 13 and Figure 14 illustrate the impact progression of each lattice at increasing time steps. These figures are used to demonstrate the way in which each lattice deforms under impact loading. The minimum ultimate stress value for PC based on the material properties is 40.05 MPa. Figure 13 and Figure 14 show that the ultimate stress is reached in certain areas of each lattice at the first time step. However, the concept FEA analysis is assumed to be linear elastic throughout the duration of impact. As mentioned previously, the selected lattice concept will require more stiffness in the final design. However, it should be noted that energy is also absorbed upon reaching the ultimate stress as the lattice members catastrophically fail.

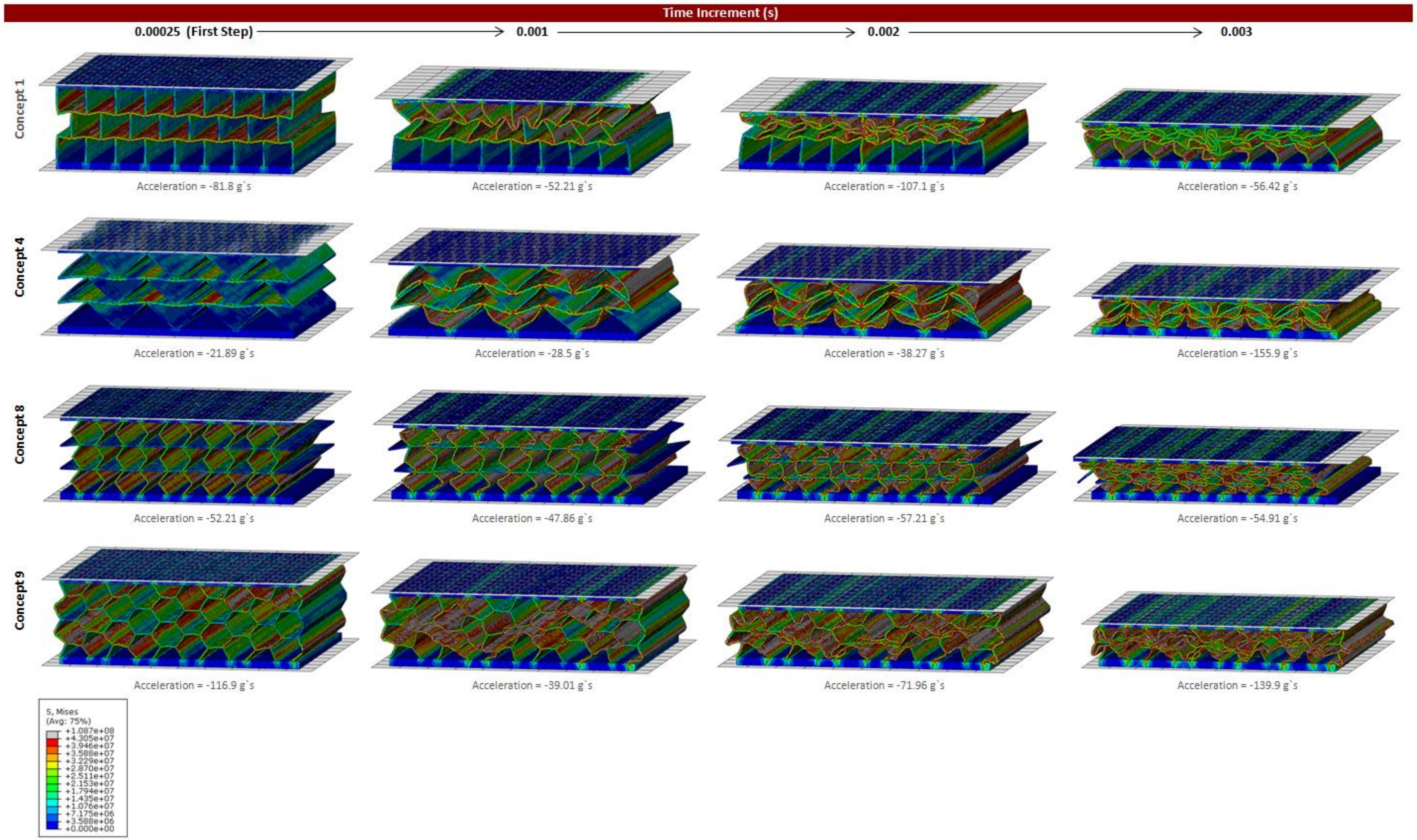

Figure 13: Four time increments of flat anvil impact FEA for concepts 1, 4, 8, and 9.

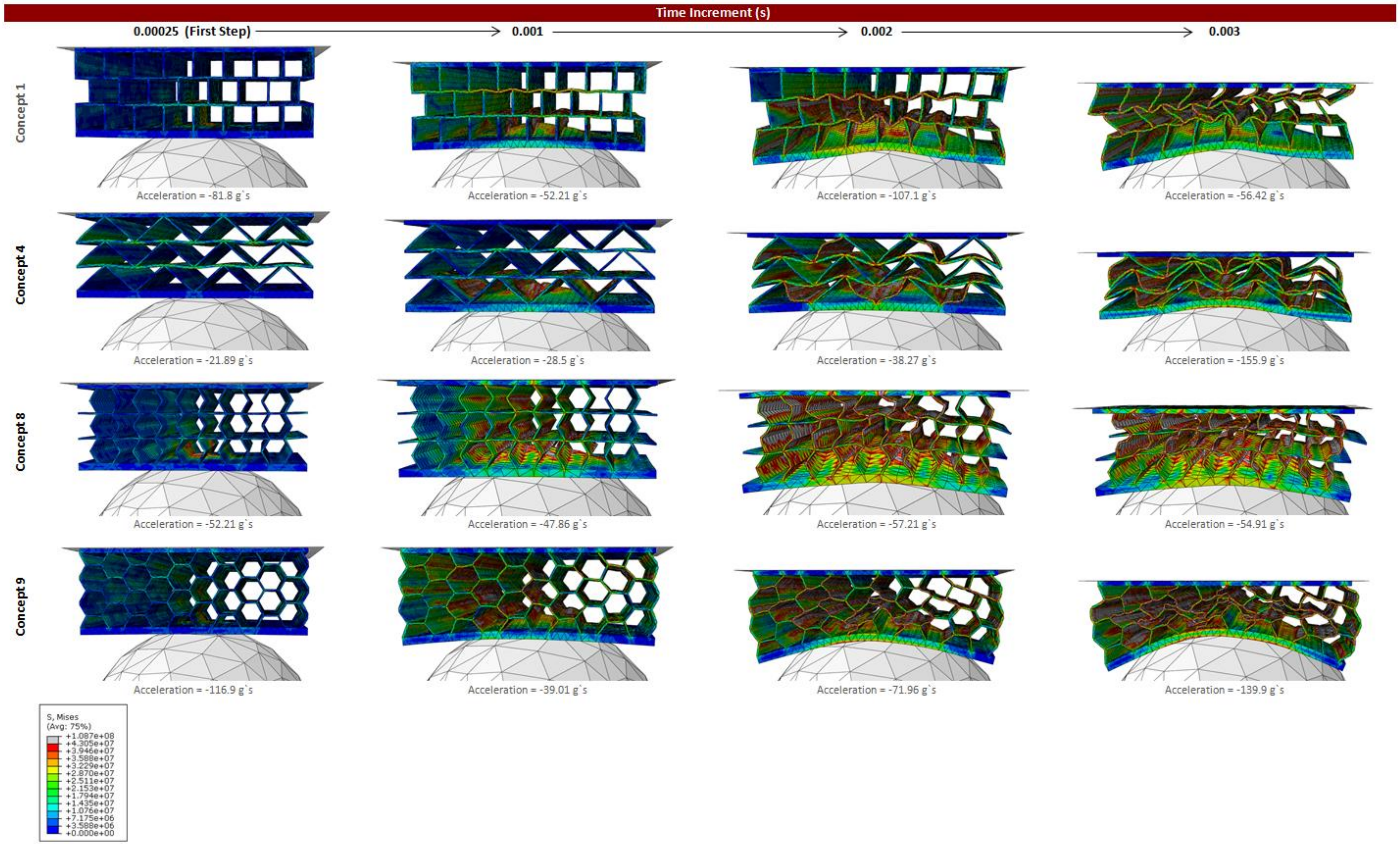

Figure 14: Four time increments of hemispherical anvil impact FEA for concepts 1, 4, 8, and 9.

3.2.3 Lattice Scoring Results

TABLE XX displays the concept scoring results. Each lattice design was evaluated against the weighted set of criteria and a total score was established.

TABLE XX : CONCEPT SCORING RESULTS

#	Concepts	Selection Criteria Weight	Simplicity 40%	Energy 60%	Total Score	Rank	Continue
1	Offset Box	Ranking	5	5	5.0	1	X
		Score	2.0	3.0			
4	Aligned Triangles	Ranking	1	3	2.2	4	
		Score	0.4	1.8			
8	Spaced Hexagons	Ranking	3	4	3.6	3	
		Score	1.2	2.4			
9	Honeycomb	Ranking	4	5	4.6	2	X
		Score	1.6	3.0			
13	Pillars	Ranking	1	N/A	0.4	5	
		Score	0.4	0			

X-Indicates that concept will progress forward for further analysis

After evaluating each concept against the established set of criteria, Concepts 4, 8, and 13 area eliminated. Based on the results, there is a distinct separation between the top two ranking concepts and the others. A sensitivity analysis was not performed due to the minimal amount of criteria used to evaluate each concept. Concepts 1 and 9 ranked highest against energy absorption and are also the concepts that will be kept. This is to be expected, as energy absorption has the highest weight since it pertains to safety.

Concept 1 - Offset Boxes:

Concept 1 achieved the maximum possible score against both criteria. The 2-dimensional, offset box style lattice was proven to be a simpler design. Out of the 5 remaining lattice structures, Concept 1 was the easiest design to model and therefore received the highest score. This concept also allows for a significant amount of flexibility in term of lattice dimensions. Upon further design, wall thicknesses, box dimensions, and the number of layers can be altered. Depending on the curvature of the helmet, the offset box design would be easier to implement than other concepts. In addition, referring back to both

Figure 11 and Figure 12, Concept 1 had the second lowest impact deceleration at 535 g's. Although it was not first, it still fell within an acceptable range to achieve a 5 for its ability to absorb energy. This concept will be kept for further design and testing.

Concept 4 - Aligned Triangles:

Concept 4 did not rank well during scoring largely due to its lack of ability to absorb energy under impact. Figure 11 and Figure 12 both show that concept 4 absorbed the least amount of energy in the early stages of impact (prior to 0.003 seconds). As a result, it also had the highest impact deceleration at 868 g's for the spherical anvil and 678 g's on the flat anvil as the crushing plane bottomed out. To improve this concept, significant amount of material to help stiffen the structure would have to be added. Adding this material results in added mass, which is not favorable for the customer. Since concept 4 was on the high end of the range for impact deceleration it was given a score of 1. Concept 4 was given a score of 3 out of 5 with respect to simplicity. The aligned triangular cross section was more complex to develop within the test piece and it could create added complexity when implementing into the curvature of the helmet. This concept ranked 4th in the scoring phase, and therefore will not be kept for further development.

Concept 8 – Spaced Hexagons:

Concept 8 provided average results. After simulating the impact, this concept resulted in the third lowest impact deceleration at 594 g's for the flat anvil and 614 g's for the spherical anvil. These values for deceleration fell within the second applicable range resulting in a score of 4 out of 5. Additionally, this concept provided some difficulty during modeling with respect to concept 1 due to its hexagonal shape. This concept uses definitive layers that must remain intact for the lattice to function under impact. Adapting this lattice to the helmet could be difficult due to the layers and curvature. Based on the results of the scores, concept 8 fell below the natural separation in the results and, therefore will not be kept.

Concept 9 - Honeycomb:

Concept 9 exhibited favorable results in both aspects of the criteria. The honeycomb structure was given a 4 out of 5 for its simplicity. Although the honeycomb shares a similar cross section as concept 8, the honeycomb lattice does not have definitive layers. Also, this lattice will have the same properties in both directions regardless of orientation. For this reason, the lattice structure could be trimmed to fit within the curvature of the helmet rather than have it wrap around the contour. This may simplify the modeling and implementation significantly. Furthermore, the lattice did provide the best impact deceleration results at 504 g's for the spherical anvil and 294 g's for the flat anvil. It is important to note that this lattice is already meeting the required impact standard for the flat anvil test of the FEA model. It still requires improvement, but it is currently the closest concept. This concept will be further developed to test its feasibility as a solution.

Concept 13 - Pillars:

Concept 13 immediately posed a series of problems when simulating the impact analysis. Due to the complexity of the structure, it was difficult to generate an effective mesh. This concept required extensive computing time to produce a set of results and ultimately it was removed. No results were plotted, and therefore this concept was given a score of 0 out of 5 for its ability to absorb energy. This concept scored the lowest out of all the options and was not be further developed.

3.3 Concept Scoring for Helmet Geometry

Since the team generated fewer helmet geometry concepts, concept screening is by-passed and only concept scoring was performed.

3.3.1 Geometry Scoring Criteria

The helmet concepts will be judged on three criteria: complexity, aesthetics and ventilation. Each criteria and its relative importance will be discussed in detail below.

Simplicity

A helmet with a lot of detail or complicated shapes may make it difficult to apply a uniform lattice structure within the helmet. Further, the level of complexity will also affect the ability to model the helmet in our short timeline and limited human resources. Complexity will be heavily weighted as the helmet geometry complexity will likely make the lattice structure more complex resulting in longer print time and higher costs. Complexity will be ranked on a scale of 1 to 5 where 1 is very complex shape and 5 is simple and this ranking is mainly concerning the easy of implementing a lattice.

Aesthetics

In order for the helmet to be a saleable product, aesthetics have to be considered. The helmet must look sleek and attractive to entice customers. Although this criteria is difficult to quantify, our team will score each design in general terms such as whether the helmet looks aerodynamic or sporty, if it looks unique, and so on. The level of complexity will likely have an impact on aesthetics and it is also secondary to the primary function of protection thus the weight will be lower for this criteria. The ranking will be on a scale of 1 to 5 where 1 is not attractive and 5 is very aesthetically pleasing.

Ventilation

The helmet must provide the wearer ventilation to mitigate overheating. The amount of venting will depend on the number of vents as well as the size of the vents. The size of the vents cannot be so large that the helmet provides inadequate protection. Conversely, if the holes are too small, the air flow rate will be too small to properly cool the cyclist. Finally, the shape of the holes may render implementing a lattice structure too difficult. This criteria will be ranked on a scale of 1 of 5 where 1 is very poor ventilation potential and 5 is for a design that will have good ventilation.

3.3.2 Geometry Scoring Results

TABLE XX displays the concept scoring results. Each lattice design was evaluated against the weighted set of criteria and a total score was established.

TABLE XXI : CONCEPT SCORING RESULTS

#	Concepts	Selection Criteria Weight	Simplicity 50%	Aesthetics 20%	Ventilation 30%	Total Score	Rank	Continue
1	Sectioned Helmet with Gap Vents	Ranking	4	5	4	4.2	1	X
		Score	2.0	1.0	1.2			
2	Built-in Vent Tubes	Ranking	2	3	3	2.5	4	
		Score	1.0	0.6	0.9			
3	Integrated Vent Design	Ranking	2	3	4	2.8	3	
		Score	1.0	0.6	1.2			
4	Modular Bicycle Helmet	Ranking	4	2	2	3.0	2	X
		Score	2.0	0.4	0.6			
5	Multi-Vent Spline Helmet	Ranking	1	4	4	2.5	4	
		Score	0.5	0.8	1.2			

X-Indicates that concept will progress forward for further analysis

After scoring, the helmet concept 1 is the clear winner. Evolutions of this design will be done iteratively with computational fluid dynamics in order to create a geometry that will be relatively simple for lattice integration, provides ventilation and is aesthetically pleasing. This process will be discussed later in section 4.0.

3.4 Concept Selection Summary

Throughout the screening and scoring phases, lattice concepts were standardized by weight, evaluated on their simplicity, and their ability to absorb energy. The ideal lattice design would be simple to allow for easy implementation into the helmet, as well to reduce computational requirements during simulations. Simplicity was evaluated on a subjective basis. Since the lattice designs were standardized by weight, a comparative analysis was done to rank concepts based on their ability to absorb energy. The concept with the lowest deceleration rate under an impact was given the best score.

17 lattice concepts were developed to begin the selection process. After the screening and scoring phases, 2 concepts were left for further development in the detailed design section. The highest scoring lattice concept was the offset box style design shown in Figure 15.

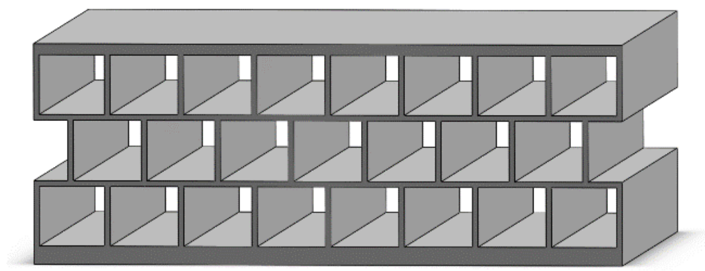

Figure 15: Offset box lattice concept.

This concept was ranked highest against both aspects of the criteria. The simple 2-dimensional style would make implementing the design into the helmet much easier, additionally this lattice effectively dissipated energy throughout the impact simulation.

The second highest overall scoring lattice concept was the honeycomb design, seen in Figure 16.

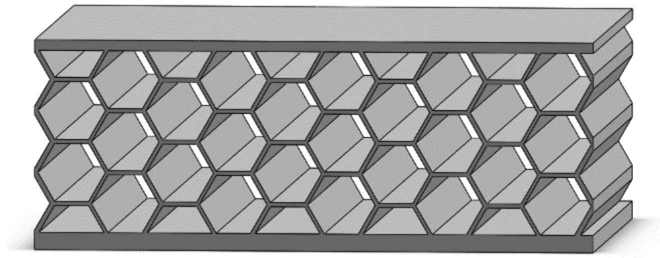

Figure 16: Honeycomb lattice concept.

The honeycomb lattice produced very similar impact energy results in comparison to the offset box style, the only difference was in the simplicity of the design. The honeycomb cell shape adds an additionally amount of complexity with respect to the offset box lattice. Ultimately, both lattice geometries produced very favorable results against the set of criteria. Further FEA analysis was done on each concept to establish the most optimal lattice design.

There were 5 different helmet geometries developed for evaluation in the scoring phase. Each geometry was evaluated against a set of criteria including complexity, aesthetics, and ventilation. Complexity was the most heavily weighted piece of criteria as it would have a large influence on the feasibility of the design and implementation of the lattice. Ventilation was the second most important aspect of the criteria since it concerned the users comfort. Aesthetics was given the lowest weight due to the main focus of the helmet being functionality.

As a result of the scoring phase, the sectioned helmet with gap vents produced the highest overall score. This concept maintained a simple helmet style, which accommodated the two selected lattice designs. The gap style vents allowed for significant customization in terms of ventilation. After the CFD analysis, if more ventilation or less drag was required the vent size could be easily adjusted without affecting the lattice structure. Figure 17 shows the general concept for the helmet geometry.

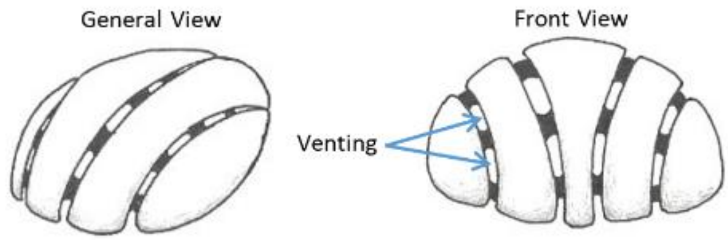

Figure 17: Sectioned helmet with gap vents.

As a result of the concept selection phase, two lattice designs were selected for further investigation along with a general helmet geometry concept. Further analysis in the detailed design section determined the most suitable lattice concept designs, as well an initial helmet geometry was developed.

4.0 Detailed Design

After the selection phase for the lattice structure and helmet shape were conducted, the combination of those two elements were performed to create a helmet. The material for the helmet is selected, while the validation of the lattice structure through FEA is performed. Finally the helmet exterior design is created, with the lattice structure included.

4.1 Material Selection

As discussed in Section 1.3, Stratasys offers a selection of 10 materials for the Fortus 400mc 3D printer. The material used in the helmet should exhibit the most ideal characteristics for an impact absorbing structure. The most important criteria for material selection is the material's density, modulus, ultimate stress, elongation at break and the types of support structure offered.

The first criteria considered when selecting the material was the support structure options. Support structure is required when material is being printed at an angle of 45° or less relative to the print bed. Since the helmet and the internal lattice structure will consist of many walls that sweeps around a radial head shape, support material will be required in many locations. Stratasys offers two types of support structures: a break away support system (BASS) or a soluble support structure [8]. Soluble support structures are removed by submerging the printed part in a solution that dissolves the support material. A break away support system must be removed physically from the structure by hand.

Since the lattice structure will consist of multiple swept cut-outs, the interior of the helmet will have many small channels, making it impossible to use a break away support system. For this reason, PC-ISO, ULTEM 9085 and PPSF/PPSU were not considered, as they only offer break away support structures. However, in order to use the soluble support structure, the helmet will require drain holes in each lattice channel. The holes will allow the dissolving solution to reach the internal support structures and drain afterwards.

After narrowing down the potential options to 7 of the available materials, the mechanical properties of each material were compared. The density, tensile modulus, ultimate tensile stress, and elongation at break are shown for each material in TABLE XXII. Each of these material properties are important to consider in the design of the bicycle helmet.

TABLE XXII: CRITICAL MATERIAL PROPERTIES FOR THE BICYCLE HELMET

Material	Plane	Density (Kg/m^3)	Tensile Modulus (MPa)	Ultimate Tensile Stress (MPa)	Elongation at Break (%)
ABSi	-	1080	1920	37	4.4
ABS ESD7	-	1040	2400	36	3
ABS-M30i	-	1040	2400	36	4
ABS-M30	XZ	1040	2230	32	7
	ZX		2180	28	2
ASA	XZ	1050	2010	33	9
	ZX		1950	30	3
PC	XZ	1200	1944	57	4.8
	ZX		1958	42	2.5
NYLON 12	XZ	1000	1282	46	30
	ZX		1138	38.5	5.4

The density will clearly affect the weight of the helmet, which is one of the metrics being considered. TABLE XXII shows that the density of each material is relatively similar, with NYLON 12 being the lowest. Since the densities are similar, this property was given less importance when deciding what material to use. Also, the density is not important compared to the other mechanical properties when considering how the lattice will respond to impact loading.

Since both lattice concepts are designed to absorb impact energy through the bending of members, the material selected should exhibit ductile behavior when loaded. A brittle material is not ideal because it is more likely to fracture without deformation upon impact. The ductility of the material is associated with material elongation. Figure 18 compares the elongation of each material in a tensile test at the point of break. The elongation for the materials with test data in two print orientations is given as an average of both.

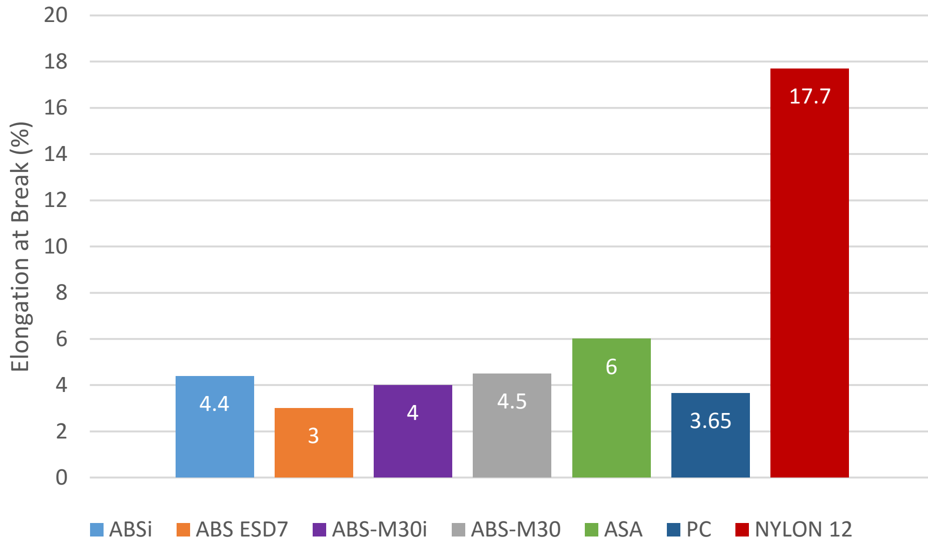

Figure 18: Comparison of material elongation at break.

Similarly, the material selected should not be too elastically stiff as characterized by the material's modulus. If the modulus is high, the material will be stiffer and will reach higher levels of stress for the same amount of strain as defined by Hooke's Law. Also, the ABAQUS FEA assumes linear elastic behavior throughout the impact. Therefore, materials with a lower modulus are ideal, as the assumption of linear elastic behavior will, in theory, hold true for a longer duration of the impact. Figure 19 compares the modulus of each material. Values are given as averages for the materials with test data in two orientations.

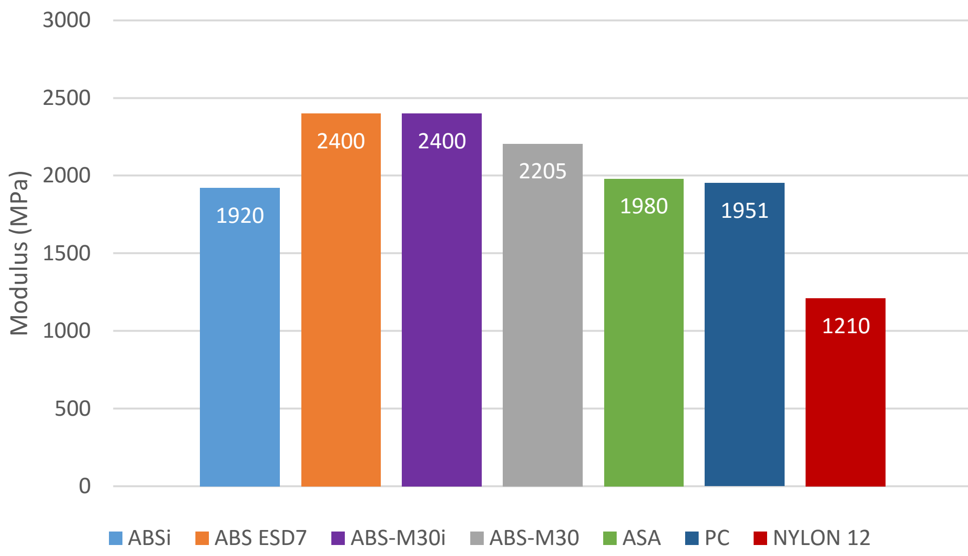

Figure 19: Comparison of material modulus.

Figure 18 and Figure 19 show that NYLON 12 is significantly more ductile and will elastically deform more than the other materials. This makes it an ideal material for impact loading. However, upon selection of this material, the technicians at Precision ADM informed the team that the minimum wall thickness they use when printing in NYLON 12 is 2.54 mm due to its thermal properties. A minimum 2.54 mm wall thickness prevents part deformation and warping. This restriction presented a possible design constraint that could prevent NYLON 12 from being the most suitable material depending on the lattice design. For this reason, a secondary material option was selected for the design.

Comparing the modulus of the remaining materials, the next best options are ABSi, ASA, and PC, which all have a similar moduli, ranging from 1920 MPa to 1980 MPa. The other options are over 2000 MPa and were removed from consideration.

To further reduce material options, the ultimate tensile stress was compared. ASA had the second lowest average ultimate tensile stress value between the two orientations compared to the other materials. Having a higher ultimate stress value was ideal because the impact FEA did not account for material damage.

PC has the highest average ultimate stress between the two orientations. It also has a low modulus, comparable to ASA and ABSi. For these reasons, PC was selected as the second option for the bicycle helmet. In terms of wall thickness, the technician at Precision

ADM suggested that a minimum thickness of 1.6 mm might be required for all walls of the helmet and internal lattice. Based on the past experience of Precision ADM, should the structure be thinner than 1.6 mm, the structure might become fragile. However, this constraint offers much more design flexibility, as compared to NYLON 12's minimum wall thickness.

Overall, NYLON 12 has the best properties for impact loading, but the wall thickness limitation presented a potential problem depending on the lattice design. PC is much more brittle than NYLON 12, but PC has the highest strength of any of the other materials. The lattice can also be designed to be much thinner using PC, which could circumvent the issue of having a higher modulus. Both NYLON 12 and PC were considered when moving into the final design of the lattice.

4.2 Helmet Lattice Design

In the lattice concept scoring stage, Concept 1 and Concept 9, were selected for further development. Ultimately, a single lattice design was selected and optimized to ensure the bicycle helmet meets safety standards. Dynamic impact FEA in ABAQUS/CAE was used to evaluate the energy absorption abilities of the lattice design.

The first step in the detailed lattice design stage was to determine the helmet material. Next, different iterations of Concept 1 and Concept 9 were designed as cubic FEA models and analyzed in ABAQUS. The resulting data was used to select the final concept. A radial lattice FEA model was designed to reflect the curvature of the helmet and used to select and optimize the final lattice design. Finally, the lattice was implemented into the interior of the bicycle helmet.

4.2.1 Cubic Lattice Analysis

In order to determine the optimum lattice design between Concept 1 and Concept 9, cubic lattice FEA models were used again in the impact analysis. This is due to the short computing time required to perform the analysis and the relative ease of adjusting the CAD models. Four iterations of each concept were designed with increasing wall thicknesses in both 3 and 4 layer configurations. The only dimension that was varied was the lattice wall thickness. The lattice wall thickness was selected so that the mass of each iteration of Concept 1 and Concept 9 were comparable. The lattice cells are evenly spaced in the vertical direction. The general dimensions of the FEA models used for Concept 1 and Concept 9 are shown in Figure 20 and Figure 21, respectively.

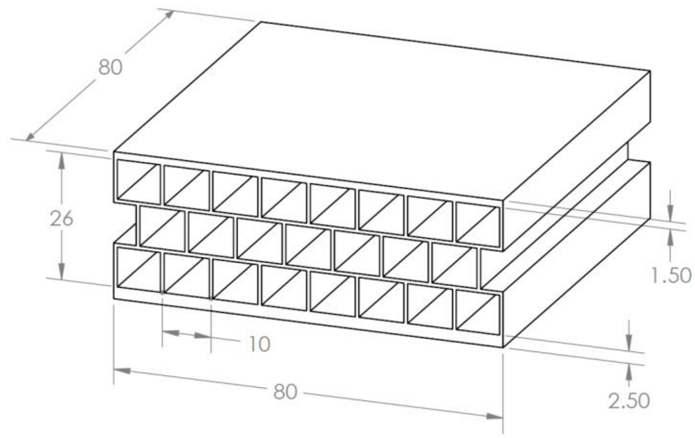

Figure 20: Three-layer Concept 1 cubic FEA model dimensions in millimeters.

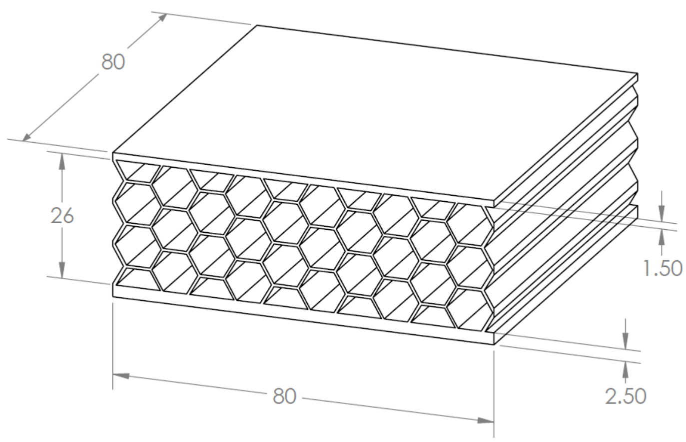

Figure 21: Three-layer Concept 9 cubic FEA model dimensions in millimeters.

Both the three layer and four layer iterations used the same general dimensions, but with different spacing. The design iterations for Concept 1 and Concept 9 are listed in TABLE XXIII.

TABLE XXIII: CONCEPT 1 AND CONCEPT 9 DESIGN ITERATIONS

Iteration Parameter		Concept 1		Concept 9	
Iteration	**# of Layers**	**Wall Thickness (mm)**	**Mass (g)**	**Wall Thickness (mm)**	**Mass (g)**
A1	3	0.75	57.5	0.6	55.5
A2	3	1.0	66.0	0.8	64.6
A3	3	1.25	74.4	1.0	72.3
A4	3	1.5	82.5	1.4	85.0
B1	4	0.75	62.5	0.6	65.7
B2	4	1.0	72.5	0.8	74.8
B3	4	1.25	82.2	1.0	83.5
B4	4	1.5	91.6	1.4	103.2

Iterations A1 through A4 have three layers and iterations B1 through B4 have four layers. The wall thicknesses were evenly incremented and the mass of each iteration is relatively close for both concepts.

Each concept iteration shown in TABLE XXIII was analyzed in ABAQUS using the same method from the concept scoring stage discussed in section 3.2. The flat anvil drop test from the CPSC standard was used as the basis for the analysis [5]. The same tetrahedral mesh with a 0.0023 meter seed size was used, and PC was chosen as the material. The wall thicknesses used are below the value recommended by Precision ADM. The purpose of this analysis was to determine the ideal concept, as well as gain a general understanding of how varying the wall thickness would affect the energy absorption capabilities of the lattice. The analysis of the three layer iterations for Concept 1 and Concept 9 were performed first. The results are shown in Figure 22 and Figure 23, respectively.

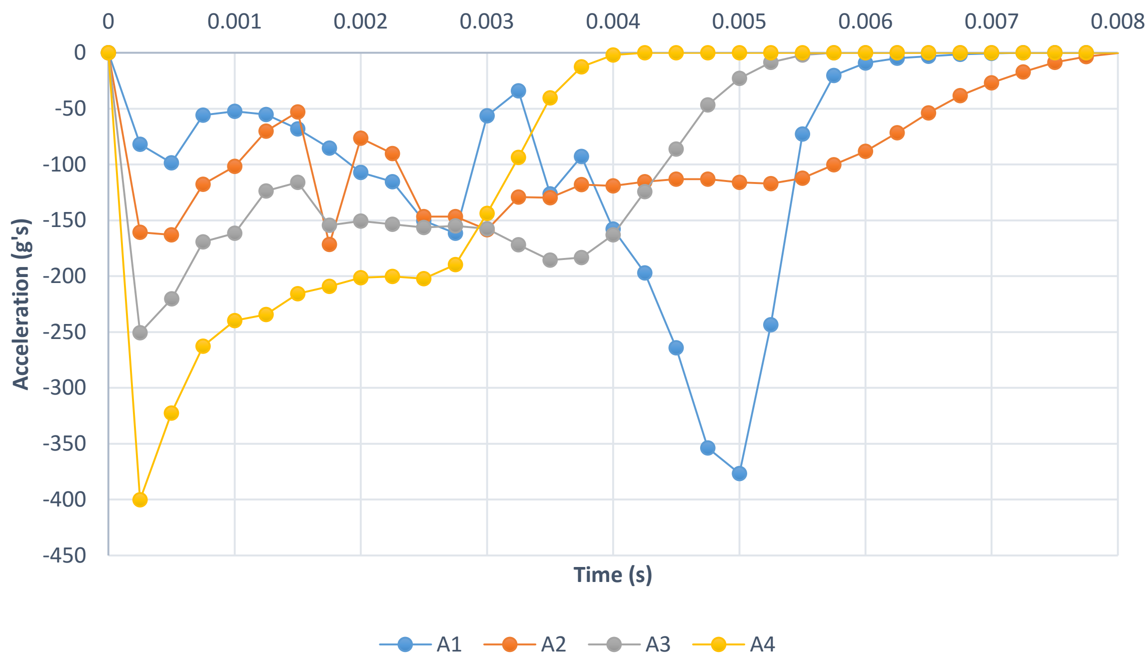

Figure 22: 3 Layer iteration comparison for Concept 1.

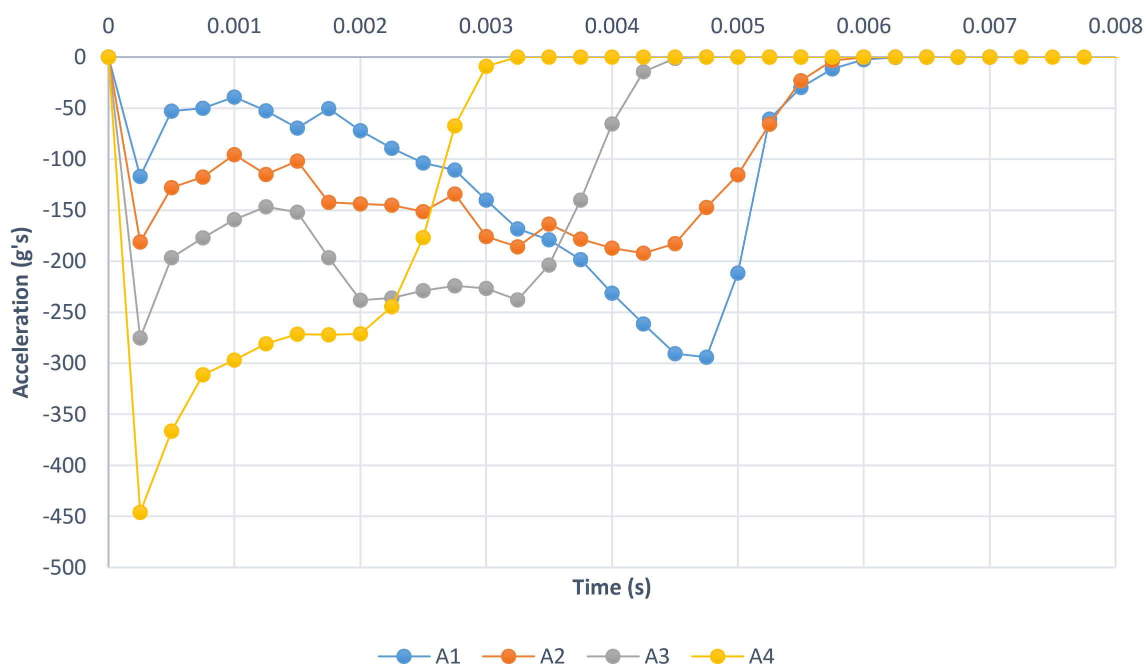

Figure 23: 3 Layer iteration comparison for Concept 9.

The results in Figure 22 and Figure 23 show that the energy absorption capabilities of the lattice structures are drastically affected by the wall thickness. As the wall thickness was increased, the overall structure stiffness increased causing a greater deceleration at the beginning of the impact. This also resulted in shorter overall impact times, as the majority of the kinetic energy was dissipated at the beginning of the impact. The peak deceleration of iteration A1 for both concepts occurred towards the end of the reaction. This is due to the lattice structure lacking stiffness, which resulted in a deceleration spike as the crushing plane bottomed out.

Each iteration for both concepts can be directly compared because they have the same approximate weight. The deceleration curves for each iteration shown in Figure 22 and Figure 23 are very similar. Figure 24 directly compares the decelerations for iteration A2 and A4 for both concepts

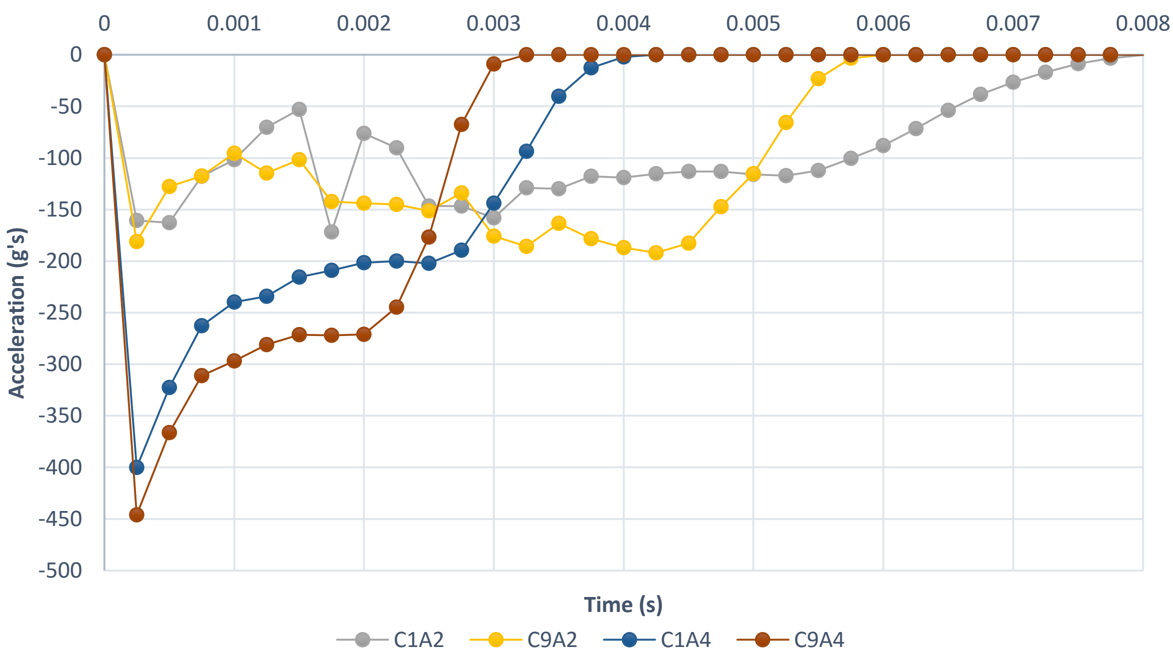

Figure 24: Comparison of three-layer iterations of Concept 1 and Concept 9.

In Figure 24, the deceleration curves follow the same general path with Concept 9, showing slightly higher deceleration during most of the impact duration. This means that Concept 9 is stiffer and could potentially be made lighter than Concept 1 if the wall thickness was reduced. However, the wall thickness is already too thin to print based on Precision ADM's suggestions. Also, implementing a swept hexagon lattice into the helmet is much more complex than implementing a swept square lattice for only minor weight savings. For these reasons, Concept 1 was selected as the best option.

The next stage in the lattice design process was to determine the optimum number of layers. Iterations B1 through B4 were analyzed in ABAQUS to compare against the 3 layer iterations. B2 and B3 have approximately the same weight as A3 and A4, and the acceleration plots for these iterations are shown in Figure 25.

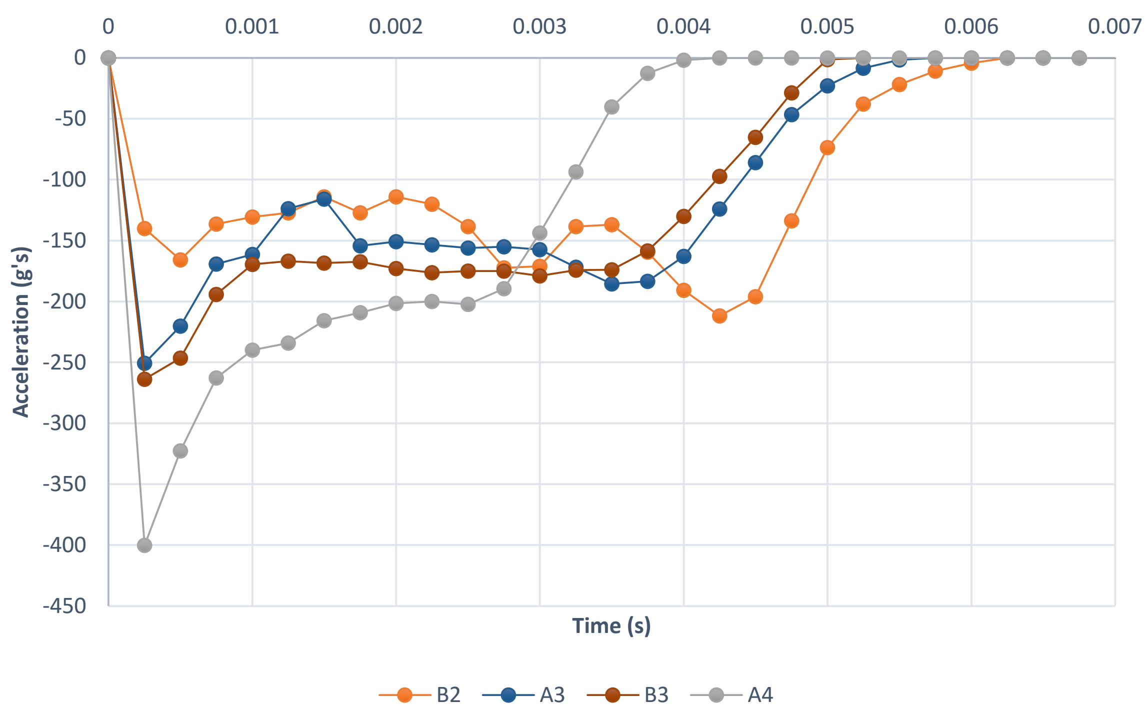

Figure 25: Comparison of three-layer and four-layer iterations of Concept 1.

Figure 25 shows that the three layer concepts are stiffer than the four layer concepts of the same weight. Intuitively, this makes sense as the wall thickness is 0.25 mm wider in the 3 layer concepts, and Figure 22 has shown that the wall thickness has a very large impact on the lattice energy absorption. Due to the minimum wall thickness restriction, it is best to have a lattice design that allows for thicker walls. Therefore, the final lattice design consists of 3 layers.

The CPSC standard dictates that the maximum deceleration cannot exceed 300 g's on a flat anvil [5]. The results show that iteration's A2 and A3 are best suited for meeting that standard. However, the wall thicknesses are too thin based on Precision ADM's recommendations. In order to increase the wall thickness, without exceeding a deceleration of 300 g's, the width of each lattice cell must be increased. The width is the distance between the vertical walls of the lattice structure. The width increase the bending moment in each horizontal lattice member and counteract the increased stiffness of the thicker walls. The width of each cell is varied in the next stage of the lattice design process.

4.2.2 Radial Lattice Analysis

The next step in the design process was to perform impact analysis on a radial FEA model. A radial FEA model was designed to represent the approximate curvature and size of the actual helmet. This was to ensure that the results of the impact FEA closely resemble what would occur within the helmet upon impact. The model was given a constant inner radius of 115 mm and a total width of 3 cm. The first iteration of the radial lattice was designed to be made of NYLON 12 since it was considered the best material for a bicycle helmet. The walls were given a thickness of 2.54 mm, as recommended by Precision ADM, and a spacing of 30 mm between the outer-most vertical walls. Figure 26 shows the general dimensions of the radial lattice model.

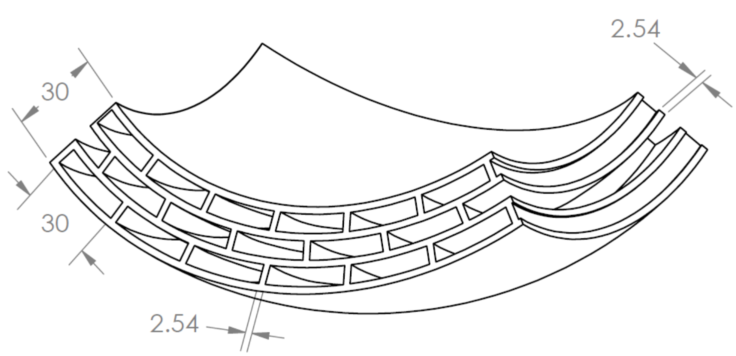

Figure 26: NYLON 12 radial FEA model dimensions in millimeters.

From the CPSC standard, helmet are dropped onto 3 different steel anvils: a flat anvil, a hemispherical anvil, and a curbstone anvil. For each test, the maximum deceleration cannot exceed 300 g's [5]. Therefore, impact analysis in ABAQUS/CAE must be performed for all three anvils to ensure that lattice design can pass the CPSC standard. Figure 27 shows the dimensions of the anvils used in the CPSC standard.

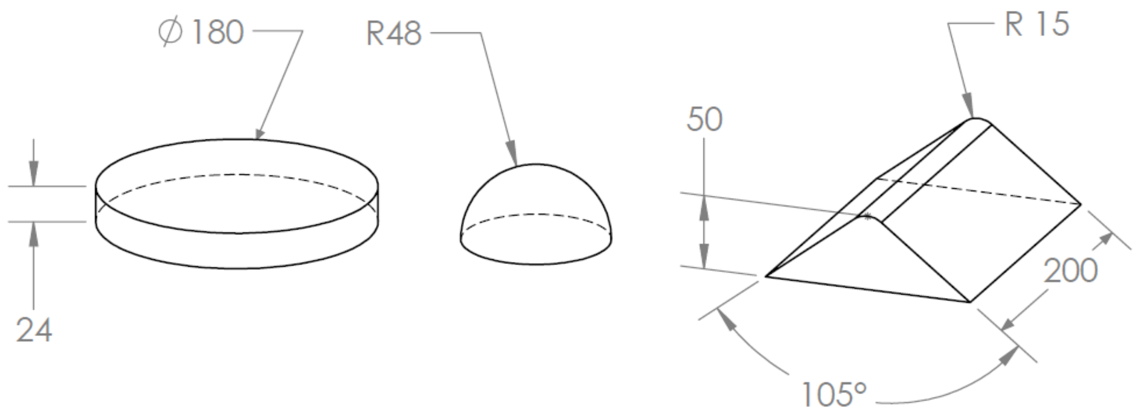

Figure 27: Flat (left), hemispherical (middle), and curbstone (right) anvil dimensions in millimeters.

The anvils were assigned material properties based on AISI 304 Stainless Steel [13]. The properties included a density of 8000 kg/m^3, a modulus of 200 GPa, and a Poisson's ratio of 0.29. The lattice model was assigned material properties for NYLON 12 in the ZX orientation as this orientation had the lowest values. This included a tensile modulus of 1138 MPa and a tensile yield stress of 28 MPa. Once again, tensile properties were used instead of compressive properties as using the compressive properties would result in a very elastically stiff material, which is not the case.

In the ABAQUS simulation, the bottom surface of each anvil was completely restrained, but the body of the anvil was given freedom to deform in every other direction. The radial lattice model was positioned directly above the center of the anvil to replicate the point of impact. The radial FEA model and the anvils were given hard-contact normal behavior and a tangential friction coefficient of 0.3 [12].

A rigid shell with a radius of 115 mm matching the inner surface of the radial FEA model was added to the simulation assembly to represent the headform. This headform shell was given a mass of 5 kg as specified in the CPSC Standard. A velocity of 6.2 m/s was applied to the headform for the flat anvil impact and a velocity of 4.8 m/s was applied for the hemispherical and curbstone impacts based on the CPSC Standards. These velocities correspond to impact energies of 96 J and 58 J, respectively [5]. The headform was also restrained to move only in the direction of the anvil.

The time period for each impact step was given a length of 0.01 seconds with a total of 40 increments. A 0.0023 meter global seed size was used to generate a tetrahedral solid mesh of the radial FEA model, similar to the cubic lattice analysis. The headform shell was meshed using quadrilateral shell elements with a seed size of 0.01 meters. The flat anvil and curbstone anvil were meshed using hexahedral solid elements with a seed size of 0.01 meters and 0.005 meters, respectively. The hemispherical anvil was meshed using tetrahedral solid elements with a seed size of 0.0035 meters. Figure 28 and Figure 29 show the fully meshed assemblies in ABAQUS/CAE.

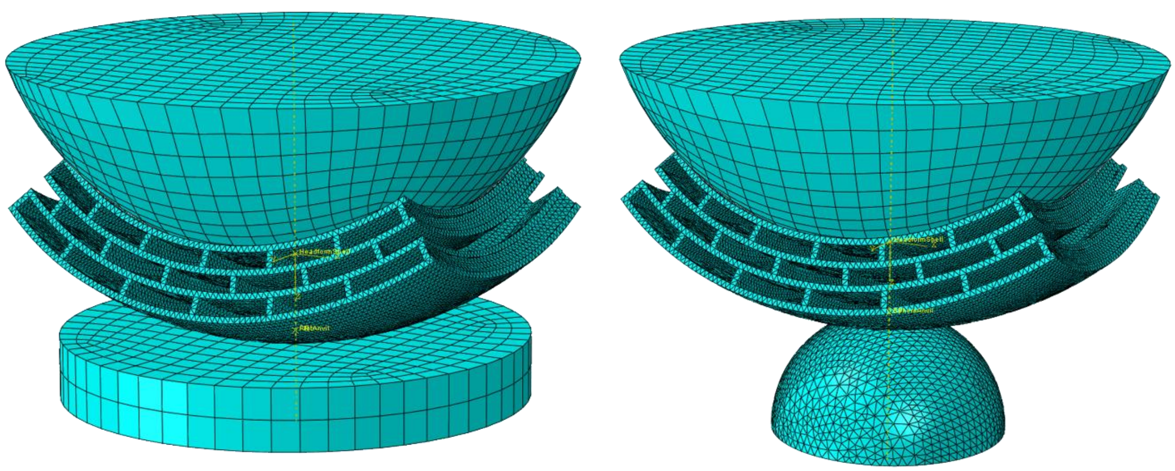

Figure 28: Radial FEA model assembly for flat and sphere anvils.

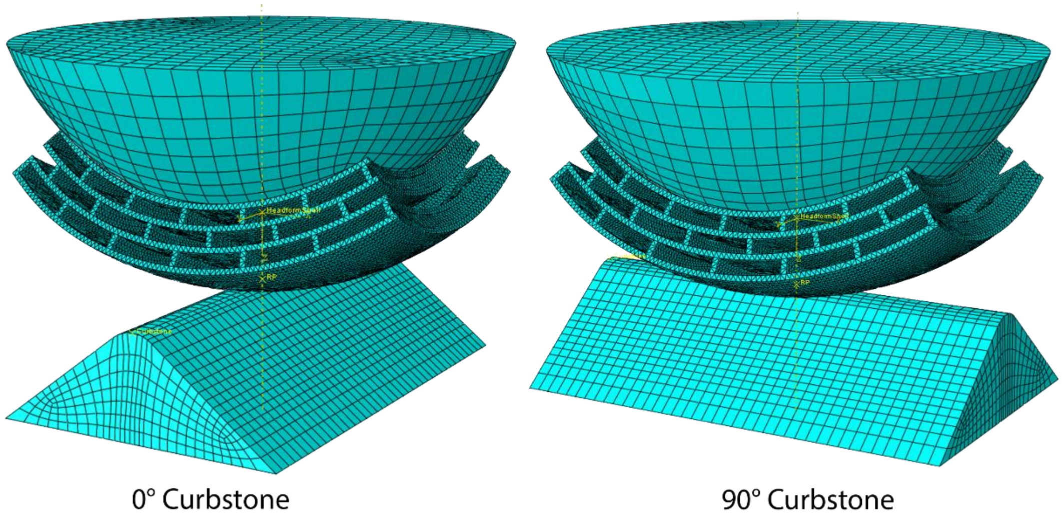

Figure 29: Radial FEA model assembly for 0° and 90° curbstone anvils.

The result of each impact test was performed for the first set of iterations of the NYLON 12 radial FEA model. The acceleration of the headform was plotted across the 0.01 time step and the results are shown in Figure 30. The overall time period was reduced to 0.008 seconds, as every impact had reached its conclusion at that time.

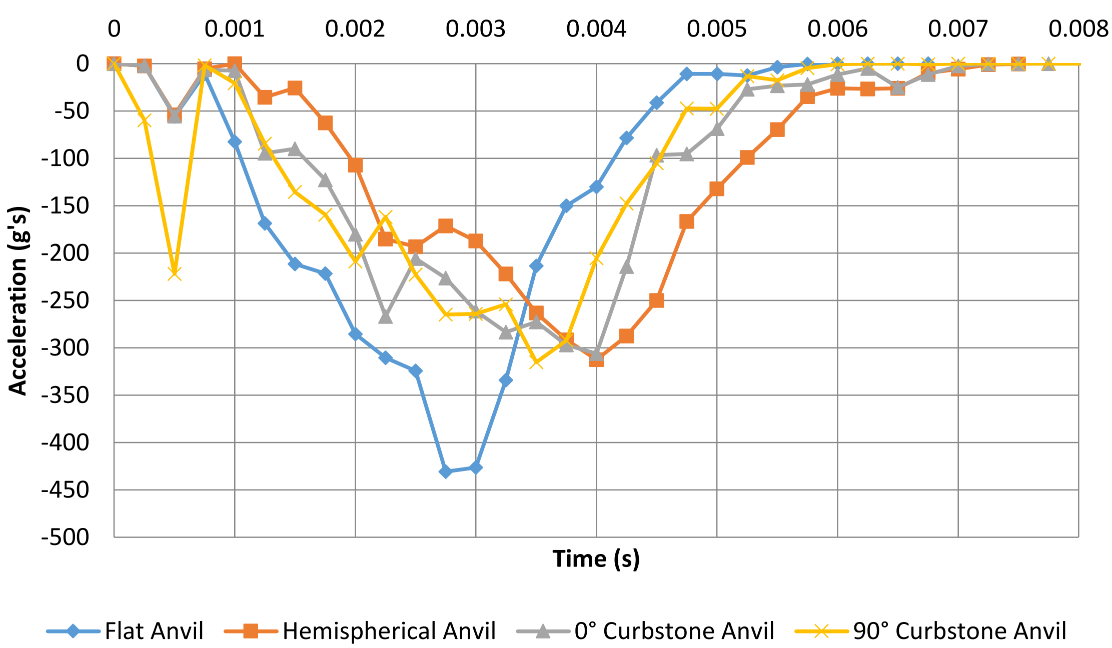

Figure 30: Comparison of anvil impacts for revision 1 radial FEA model.

Figure 30 shows that the flat anvil has the highest peak deceleration. Therefore, all further analysis was performed on the flat anvil since it can be assumed that the other anvil tests would pass the CPSC standard. Figure 30 also shows that the peak declaration for the flat anvil is well over the limit of 300 g's. To reduce the deceleration, the stiffness of the structure must be reduced by increasing the distance between the vertical walls. Two more versions of the NYLON 12 radial lattice were analyzed with 40 mm and 55 mm spacing. The wall thickness of 2.54 mm was held constant. The results for all three versions of the NYLON 12 radial lattice simulations are compared in Figure 31.

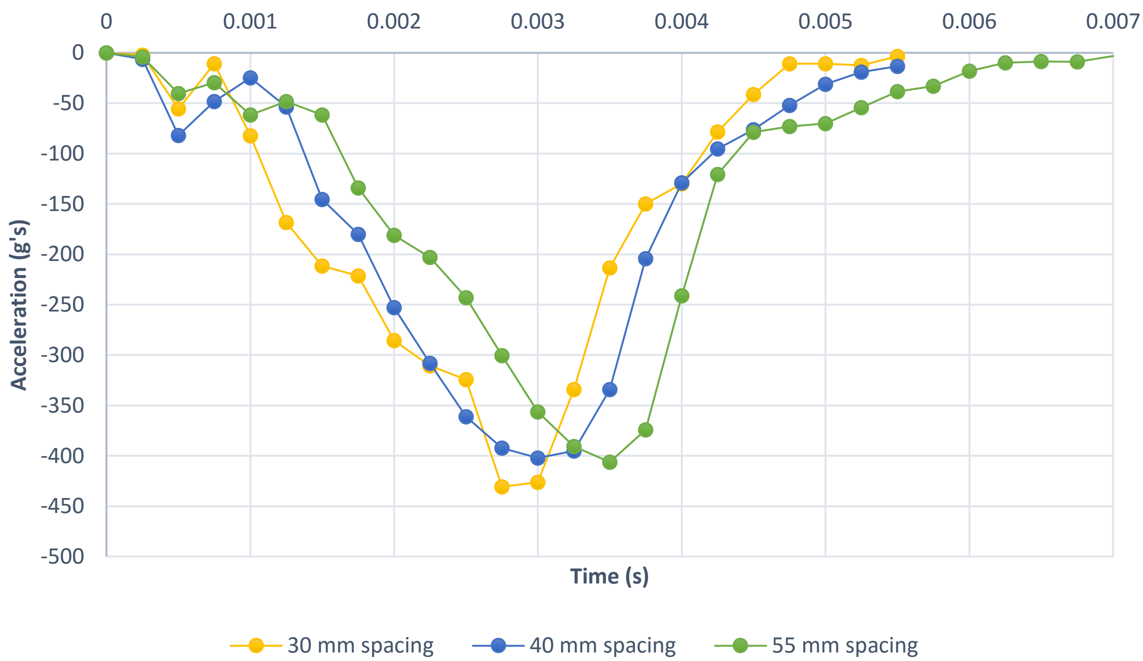

Figure 31: Comparison of NYLON 12 radial FEA models with 2.54 mm wall thickness.

Figure 31 shows that even with a much larger wall spacing, the results improved only marginally. The deceleration curves shifted slightly, but the peak deceleration is at least 100 g's over the 300 g limit for each version. Further increasing the wall spacing would make it difficult to implement the lattice into the helmet. Moreover, 30 mm wall spacing is too wide if the lattice was to be swept longitudinally across the helmet. Instead, the 30 mm spacing could be implemented if the lattice was swept laterally across the helmet.

To properly remove the support structure after printing, drain holes were required in the final design. These drain holes would have to be positioned along the sides of the helmet, but that positioning could cause disruptions to the airflow along the side of the helmet; and potentially increase the helmet's aerodynamic drag. Therefore, it would be ideal to sweep the lattice longitudinally and position the drain holes at the rear of the helmet where they would not affect the airflow. In order to properly implement the lattice into that helmet at this orientation, the wall spacing should ideally be less than 30 mm. This is to ensure that a consistent number of lattice cells can fit into each swept profile of the helmet. Consequently, a NYLON 12 helmet was deemed not feasible based on the team's current design.

Next, a radial FEA model designed to be printed in PC was created with a minimum wall thickness of 1.6 mm as suggested by Precision ADM. The first iteration used an outermost wall spacing of 23 mm. The maximum deceleration of the headform was 178 g's over the maximum allowable deceleration, hence two more iterations with 30 mm and 40 mm spacing were performed. The results for all three iterations are shown in Figure 32.

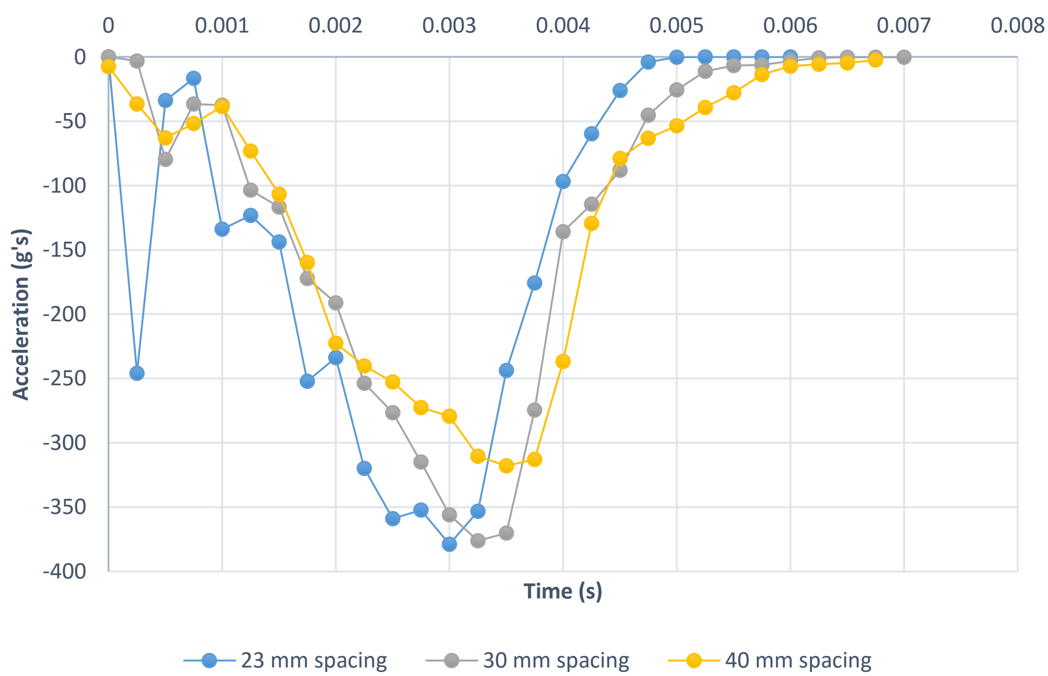

Figure 32: Comparison of PC radial FEA models with 1.6 mm wall thickness.

None of the iterations with 1.6 mm thick walls were successful without increasing the wall spacing beyond acceptable limits. Therefore, the wall thickness was reduced to 1.5 mm. Although this thickness is below the recommendation given by Precision ADM however, the difference is only 0.1 mm, which was deemed insignificant for the overall strength of the structure. Three iterations with 20 mm, 25 mm, and 28 mm wall spacing were analyzed and the results are shown in Figure 33.

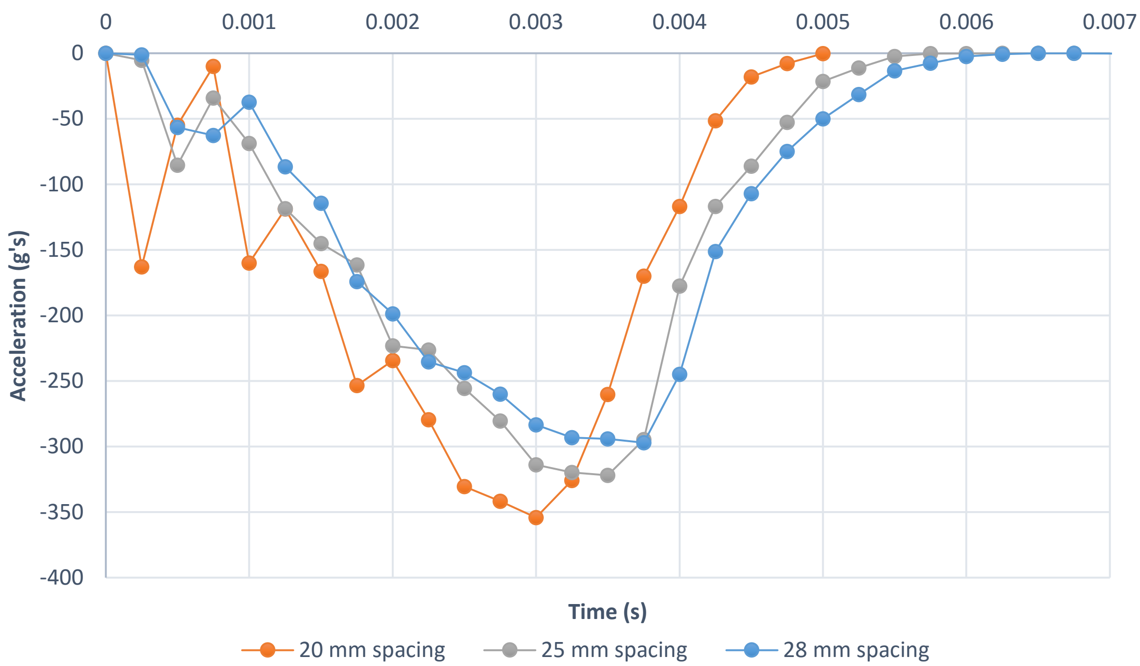

Figure 33: Comparison of PC radial FEA models with 1.5 mm wall thickness.

Figure 33 shows that the radial FEA model with 28 mm wall spacing is below the maximum specified deceleration of 300 g's. Since this design passed the requirements for the flat anvil impact in the CPSC Standard, it was selected as the final design.

4.2.3 Analysis of Final Lattice Design

From the iterative analysis of the radial FEA lattice models, a final design made of PC was selected to implement into the interior of the helmet. The design consists of 1.5 mm thick walls with an outermost wall spacing of 28 mm. The design is shown in Figure 34.

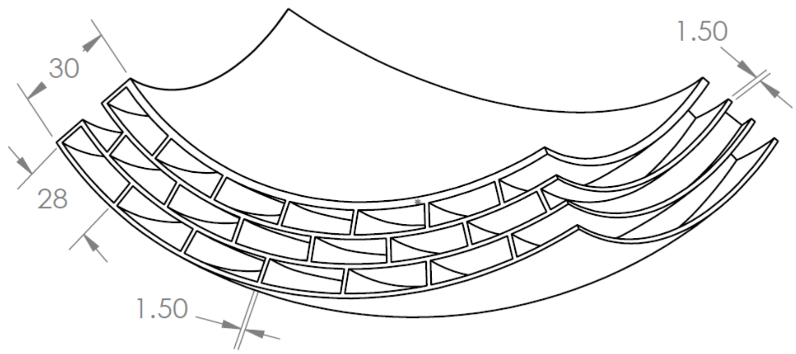

Figure 34: Final radial lattice design dimensions in millimeters.

In order to verify that the final lattice design is capable of passing the requirements of the CPSC Standard, impact analysis was performed on each anvil type. The resulting decelerations of the headform are plotted in Figure 35.

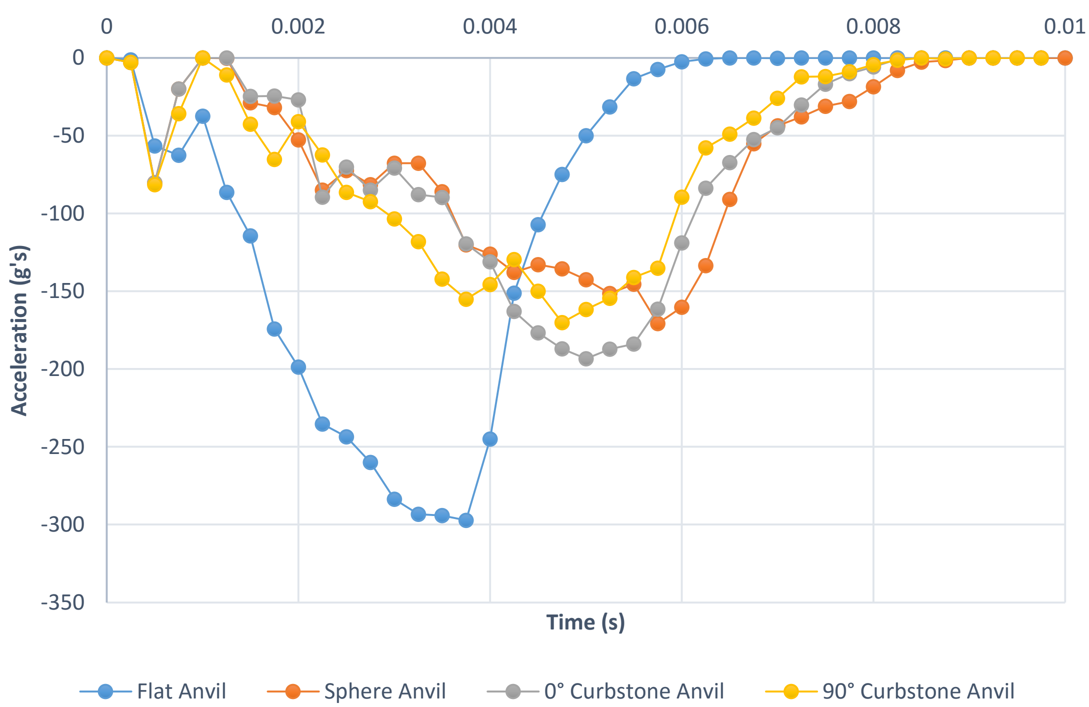

Figure 35: Impact decelerations of final lattice design for each anvil type.

Figure 35 shows that every anvil impact is below the maximum of 300 g's. Thus, the lattice design passes the main impact requirements of the CPSC Standard. The results shown in Figure 35 were calculated using a 0.0023 meter global seed size.

In order to verify the accuracy of the FEA results, the impact studies were performed with increasingly fine meshes to confirm that the resulting deceleration plots converge to the same result. The results of the convergence studies for the flat anvil and hemispherical anvil studies are shown in Figure 36 and Figure 37, respectively. Figure 36 and Figure 37 clearly show that the deceleration curves are converging to the same result as the global seed size is decreased.

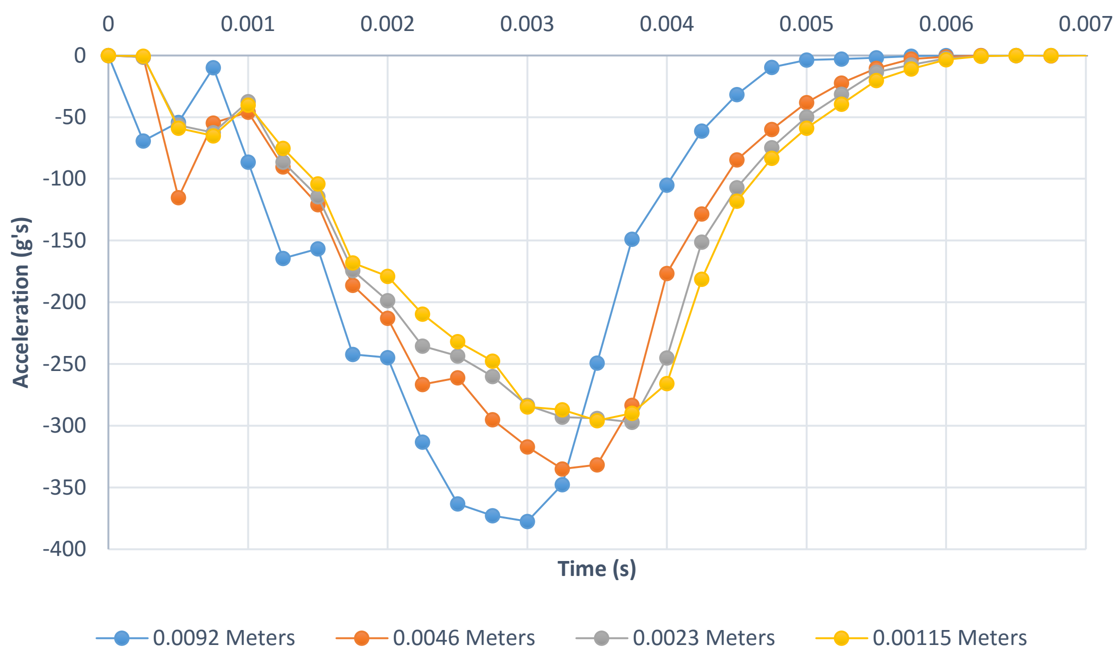

Figure 36: Convergence of flat anvil study results using decreasing mesh seed sizes.

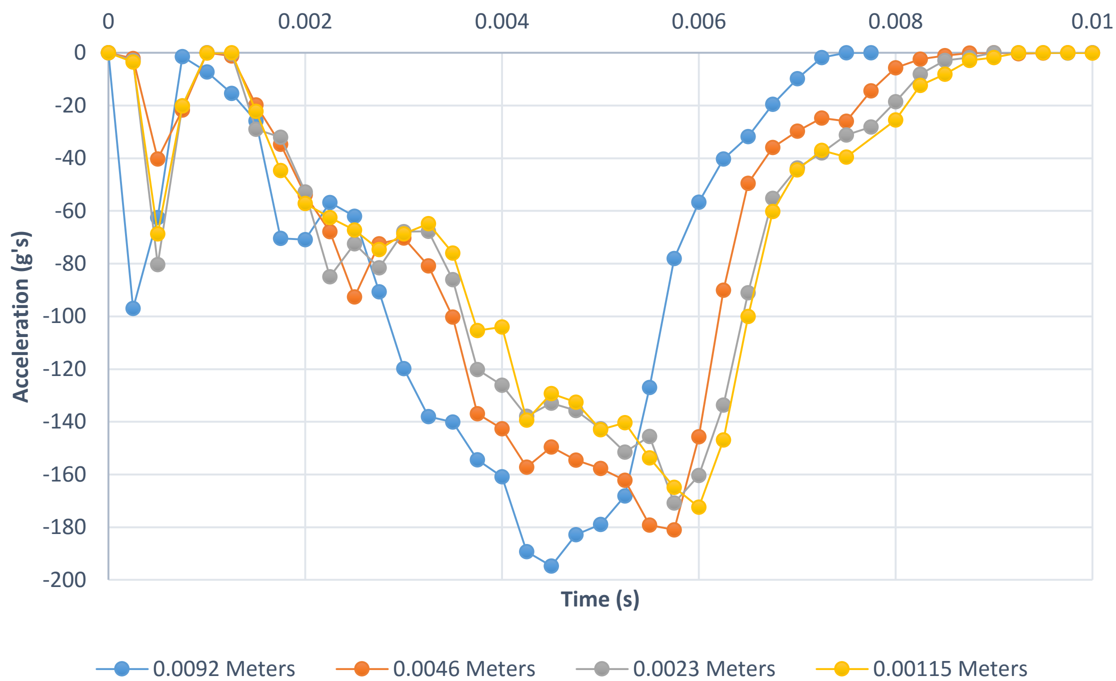

Figure 37: Convergence of hemispherical anvil study results using decreasing mesh seed sizes.

The mesh with a global seed size of 0.0023 meters can be considered relatively identical to the results of the 0.00115 meter seed size mesh. Therefore, the accuracy of the results shown in Figure 35, which were found with a 0.0023 meter seed size, can be considered accurate. It is also worth noting that as the mesh became finer, the maximum deceleration decreased. With that, it is unlikely the maximum deceleration would increase when further decreasing the global seed size.

Another aspect of the impact FEA to consider is the amount of solved increments within the 0.01 time step. Although 40 increments were used in the impact FEA, there is the possibility that decelerations spikes occurred between these increments. An analysis was performed with 160 increments and compared against the results using 40 increments. Figure 38 shows the results of this comparison.

UNIVERSITY OF MANITOBA

PRECISION ADM
ADVANCED DIGITAL MANUFACTURING

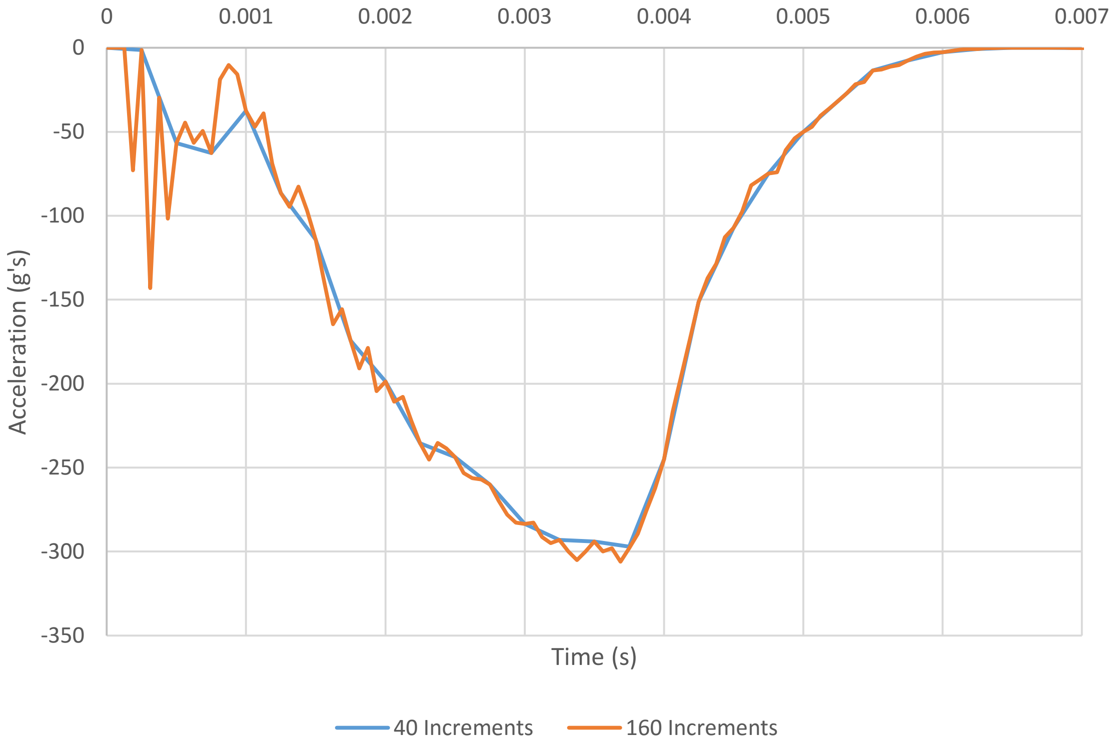

Figure 38: Comparison of 40 and 160 increments for flat anvil impact FEA.

Figure 38 shows that the results are virtually the same when using 40 or 160 increments because the deceleration curves follow the same general path. It should be noted that the 160 increment deceleration curve is slightly over 300 g's for a few small time increments. Despite this, the lattice was not considered a failure as the occurrences are only a maximum of 5 g's over the limit, which is not large enough to be conclusive. The peak deceleration also occurs during a time period of 6.24×10^{-5} seconds. It is possible that the accelerometer used in physical testing would not be able to capture peaks that occur at such a high frequency.

The only large discrepancy between the 40 and 160 increment deceleration curves occurs between 0 and 0.001 seconds. The likely cause of the large peaks is due to the fact that the rigid headform is making contact with the radial FEA model creating oscillation before leveling out. This behavior can be ignored in the analysis as the oscillations are likely being caused by the free ends of the radial FEA model, which are not connected to any rigid body in the analysis.

The final consideration for the design of the lattice is the distribution of stress throughout the structure. The stress plots provide insight into when and where the lattice structure will fail throughout the impact. Also, since damage properties were not used in the FEA, any elements in the lattice that reach the ultimate stress will not behave the same way in reality. The lattice has different material properties in each direction as determined by the print orientation so the lowest ultimate stress value was used as a worst case scenario. The lowest ultimate stress value for PC is 42 MPa in the ZX orientation, which was given the red colour in the stress plot legend. Figure 39 shows the stress plot of the entire lattice design on the flat anvil during the maximum deceleration impact. The plot has a deformation scale value of 1.

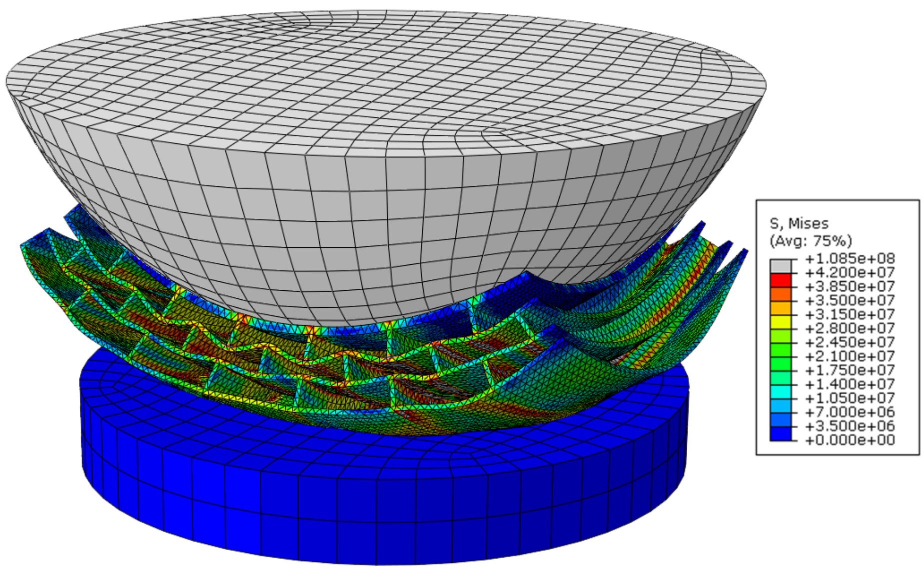

Figure 39: Stress plot of final lattice design at maximum deceleration increment.

Figure 39 shows how the deformation of the lattice dissipates towards the outer edge of the radial FEA model. In the actual helmet, the swept lattice will terminate against walls and there will be no free edges. However, the radial FEA model is large enough to give valuable insight into the lattice structure's behaviour upon impact.

Figure 40, Figure 41, Figure 42, and Figure 43 show stress plots on each type of anvil throughout the impact. The stress plots have a section cut on the center plane to show the lattice at the center of impact and the deformation scale has a value of 1. Once again, the lowest ultimate stress value was used as the maximum on the legend. The impact increments used in the figures are between the beginning on the impact and the maximum deceleration increment. The increments were chosen to best display the continued deformation of the lattice throughout the impact. The headform was also hidden from view so the lattice could be seen clearly.

Figure 40 through Figure 43 show that failure most commonly occurs along the horizontal members of the lattice where they connect to the vertical members. This occurs as designed in order to absorb impact energy through the bending and eventual fracture of the lattice members. Also, as the vertical members begin to buckle, they reach the ultimate stress along the wall.

The sphere and curbstone impacts show that the outer layer of the lattice begins to fail at the point of contact with the anvil and propagates outward as the impact continues. This is due to localized force being applied to the lattice by the anvil. The stress in the flat anvil is more distributed due to the large surface area. Also, the reason that the curbstone and hemispherical anvils have a smaller peak deceleration can be attributed to the fact that the lattice slowly wraps around the anvil over a longer impact duration. The impact on the flat anvil occurs at a much faster rate causing a higher deceleration curve.

The stress along the top surface shows a series of circular stress concentrations. These concentrations are caused by the course mesh of the headform anvil and can be neglected.

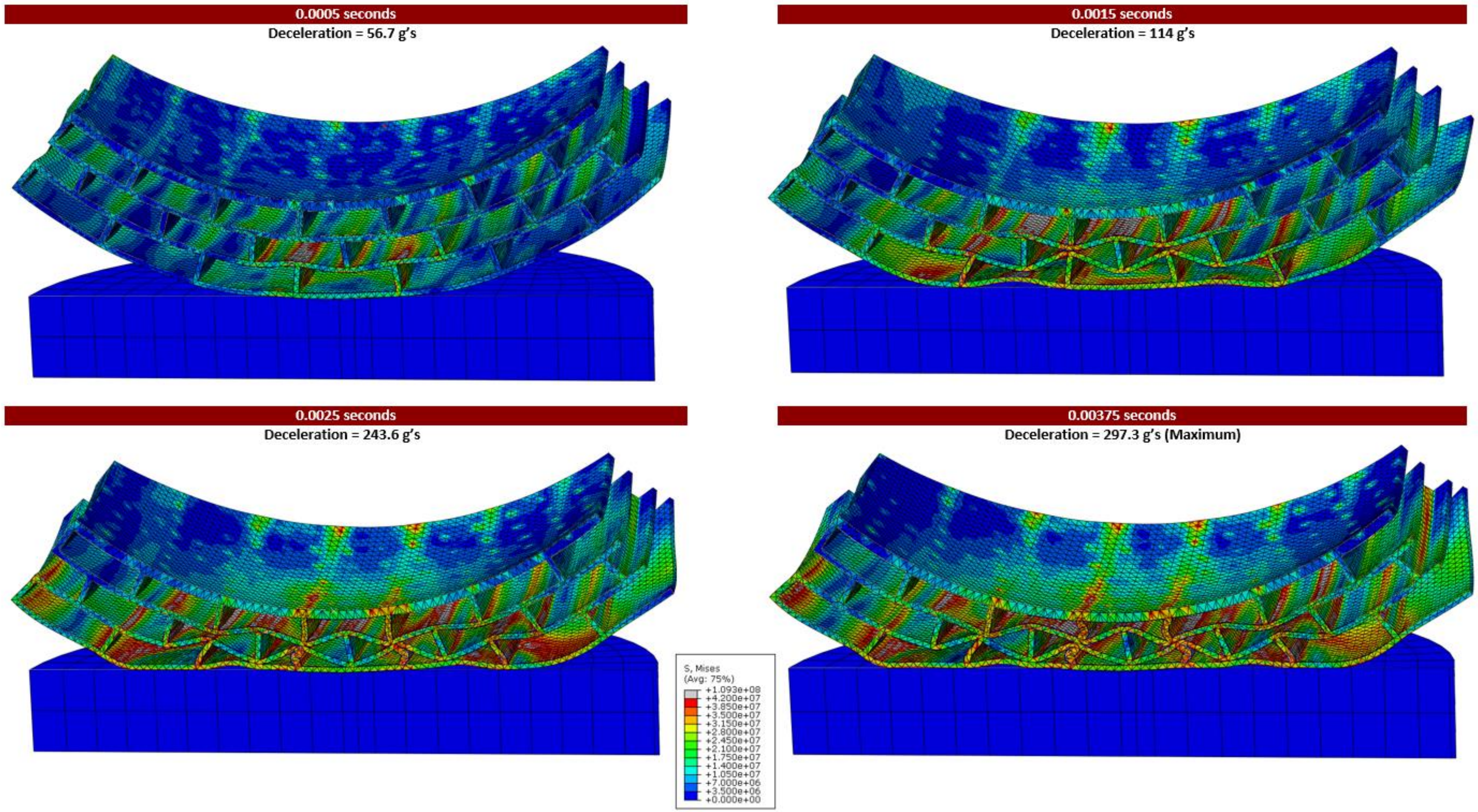

Figure 40: Impact analysis of final lattice model on the flat anvil.

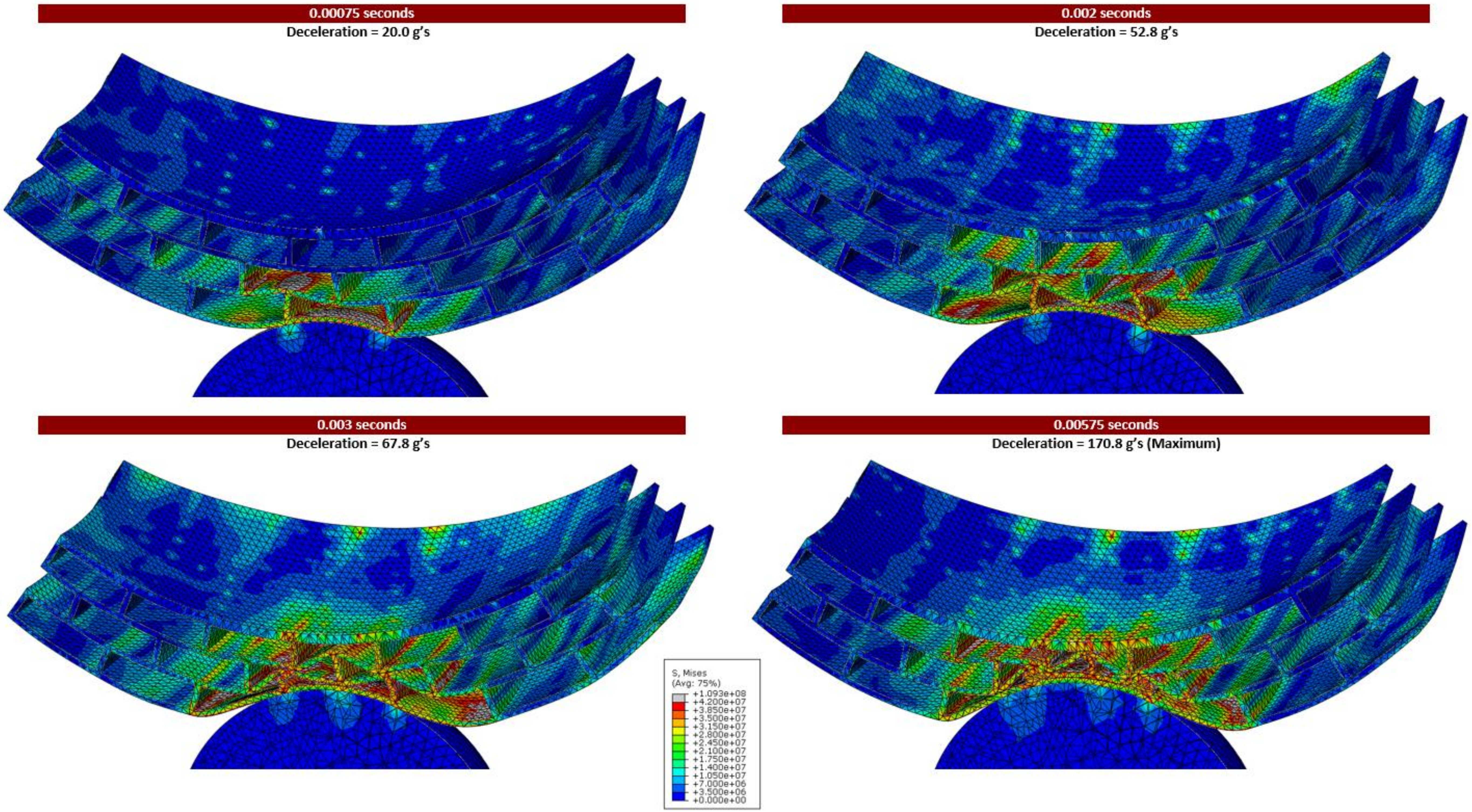

Figure 41: Impact analysis of final lattice model on the hemispherical anvil.

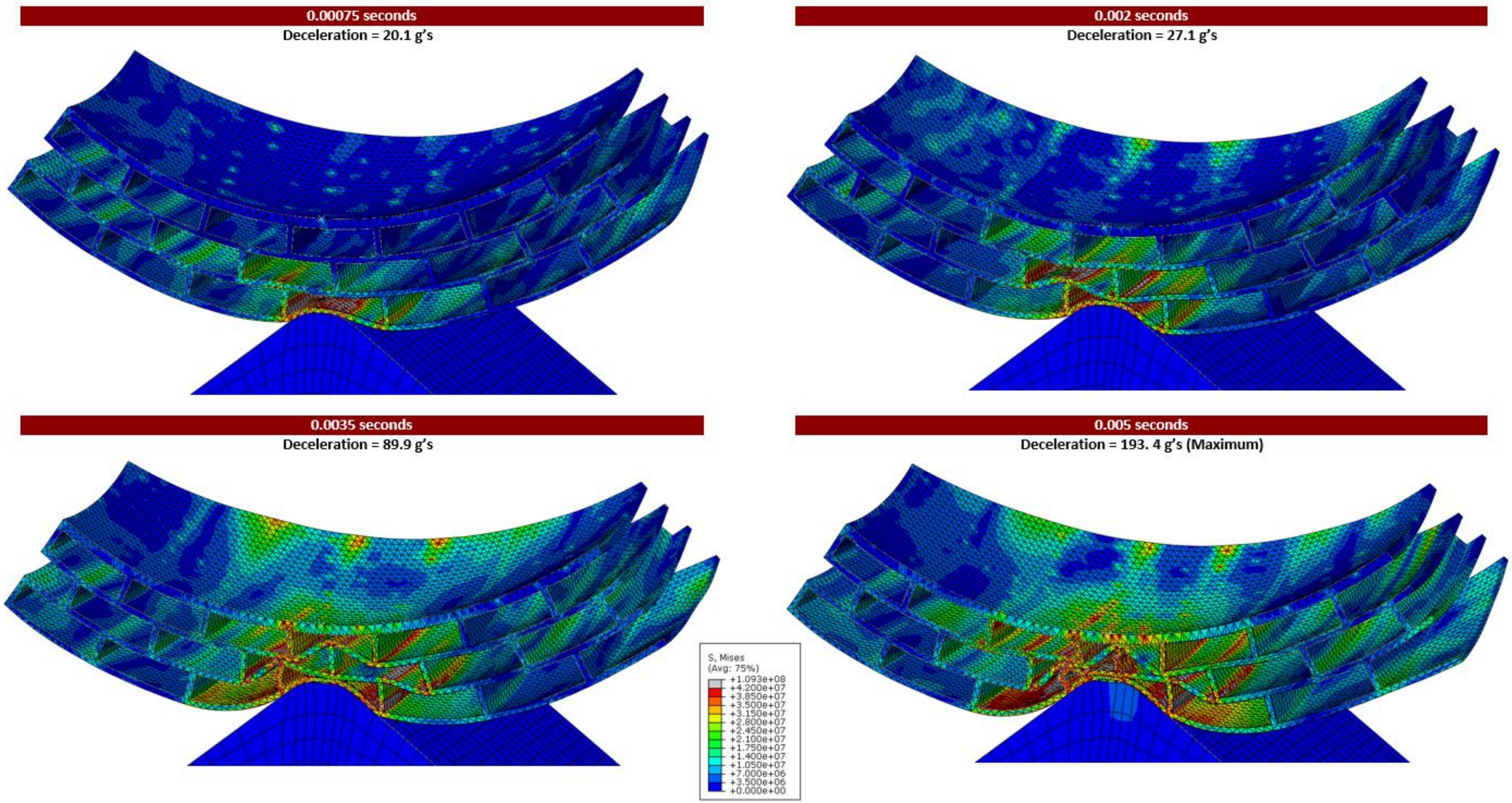

Figure 42: Impact analysis of final lattice model on the 0° curbstone anvil.

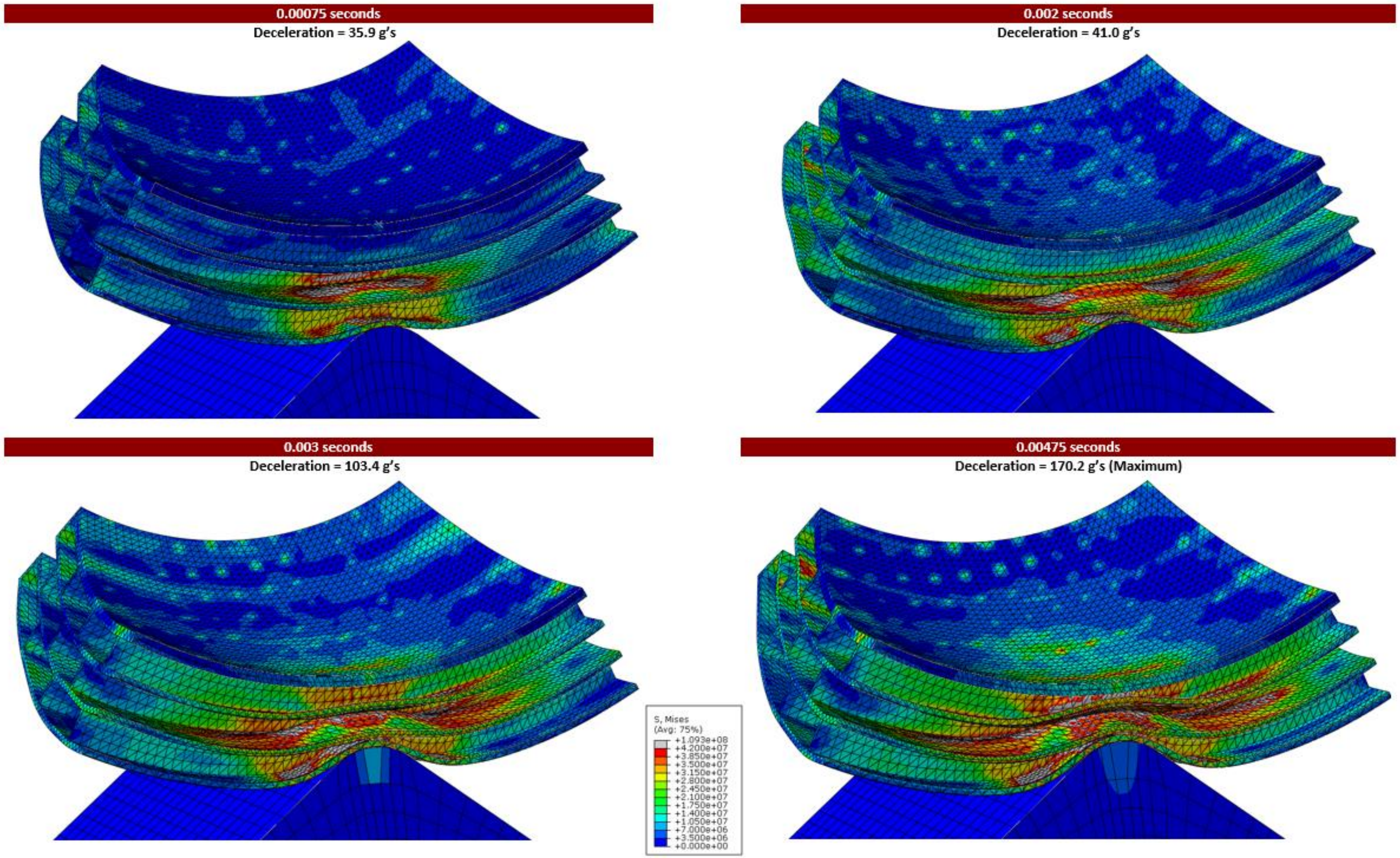

Figure 43: Impact analysis of final lattice model on the 90° curbstone anvil.

Figure 44 shows the propagation of stress on the outer layer of the lattice model during the flat anvil impact. The anvil has been hidden to show the distribution of stress. At the 0.00075 second increment, the section of the lattice making contact with the anvil has reached failure. As the impact continues, the stress propagates causing failure throughout the whole bottom layer of the lattice.

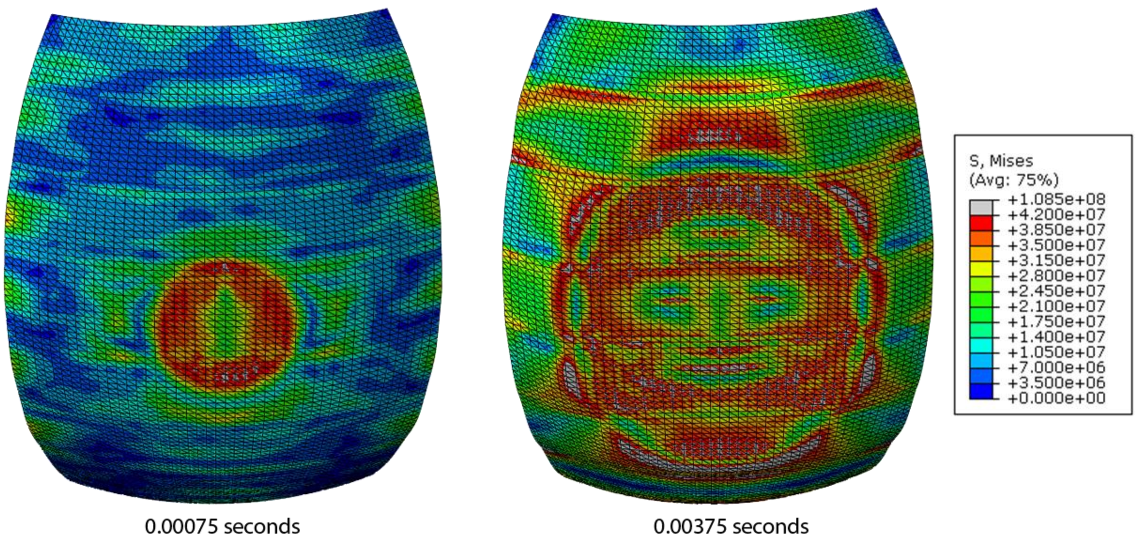

Figure 44: Flat anvil stress propagation of the outer lattice layer.

Figure 40 through Figure 44 show that the lattice structure will fail in multiple locations throughout the impact. However, these stress plots use the smallest ultimate stress value of 42 MPa as the maximum value in the legend. The ultimate stress value in the XZ orientation is 57 MPa and using this value has a significant impact on the results. Figure 45 shows a section view of the flat anvil impact at 0.00125 seconds where the maximum stress value in the legend is 42 MPa. Figure 46 is the same stress plot with a maximum stress value of 57 MPa in the legend.

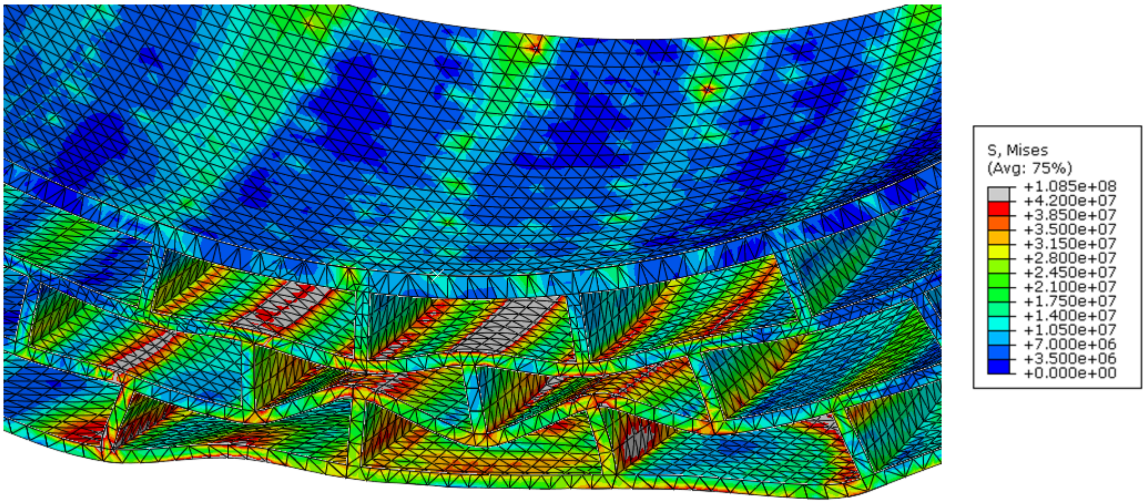

Figure 45: Flat anvil impact at 0.00125 seconds with an ultimate stress of 42 MPa.

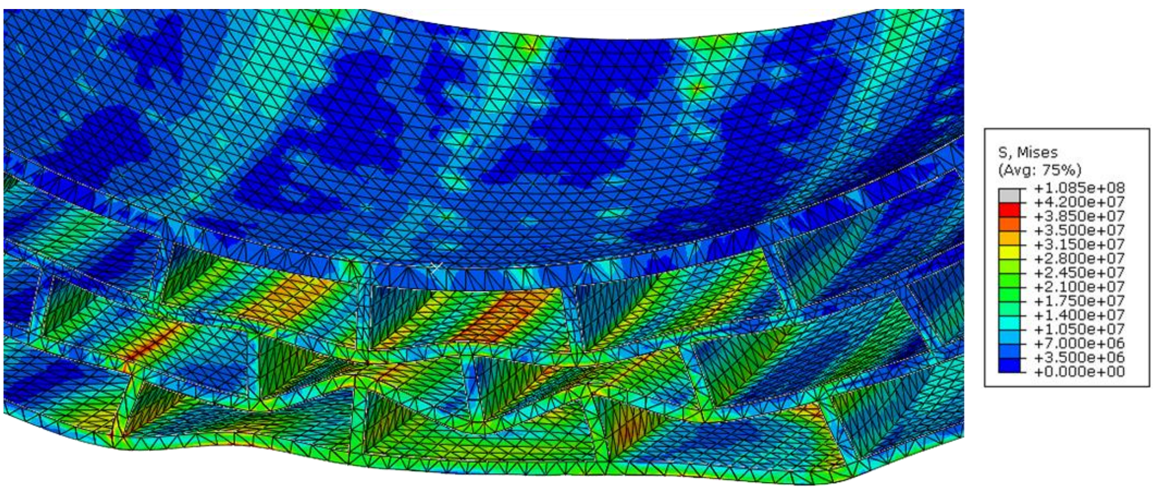

Figure 46: Flat anvil impact at 0.00125 seconds with an ultimate stress of 57 MPa.

Figure 46 shows that when using the higher ultimate stress value, the amount of elements reaching ultimate stress is significantly reduced. Failure only occurs along a couple rows of elements in the horizontal walls. Figure 47 shows that the outer surface of the lattice has minimal failure at 57 MPa compared to 42 MPa.

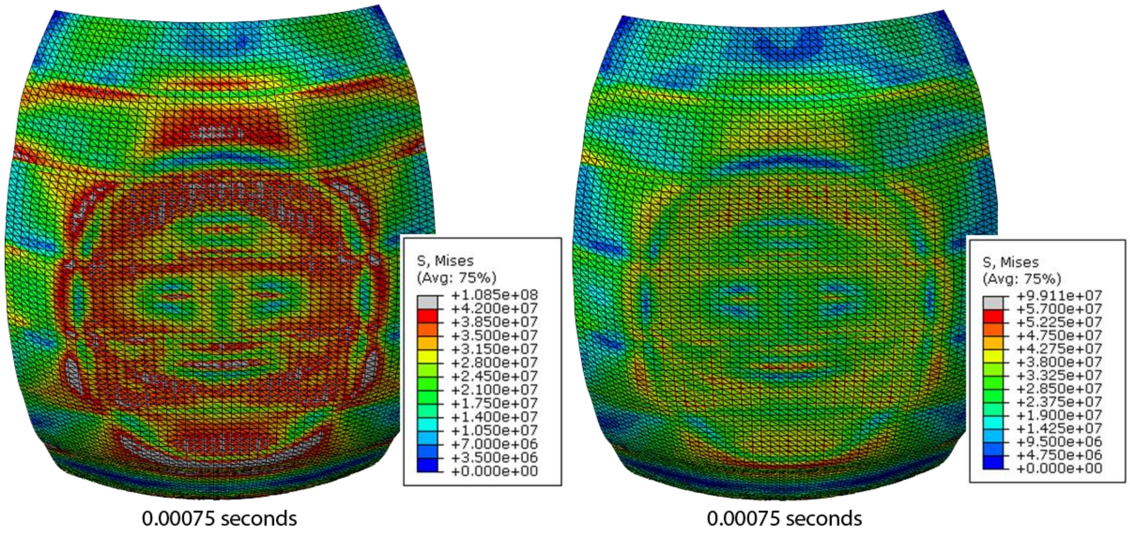

Figure 47: Comparison of flat anvil stress in the outer lattice layer at different stress plot scales.

Since the printed helmet will consist of a combination of orientations, the ultimate stress will vary between 42 MPa and 57 MPa throughout the structure. The compressive ultimate stress values are higher than 57 MPa and can be ignored since every member is in bending and will experience both tensile and compressive stress. Therefore, it is safe to assume that the actual damage to the helmet's lattice during an impact will be somewhere between the results seen in Figure 45, Figure 46, and Figure 47. Physical testing must be performed to confirm the results of the FEA and evaluate the amount of fracture in the lattice structure. However, the impact FEA has given valuable insight into how the lattice will be behave upon impact.

4.3 Helmet Exterior Design

One of the main factors influencing the design of the helmet was the style of the lattice. The helmet geometry must complement the lattice style to maximize the lattice functionality. Based on initial FEA results and simplicity in the design, a 2-dimensional swept style lattice will be used. To complement this lattice design, the helmet should also follow a similar swept style to ensure that the lattice is oriented correctly with respect to the impact direction.

A study performed by the Civil Aeromedical Institute in Oklahoma [14]. This study was done to determine a range of head dimensions that can be used for basic conceptual design of protective equipment. Head width and head length were the two main dimensions that were considered when the helmet model was developed. As defined by the Civil Aeromedical Institute, the 90th percentile male head length (distance from the forehead to the rear most point of the head) is 8.23 in, and the head width (maximum lateral distance) is 6.26 in. To accommodate more head sizes, the prototype was designed to fit the 90th percentile male head. Figure 48 and Figure 49 shows the base dimensions that the helmet was designed around with respect to the human head.

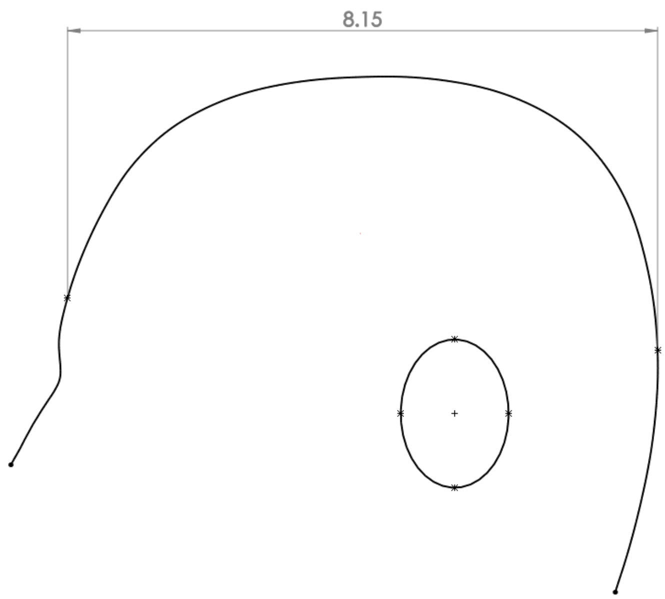

Figure 48: Side profile head length dimension in inches.

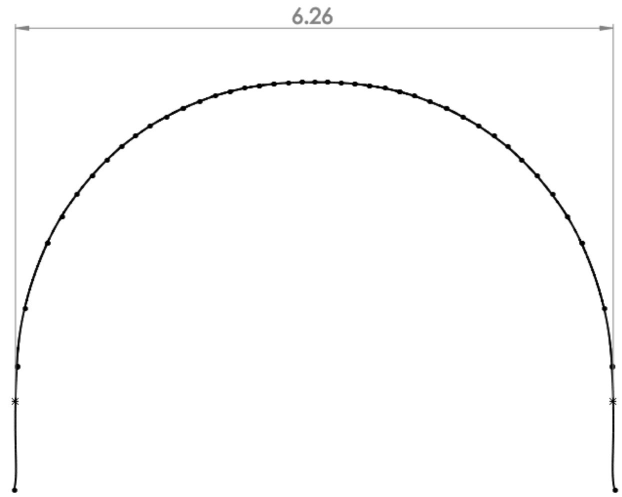

Figure 49: Front profile head width dimension in inches.

These sketches were used as a basis for defining the interior skin of the helmet. Using these sketches as reference, a general head profile was made. This head profile was used as the foundation for the helmet design. Additionally, the ventilation cuts were incorporated into the surface to define the path of the vents along the helmet, the remaining surfaces will be used as the base for the structural bodies of the helmet.

Figure 50: Interior helmet skin.

Based on the helmet concept scoring results, the helmet geometry will be defined by 3 distinct bodies with ventilation channels and structural supports between each body. By splitting the helmet structure into 3 bodies, the helmet model can be easily modified to adjust the amount of ventilation; additionally the lattice can be adjusted within each body of the helmet to better suit the curvature. The general structure of the helmet geometry is shown in Figure 51.

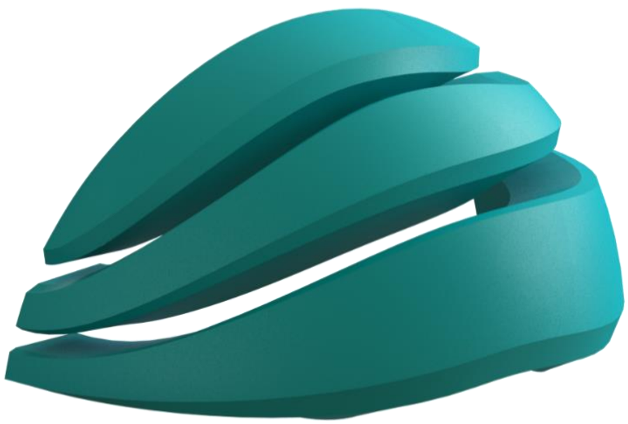

Figure 51: Multiple body helmet design.

In Figure 51, the concept features swept bodies running lengthwise along the helmet. To ensure uniform structural properties, each body is held to a minimum of a 3 cm thickness. The next step in the model is to incorporate supports between the bodies to unify the helmet. The supports can also be used as a method for controlling ventilation. Adding in more supports, or increasing the size of the supports, will decrease the amount of airflow, but also improve structural integrity between the bodies. Support design will be further optimized through the CFD results.

This concept features 3 main supports between each body. Furthermore, the supports have an elliptical cross-section to reduce their impact on the aerodynamic drag. The support members are intentionally positioned away from the interior surface of the helmet to improve airflow around the head. The initial design for the supports between each body can be seen in Figure 52.

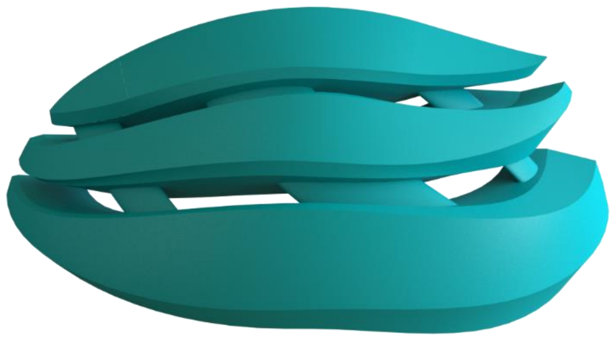

Figure 52: Structural support member concept.

In addition to the added structural supports, the tail of the helmet was flared to improve the aesthetic appeal. This implementation of the flare can be evaluated using CFD and further refinements can be made to improve the performance of the helmet. The first iteration of the exterior helmet design, *H1*, can be seen in Figure 53 and Figure 54.

Figure 53: Exterior of H1 front view.

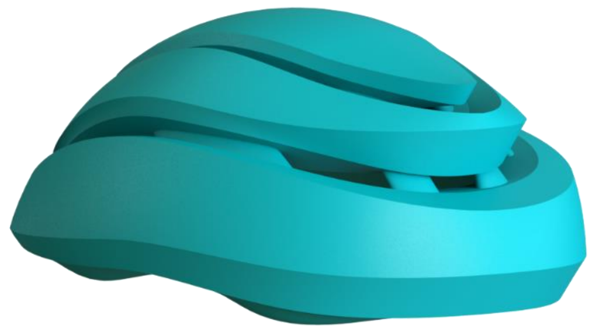

Figure 54: Exterior of H1 rear view.

To ensure that a sufficient field of view was provided for the rider a side view of the helmet with a plane at eye level was made, Figure 55 illustrates this.

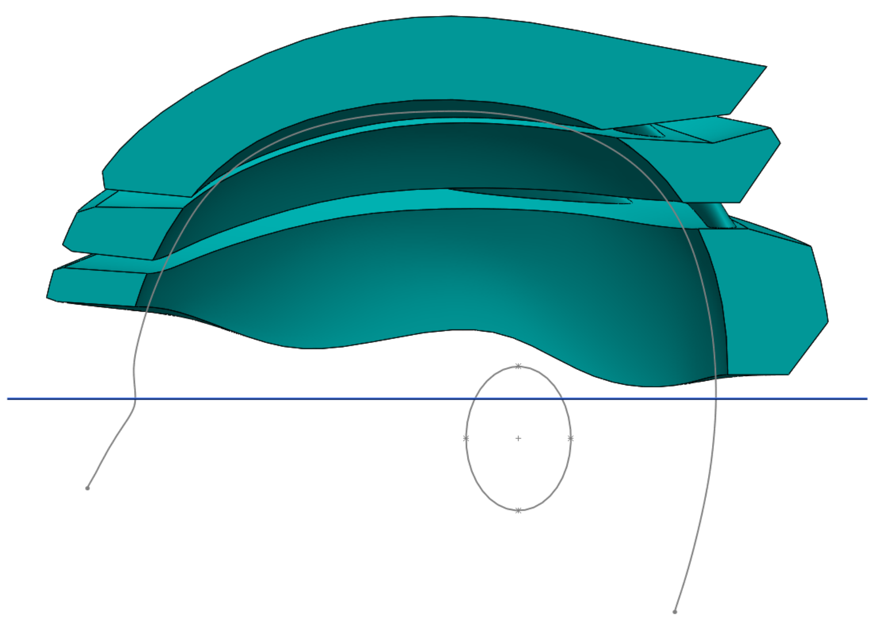

Figure 55: Side view of helmet for field of view.

Since the helmet does not block any portion of the user's eyes at any point in the side view, it can be concluded that the helmet allows for an adequate field of view. The helmet does not intrude the peripheral vision of the rider at any point and therefore provides a field of view greater than 180 degrees.

Analysis through CFD was used to refine the exterior shape, reduce the drag force, and improve ventilation. An optimized lattice geometry will be implemented into the model of the helmet.

4.4 Lattice Implementation in Helmet

Due to the spherical shape of the helmet and the 2-dimensional lattice design, the lattice had to be swept along the surface of the helmet. Two methods for lattice implementation were evaluated. The first method being a longitudinal sweep from the front of the helmet to the back of the helmet. The second potential method being a lateral sweep from one side of the helmet to the other. Based on the first exterior helmet model, the most influential factor in the lattice orientation will be the method used to implement drainage holes. Subsequently, the structural supports and the aerodynamics of the helmet will be affected by the position of the drain holes.

As a result of the internal lattice, there is potential that support structure can be printed inside of the helmet. For this reason all lattice cells must be exposed, for example drain holes should be incorporated into the design to allow the solvent to wash away the support structure. The position of these drain holes could have a large influence on the structural integrity, aerodynamic properties, and design of the helmet.

By sweeping the lattice laterally across the helmet, this would force the drain holes to be exposed on the side of the bodies, this would hinder the air flow through the vents as well as it could compromise the structural support mounting [3]. For these reasons a longitudinal sweep from front to back was more favorable. This method allowed the drain holes to be located at the rear of the helmet as well as the structural supports would be unaffected. Figure 56 shows a cross-section view of the lattice within the helmet.

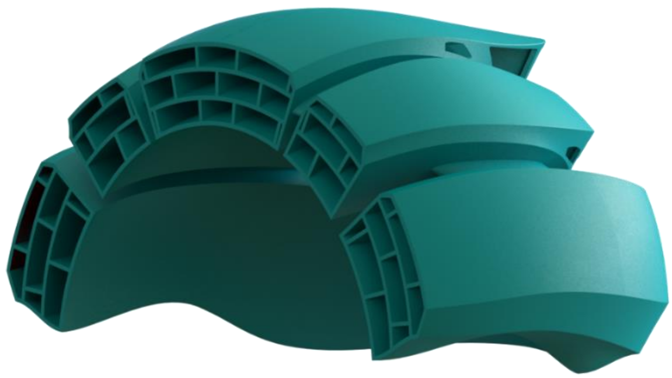

Figure 56: Cross section view of helmet.

The variability in curvature and changing cross section between each body of the helmet added complexity when implementing the lattice. The method used to sweep the lattice changed depending on which body of the helmet was being modeled. In Figure 57, the cross sections of all three helmet members are displayed.

(A) (B) (C)

Figure 57: Cross sections of the helmet body (A) Upper (B) Middle (C) Lower sections.

On the left of Figure 57 the upper body follows an arch over the top of the head and therefore allows for a simple sweep that follows the same path. A similar approach was used for the middle body of the helmet seen in the center of Figure 57. The lower body of the helmet wraps around the side of the head, and therefore the lattice follows the same path. This ultimately led to some inconsistencies in lattice structure near the back of the helmet. Since the helmet must have drain holes for all lattice cells there is a slight amount of separation between the left and right halves of lattices in the lower body at the back of the helmet. This can be seen below in Figure 58.

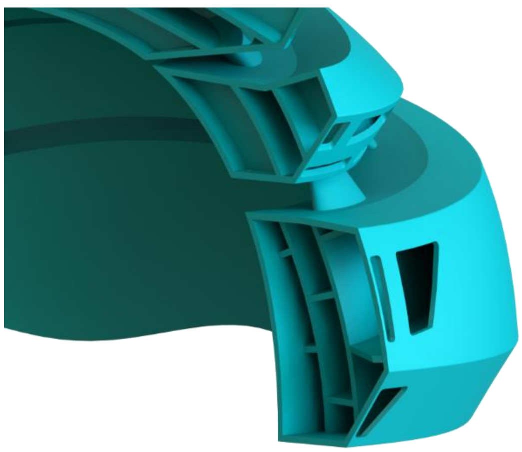

Figure 58: Lower body separation of lattice.

The separation in the lattice could compromise the structural integrity at the back of the helmet. To ensure that the helmet still remains structurally sound, physical testing must be done to verify impact absorption properties at this location. The helmet as a whole is illustrated in Figure 59.

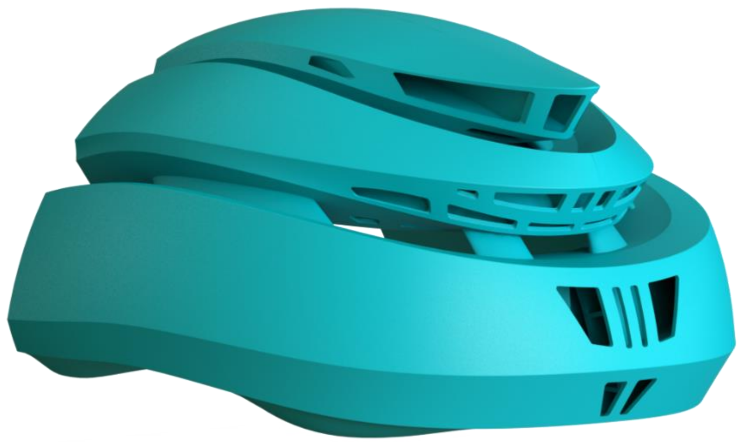

Figure 59: Drain hole locations on rear of helmet.

Ultimately, due to the longitudinal swept lattice, the drain holes were incorporated at the back of the helmet. This can be seen above in Figure 59. The drain holes expose cells within the lattice allowing for proper drainage to remove support structure after printing.

4.5 Detailed Design Summary

The detailed design portion of the project encompassed material selection, the development of the lattice design, exterior helmet design, and the lattice implementation. The first step in the design phase was to select suitable materials for the helmet. Stratasys offers 10 different materials to choose from. The ideal material for an impact absorbing material would have a lower modulus, high elongation, and a high ultimate stress. This combination of material properties makes the material ductile, yet less likely to fracture under sudden impact. NYLON 12 exhibited the best set of properties, but due to printing thickness constraints, was not used in the final lattice design. Alternatively, PC has the next best combination of properties. PC has a higher modulus and less elongation at break, but also has a higher ultimate stress with respect to NYLON 12. PC also allows for a greater range of printable wall thicknesses. For this reason PC will be used for the final lattice design.

After many iterations of impact simulations were completed, the offset rectangular cell style lattice ultimately outperformed the honeycomb lattice in the cubic test piece analysis.

Therefore, the honeycomb lattice was eliminated from the potential design concepts. In an effort to replicate the geometry of the helmet, radial models were produced to simulate a more accurate impact scenario. After refining the model, the final lattice geometry produced a maximum head deceleration of 297 g's in a 6.2 m/s impact on a flat anvil. The maximum head declaration in the CPSC standard is 300 g's. Every other anvil impact analysis met the standard as well. To verify the simulation results, physical testing must be done to ensure the helmet can actually meet the CPSC standard.

Once the lattice was finalized, the exterior helmet design was developed. Following along with the established concept from section 3.3, the helmet was designed to complement the lattice style. The lattice was modeled by sweeping a 2-dimensional profile through the length of the helmet. With that in mind, the helmet was modeled in a similar fashion. The geometry was defined by three distinct bodies, each of which are swept along the length of the helmet. Additionally, aerodynamically profiled supports were added between the bodies to give the helmet structure and improve ventilation through the helmet. Finally, drain holes were added to the back of the helmet to ensure that added support structure from the printing process could be removed from within the helmet. With the addition of the drain holes, the first full helmet model with an internal lattice structure was complete. Further helmet revisions are developed in the aerodynamic analysis section to reduce drag and improve ventilation.

5.0 Aerodynamic Analysis

In order to determine the ideal helmet shape, computational fluid dynamic (CFD) analysis was performed. Multiple helmet iterations were developed and tested in order to improve the final design. The target value for the drag coefficient and head temperature was based on the study performed by Alam *et al*. [6] [3]. Only the drag coefficient of the concept helmets developed were compared with the study conducted by Alam *et al*. The head temperature is instead evaluated through the correlation of the heat transfer and velocity. With an increase in velocity, an increase in heat transfer can be expected. Additionally, helmet concepts will be tested in conjunction with the Biosystems helmet to perform a comparative analysis.

5.1 Background

The helmet's performance is evaluated based on its aerodynamic performance and the ability to provide thermal comfort to the user. There are several theoretically concepts that have to be considered to evaluate to helmet's aerodynamic performance.

For aerodynamic performance, the drag force for an object in motion can be determined by equation 1

$$D = C_D \frac{1}{2} \rho V^2 A \qquad \text{Eq. 1}$$

Rearranging equation 1 to calculate the drag coefficient leads to equation 2

$$C_D = \frac{2D}{\rho V^2 A} \qquad \text{Eq. 2}$$

D, ρ, V, C_D and A represent drag force (N), density (kg/m^3), velocity (km/h), drag coefficient (unitless) and the projected frontal area (m^2), respectively.

In addition to finding the drag coefficient of the helmet, the thermal comfort of the helmet was also found. In order for the thermal comfort calculations to be valid, three assumptions were made:

- The helmet was approximated to be a spherical shape

- The heat transfer is mainly due to forced convection provided by the air flowing through the vents
- To properly choose tabulated values, an air temperature would also have to be set

The air velocity and the temperature of the cyclist head is related through several equations. The air flow can be generally described by the Reynolds number, which is defined by equation 3 below.

$$Re = \frac{\rho V D}{\mu} \qquad \text{Eq. 3}$$

V and *D* are the velocity (m/s) and projected diameter (m) of an object, respectively. This equation describes the ratio of momentum forces to viscous forces of the air flow. The Nusselt number ($\overline{Nu_D}$) is a value that describes interaction of convection and conduction at the surface within a fluid [15]. For example, the boundary layer would be close to the cyclist scalp; while the interaction of convection from the air movement and the conduction from the riders skin would be described by the Nusselt Number. The cyclist head can be assumed to be a spherical object and the Nusselt number is defined by equation 4 as described by the Whitaker method.

$$\overline{Nu_D} = 2 + \left(0.4Re_D^{\frac{1}{2}} + 0.06Re_D^{\frac{2}{3}}\right) Pr^{0.4} \left(\frac{\mu}{\mu_s}\right)^{\frac{1}{4}} \qquad \text{Eq. 4}$$

Re_D, Pr and ($\mu/\ \mu_s$) are the Reynolds number relative to diameter, the Prandtl number and the dynamic to static viscosity ratio, respectively. The values of Re_D, Pr and ($\mu/\ \mu_s$) have a range that depends on the flow temperature as listed in TABLE XXIV.

TABLE XXIV: VALUE RANGES FOR PRANDLT NUMBER, REYNOLDS NUMBER AND VISCOSITY RATIO [2]

Lower Bound		Parameter		Upper Bound
0.71	≤	Pr	≤	380
3.5	≤	Re_D	≤	7.6×10^4
1.0	≤	$(\frac{\mu}{\mu_s})$	≤	3.2

The Nusselt number can then be used to find the heat convective coefficient from the relation, as shown in equation 5.

$$\bar{h} = \overline{Nu_D}\frac{k}{D} \quad \text{Eq. 5}$$

$\bar{h}$ and k are the convective heat transfer coefficient (W/m^{2}K) and thermal conductivity (W/mK), respectively. The heat transfer rate is dependent on the heat flux and temperature difference between a solid and surrounding flow. The heat convective coefficient is shown in equation 6.

$$q = \bar{h}A(T_s - T_\infty) \quad \text{Eq. 6}$$

q, T_∞ and T_s are the heat transfer rate (W), temperatures (K) of the air and surface of the riders head (K), respectively. Substituting equation 4 into 5, then substituting the result into equation 6 gives equation 7, which is the heat transfer rate in terms of Prandtl and Reynolds numbers.

$$q = (Ts - T_\infty)\frac{\left(2+\left(0.4\left(\frac{\rho VD}{\mu}\right)^{\frac{1}{2}}+0.06\left(\frac{\rho VD}{\mu}\right)^{\frac{2}{3}}\right)Pr^{0.4}\left(\frac{\mu}{\mu_S}\right)^{\frac{1}{4}}\right)kA}{D} \quad \text{Eq. 7}$$

From equation 7, it can be seen that an increase in velocity has an increase in the heat transfer rate. Therefore, a higher velocity of air flowing through the vents will lead to greater heat transfer from the rider's head. As there are many variables that would have to be assumed, it would be difficult to produce accurate results. Thus, the temperature of the cyclist's head while wearing the helmet will not be calculated, only the relationship of velocity to the heat transfer rate will be discussed.

5.2 Aerodynamic Evaluation

In order to compute the aerodynamic performance of each of the concepts, Star CCM+ was used for the CFD. The helmet was designed as a solid model without the internal lattice structure to simplify the setup of the analysis. A head was required for each of the concept helmets for simulation. Since the inner shell of the helmet was the same for each of the concepts, a universal head was produced. The head was created by offsetting a surface from the inner shell of the helmet. Having a head model in the simulation was important as this would allow for a more realistic airflow between the head and helmet. The helmet was then imported into Star CCM+.

Meshing of the Helmet

An automatic surface mesh was generated when the CAD models were imported into STAR CCM+ from SolidWorks. Since there is no internal flow in the simulation, a surface mesh is sufficient for analysis. A triangular surface mesh geometry was used, as this provides an adequate meshing geometry, which is illustrated in Figure 60 and Figure 61.

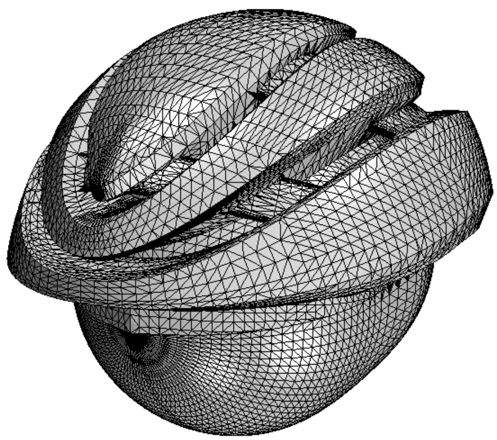

Figure 60: Triangular mesh surface geometry on concept 1 of the bicycle helmet.

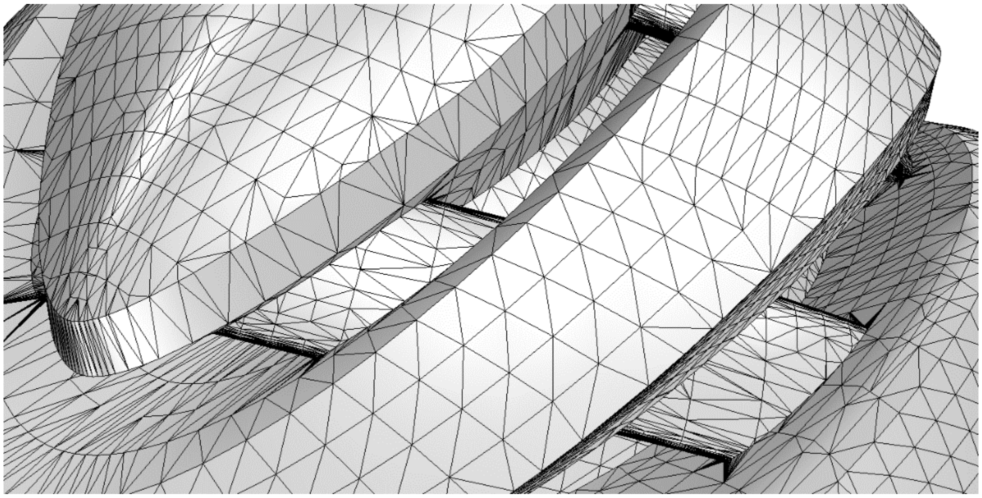

Figure 61: Close up image of surface triangular mesh in Star CCM+.

The default mesh size was used for the helmets. There were 214,040 mesh triangles and 107,002 vertices used for the simulation. The minimum mesh size for the helmet was set to 0.00125 m.

Parameters Used for the Simulation

To compare the aerodynamic performance of the concept helmets, the drag coefficient (C_D) was calculated directly by Star CCM+. The Biosystems helmet and each of the concepts were oriented at two pitch angles, 0° and 45°, with respect to the ground, as illustrated in Figure 62. The 0° orientation was used to find the lowest drag value possible to provide a base value since the cross sectional area would be lowest. The 45° angle was used as it is the most common angle that a rider would situate their head [6].

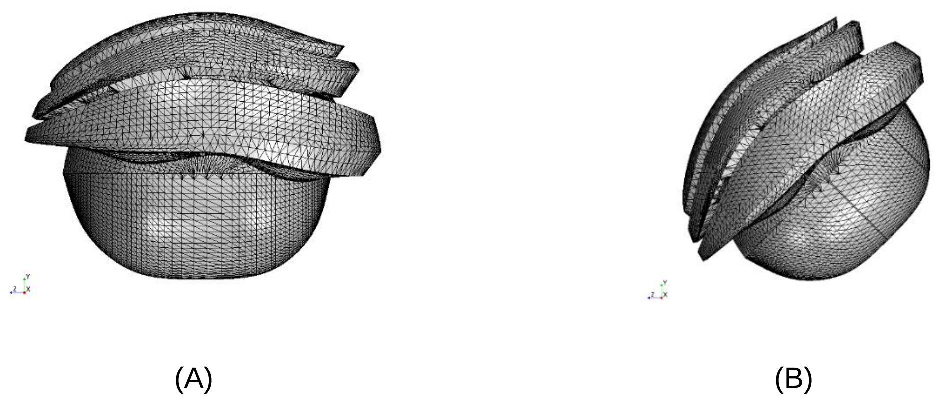

Figure 62: Side view of concept helmet with different orientations using Star CCM+ (A) 0° pitch angle (B) 45° pitch angle.

For the calculation of the drag coefficient, the simulation closely resembled the study performed by Alam *et al* [6]. The industrial wind tunnel used at RMIT University has a maximum test speed of 150 km/hr and a test section size of 3 meters wide, 2 meters high and 9 meters long. A wind tunnel was modelled around the helmet with the same dimensions as the one used in the study. The helmet was situated at the same position as the study; placed at the 6m point from the inlet of the wind tunnel [6]. The wind tunnel is depicted in Figure 63.

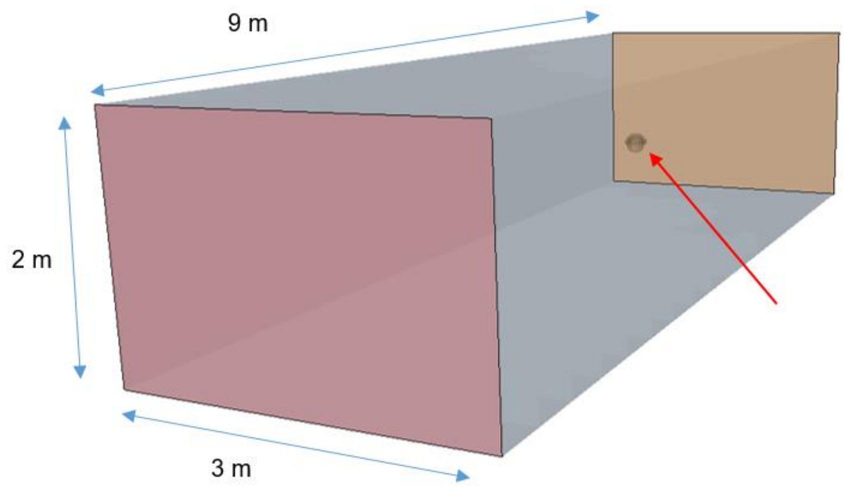

Figure 63: Dimensions of wind tunnel model made around helmet concepts in Star CCM+, with a helmet inside as indicated with red arrow.

To aid in the running computation time of the simulation, a subtract was created between the wind tunnel and the helmet. Since the wind tunnel was created in Star CCM+, creating a subtract removes the equivalent helmet model volume from the wind tunnel. The subtract allows for the simulation to take place within the wind tunnel model itself, thereby reducing the computing time that would have been required for running a simulation on a wind tunnel and helmet model directly.

The number of curvature nodes about a curved surface was also set to 120 points, increasing the node density about the helmet. The density of mesh was further increased by the change in the number of prisms layers to 4. The physical models used for the flow simulations is summarized in TABLE XXV.

TABLE XXV: PHYSICAL MODELS SELECTED FOR FLOW SIMULATION IN STAR CCM+

Parameter	Models Selected
Time	Steady State
Material	Gas
Flow	Segregated Flow
Viscous Regime	Turbulent
Equation State	Constant Density
Reynolds-Averaged Turbulence	K-Omega Turbulence

There are some parameters that had to be assumed since they were not mentioned by the RMIT study, which included the air pressure and density in the wind tunnel during testing. Therefore, it was assumed that the helmet would be run at standard sea level conditions. Pressure was set to 101325 Pa, while the air density had a value of 1.225 kg/m^3 [2].

During the simulations, momentums in the x, y and z coordinates, turbulence dissipation rate (Tdr) residual, turbulence kinetic energy (Tke) residuals were calculated. When these values have a reduction in magnitude from 3 to 4 and level off, then the results have converged. The simulations were run for a 1000 iterations to ensure convergence to a solution would be obtained. Figure 64 is an example of a plotted residual graph from calculated values demonstrating convergence.

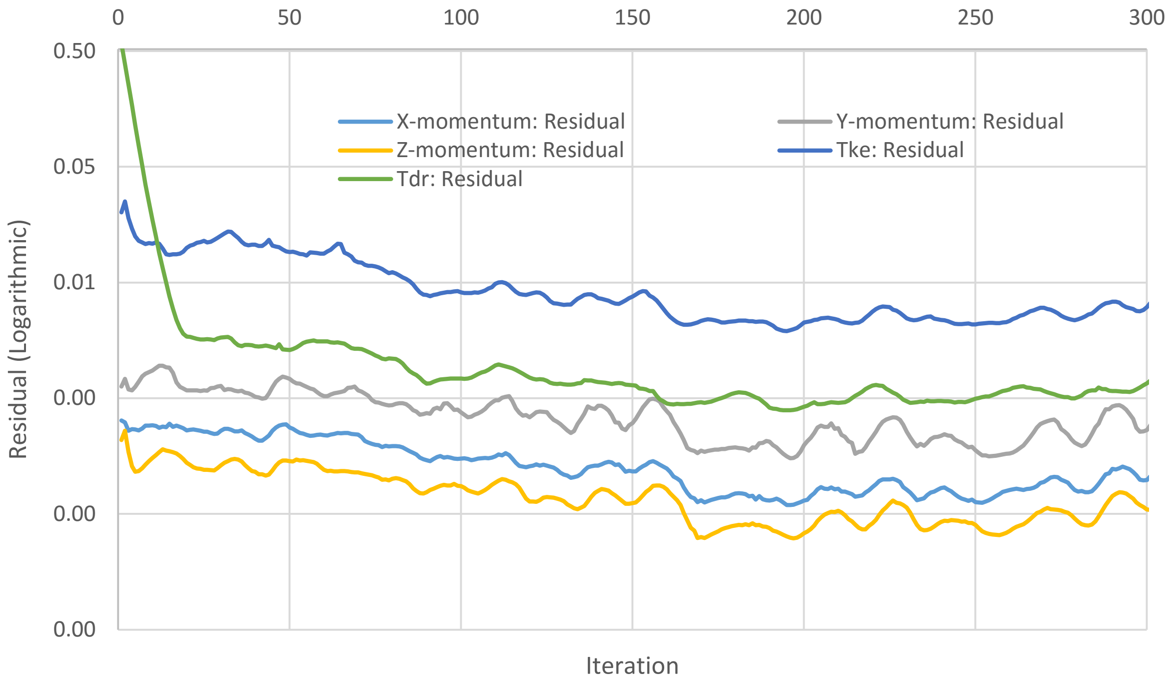

Figure 64: Example of a residual plot obtained from Star CCM+ for 300 iterations.

5.3 Results of CFD

The frontal area of the helmets as well as the drag coefficient were determined from CFD for the helmet iterations and Biosystems helmet and summarized in TABLE XXVI.

TABLE XXVI: DRAG COEFFICIENT AND FRONTAL AREA OF THE HELMET CONCEPTS

Pitch Angle	Helmet Style	Frontal Area (m^2)	Drag Coefficient	Rank
0°	Biosystems	0.0242	0.3602	4
	H1	0.0233	0.2736	2
	H2	0.0235	0.3284	3
	H3	0.0234	0.2708	1
45°	Biosystems	0.0394	0.5792	3
	H1	0.0408	0.4598	1
	H2	0.0403	0.6057	4
	H3	0.0403	0.4644	2

The result of the C_D was used as a basis to rank the helmets amongst each other, where the helmet iteration 1, 2 and 3 equate to H1, H2 and H3, respectively. The helmet with the lowest C_D for each pitch angle was used as a base to rank the other helmets accordingly. For example, for the pitch angle of 0°, H3 had the lowest C_D and received a rank of 1. Therefore, the next lowest C_D then belonged to H1, and so forth.

Biosystems Helmet

The helmet created by the Biosystems team was analyzed and provided a benchmark that the concept helmets would be compared to. The Biosystems helmet was initially comprised of two nested shells with EPS foam filling in between. The helmet CAD model was converted into a solid body and simulated in Star CCM+. The shape of the helmet has a more elongated shape, which would be comparable to helmets used for racing. There are four sets of vent channels that run the longitudinal length of the helmet. The air would ideally flow into the front facing vents and flow through the head, and exit the rear of the helmet. The rear vents line up at the same plane as the front facing vents. For the 0° and 45°, the C_D calculated was 0.3602 and 0.5792, respectively. The Biosystems helmet ranked 4 and 3 for the C_D for the 0° and 45° pitch angle, accordingly.

H1

The concepts created deviated from a racing helmet to a more conventional helmet shape. The first concept created utilized a three tiered geometry, which created two venting channels that ran from the front to the back of the helmet. The vent size was maximized for this design, which would provide the maximum amount of ventilation, while staying structurally sound. The C_D was calculated to be 0.2736 for 0° and 0.4553 for 45°. H1 ranked 2 and 1 for the C_D for the 0° and 45° pitch angle, respectively. The drag coefficient values were lower than the Biosystems helmet, which could be due to the overall height of H1. The more aerodynamic shape allowed for passing of the air more efficiently than the Biosystems helmet.

H2

The size of the venting area was reduced in H2, with the premise that a reduction in vent size would decrease the aerodynamic drag [3]. H2 has the same shape as H1, except that it has the front vent replaced with a solid surface, which is shown in Figure 65.

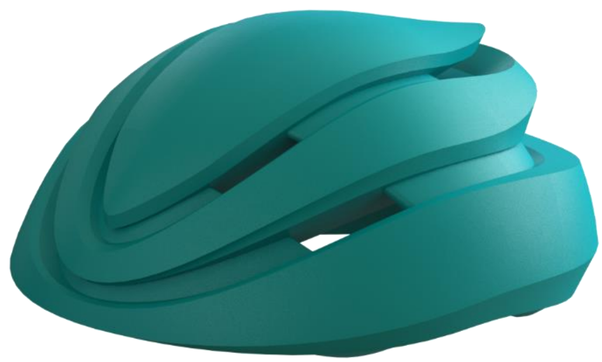

Figure 65: Isometric view of H3 concept.

The drag coefficient for the helmet was 0.3284 for 0° and 0.6057 for 45° pitch angle, respectively. H2 was ranked 3 and 4 for the C_D for the 0° and 45° pitch angles, respectively. This increase in the C_D as compared to H1 was likely due to a larger boundary layer created by the added surface.

As a fluid travels across a surface, the boundary layer, where viscous effects heavily impact flow velocity, continually grows. The added surfaces induced a larger boundary layer because the flow continued to build a larger boundary layer making it more difficult for the flow to travel over the helmet. By contrast, when the vent was open to the flow as in H1, the flow traveling across the first tier of the helmet structure could then separate from the helmet surface and flow through the vent. In other words, the covered surface increases the boundary layer, consequently increasing the displacement thickness, which increases the pressure drag. Additionally, there is an increase in shear forces at the surface of the helmet increasing skin friction drag. One or both of these factors would have contributed to the increase of the drag coefficient.

H3

The delay in separation of the air from the helmet was a focal point for this iteration, reverting back to the shape of H1 and altering the rear of the helmet. H3 has similar characteristics of the H1, except for the elongated tip at the rear of the helmet, which can be shown in Figure 66

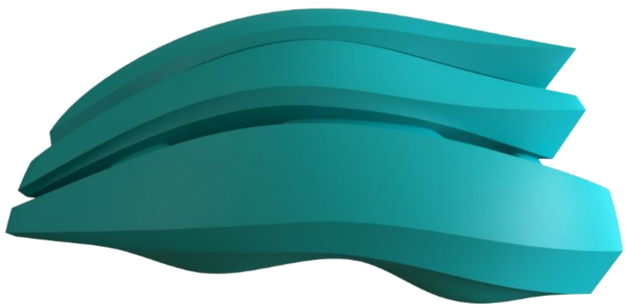

Figure 66: Side view of H3 concept.

The C_D was 0.2708 in the 0° test and 0.4644 for the 45° orientation. C_D was decreased at the 0° and 45° pitch angle, as compared to H2. H3 ranked 1 and 2 for the 0° and 45° pitch angle, respectively.

The streamlines at the mid-plane of the helmets at 0° and 45° are illustrated in Figure 67 and Figure 68, respectively. It should be noted that the results below the head is not taken into consideration, as a body was not incorporated in the simulation. Incorporating a body would have increased simulation time.

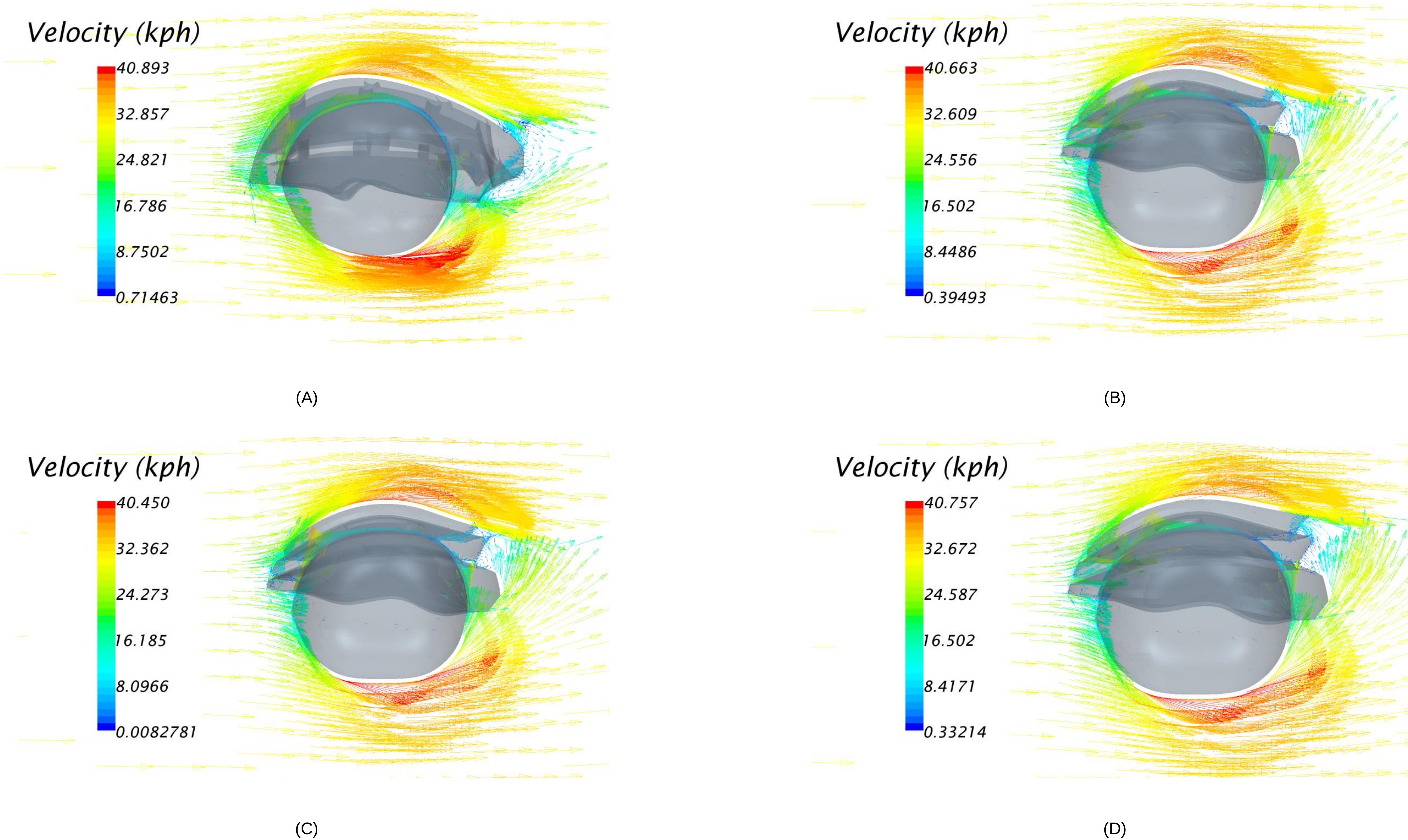

Figure 67: Mid-plane streamlines of helmet concepts with zero pitch angle at wind velocity of 30 km/h for (A) Biosystems Helmet (B) H1 (C) H2 (D) H3.

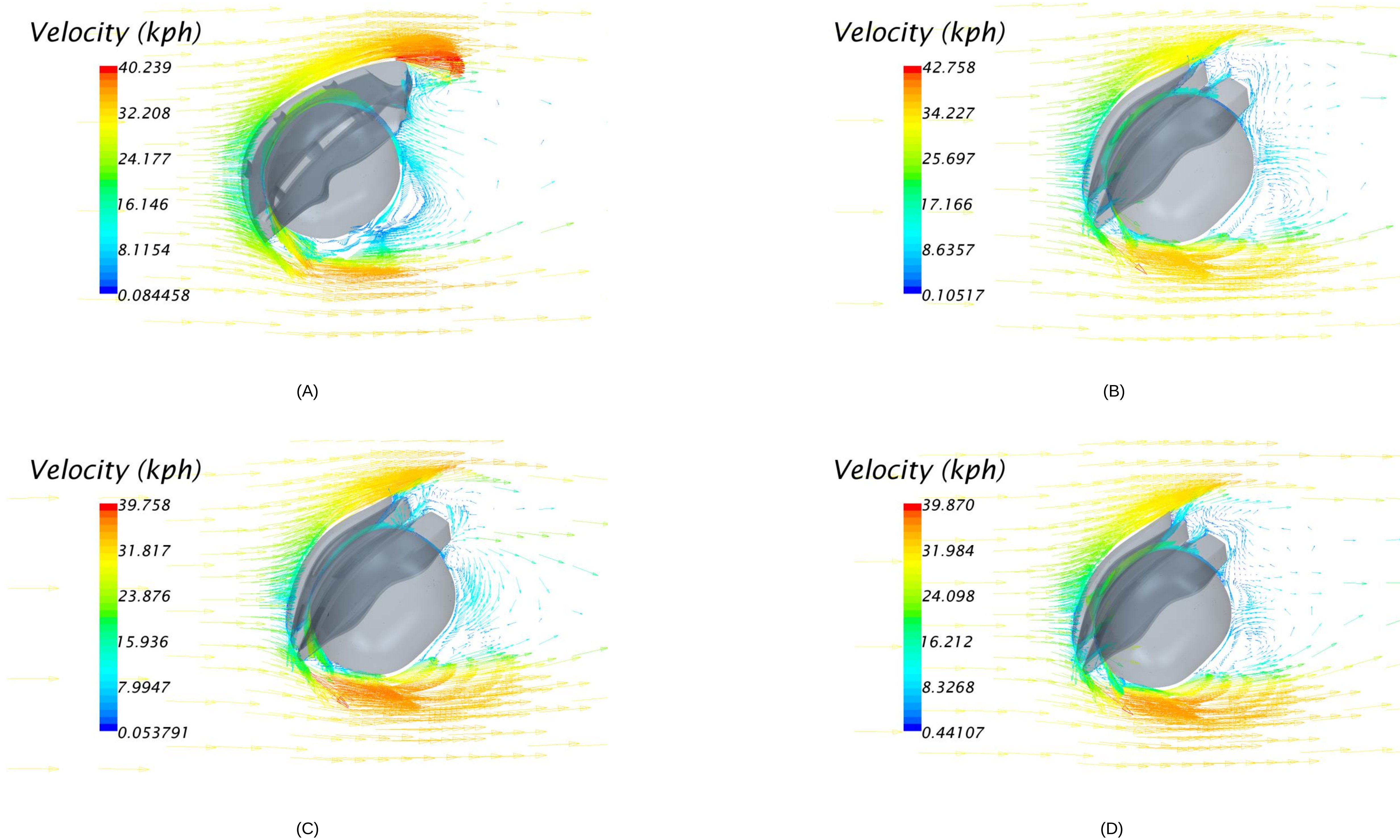

Figure 68: Mid-plane streamlines of helmet concepts with 45° pitch angle at wind velocity of 30 km/h for (A) Biosystems helmet (B) H1 (C) H2 (D) H3.

Figure 67 shows that the air velocities changes more while flowing around the Biosystems helmet as compared to the Concept helmets. In Figure 68, the velocities ranges at the top of the Biosystems helmet is broader, as compared to the concept helmets. The lowest C_D was found for the four helmets and used as a base, to compare and compute the percent difference with the other helmets. The values obtained are summarized in TABLE XXVII.

TABLE XXVII: THE PERCENT DIFFERENCE OF THE C_D WITH THE LOWEST C_D FOR DIFFERENT PITCH ANGLES

Pitch Angle	Helmet Style	% Difference with Lowest C_D
0°	Biosystems	28.33%
	H1	1.03%
	H2	19.24%
	H3	0.00%
45°	Biosystems	22.99%
	H1	0.00%
	H2	27.38%
	H3	0.99%

From TABLE XXVII, H3 had the lowest C_D of 0.2708 at the 0° pitch, while H1 had the lowest C_D of 0.4598 at 45°. H3 also had the second lowest C_D value of 0.4644 at the 45° pitch with a percent difference of 0.99% compared to H1. On the other hand, H1 has the lowest C_D of 0.4598 and had a percent difference of 1.03% when compared to H3 at the 0° pitch angle. Even though H3 was ranked second for the C_D at 45°, the percent difference is lower than compared to percent difference for H1. Therefore, it was concluded that H3 performed better aerodynamically, and would move on for further analysis.

5.4 Final Design Evaluation

The final helmet shape was analyzed by two aspects, the aerodynamic performance and the thermal comfort. For the aerodynamic performance, CFD is simulated under various velocities and pitch angles to determine the C_D. The thermal comfort would be determined by measuring the velocity of the air through the helmet vents.

5.4.1 Aerodynamic Performance

Further analysis of H3 was performed to reflect the study done by Chowdhury and Alam [6]. Additional pitch angles of 0° and 15° were simulated in CFD in comparison to the Chowdury and Alam study, as to provide supplementary data. This resulted in simulations of H3 at pitch angles of 0°, 15°, 30°, and 45° at varying velocities ranging from 30 km/h to 70 km/h with 10 km/h increments. This process is visualized in Figure 69.

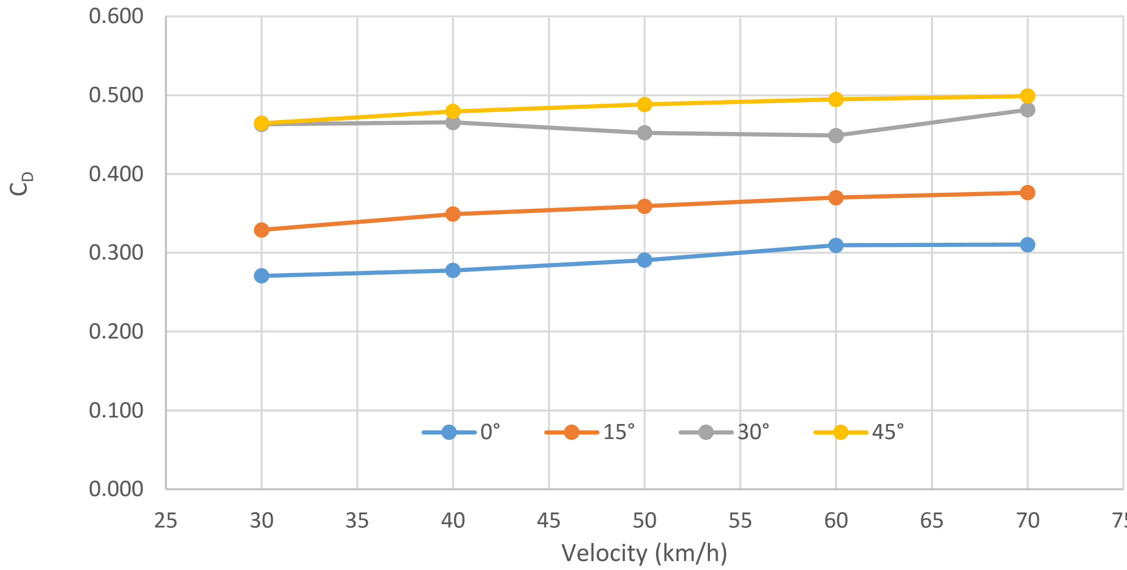

Figure 69: Comparison of C_D for different pitch angles at varying velocities for helmet 3.

The C_D values for H3 increase as the pitch angle increases, this is to be expected since the frontal area increases as the pitch angle increases. The C_D at each pitch angle does not vary significantly as the velocity is increased. For example, the C_D value for H3 at a pitch angle of 30° ranges from 0.4630 to 0.4814 as the velocity increases from 30 km/h to 70 km/h.

A comparison of the drag coefficients for H3 and the Biosystems helmet at varying velocities is depicted in Figure 70.

.

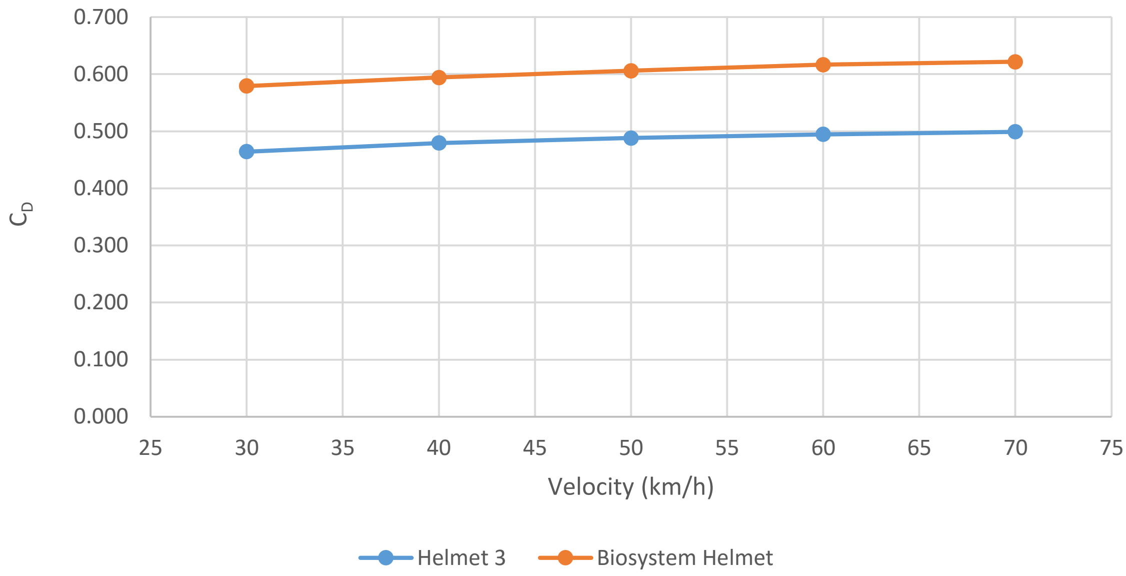

Figure 70: Comparison of C_D of concept 3 and Biosystems helmet with varying velocity at a pitch angle of 45°.

Figure 70 illustrates that for the velocities ranging from 30 km/h to 70 km/h, H3 had a lower C_D than the Biosystems helmet. The difference in C_D is primarily due to the overall shape of the helmets, which is heavily influenced by the frontal area of the helmet. At a pitch angle of 45°, the frontal area of the H3 and the Biosystems helmet the C_D is 0.4544 and 0.5792, respectively. Since H3 has a more gradually sloped front than the Biosystems helmet, there is less of a wake produced resulting in a lower C_D. A residual plot was created from the simulation and shown in Figure 71.

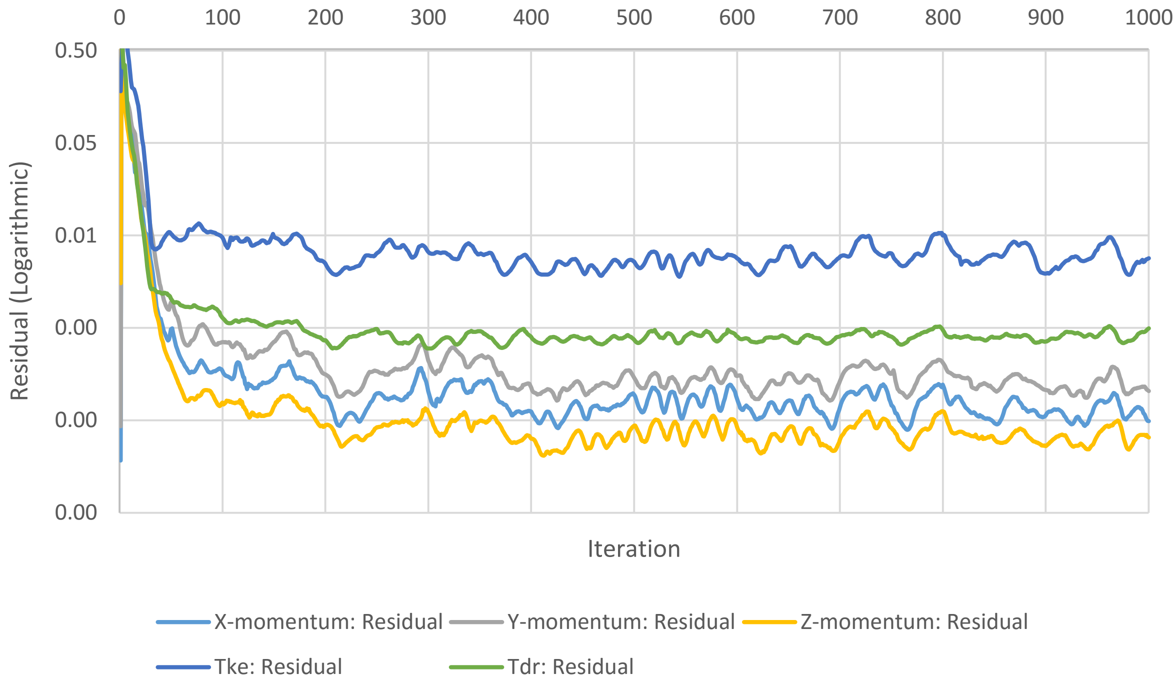

Figure 71: Residual plot for Concept 3 in 30 km/h at a pitch angle of 45° in Star CCM+.

As demonstrated in the residual plot in Figure 71, values were calculated for the x, y and z momentums as well as the Tdr and Tke residuals for 1000 iterations. At the 50th iteration, the values dropped well below the 3 to 4 orders of magnitude and began to level off to interpret that the values obtained in the simulation are valid.

5.4.2 Thermal Comfort

To determine the airflow through the helmet, probes were created at various points to obtain an average velocity within the helmet. This included points near the vent entrances as well as the areas in-between the helmet and the head model. The probes are highlighted in purple and illustrated in Figure 72.

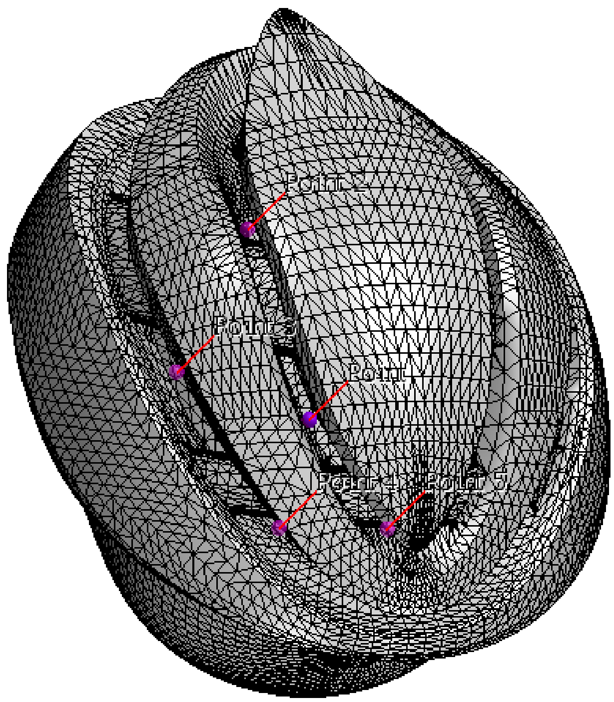

Figure 72: Example of location of probes used to measure the average airflow velocity in Star CCM+.

The probes were located at areas that would best represent the flow of air through the helmet. The varying velocities from the five probes are summarized in TABLE XXVIII.

TABLE XXVIII: AVERAGE VELOCITY OF AIR FLOW THROUGH HELMETS WITH INITIAL WIND TUNNEL VELOCITY OF 30 KM/H.

Helmet	Pitch Angle	Probe (km/h)					Average Velocity (km/h)
		1	2	3	4	5	
H3	0°	21.471	21.195	30.192	30.778	39.027	28.533
	45°	21.448	31.587	19.649	22.473	17.19	22.469
Biosystems	0°	5.318	29.394	33.23	30.077	33.746	26.353
	45°	17.39	19.298	20.434	22.727	23.424	20.655

From TABLE XXVIII, the average velocity of H3 was 28.533 and 24.469 km/h at pitch angles of 0° and 45°, respectively. Conversely, the average velocity of Biosystems helmet was

26.353 and 20.655 km/h at the pitch angles of 0° and 45°, respectively. H3 had a reduction of velocity of 6.064 km/h, while the Biosystems helmet had reduction of velocity of 5.698 km/h as the pitch angle increased from 0° and 45°. With the larger average velocity, H3 will have a higher heat transfer rate as compared to the Biosystems helmet due to the higher average velocity, as dictated by equation 7. The higher the heat transfer rate, the better the helmet to transferring heat from the riders head to the moving air. Therefore, H3 has a better thermal comfort properties as compared to the Biosystems helmet.

5.5 Aerodynamic Analysis Summary

The goal of the aerodynamic analysis section was to further refine the geometry of the helmet to reduce drag and improve ventilation. To develop the helmet, three iterations were made and evaluated against the Biosystems helmet model. A study performed by RMIT evaluated helmets at a series of different pitch angles and velocities. The same methodology was used to study the three helmet concepts in comparison with the Biosystems helmet.

Through further studies, an inverse relationship was established between the amount of ventilation and the drag force the helmet produced. As a result, a compromise between the two parameters would be made. After running the simulations, H3 produced the most favorable results throughout the range of pitch angles. The final drag coefficient for H3 at 30 km/h and a pitch angle of 0° was 0.278. H3 at 30 km/h and a pitch angle of 45° produced a drag coefficient of 0.4644. With respect to the Biosystems helmet, H3 provided a 28% difference in drag reduction at 0° and 30 km/h, as well H3 provided a 23% difference in drag reduction at 45° and 30 km/h. One item to note, is that parameters such as density and pressure are unknown from the RMIT study. Therefore the drag coefficient values differ from the metrics as outlined in section 1.2.2.

The final aspect of the aerodynamic analysis was to evaluate the air flow velocity through the vents. At both angles of 0° and 45°, H3 produced an additional 2 km/h of air flow velocity through the vents with respect to the Biosystems helmet. The values for the heat transfer rate could not be found, as there were too many unknown variables to calculate a reasonable heat transfer rate. So the correlation of the vent velocity and the heat transfer rate is taken into consideration. H3 has a better heat transfer rate as the ventilation velocity is higher in comparison to the Biosystems helmet.

6.0 Final Specifications

The final specifications of the helmet encompass the details of the helmet's design, the results of the FEA and CFD analysis, and the helmet's cost. Recommendations for the future development of the helmet's design are discussed as well.

6.1 Final Helmet Design

Developing the final geometry of the helmet was split into two separate stages. The first stage was developing the exterior of the helmet, which includes defining the body and the shape of the helmet. The second stage was the implementation of the lattice structure within the helmet body. Both aspects were developed with adjustability in mind to ensure that the design could be easily revised and improved after FEA and CFD results were collected.

Helmet Exterior

The helmet is made up of 3 distinct bodies with small aerodynamically profiled structural supports. Throughout the helmet exterior's development, three concepts were modeled and tested with CFD. Ultimately the third iteration was used as the final design. This concept features long sweeping vents between the helmet's three bodies. Figure 73 shows the final helmet exterior design. The aerodynamically profiled supports are highlighted in red.

Figure 73: Final helmet exterior design.

Other helmet concepts were developed with larger structural supports in an effort to reduce the drag at the expense of better ventilation. It was deemed that ventilation was a more important factor in the design and therefore, alternative methods for reducing drag were explored. By implementing the flare at the top of the back of the helmet, drag is reduced while maintaining a sufficient amount of ventilation. Furthermore, the tail flare adds to the overall aesthetic appeal of the helmet. A technical drawing of the helmet can be seen in Appendix G.

Helmet Lattice Structure

The swept body style of the helmet is designed intentionally to compliment the lattice structure. It was important to design a helmet exterior that would be easily adapted to encompass the final design of the lattice. In Figure 74, a cross section of the helmet with and without the lattice structure can be seen. This illustrates how the helmet exterior was developed to allow for a variety of lattice styles to be implemented. Any style of lattice with a 2-dimensional type cross section could be swept through the interior along the contours of the helmet. Thus, designing the offset rectangular cell lattice to fit the helmet only required minor adjustments to be fully implemented into the final design.

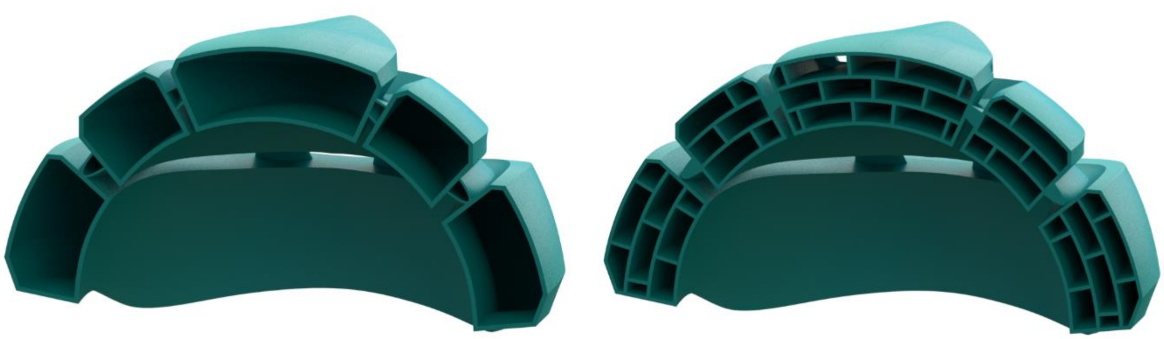

Figure 74: Hollow and filled lattice cross section.

Once the lattice had been fully developed within the helmet, every cell had to be given holes to allow for the dissolving solution to enter the helmet to remove the internal support structures. The drain holes were incorporated at the back of the helmet to ensure that they do not disrupt the air flow over the surface of the helmet. Each drain hole is strategically positioned to give access to all cells of the lattice, as well as minimize their impact on the helmet's structural integrity. Figure 75 shows the final helmet design with the drain holes implemented on the back side.

Figure 75: Final helmet drain hole geometry.

FEA of Final Lattice Design

Impact FEA in ABAQUS/CAE was used to analyze the final lattice design. The test parameters of the CPSC standard were replicated in the FEA analysis to verify that the lattice structure can protect the wearer's head from injury. The deceleration of the head was plotted at 40 time increments for impacts on a flat anvil, hemispherical anvil, and a curbstone anvil at 0° and 90°. A radial FEA model was used in the analysis that was designed to match the curvature of the actual helmet. The radial FEA model was used instead of the actual helmet model in order to reduce the computing time and limit the potential errors that can occur when generating a mesh for a complicated solid model. Figure 76 compares the radial FEA model to the actual helmet design.

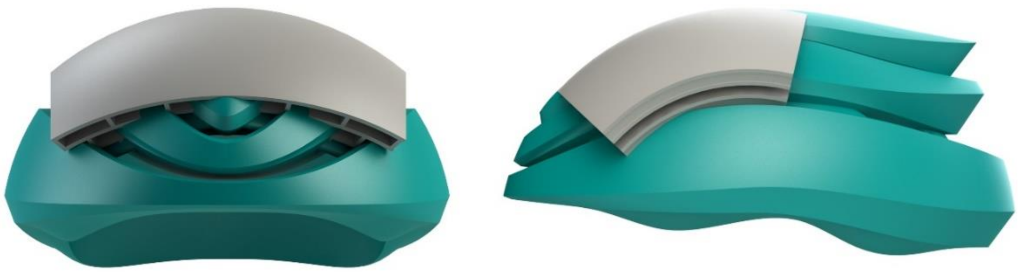

Figure 76: Comparison of radial FEA model (grey) to the helmet.

The dimensions of the lattice geometry were varied until the deceleration results were below the maximum value specified by the CPSC standard. The FEA deceleration results of the final lattice design are summarized in TABLE XXIX. The final dimensions of the lattice geometry determined using the FEA are shown in Figure 77.

TABLE XXIX: FEA HEAD DECELERATION RESULTS SUMMARY

Anvil	Impact Velocity (m/s)	Maximum Allowable Deceleration (g's)	Maximum Calculated Declaration (g's)
Flat	6.2	300	297
Hemispherical	4.8	300	171
Curbstone 0°	4.8	300	193
Curbstone 90°	4.8	300	170

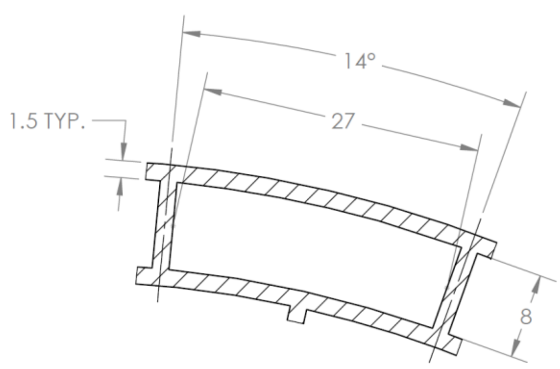

Figure 77: General dimensions of the final lattice geometry.

In reality, the actual helmet might behave differently in an impact compared to the radial FEA model. This is due to the fact that helmet consists of three swept segments containing the lattice geometry instead of a single segment as seen in the radial FEA model. However, the purpose of the FEA was to provide insight into the behavior of the lattice structure in an impact, not guarantee that the actual helmet will pass the CPSC standard in its first iteration. The accuracy of the FEA results was verified by examining the convergence of the deceleration results at various mesh sizes, but this does not prove that the lattice will actually behave this way in real life. This is largely due to the fact that the impact was assumed to be linear elastic throughout its duration. The FEA does provide a foundation for the design of the lattice structure. Future development of the helmet's design would require physical impact testing to validate the results of the FEA.

CFD of Final Design

The drag coefficient at different velocities of the final helmet design iteration, H3, and the Biosystems helmet are tabulated in TABLE XXX.

TABLE XXX: DRAG COEFFICIENT FOR HELMET 3 AND BIOSYSTEMS HELMET AT 45° AND THE CORRESPONDING PERCENT DECREASE

Velocity (km/h)	H3	Biosystems	% Decrease
30	0.464361	0.579233	19.83%
40	0.479375	0.594202	19.32%
50	0.48805	0.606062	19.47%
60	0.494684	0.616723	19.79%
70	0.499001	0.621526	19.71%

For all of the air velocities, H3 had a reduction in the drag coefficient. These values ranged from 19.32% to 19.83%, thereby concluding that H3 had a better aerodynamic performance as compared to the Biosystems helmet.

The values for the average velocity within the vents of Concept 3 and the Biosystems helmet were also found. The velocity of the air through the helmet's vents correlates to the degree of convective heat transfer out of the wearer's head. Therefore, the velocity of the air through the vents was used to gain insight into the amount of cooling. Performing numerical heat transfer analysis was deemed out of the scope of the project due to it's complexity. The average velocities and percent difference are listed in TABLE XXXI.

TABLE XXXI: PERCENT INCREASE IN AIR VELOCITY IN HELMET VENTILATION

Pitch Angle	Biosystems Helmet (km/h)	H3 (km/h)	% Increase
0°	26.35304	28.5326	7.94%
45°	20.6546	22.4694	8.42%

H3 exhibited a percent increase of 7.94% and 8.42% in the velocity of the air in the helmet ventilation for 0° and 45°, respectively. Thereby, concluding that H3 has a higher heat transfer rate, as compared to the Biosystems helmet.

6.2 Cost

A CAD model of the rear section of the final helmet design was provided to Precision ADM to be printed. The helmet was printed with the intention to show the internal lattice structure. The printed helmet with the exposed lattice structure is shown in Figure 78.

Figure 78: Printed back section of the helmet (black) with printing support structure (white) [16].

Figure 78 shows that a large amount of support material is required to print the helmet. The support structure appears to completely fill every lattice cell. This support material adds to the material costs and the total manufacturing time as it must all be dissolved.

Print time is the main factor for the cost of the helmet. The helmet in Figure 78 required 81 hours to print. If the helmet were to be produced at a high volume rather than a one-time product, Precision ADM would charge 10$ per hour of print time. Additionally, 1-2 hours of print set up time, dissolving and post processing can be charged at a rate of $80-$100 per hour. Finally, material costs are $5 per cubic inch, which includes both the support material and model material. A breakdown of the costs for the partial helmet printed by Precision ADM is given in TABLE XXXII.

TABLE XXXII: COST BREAKDOWN FOR BACK PORTION OF HELMET

Time Rate	Rate	Quantity	Sub Total
Print Time (per hr)	$ 10.00	81	$ 810.00
Set up (per hour)	$ 80.00 - $ 100.00	1 - 2	$ 80.00 - $ 200.00
Material (per in^3)	$ 5.00	29.1	$ 145.50
		Total	$ 1,035.50 - $ 1,155.50

The price of a helmet can be prorated into a cost per inch cubed (in^3). The volume of the printed part was 29.1 in^3 for a total cost ranging from $1035.50 to $1155.50 as outlined in TABLE XXXII. The full helmet has volume of 39.6 in^3, thus the cost of the full helmet is tabulated in TABLE XXXIII.

TABLE XXXIII: COST BREAKDOWN FOR FULL HELMET

Time Rate	Rate	Quantity	Sub Total
Print Time (per hr)	$ 10.00	110.23	$ 1,102.27
Set up (per hour)	$ 80.00 - $ 100.00	1 - 2	$ 80.00 - $ 200.00
Material (per in^3)	$ 5.00	39.6	$ 198.00
		Total	$ 1,380.27 - $ 1,500.27

With an increase in print volume, the helmet cost increases from $145.50 to $198.00. The total cost of a full helmet would then approximately range from $1380.27 to $1500.27. Due to the small difference between the high cost estimate and budget, the part could be kept within budget by designing an efficient pre-printing and post-printing process.

6.3 Recommendations

One of the main constraints the team faced throughout the project was time. As a result, many aspects of the final design could be further refined and optimized to produce an improved result. For example, physical testing could be performed in order to verify the simulation values, FEA models could be made to more accurately represent the final helmet geometry, and alternative software and simulations could be used to refine the design.

As with any simulation, all results must be verified though some form of physical testing. Due to time constraints, the schedule did not allow for physical crush testing and wind tunnel testing. Although the FEA and CFD analysis was proven valid through convergence and residual plots, physical testing must be done in the future to verify the results. In the scenario where physical test data does not agree with simulation results, FEA methods may have to be altered to better represent the helmet. An alternative approach may have to be developed in an effort to produce a valid simulation. After analyzing the final FEA simulation from ABAQUS, the ultimate stress was exceeded in some cases depending on the print orientation of the structure. Physical testing should be performed to predict the effects of the printing orientation, as well as the fracture characteristics of the helmet. Since fracture was not accounted for in the simulation, this could be a potential discrepancy between simulation results and physical test results. Therefore, data analyzing the influence of fracture on the helmet must be collected. With additional time, simulations could be developed to incorporate plasticity through a non-linear solution.

Additionally, wind tunnel testing should be performed to ensure agreement with calculated drag coefficient and velocity values. Heat transfer and ventilation data could also be collected through the use of physical testing. This would provide a direct correlation between changes in helmet geometry and ventilation. Ultimately, physical data is required to make further refinements and optimizations to the final helmet design. Simulation models need to be verified to ensure that they are producing adequate results, thus allowing for further helmet modifications to be made.

To simplify simulation and computational requirements, representative FEA models were developed to replicate portions of the helmet structure. With additional time, further FEA models should be developed to better replicate the final design, and ultimately a simulation of the final helmet in its entirety should be tested. A few critical aspects of the helmet such as the structural supports and rear portion of the helmet need to be analyzed before final conclusions can be made with respect to the standards. Detailed FEA models of the supports should be made to quantify their effect on the helmets integrity. The current final design features solid supports to ensure structural integrity. With further analysis, wall thicknesses of the supports could be reduced to optimize the final design. As discussed in the lattice implementation section, discrepancies within the lattice structure occur at the back of the helmet. Therefore, analysis must be done on this location to ensure that the helmet meets standards. In the event that the back of the helmet does not meet standards, an alternative method to implement the lattice must be developed.

Alternative software such as Altair Optistruct or Within by Autodesk could be used to develop optimized lattice designs. These programs are designed to optimize structures based on established constraints through the implementation of internal lattice structures. Using these programs, constraints and boundary conditions for the helmet can be imposed on the geometry, allowing for the software to develop the lattice structure. This would significantly minimize lattice development time, as well as allow for the development of complex geometries. Implementing this kind of software in the lattice structure development process would provide a significant amount of insight into a further optimized design.

Recently Precision ADM acquired a Selective Laser Sintering (SLS) 3D printing machine. As recommended by the client, SLS is a potential alternative method of printing that can be used in the future. SLS printing can possibly provide lower material costs, faster production, and a wider range of capabilities. One of the main limitations with FDM is the need for support material. Due to the internal geometry of the lattice, drain holes were needed to allow for the support structure to be removed after printing. Upon completion of the helmet the drain holes should be evaluated to determine if they provide adequate access to the lattice. On the other hand, SLS printing does not require the addition of support material and the helmet would not require drain holes. Instead, the helmet would require a method to remove unsintered material. Further research would have to be done to establish all of the potential benefits of switching to a SLS printer.

Material testing considering environmental conditions should be further evaluated. Stratasys provides limited information on how certain materials react under prolonged exposure to varying temperatures and humidity. A study should be performed to evaluate the helme’s structural integrity across all potential environmental conditions to ensure it continues to meet the standards requirements.

For future development, outside of the scope of this project, methods for implementing head padding, fastening straps, and customization options should be developed. Internal padding should be added to provide comfort for the user and minimize pressure points. Fastening straps would require further design so that the straps are implemented without affecting the structural integrity of the helmet. Finally, due the flexibility in the manufacturing process of FDM, this allows for a significant amount of customization in the helmet design. By implementing 3-Dimensional scanning technology, customers could have a helmet specifically printed to their head dimensions to maximize comfort. Applying these aspects would entail future development in the production phase of the project, thus requiring the completion and finalization of the helmet design.

7.0 Summary

A 3D printed bicycle helmet with an internal lattice structure has been designed by the team, which meets the specifications required by the client, Precision ADM. The bicycle helmet has been designed to be printed as a single piece using fused deposition modeling, which was the main objective of the project. Impact FEA was performed to evaluate and optimize the internal lattice structure's ability to absorb energy in an impact. CFD was used to determine the optimum ventilation geometry and evaluate the aerodynamic performance of the helmet.

The helmet was designed with three swept segments, each containing the internal lattice geometry. The three segments are connected with structural supports and the gaps between the structural supports provide ventilation to the wearer's head. The segmented design of the helmet contributes to the helmet's aesthetics, as well as provides an effective way to implement the internal lattice geometry and ventilation. The helmet has been designed to be printed in polycarbonate (PC) and the total weight of the helmet including the internal lattice structure is 779 grams.

The lattice structure inside the helmet consists of rectangular cells swept longitudinally along the helmet. The rows of lattice cells are offset to induce bending during an impact, which contributes to absorbing energy and reducing the deceleration of the head. To evaluate the ability of the lattice structure to absorb energy, impact FEA was performed on a simplified FEA model that reflects the general curvature of the helmet. The parameters of the impact testing in the CPSC standard have been used as baseline for the FEA. Therefore, the results of the FEA give insight into the helmet's ability to meet the CPSC standard and protect the wearer's head from injury. Many lattice design iterations were analyzed until the final lattice design that best meets the criteria of the CPSC standard was selected.

The CPSC standard dictates that the maximum head deceleration must be less than 300 g's for impacts on 3 different anvils: a flat anvil, hemispherical anvil, and a curbstone anvil. The flat anvil impacts are at a velocity of 6.2 m/s and the hemispherical and curbstone impacts are at a velocity of 4.8 m/s. In the flat anvil and hemispherical anvil impacts, the maximum calculated head decelerations are 297 g's and 171 g's, respectively. In the curbstone anvil impacts, the maximum calculated head decelerations are 193 g's and 170 g's at the 0° and 90° orientations, respectively.

The aerodynamic performance of the helmet has also been assessed. CFD has been used to determine the optimal structural support configuration and surface geometry. The helmet iteration with the lowest drag coefficient was selected as the helmet's final design. CFD simulations have been performed to calculate the drag coefficient of the helmet at varying pitch angles and velocities. At the ideal pitch angle of 45° with a wind tunnel velocity of 30 km/h, the drag coefficient of the helmet was 0.4644. The aerodynamic performance of the helmet was also compared to a bicycle helmet design that was previously made for Precision ADM by Biosystems students. The new helmet design had a drag coefficient reduction of 19.83% compared to the Biosystems student's design.

It was not feasible in the project timeline to run a heat transfer simulation due to the complexity of the analysis. Instead, the thermal comfort was evaluated using the ventilation velocity calculated through CFD. The dissipation of heat is related to the velocity of the airflow through the vents. The average velocity of the air flow through the vents is 22.469 km/h, with an initial wind tunnel speed of 30 km/h. In comparison with the Biosystems student's helmet design, the new design had an 8.42% increase of air flow velocity through the vents.

A section of the helmet has been printed as a test piece. The test piece's estimated cost is $1035.50 to $1155.50 based on the print time, set up time, and material costs. Using the cost of the printed test piece as a baseline, the estimated cost of the full helmet is $1380.27 to $1500.27, which is within the range specified by Precision ADM at the beginning of the project.

The team has successfully met the critical needs of the project. The helmet design is ready to be fully printed and undergo physical testing to verify that it can pass the required safety standards. The FEA has provided insight into the behavior of the lattice structure upon impact and the calculated head impact decelerations are below the CPSC standard's limit. CFD analysis of the helmet design has allowed the team to reduce the drag coefficient of the helmet while ensuring the helmet can provide ventilation to the wearer's head.

8.0 References

[1] J. Bell, P. Botha, M. Karpowicz, P. Logan, P. Mugova and J. Schwartz, "*3D Printing a Better Fitting Bicycle Helmet*," Winnipeg, 2014.

[2] V. Cormier, "*3D Prototype of Biosystems Helmet*," Winnipeg: Design Eng., Univ Manitoba, Winnipeg, MB , 2015.

[3] F. Alam, H. Chowdhury, Z. Elmir, A. Sayogo, J. Love and A. Subic, "*An Experimental Study of Thermal Comfort and Aerodynamic Efficiency of Recreational and Racing Bicycle Helmets*," Elsevier Ltd., Melbourne, 2010.

[4] C. S. Association, "*Cycling Helmets*". Canada Patent CAN/CSA-D113.2-M89, September 1989.

[5] T. A. Stevenson, "*Consumer Product Safety Commission*," 10 March 1998. [Online]. Available: http://www.cpsc.gov//PageFiles/86318/10mr98r.pdf. [28 September 2015].

[6] H. Chowdhury and F. Alam, "*An experimental study on aerodynamic performance of time trial bicycle helmets*," *Sports Engineering,* vol. 17, pp. 165-170, 2014.

[7] CompetitiveCyclist.com, "*Road Bike Helmets*," Competitive Cyclist, [Online]. Available: http://www.competitivecyclist.com/road-bike-helmets. [28 September 2015].

[8] stratasys.com, "*FDM Thermoplastics*," Stratasys, 2015. [Online]. Available: http://www.stratasys.com/materials/fdm. [27 September 2015].

[9] stratasys.com, "*Fortus 380mc and Fortus 450mc*," Stratasys, 2015. [Online]. Available: http://www.stratasys.com/3d-printers/production-series/fortus-380-450mc. [27 September 2015].

[10] J. Heimenz, "*3D Printing With FDM," 2014*. [Online]. Available: http://usglobalimages.stratasys.com/Main/Files/White%20Papers/WP_FDM_3D%20PrintingWithFDM.pdf?v=635786177472811876. [28 September 2015].

[11] J. Lawrence, "*3D Printing Material and Support Build Options*," CAPUniversity, 9 January 2015. [Online]. Available: http://blog.capinc.com/2015/01/3d-printing-material-and-support-build-options/. [25 October 2015].

[12] Tribology-abc, "*Coefficient of friction for a range of material combinations*," [Online]. Available: http://www.tribology-abc.com/abc/cof.htm. [29 10 2015].

[13] ASM, "*ASM Material Data Sheet*," [Online]. Available: http://asm.matweb.com/search/SpecificMaterial.asp?bassnum=MQ304A. [07 December 2015].

[14] J. W. Young, "*Head and Face Anthropometry of Adult U.S. Civilians*," National Technical Information Service, Springfield, 1993.

[15] F. P. Incropera and D. P. Dewitt, *Fundamentals of Heat and Mass Transfer*, 7th ed., John Wiley & Sons, Inc, 2007.

[16] T. Gascoyne, "*Final helmet design with lattice structure and support structure*," Precision ADM, Winnipeg, Manitoba, 2015.

Appendix for Final Design Report

Table of Contents

List of Figures

List of Tables

Appendix A: **Research**

Literature research and competitor benchmarking are crucial components for gathering information that can be applied towards the design of the helmet. The helmet design research was divided into three key areas: the lattice structure, ventilation, and the material properties.

Appendix A.1. Lattice Design

A study by Moon *et al.* investigated the optimal elastic performance of three lattice structures for the development of a deployable UAV wing design [1]. The team compared three lattice structures: 3D Kagome, 3D pyramidal, and hexagonal diamond structures, as illustrated in Figure 1

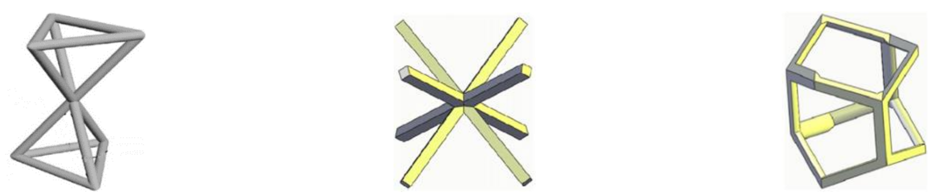

3D Kagome 3D Pyramidal Hexagonal Diamond

Figure 1: 3D Lattice structures analyzed by Moon et al. [1].

The structures were compared in a compression test and the results showed that the 3D Kagome structure had the highest load capacity, but the hexagonal diamond exhibited the ideal energy absorption properties.

Another informative journal article written by Soe *et al.* studied the application of 3D printing for bicycle helmets [2]. Using thermoplastic elastomers (TPE) and selective laser sintering (SLS), the Soe team evaluated the energy absorption capabilities of the lattice structures illustrated in Figure 2.

Fully Filled Liner | 25% Density using Tubular Cross Sections | 10% with Tubular Cross Sections

Figure 2: The three energy absorbing layers [2].

The study used dynamic FEA to simulate an impact similar to the requirements for this project [2]. A simplified helmet was modeled with an inner and outer shell, and an internal lattice structure. Simplified versions of a headform and anvil were modeled to simulate an EN:BS1078 helmet impact test. The helmet model was perfectly fixed to the headform, while the anvil was constrained along its lower surface. The helmet outer shell and anvil were given a frictionless surface to surface contact interaction. A mesh was automatically generated using brick and tetrahedral elements. The headform was given a mass of 4.2 kg and an impact velocity of 2.2 m/s. Soe *et al.* found that peak translational accelerations decreased with a decrease in cellular density, while acceleration pulse durations were increased. These parameters and results could be used as guidelines for our dynamic FEA testing.

Another article related to impact absorbing lattice structure is the work of J Brennan-Craddock *et al.* in "*The Design of Impact Absorbing Structure for Additive Manufacture*" [3]. Although the paper is for body conforming impact protection, the paper is strongly related to the function of a helmet composed of an impact absorbing lattice. The article goes into detail regarding lattice design and the ability of a lattice to conform to curvature. Figure 3 shows four different ways a lattice can be conformed to curved geometry.

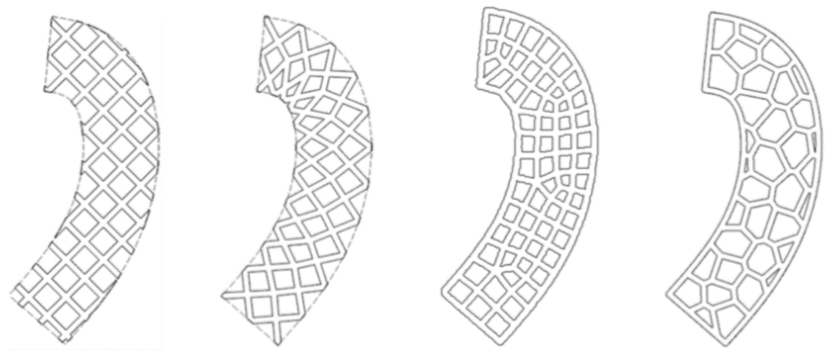

Figure 3: Methods of conforming lattice to curvature [12].

Conformity is an important consideration in the design of a lattice structure since the bike helmet will have curvatures of varying radii and ventilation. The far left geometry, known as a “trimmed” conformal method, is not ideal in the case of a bicycle helmet lattice structure because the variability of the trim locations could lead to varying stiffness characteristics. The second “swept” geometry or third “meshed” geometry proved to be more adept at providing uniform stiffness throughout the structure.

Appendix A.2. Helmet Ventilation

The number, position, and shape of vents have an impact on the aerodynamic performance as well as on the heat dissipation characteristics for a bicycle helmet. Firoz Alam and his team at RMIT University conducted a study to determine the thermal comfort and aerodynamic efficiency that bicycle helmets provide. Alam *et al.* analyzed six commercial helmets using an RMIT industrial wind tunnel [4]. Using force sensors, thermocouples, and a mannequin with an integrated heater mat to simulate heat generation, Alam *et al.* were able to conclude that the Giro Advantage helmet had the best aerodynamic performance. They also modified the helmets by taping over certain portions. Alam *et al.* determined that the position of the vents can increase aerodynamic performance while maintaining thermal comfort.

The shape of the venting was also studied by Alam *et al.* Using the same wind tunnel as the previous study, a pitot tube was integrated into the testing apparatus. Using five helmets, the venturi shape of the venting holes was measured and the effect on the aerodynamic drag was measured. Alam *et al.* concluded that an increase in venturi effectiveness correlated to higher aerodynamic drag [4].

Appendix A.3. Materials

Information for the material properties based on the environmental conditions are explained in this section.

Appendix A.3.1: Environmental Conditions Effects on Material Properties

Stratasys performed extensive testing to determine the effects that the environment has on the material properties of polycarbonate (PC) [5] and ABS-M30 [6]. Test samples were stored in three conditions: dry (15% relative humidity), wet (immersed in water), and controlled (50% relative humidity). Test samples were made to a 0.18 mm slice height, using a T12 printer tip, and produced using the Fortus 400mc 3D production system. After the test samples were conditioned, the material properties for tensile strength, flexural modulus, and percent elongation break were measured. Stratasys tested 10 samples for the three mechanical properties using IS0 527 and IS0 178 testing standards. The results show that the tensile strengths of the PC and ABS-M30 decreases as the temperature of the polymers is increased, as shown in Figure 4.

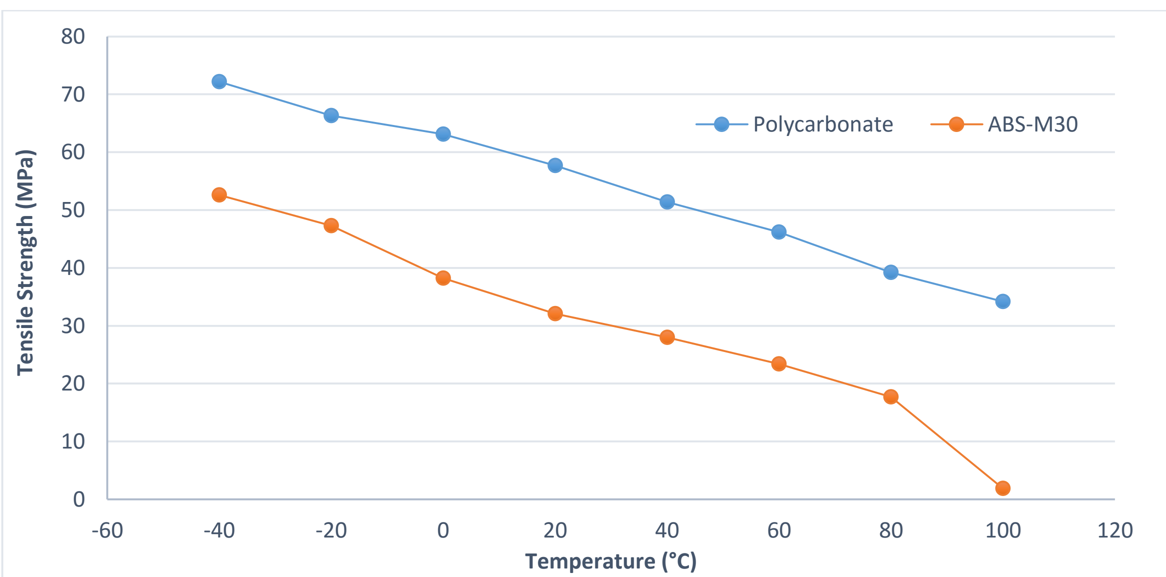

Figure 4: Tensile strength as function of temperature for polycarbonate and ABS-M30 [6] [5].

The tensile strength ranges between 72.2 to 34.2 MPa for PC. and 52.6 to 1.9 MPa for ABS-M30 throughout the given temperature range. The flexural modulus of PC and ABS-M30 follow the same trend as the tensile strength; however, ABS-M30 does have a significant drop in flexural modulus at 100 °C. Polycarbonate has a value of 1671 MPa while ABS-M30 has a value of 1154 MPa at 100 °C. The trends are shown in Figure 5.

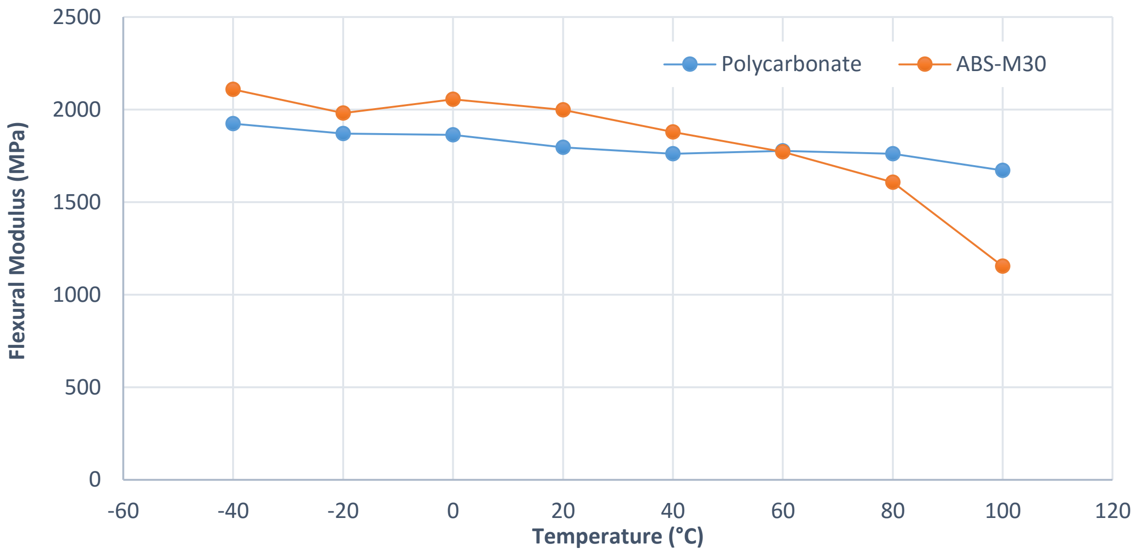

Figure 5: Flexural modulus as a function of temperature for polycarbonate and ABS-M30 [6] [5].

The percent elongation at break for PC has a downward trend ranging from 10.4% to 4% as the temperature was increased, while ABS-M30 has an overall increase in elongation ranging from 5.3% to 8.7%.

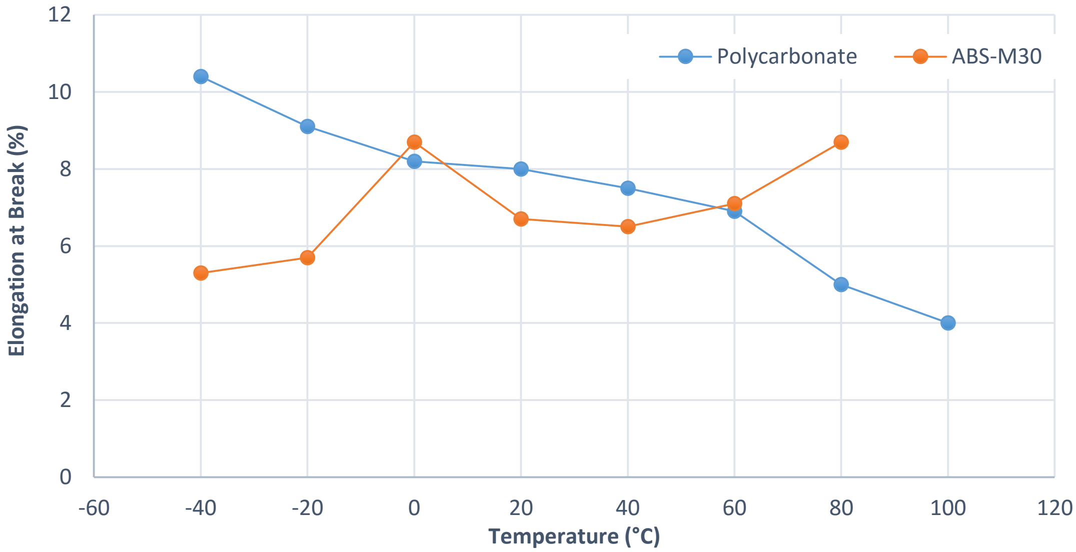

Figure 6: Elongation at break as function of temperature for polycarbonate and ABS-M30 [6] [5].

The graphical data shown was for the controlled sample pieces, and the tabulated values are shown below.

The effects of temperature and material properties are tabulated in TABLE I, TABLE II and TABLE III for tensile strength, flexural modulus, and percent elongation at break for polycarbonate.

TABLE I: ENVIRONMENTAL EFFECTS ON TENSILE STRENGTH OF POLYCARBONATE [5]

Condition	Tensile Strength (MPa)		Temperature (°C)				
Wet	55.2	Condition	-40	0	40	80	120
Dry	56.9	Wet	71.5	60.3	49.2	37.7	27.2
Controlled	57.7	Dry	70.3	62.2	51.7	40	28.6
* 20 Deg. C 4 week old sample		Controlled	72.2	63.1	51.4	39.2	26.4

TABLE II: ENVIRONMENTAL EFFECTS ON FLEXURAL MODULUS OF POLYCARBONATE [5]

Condition	Flexural Modulus (MPa)		Temperature (°C)				
Wet	1799	Condition	-40	0	40	80	120
Dry	1818	Wet	2274	1850	1771	1714	1633
Controlled	1797	Dry	1819	1808	1829	1742	1659
* 20 Deg. C 4 week old sample		Controlled	1924	1863	1762	1761	1625

TABLE III: ENVIRONMENTAL EFFECTS ON ELONGATION AT BREAK OF POLYCARBONATE [5]

Condition	Elongation Break (%)		Temperature (°C)				
Wet	7.9	Condition	-40	0	40	80	120
Dry	8	Wet	10.5	8.6	6.6	6.3	3.9
Controlled	8	Dry	9.2	8.6	7.6	7.2	3.9
* 20 Deg. C 4 week old sample		Controlled	10.4	8.2	7.5	5	2.9

The effects of temperature and material properties are tabulated in TABLE IV, TABLE V, and TABLE VI for tensile strength, flexural modulus, and percent elongation at break for ABS M-30.

TABLE IV: ENVIRONMENTAL EFFECTS ON TENSILE STRENGTH OF ABS-M30 [6]

Condition	Tensile Strength (MPa)		Temperature (°C)				
Wet	33.8	Condition	-40	0	40	80	100
Dry	31.8	Wet	50.1	43.6	27.2	14.9	0.4
Controlled	32.1	Dry	49.7	37.5	28.5	18.3	2.6
* 20 Deg. C 4 week old sample		Controlled	52.6	38.2	28	17.9	2.8

TABLE V: ENVIRONMENTAL FLEXURAL MODULUS OF ABS-M30 [6]

Condition	Flexural Modulus (MPa)		Temperature (°C)				
Wet	1949	Condition	-40	0	40	80	100
Dry	1909	Wet	2347	2047	1862	1367	161
Controlled	1999	Dry	2403	1964	1937	1477	999
* 20 Deg. C 4 week old sample		Controlled	2109	2055	1879	1607	1154

TABLE VI: ENVIRONMENTAL ELONGATION AT BREAK OF ABS-30 [6]

Condition	Elongation of Break (%)		Temperature (°C)				
Wet	5	Condition	-40	0	40	80	100
Dry	6.7	Wet	4.1	4.8	5.7	3.1	0
Controlled	6.7	Dry	4.7	8.7	7.6	7.3	0
* 20 Deg. C 4 week old sample		Controlled	5.3	8.7	6.5	8.7	0

In addition to literature research, consumer reviews were found in bicycle magazines and collected to create a set of competitor data that includes durability, affordability, and subjective values such as comfort [6]. These results, combined with the values obtained from the literature reviews, allowed for the production of marginal and ideal values that the helmet can be compared to.

Appendix B: **House of Quality**

Now that the client's needs and corresponding metrics have been defined in addition to collecting literature research and competitor benchmarking information, a house of quality (HOQ) can be created to visually represent the relation between all of our collected data.

First, the HOQ relationships between the needs and metrics must be established. The relationships were assigned values of 1, 3, and 9 to evaluate the strength of those relationships. A value of 1 is a weak relationship while a value of 9 is a strong relationship. For example, the "helmet is affordable to customer" need has a strong relationship with the cost of the helmet, and a value of 9 was given. Additionally, the relationship between metrics were also quantified. For example, head temperature and drag coefficient would have a negative relationship, because a decrease in head temperature would relate to an increase in ventilation. Consequently, an increase ventilation would result in increase in aerodynamic drag coefficient.

All the metrics, needs, constraints and benchmarking relationship data was collected in the HOQ, which is shown in TABLE VII. For values that are left blank, the correlating data was not available.

TABLE VII: HOUSE OF QUALITY FOR THE 3D PRINTED BICYCLE HELMET

Legend

θ	Strong Relationship
o	Moderate Relationship
Δ	Weak Relationship
++	Strong Positive Correlation
+	Positive Correlation
–	Negative Correlation
v	Strong Negative Correlation
↓	Objective Is to Minimize
↑	Objective is to Maximize
X	Objective is to Hit Target

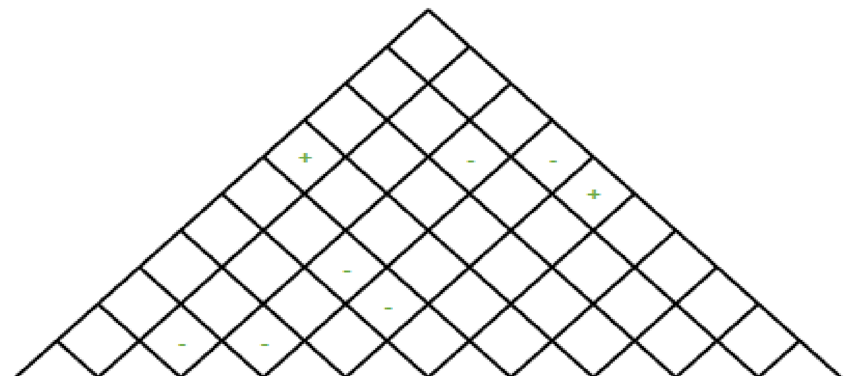

			Column #	1	2	3	4	5	6	7	8	9	10	Competivive Analysis (0=Worst, 5 = Best)										
			Direction of Improvement	↓	↓	↓	↓	↑	↓	X	X	X	X											
Row #	Relative Weight	Weight/Importance	Quality Characteristics / Demand Quality (Customer Needs)	Cost [$ CAD]	Impact Deceleration [G-Force]	Weight [g]	Head Temperature [Celsius]	Field of Vision [Degree]	Drag Coefficient [Non Dimensional]	Helmet is 3D printed [Y/N]	Fits Wearer's Head [sub]	No Pressure Points [sub]	Visually Appealing [sub]	Biosystems Helmet	Bell Array	Bell Star Pro	Giro Advantage	Giro Aeon	Giro Atmos	Giro Synthe Helmet	Kask Vertigo	LG Rocket	Limar UltraLight	POC Octal
1	15.15	5.0	Entirely 3D printed		Δ	Δ				θ		o		1	0	0	0	0	0	0	0	0	0	0
2	15.15	5.0	Prevents head injury		θ	o				Δ						4			4	3		4	4	5
3	12.12	4.0	Provides ventilation to the head				θ		θ					2				5	5		4			5
4	12.12	4.0	Can withstand environmental conditions											3				2	3		4			4
5	9.09	3.0	Does not obstruct vision											5	5	5	5	5	5	5	5	5	5	5
6	9.09	3.0	Helmet is aerodynamic		o		o		θ								3		5					
7	9.09	3.0	Helmet is lightweight		θ	θ			o			Δ		0		2		5	5	3	3	5	5	5
8	9.09	3.0	Helmet is visually appealing										θ	2										
9	6.06	2.0	Helmet is affordable to customer	θ						o				1	5	1				1		2	2	1
10	3.03	1.0	Helmet is comfortable			Δ	Δ	Δ			θ	θ		1				4	4		3			3
			Target or Limit Value	1500	300	252	29.1	105	0.27	Yes	1	4	4											
			Relative Difficulty (1=Easy to Accomplish, 10=Extremely)	4	8	7	7	2	8	5	3	3	5											
			Weight/Importance	54.5	236.3	145.5	115.1	3.0	145.4	169.7	27.3	81.8	81.8											
			Relative Weight	5.1	22.3	13.7	10.9	0.3	13.7	16.0	2.6	7.7	7.7											
			Rank	8	1	3	5	10	4	2	9	7	6											

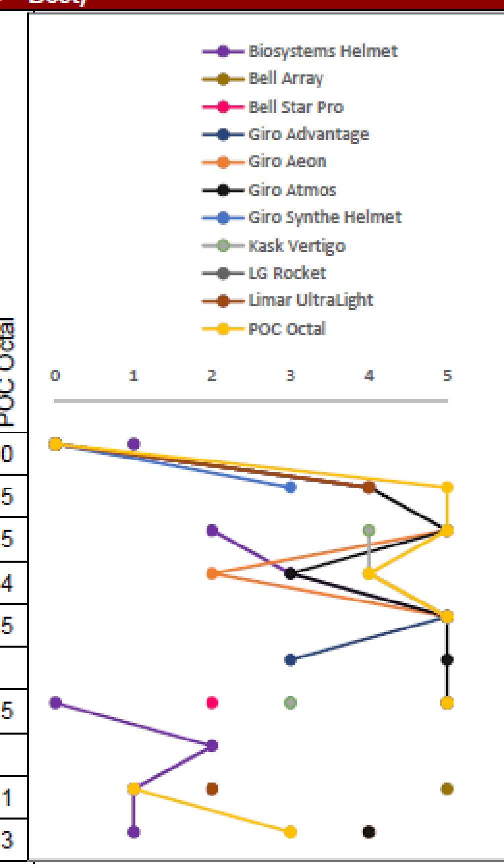

The relative weights of the metrics are summarized in the HOQ, then ranked for importance. The *Impact Deceleration* received a rank of 1, which indicates that impact deceleration of the helmet is priority for the design. The quality characteristics *Fits Wearer's Head* and *Field of Vision* have the lowest ranks, as these aspects are not as important.

The graph on the right of the HOQ aids in the visualization of the needs that certain competitor helmets exceed in. For example, the Giro Atoms outlined in black has values that range from 0 to 5 for the given client needs, which is tracked by the graph in the HOQ. The helmets that scored values of 4 or 5 in the client's needs were used as a basis for the target values.

Appendix C: **Project Schedule**

The team had an overall timeline from September 24th to December 9th for the completion of the project. The project is broken down into two work breakdown structures (WBS): one for the Helmet Design and another for the Team Deliverables as shown in Figure 22 and Figure 23, respectively. The Helmet Design WBS breaks down the deliverables needed to conceptualize, build, and test our designs whereas the Team Deliverables WBS shows the deliverables required by the client to document and present the design work.

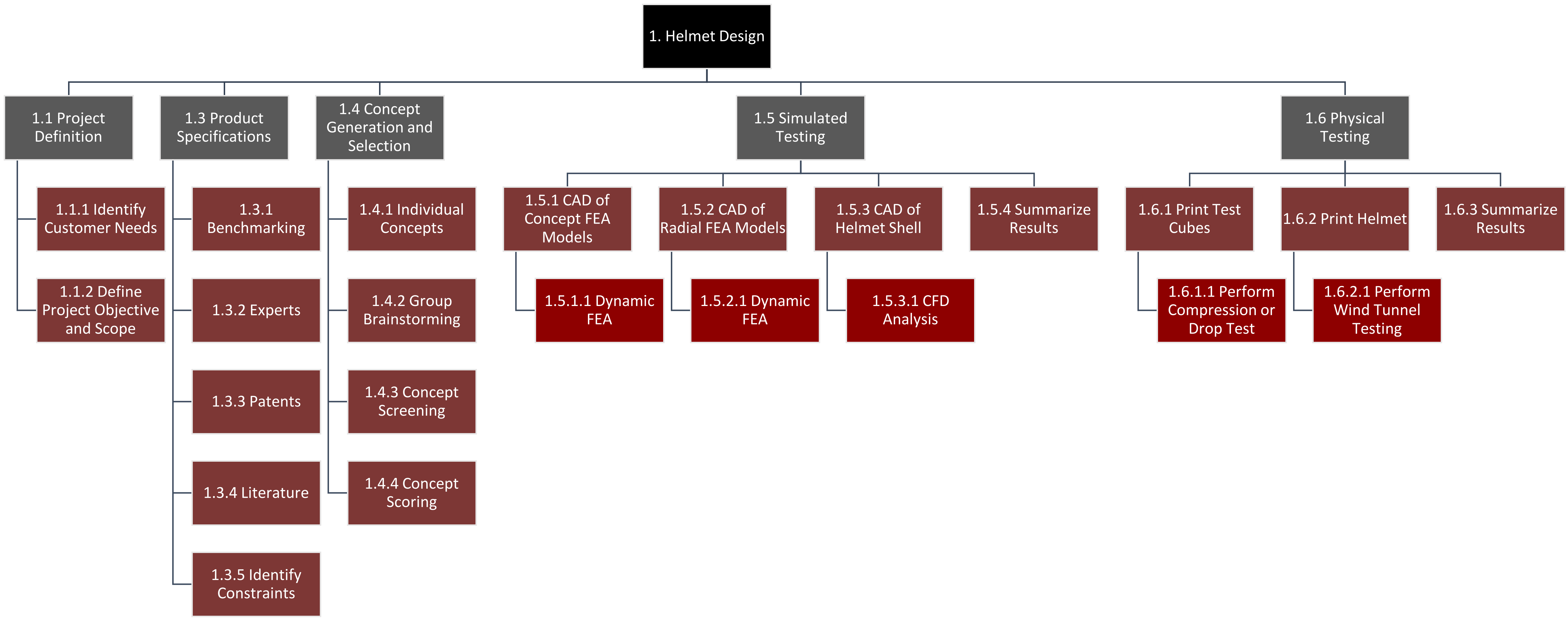

Figure 7: WBS for the project design.

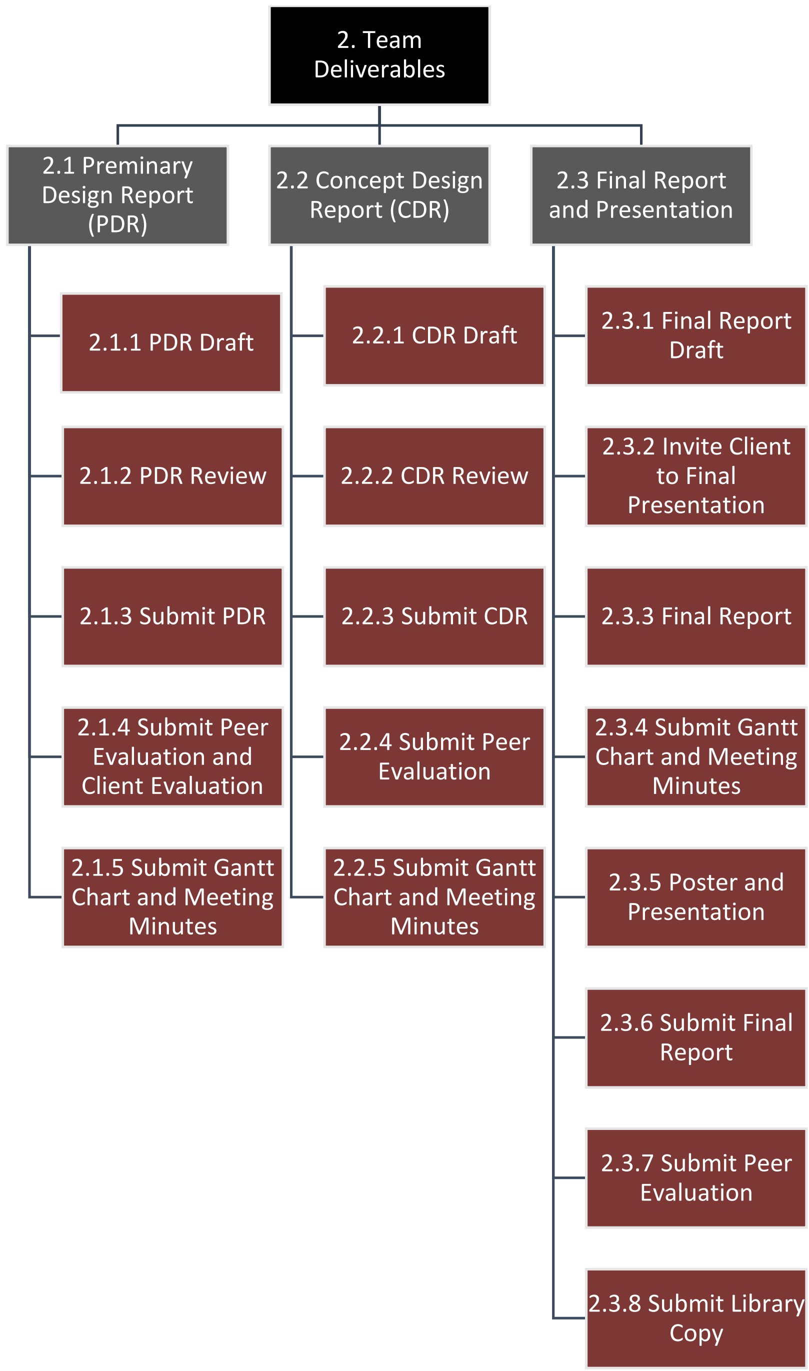

Figure 8: WBS for the project deliverables.

A tentative schedule was created at the beginning of the project as a means of tracking progress. Since the original schedule was set, some slipping had occurred as shown by the black horizontal lines in the Gantt chart in Figure 24. The slip in the schedule was mainly due to the fact that the team could not properly score the concepts without modeling each concept and performing preliminary compression analysis. The concepts resulting from brainstorming were all modelled and were also designed with the same volumetric dimensions and mass for potential FEA analysis. The added time to model the rectangular lattice FEA models and the preliminary impact FEA for the concept scoring added a significant amount of time to the original schedule. The primary method for dealing with the time slip was to compress the lead times for the 3D printing of lattice test cubes and helmet for impact testing and wind tunnel testing respectively.

Eventually, the wind tunnel testing and drop testing were removed from the schedule, hence they are no longer included in the Gantt chart shown in Figure 9. The FEA and CFD analysis for design optimization required more time than initially anticipated. The team had to work with unfamiliar software and run several iterations for each design modification. Furthermore, the physical tests were not required by Precision ADM and only served to validate the helmet's final design specifications. Consequently, physical testing was removed from the project scope and schedule.

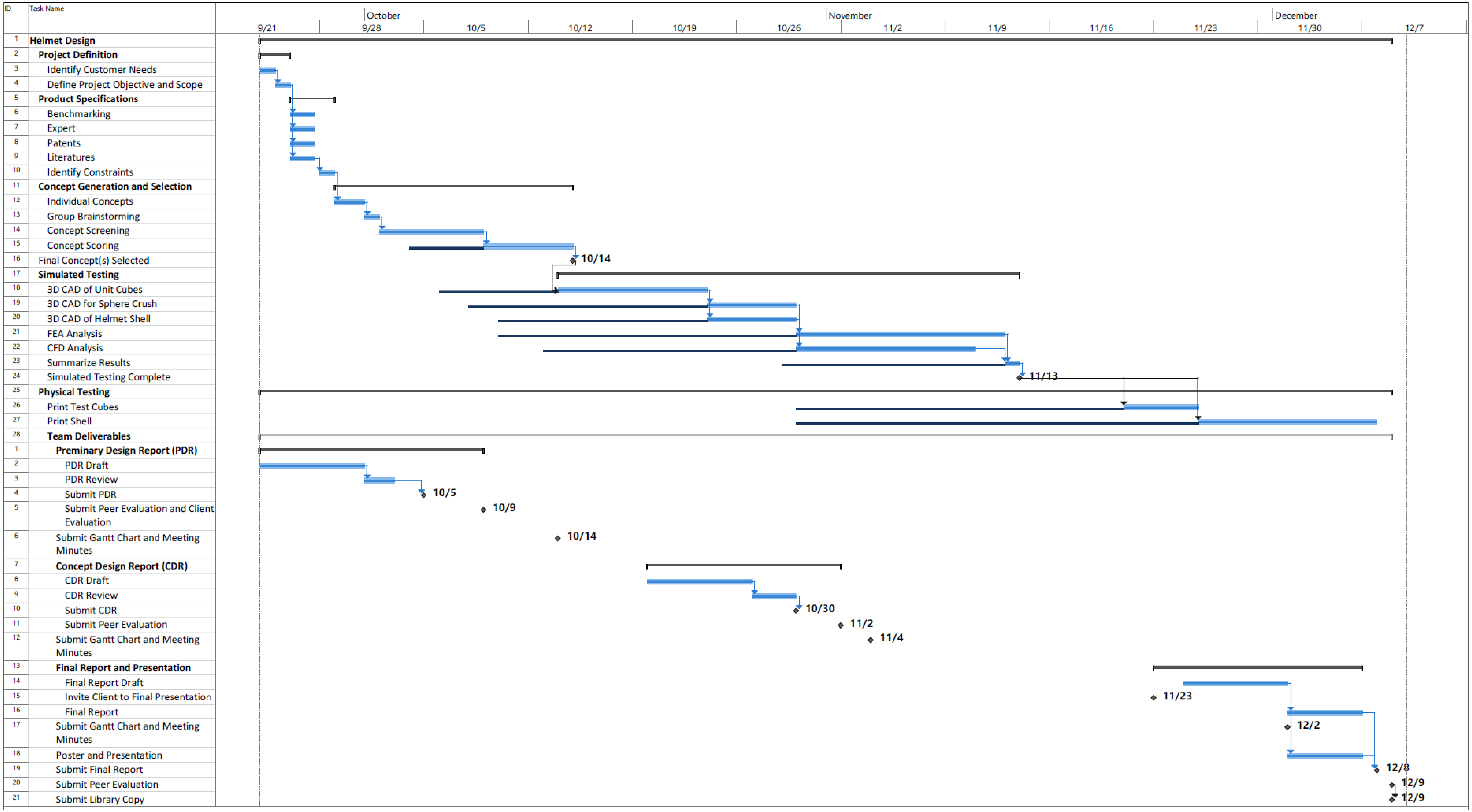

Figure 9: Final Gantt chart for project schedule

Appendix D: **SolidWorks FEA for Concept Screening**

Seventeen concepts were considered for the lattice structure of the bicycle helmet. The screening process for the concepts included assigning values of 1 to 5 for two categories: simplicity and energy absorption ability. The top five concepts were considered for further concept scoring. To aid in the visualization of how the lattice structure responds to an applied load, rectangular finite element analysis (FEA) models were designed using SolidWorks. Concepts with 8x8x3 cm dimensions were modelled and static FEA was performed. To standardize the FEA process, a static load of 300 N was applied with a semi-fine mesh. Acrylonitrile butadiene styrene (ABS) used as the material. The samples were also made to have a weight of 50 +/- 1g. The stress and displacement plots were then collected and aided in the concept screening. The stress and displacement plots are summarized in TABLE VIII.

TABLE VIII: STRESS AND DISPLACEMENT PLOTS FOR CONCEPT SCREENING

<table>
<tr><th colspan="2">Concept 1 – Offset Boxes</th></tr>
<tr><td>Stress Plot</td><td>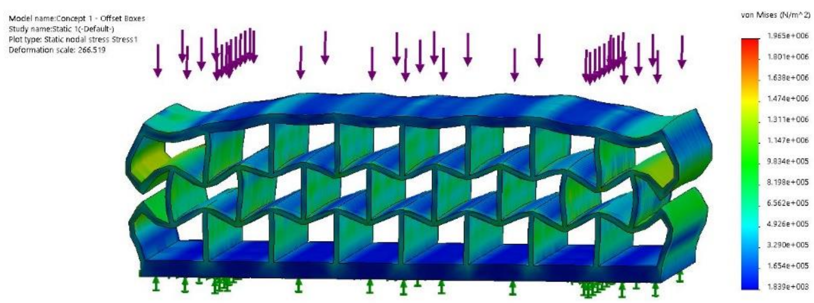
</td></tr>
<tr><td>Displacement Plot</td><td>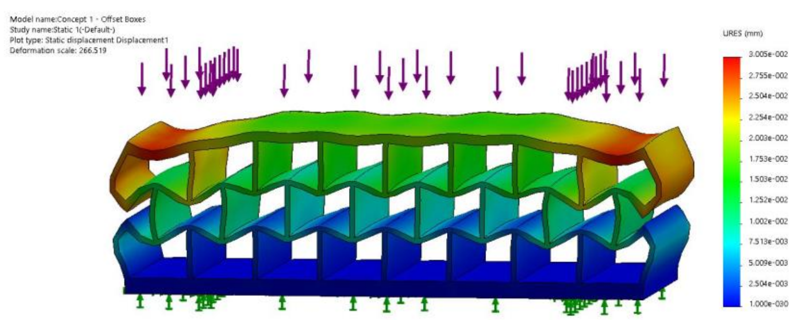
</td></tr>
</table>

Concept 2 – Aligned Boxes

Stress Plot

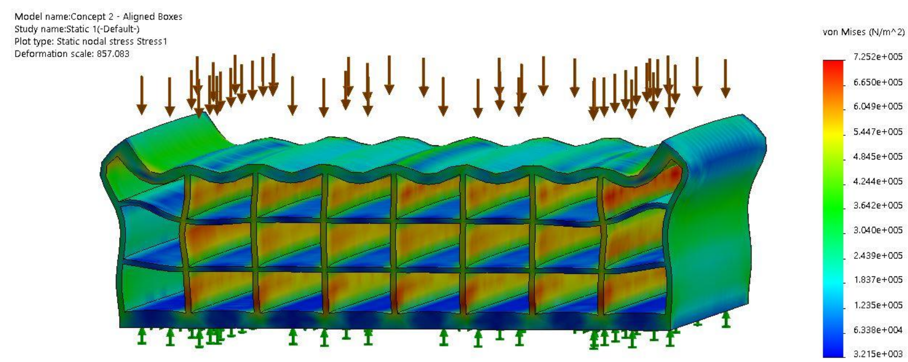

Displacement Plot

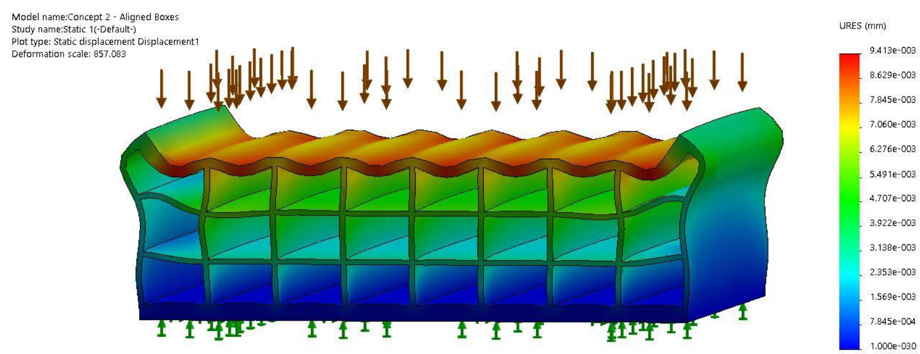

Concept 3 – Offset Triangles

Stress Plot

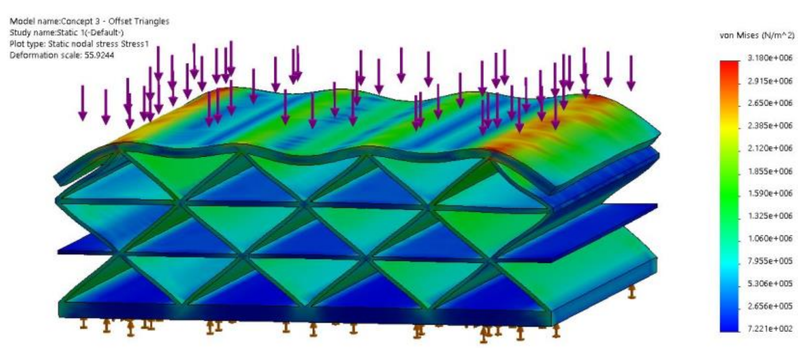

<table>
<tr>
<td>Displacement Plot</td>
<td>
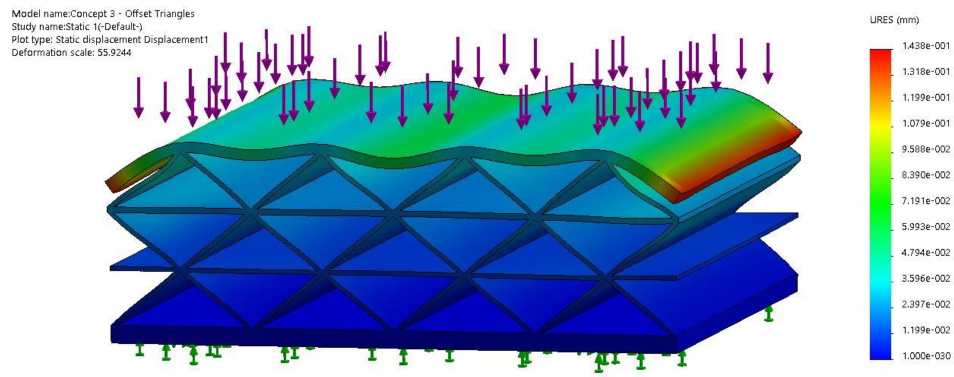

</td>
</tr>
<tr>
<td colspan="2">Concept 4 – Aligned Triangles</td>
</tr>
<tr>
<td>Stress Plot</td>
<td>
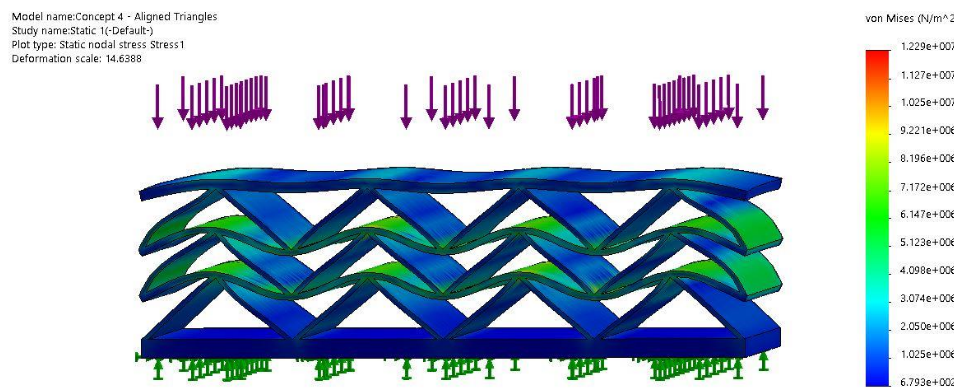

</td>
</tr>
<tr>
<td>Displacement Plot</td>
<td>
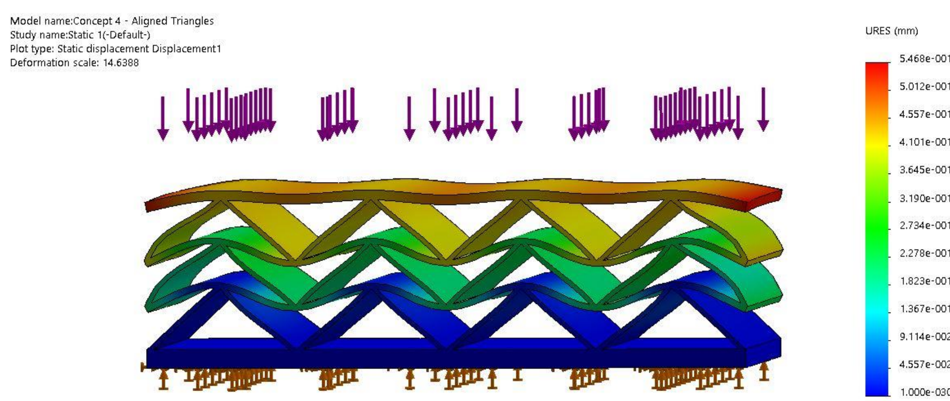

</td>
</tr>
</table>

Concept 5 – Offset Circles

Stress Plot

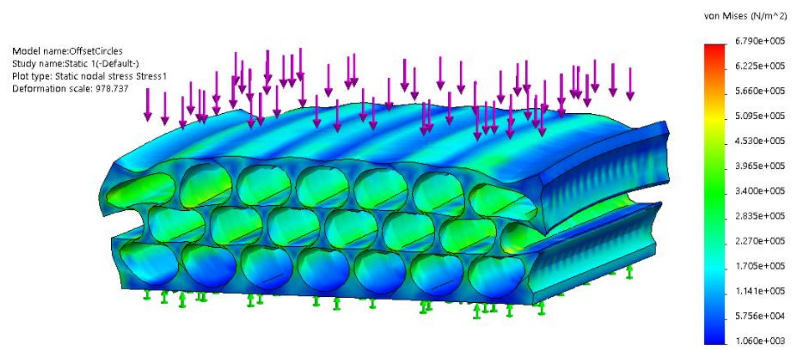

Displacement Plot

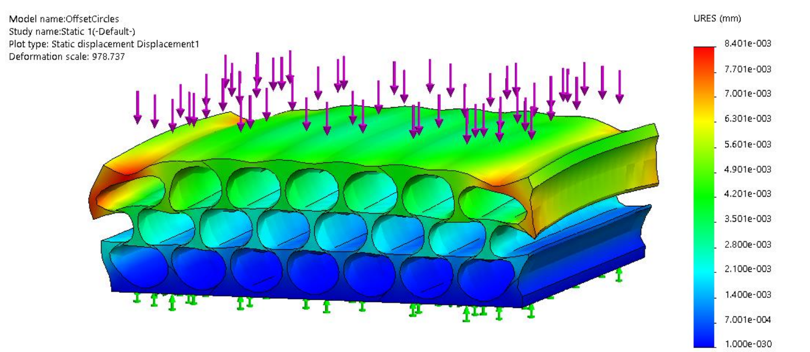

Concept 6 – Aligned Circles

Stress Plot

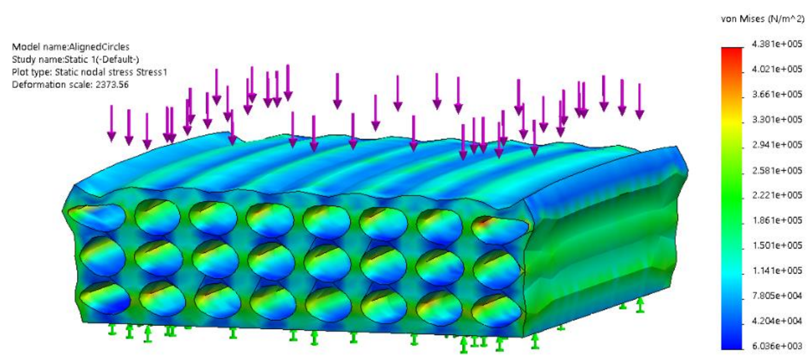

<table>
<tr><td>Displacement
Plot</td><td>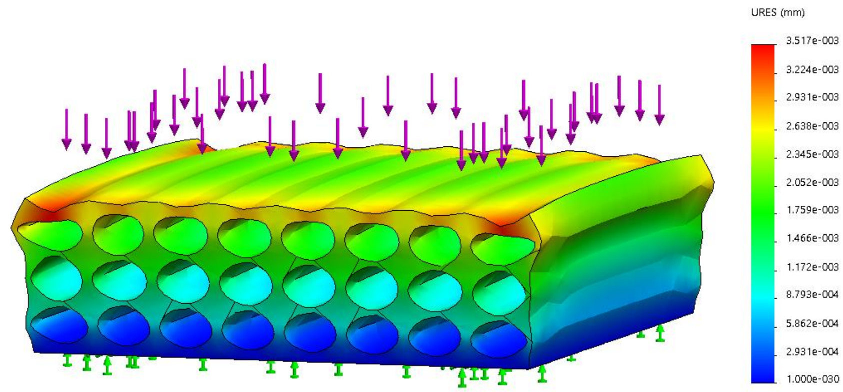
</td></tr>
<tr><td colspan="2">Concept 7 – Aligned Hexagons</td></tr>
<tr><td>Stress Plot</td><td>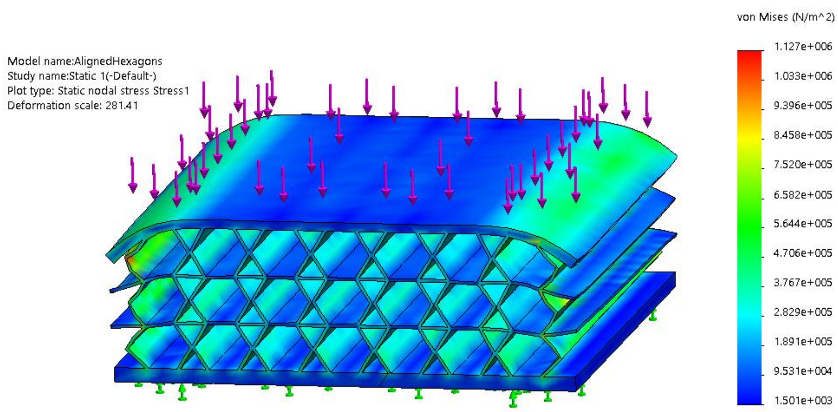
</td></tr>
<tr><td>Displacement
Plot</td><td>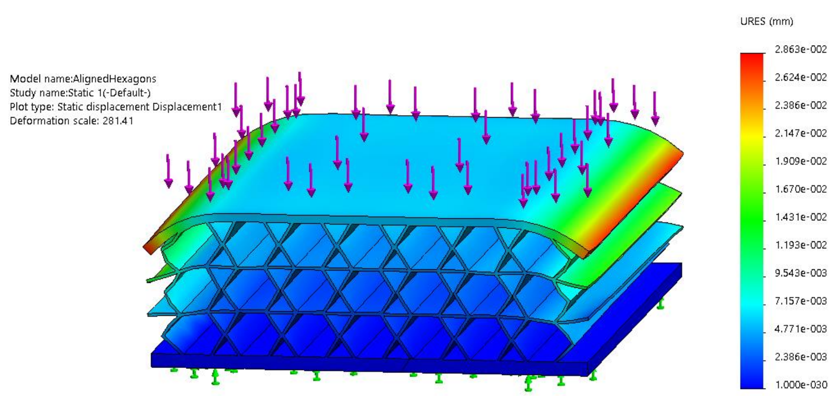
</td></tr>
</table>

Concept 8 – Spaced Hexagons

Stress Plot

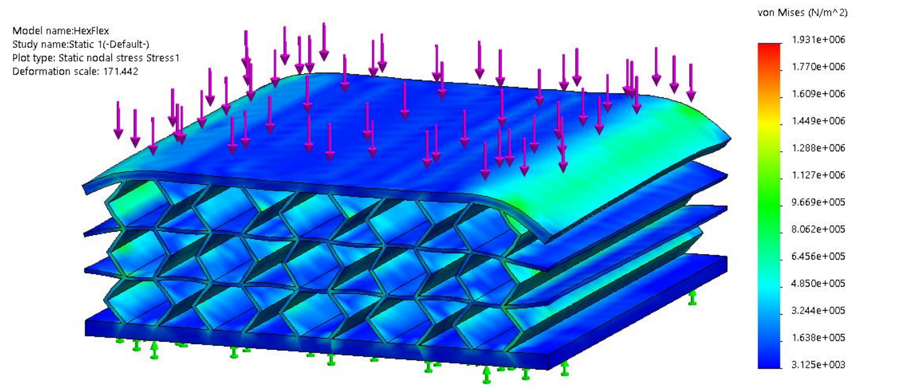

Displacement Plot

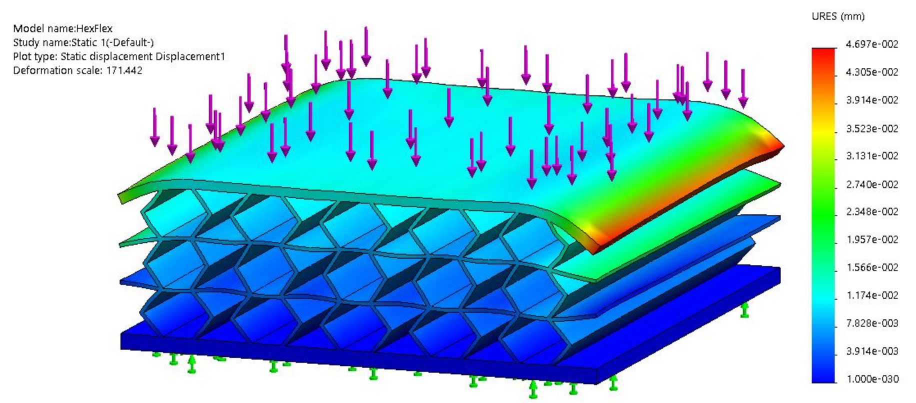

Concept 9 - Honeycomb

Stress Plot

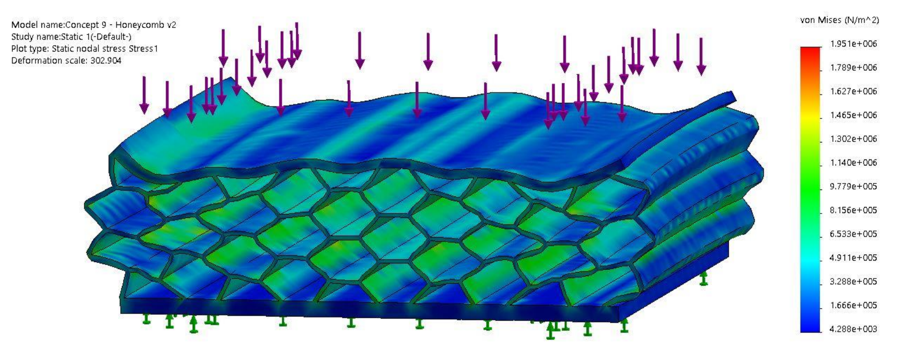

<table>
<tr><td>Displacement Plot</td><td>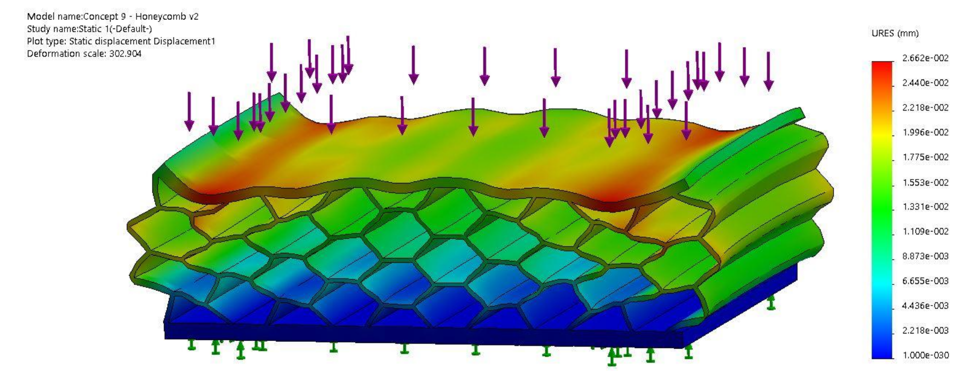
</td></tr>
<tr><td colspan="2">Concept 10 – Octet Truss</td></tr>
<tr><td>Stress Plot</td><td>Unable to mesh</td></tr>
<tr><td>Displacement Plot</td><td>Unable to mesh</td></tr>
<tr><td colspan="2">Concept 11 – 3D Kagome Structure</td></tr>
<tr><td>Stress Plot</td><td>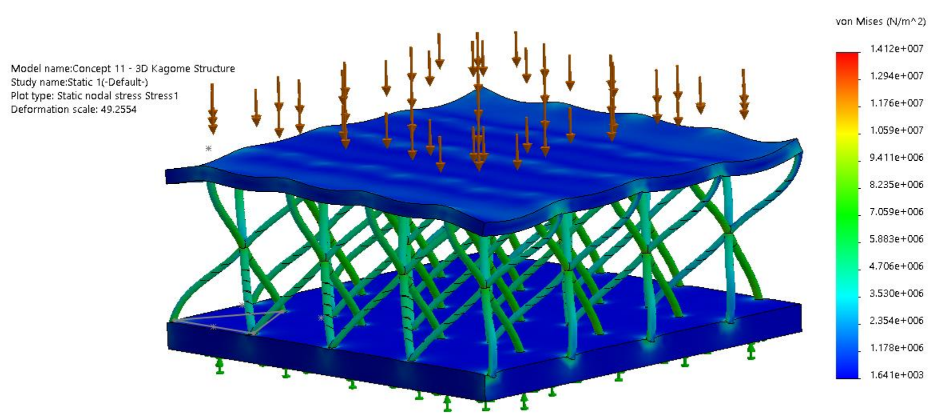
</td></tr>
</table>

<table>
<tr><td>Displacement
Plot</td><td>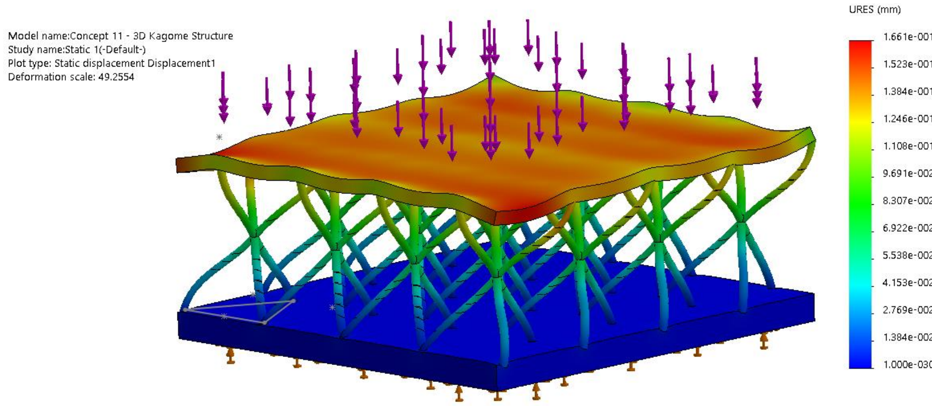
</td></tr>
<tr><td colspan="2">Concept 12 – Cubic Nodal Lattice</td></tr>
<tr><td>Stress Plot</td><td>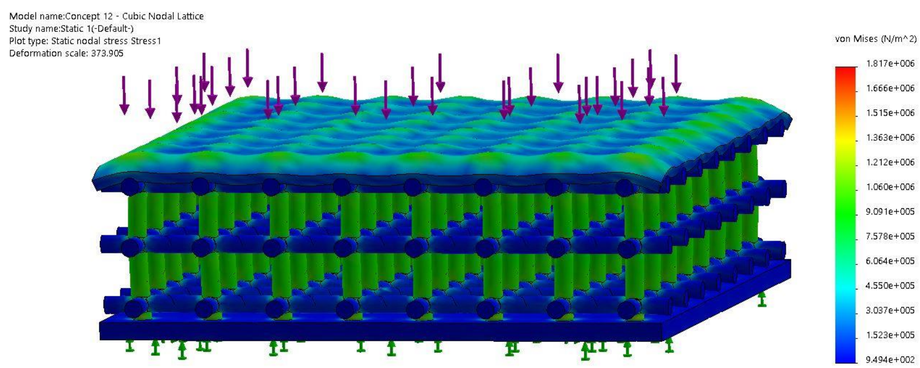
</td></tr>
<tr><td>Displacement
Plot</td><td>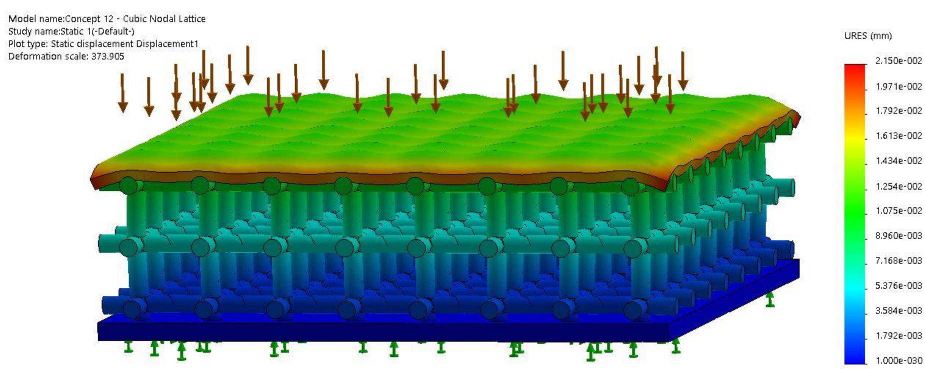
</td></tr>
</table>

Concept 13 - Pillars	
Stress Plot	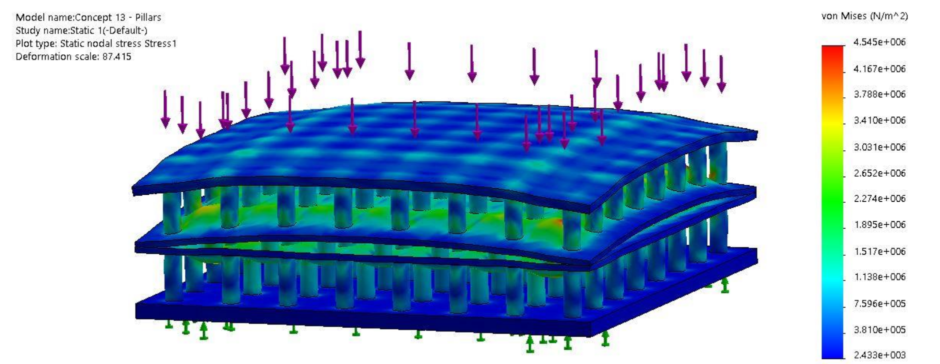
Displacement Plot	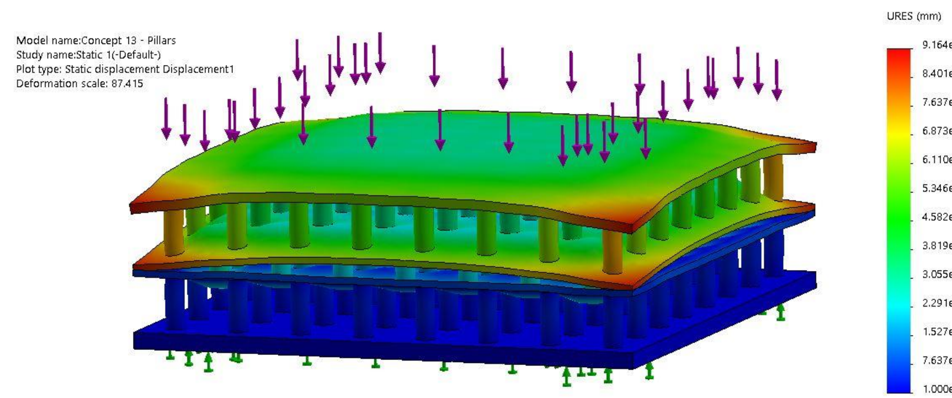
Concept 14 Lateral Voids	
Stress Plot	Not Designed
Displacement Plot	Not Designed

Concept 15 – Asterisk Lattice	
Stress Plot	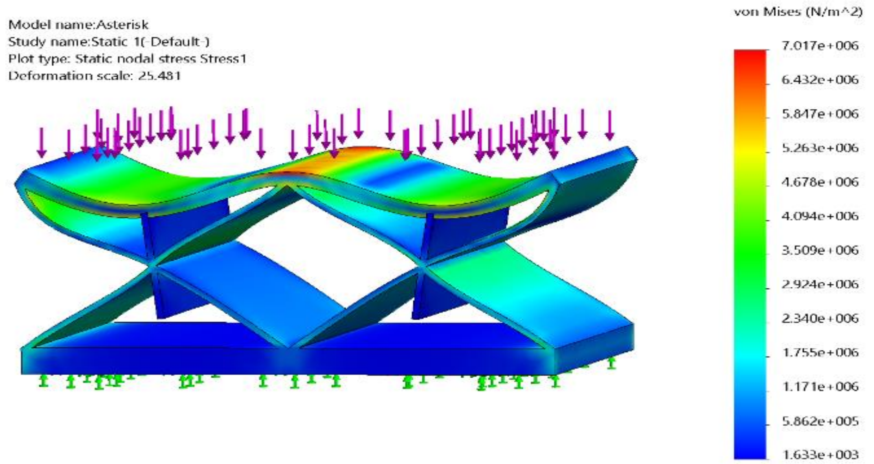
Displacement Plot	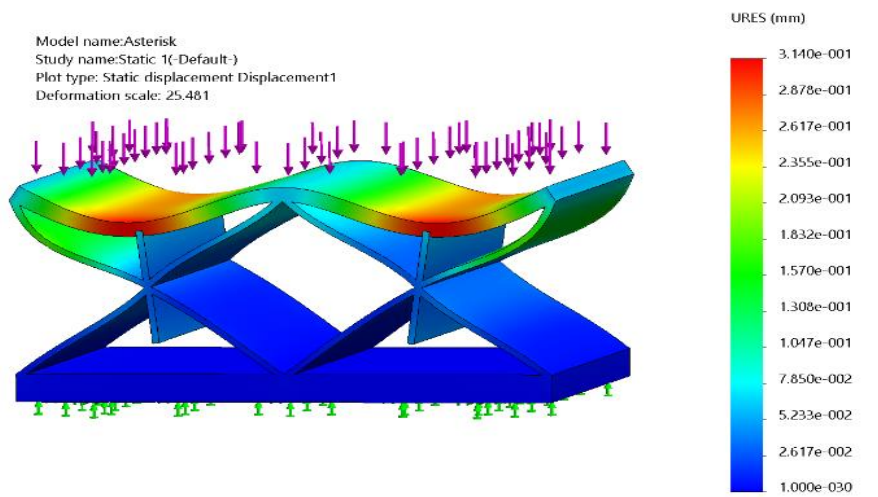

Appendix E: **Generated Mesh for Concept Impact FEA**

A tetrahedral mesh was automatically generated for each concept FEA model. A seed size of 0.0023 meters was used. The generated mesh for concepts 1, 4, 8, 9, and 13 are shown in Figure 10 to Figure 14.

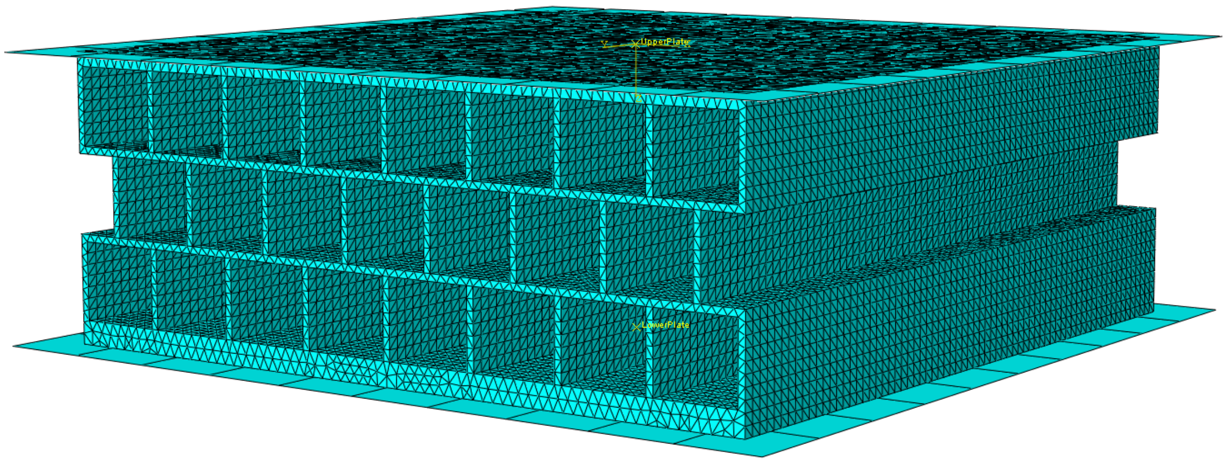

Figure 10: Generated Tetrahedral Solid Mesh of Concept 1 with a 0.0023 meter Seed Size

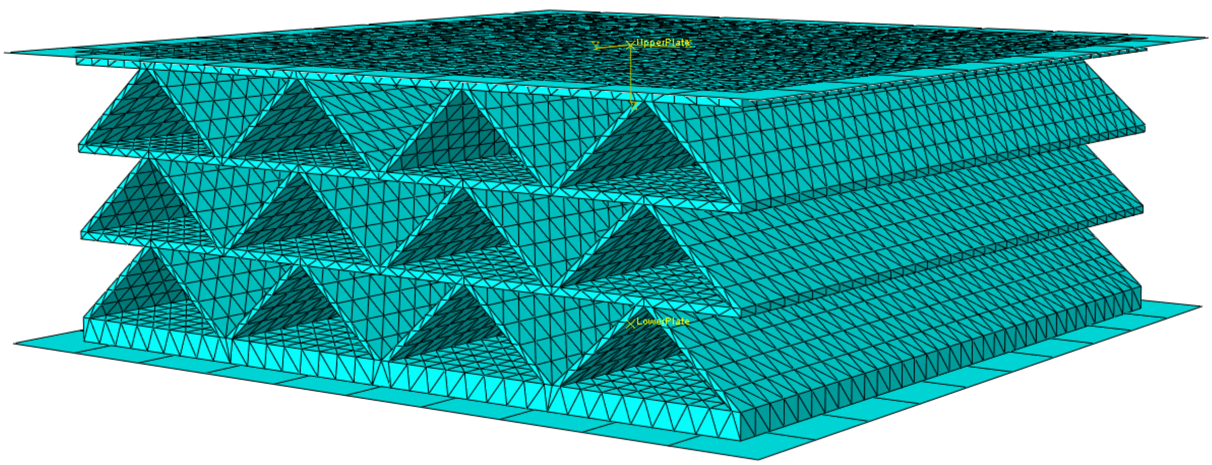

Figure 11: Generated Tetrahedral Solid Mesh of Concept 4 with a 0.0023 meter Seed Size

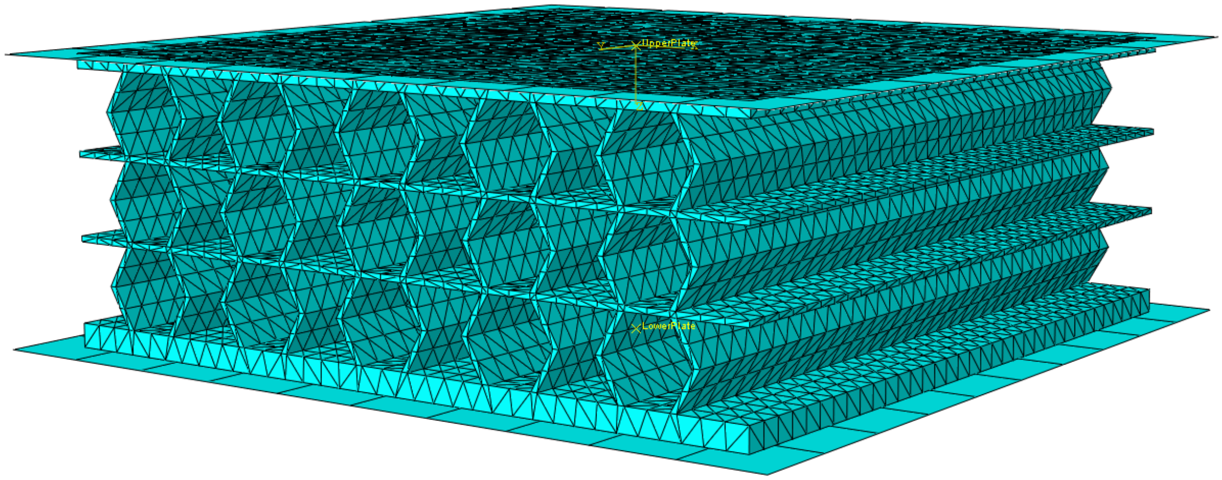

Figure 12: Generated Tetrahedral Solid Mesh of Concept 8 with a 0.0023 meter Seed Size

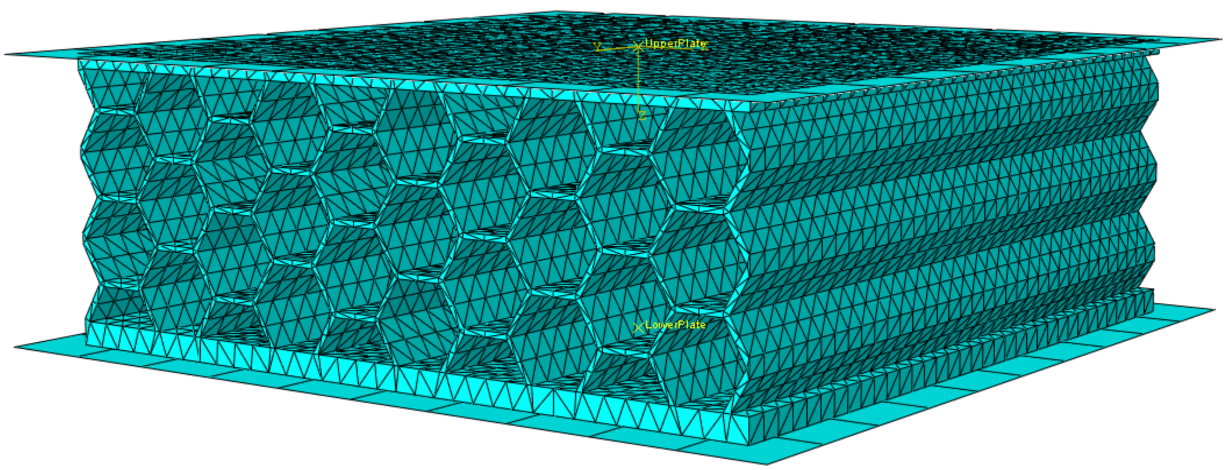

Figure 13: Generated Tetrahedral Solid Mesh of Concept 9 with a 0.0023 meter Seed Size

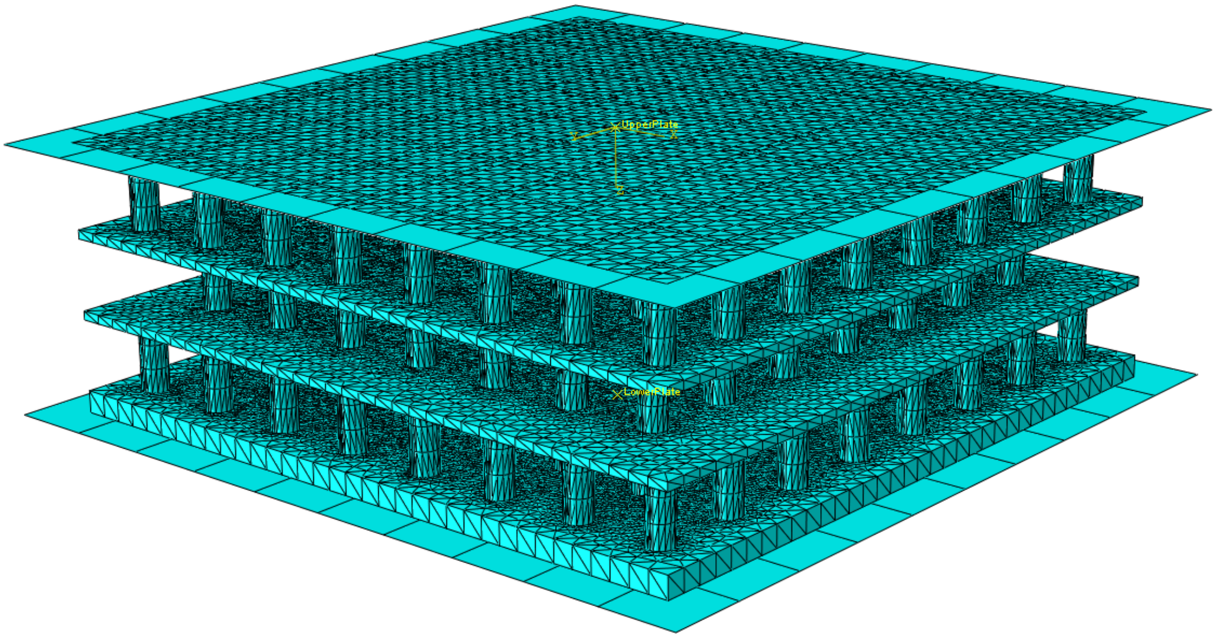

Figure 14: Generated Tetrahedral Solid Mesh of Concept 13 with a 0.0023 meter Seed Size

Appendix F: **Technical Drawings for Helmet**

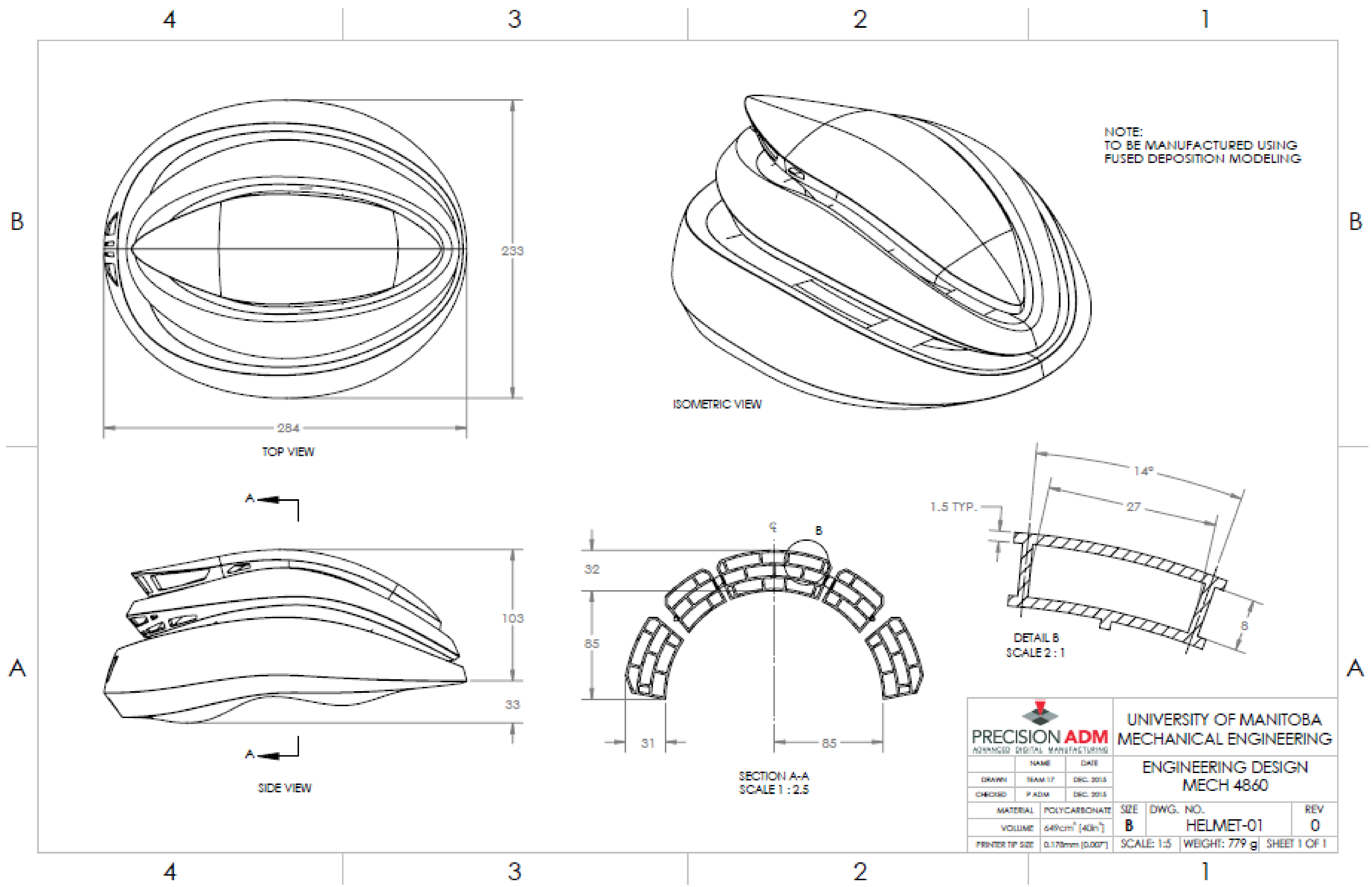

Appendix G: **References**

[1] S. K. Moon, Y. E. Tan, J. Hwang and Y.-J. Yoon, "*Application of 3D Printing Technology for Designing Light-weight Unmanned Aerial Vehicle Wing Structure*," *International Journal of Precsision Engineering and Manufacturing-Green Technology,* vol. 1, no. 3, pp. 223-228, 2014.

[2] S. Soe, P. Martin, M. Jones, M. Robinson and P. Theobald, "*Feasibility of optimising bicycle helmet design safety through the use of additive manufacturing TPE cellular structures*," *International Journal of Advance Manufacturing Technology,* no. 79, pp. 1975-1982, 2015.

[3] D. B. R. W. a. R. H. J Brennan-Craddock, "*The design of impact absorbing structures for additive manufacture*," *Journal of Physics,* vol. 382, p. 7, 2012.

[4] F. Alam, A. Subic and A. Akbarzadeh, "*Aerodynamics of Bicycle Helmets (P68)*," in *The Engineering of Sport 7*, Paris, Springer, 2008, pp. 337-344.

[5] Stratasys, "*FORTUS PC (Polycarbonate) Characterization of Material Properties*," Stratasys, Eden Prairie, 2013.

[6] Stratasys, "*FORTUS ABS-M30 Characterization of Material Properties*," Stratsys, Eden Prairie, 2013.

[7] H. Chowdhury and F. Alam, "*An experimental study on aerodynamic performance of time trial bicycle helmets*," *Sports Engineering,* vol. 17, pp. 165-170, 2014.

[8] stratasys.com, "*FDM Thermoplastics*," Stratasys, 2015. [Online]. Available: http://www.stratasys.com/materials/fdm. [27 September 2015].

Appendix for Final Design Report

Table of Contents

List of Figures

List of Tables

Appendix A: Research

Literature research and competitor benchmarking are crucial components for gathering information that can be applied towards the design of the helmet. The helmet design research was divided into three key areas: the lattice structure, ventilation, and the material properties.

Appendix A.1. Lattice Design

A study by Moon *et al.* investigated the optimal elastic performance of three lattice structures for the development of a deployable UAV wing design [1]. The team compared three lattice structures: 3D Kagome, 3D pyramidal, and hexagonal diamond structures, as illustrated in Figure 1

[redacted]

Figure 1: 3D Lattice structures analyzed by Moon et al. [1].

The structures were compared in a compression test and the results showed that the 3D Kagome structure had the highest load capacity, but the hexagonal diamond exhibited the ideal energy absorption properties.

Another informative journal article written by Soe *et al.* studied the application of 3D printing for bicycle helmets [2]. Using thermoplastic elastomers (TPE) and selective laser sintering (SLS), the Soe team evaluated the energy absorption capabilities of the lattice structures illustrated in Figure 2.

[redacted]

Figure 2: The three energy absorbing layers [2].

The study used dynamic FEA to simulate an impact similar to the requirements for this project [2]. A simplified helmet was modeled with an inner and outer shell, and an internal lattice structure. Simplified versions of a headform and anvil were modeled to simulate an EN:BS1078 helmet impact test. The helmet model was perfectly fixed to the headform, while the anvil was constrained along its lower surface. The helmet outer shell and anvil were given a frictionless surface to surface contact interaction. A mesh was automatically generated using brick and tetrahedral elements. The headform was given a mass of 4.2 kg and an impact velocity of 2.2 m/s. Soe *et al.* found that peak translational accelerations decreased with a decrease in cellular density, while acceleration pulse durations were increased. These parameters and results could be used as guidelines for our dynamic FEA testing.

Another article related to impact absorbing lattice structure is the work of J Brennan-Craddock *et al.* in "*The Design of Impact Absorbing Structure for Additive Manufacture*" [3]. Although the paper is for body conforming impact protection, the paper is strongly related to the function of a helmet composed of an impact absorbing lattice. The article goes into detail regarding lattice design and the ability of a lattice to conform to curvature. Figure 3 shows four different ways a lattice can be conformed to curved geometry.

Trimmed Swept Meshed Random

Figure 3: Methods of conforming lattice to curvature [12].

Conformity is an important consideration in the design of a lattice structure since the bike helmet will have curvatures of varying radii and ventilation. The far left geometry, known as a “trimmed” conformal method, is not ideal in the case of a bicycle helmet lattice structure because the variability of the trim locations could lead to varying stiffness characteristics. The second “swept” geometry or third “meshed” geometry proved to be more adept at providing uniform stiffness throughout the structure.

Appendix A.2. Helmet Ventilation

The number, position, and shape of vents have an impact on the aerodynamic performance as well as on the heat dissipation characteristics for a bicycle helmet. Firoz Alam and his team at RMIT University conducted a study to determine the thermal comfort and aerodynamic efficiency that bicycle helmets provide. Alam *et al.* analyzed six commercial helmets using an RMIT industrial wind tunnel [4]. Using force sensors, thermocouples, and a mannequin with an integrated heater mat to simulate heat generation, Alam *et al.* were able to conclude that the Giro Advantage helmet had the best aerodynamic performance. They also modified the helmets by taping over certain portions. Alam *et al.* determined that the position of the vents can increase aerodynamic performance while maintaining thermal comfort.

The shape of the venting was also studied by Alam *et al.* Using the same wind tunnel as the previous study, a pitot tube was integrated into the testing apparatus. Using five helmets, the venturi shape of the venting holes was measured and the effect on the aerodynamic drag was measured. Alam *et al.* concluded that an increase in venturi effectiveness correlated to higher aerodynamic drag [4].

Appendix A.3. Materials

Information for the material properties based on the environmental conditions are explained in this section.

Appendix A.3.1: Environmental Conditions Effects on Material Properties

Stratasys performed extensive testing to determine the effects that the environment has on the material properties of polycarbonate (PC) [5] and ABS-M30 [6]. Test samples were stored in three conditions: dry (15% relative humidity), wet (immersed in water), and controlled (50% relative humidity). Test samples were made to a 0.18 mm slice height, using a T12 printer tip, and produced using the Fortus 400mc 3D production system. After the test samples were conditioned, the material properties for tensile strength, flexural modulus, and percent elongation break were measured. Stratasys tested 10 samples for the three mechanical properties using IS0 527 and IS0 178 testing standards. The results show that the tensile strengths of the PC and ABS-M30 decreases as the temperature of the polymers is increased, as shown in Figure 4.

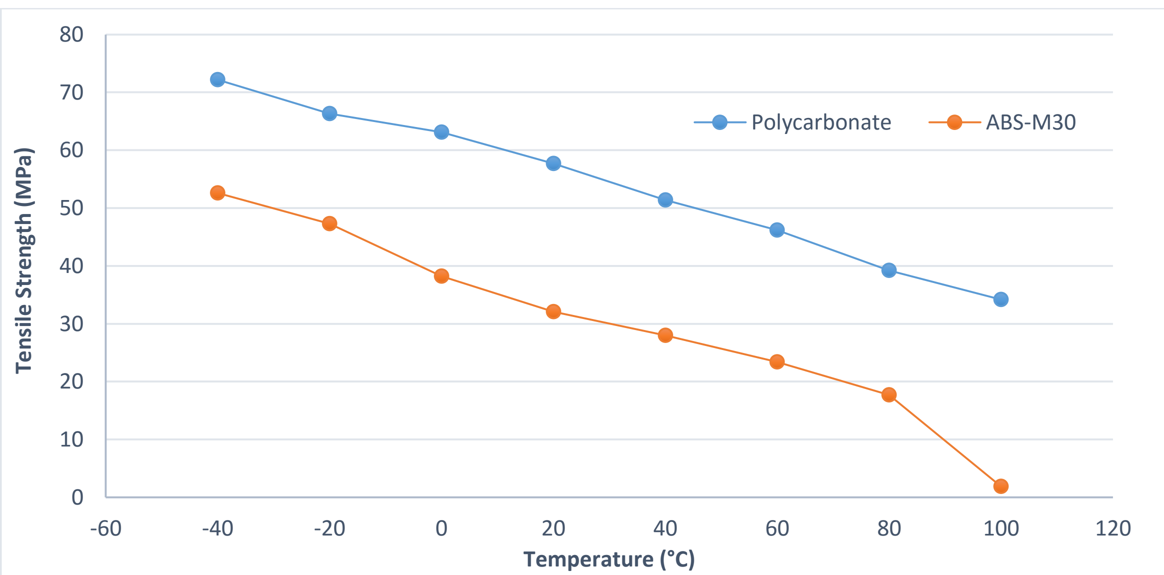

Figure 4: Tensile strength as function of temperature for polycarbonate and ABS-M30 [6] [5].

The tensile strength ranges between 72.2 to 34.2 MPa for PC. and 52.6 to 1.9 MPa for ABS-M30 throughout the given temperature range. The flexural modulus of PC and ABS-M30 follow the same trend as the tensile strength; however, ABS-M30 does have a significant drop in flexural modulus at 100 °C. Polycarbonate has a value of 1671 MPa while ABS-M30 has a value of 1154 MPa at 100 °C. The trends are shown in Figure 5.

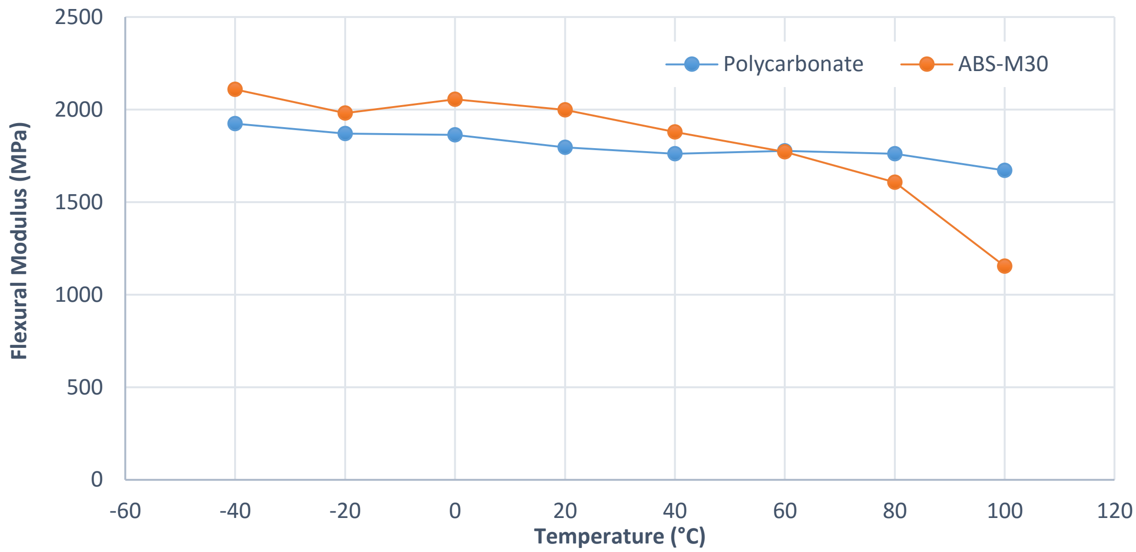

Figure 5: Flexural modulus as a function of temperature for polycarbonate and ABS-M30 [6] [5].

The percent elongation at break for PC has a downward trend ranging from 10.4% to 4% as the temperature was increased, while ABS-M30 has an overall increase in elongation ranging from 5.3% to 8.7%.

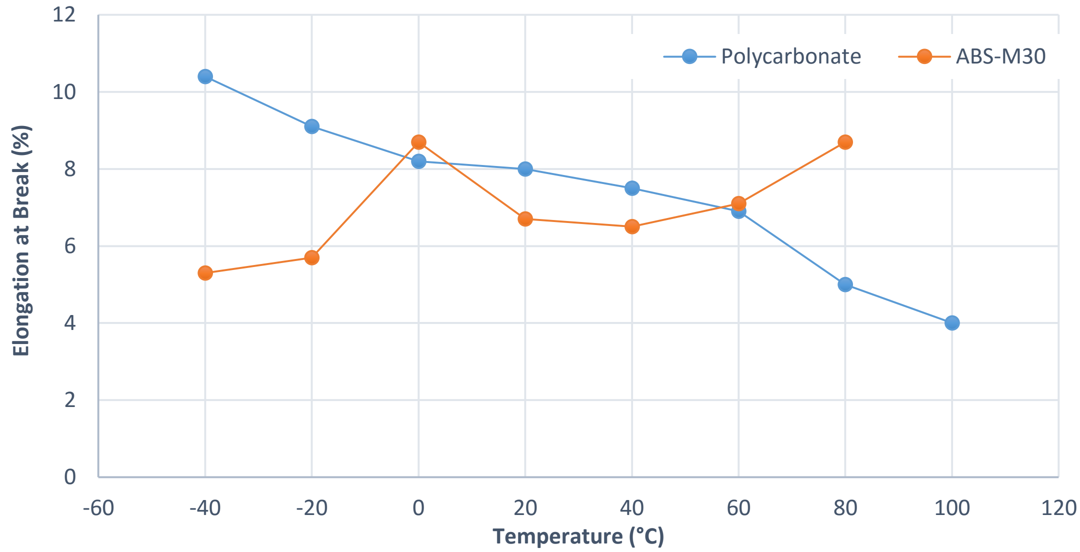

Figure 6: Elongation at break as function of temperature for polycarbonate and ABS-M30 [6] [5].

The graphical data shown was for the controlled sample pieces, and the tabulated values are shown below.

The effects of temperature and material properties are tabulated in TABLE I, TABLE II and TABLE III for tensile strength, flexural modulus, and percent elongation at break for polycarbonate.

TABLE I: ENVIRONMENTAL EFFECTS ON TENSILE STRENGTH OF POLYCARBONATE [5]

Condition	Tensile Strength (MPa)		Temperature (°C)				
Wet	55.2	Condition	-40	0	40	80	120
Dry	56.9	Wet	71.5	60.3	49.2	37.7	27.2
Controlled	57.7	Dry	70.3	62.2	51.7	40	28.6
* 20 Deg. C 4 week old sample		Controlled	72.2	63.1	51.4	39.2	26.4

TABLE II: ENVIRONMENTAL EFFECTS ON FLEXURAL MODULUS OF POLYCARBONATE [5]

Condition	Flexural Modulus (MPa)		Temperature (°C)				
Wet	1799	Condition	-40	0	40	80	120
Dry	1818	Wet	2274	1850	1771	1714	1633
Controlled	1797	Dry	1819	1808	1829	1742	1659
* 20 Deg. C 4 week old sample		Controlled	1924	1863	1762	1761	1625

TABLE III: ENVIRONMENTAL EFFECTS ON ELONGATION AT BREAK OF POLYCARBONATE [5]

Condition	Elongation Break (%)	Temperature (°C)					
Wet	7.9	Condition	-40	0	40	80	120
Dry	8	Wet	10.5	8.6	6.6	6.3	3.9
Controlled	8	Dry	9.2	8.6	7.6	7.2	3.9
* 20 Deg. C 4 week old sample		Controlled	10.4	8.2	7.5	5	2.9

The effects of temperature and material properties are tabulated in TABLE IV, TABLE V, and TABLE VI for tensile strength, flexural modulus, and percent elongation at break for ABS M-30.

TABLE IV: ENVIRONMENTAL EFFECTS ON TENSILE STRENGTH OF ABS-M30 [6]

Condition	Tensile Strength (MPa)	Temperature (°C)					
Wet	33.8	Condition	-40	0	40	80	100
Dry	31.8	Wet	50.1	43.6	27.2	14.9	0.4
Controlled	32.1	Dry	49.7	37.5	28.5	18.3	2.6
* 20 Deg. C 4 week old sample		Controlled	52.6	38.2	28	17.9	2.8

TABLE V: ENVIRONMENTAL FLEXURAL MODULUS OF ABS-M30 [6]

Condition	Flexural Modulus (MPa)	Temperature (°C)					
Wet	1949	Condition	-40	0	40	80	100
Dry	1909	Wet	2347	2047	1862	1367	161
Controlled	1999	Dry	2403	1964	1937	1477	999
* 20 Deg. C 4 week old sample		Controlled	2109	2055	1879	1607	1154

TABLE VI: ENVIRONMENTAL ELONGATION AT BREAK OF ABS-30 [6]

Condition	Elongation of Break (%)	Temperature (°C)					
Wet	5	Condition	-40	0	40	80	100
Dry	6.7	Wet	4.1	4.8	5.7	3.1	0
Controlled	6.7	Dry	4.7	8.7	7.6	7.3	0
* 20 Deg. C 4 week old sample		Controlled	5.3	8.7	6.5	8.7	0

In addition to literature research, consumer reviews were found in bicycle magazines and collected to create a set of competitor data that includes durability, affordability, and subjective values such as comfort [6]. These results, combined with the values obtained from the literature reviews, allowed for the production of marginal and ideal values that the helmet can be compared to.

Appendix B: **House of Quality**

Now that the client's needs and corresponding metrics have been defined in addition to collecting literature research and competitor benchmarking information, a house of quality (HOQ) can be created to visually represent the relation between all of our collected data.

First, the HOQ relationships between the needs and metrics must be established. The relationships were assigned values of 1, 3, and 9 to evaluate the strength of those relationships. A value of 1 is a weak relationship while a value of 9 is a strong relationship. For example, the "helmet is affordable to customer" need has a strong relationship with the cost of the helmet, and a value of 9 was given. Additionally, the relationship between metrics were also quantified. For example, head temperature and drag coefficient would have a negative relationship, because a decrease in head temperature would relate to an increase in ventilation. Consequently, an increase ventilation would result in increase in aerodynamic drag coefficient.

All the metrics, needs, constraints and benchmarking relationship data was collected in the HOQ, which is shown in TABLE VII. For values that are left blank, the correlating data was not available.

TABLE VII: HOUSE OF QUALITY FOR THE 3D PRINTED BICYCLE HELMET

Legend

θ	Strong Relationship
o	Moderate Relationship
Δ	Weak Relationship
++	Strong Positive Correlation
+	Positive Correlation
–	Negative Correlation
v	Strong Negative Correlation
↓	Objective Is to Minimize
↑	Objective is to Maximize
X	Objective is to Hit Target

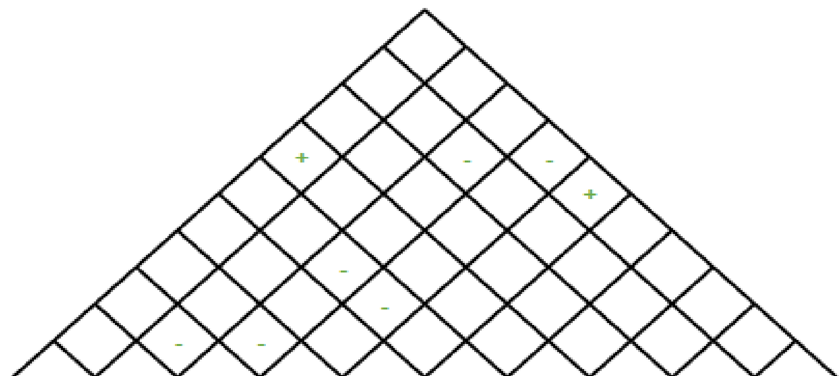

Row #	Relative Weight	Weight/Importance	Demand Quality (Customer Needs) / Quality Characteristics	Cost [$ CAD]	Impact Deceleration [G-Force]	Weight [g]	Head Temperature [Celsius]	Field of Vision [Degree]	Drag Coefficient [Non Dimensional]	Helmet is 3D printed [Y/N]	Fits Wearer's Head [sub]	No Pressure Points [sub]	Visually Appealing [sub]
			Column #	1	2	3	4	5	6	7	8	9	10
			Direction of Improvement	↓	↓	↓	↓	↑	↓	X	X	X	X
1	15.15	5.0	Entirely 3D printed		Δ	Δ				θ		o	
2	15.15	5.0	Prevents head injury		θ	o				Δ			
3	12.12	4.0	Provides ventilation to the head				θ		θ				
4	12.12	4.0	Can withstand environmental conditions										
5	9.09	3.0	Does not obstruct vision										
6	9.09	3.0	Helmet is aerodynamic		o		o		θ				
7	9.09	3.0	Helmet is lightweight		θ	θ			o			Δ	
8	9.09	3.0	Helmet is visually appealing										θ
9	6.06	2.0	Helmet is affordable to customer	θ						o			
10	3.03	1.0	Helmet is comfortable			Δ	Δ	Δ			θ	θ	
			Target or Limit Value	1500	300	252	29.1	105	0.27	Yes	1	4	4
			Relative Difficulty (1=Easy to Accomplish, 10=Extremely)	4	8	7	7	2	8	5	3	3	5
			Weight/Importance	54.5	236.3	145.5	115.1	3.0	145.4	169.7	27.3	81.8	81.8
			Relative Weight	5.1	22.3	13.7	10.9	0.3	13.7	16.0	2.6	7.7	7.7
			Rank	8	1	3	5	10	4	2	9	7	6

Competivive Analysis
(0=Worst, 5 = Best)

Row #	Biosystems Helmet	Bell Array	Bell Star Pro	Giro Advantage	Giro Aeon	Giro Atmos	Giro Synthe Helmet	Kask Vertigo	LG Rocket	Limar UltraLight	POC Octal
1	1	0	0	0	0	0	0	0	0	0	0
2			4			4	3		4	4	5
3	2				5	5		4			5
4	3				2	3		4			4
5	5	5	5	5	5	5	5	5	5	5	5
6				3		5					
7	0		2		5	5	3	3	5	5	5
8	2										
9	1	5	1				1		2	2	1
10	1				4	4		3			3

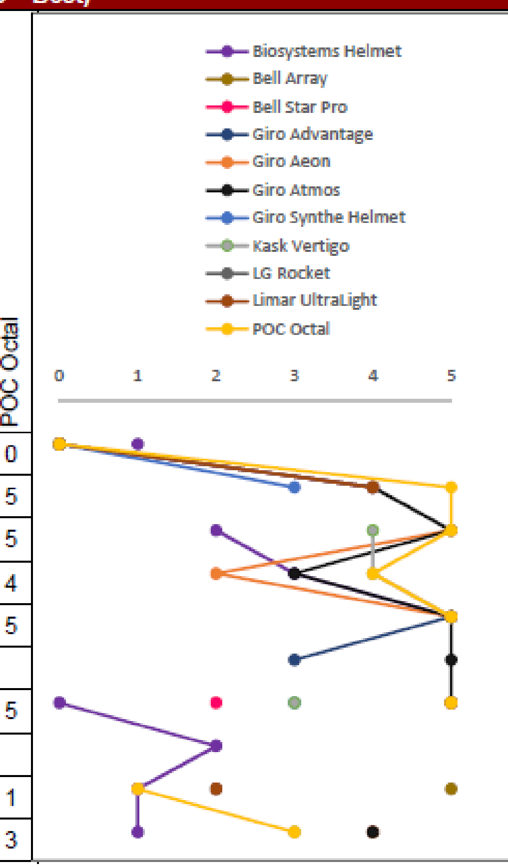

University of Manitoba

PRECISION ADM
ADVANCED DIGITAL MANUFACTURING

The relative weights of the metrics are summarized in the HOQ, then ranked for importance. The *Impact Deceleration* received a rank of 1, which indicates that impact deceleration of the helmet is priority for the design. The quality characteristics *Fits Wearer's Head* and *Field of Vision* have the lowest ranks, as these aspects are not as important.

The graph on the right of the HOQ aids in the visualization of the needs that certain competitor helmets exceed in. For example, the Giro Atoms outlined in black has values that range from 0 to 5 for the given client needs, which is tracked by the graph in the HOQ. The helmets that scored values of 4 or 5 in the client's needs were used as a basis for the target values.

Appendix C: **Project Schedule**

The team had an overall timeline from September 24th to December 9th for the completion of the project. The project is broken down into two work breakdown structures (WBS): one for the Helmet Design and another for the Team Deliverables as shown in Figure 22 and Figure 23, respectively. The Helmet Design WBS breaks down the deliverables needed to conceptualize, build, and test our designs whereas the Team Deliverables WBS shows the deliverables required by the client to document and present the design work.

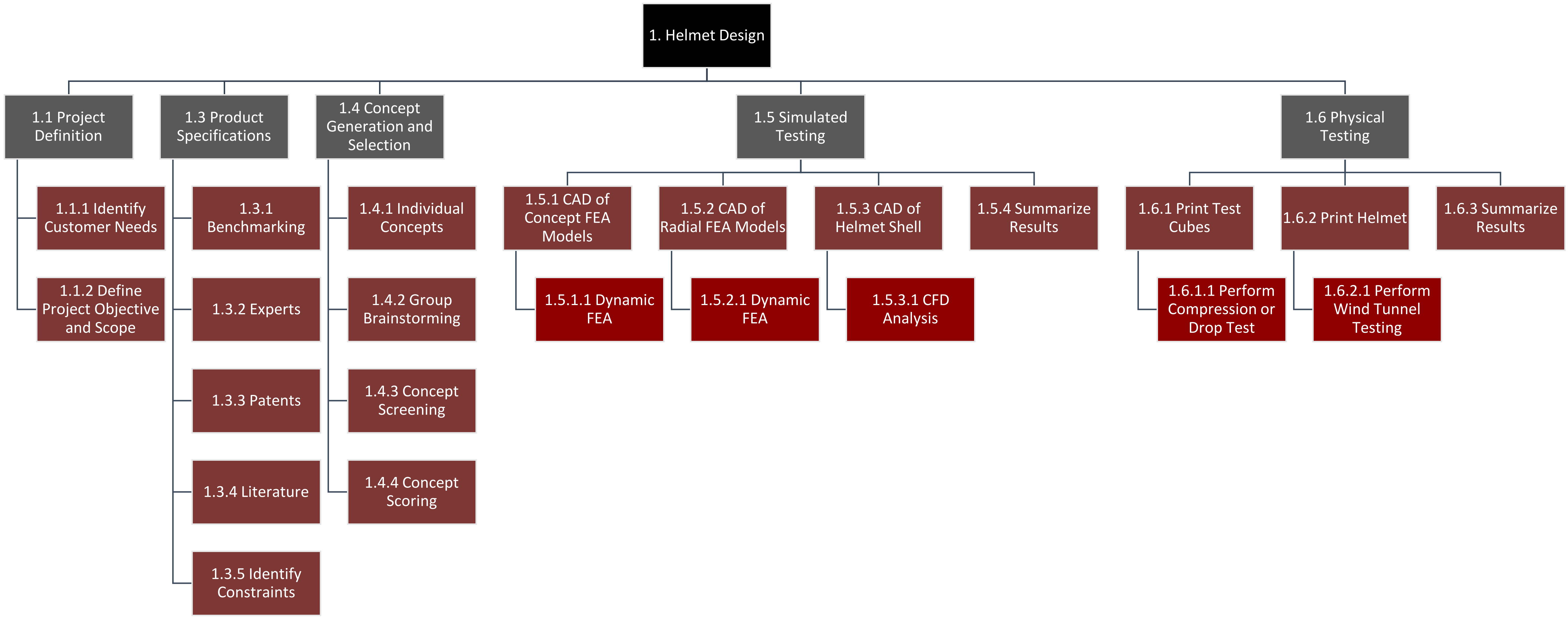

Figure 7: WBS for the project design.

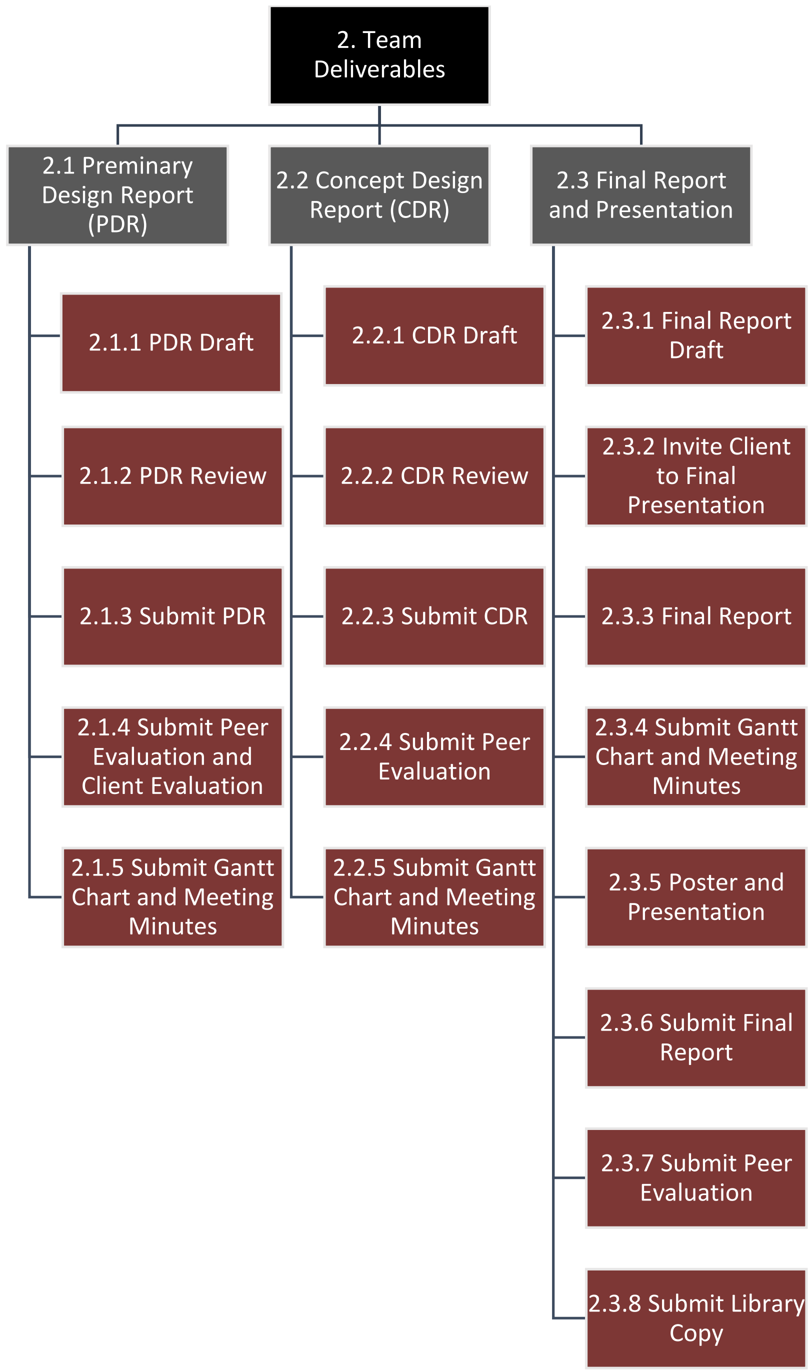

Figure 8: WBS for the project deliverables.

A tentative schedule was created at the beginning of the project as a means of tracking progress. Since the original schedule was set, some slipping had occurred as shown by the black horizontal lines in the Gantt chart in Figure 24. The slip in the schedule was mainly due to the fact that the team could not properly score the concepts without modeling each concept and performing preliminary compression analysis. The concepts resulting from brainstorming were all modelled and were also designed with the same volumetric dimensions and mass for potential FEA analysis. The added time to model the rectangular lattice FEA models and the preliminary impact FEA for the concept scoring added a significant amount of time to the original schedule. The primary method for dealing with the time slip was to compress the lead times for the 3D printing of lattice test cubes and helmet for impact testing and wind tunnel testing respectively.

Eventually, the wind tunnel testing and drop testing were removed from the schedule, hence they are no longer included in the Gantt chart shown in Figure 9. The FEA and CFD analysis for design optimization required more time than initially anticipated. The team had to work with unfamiliar software and run several iterations for each design modification. Furthermore, the physical tests were not required by Precision ADM and only served to validate the helmet's final design specifications. Consequently, physical testing was removed from the project scope and schedule.

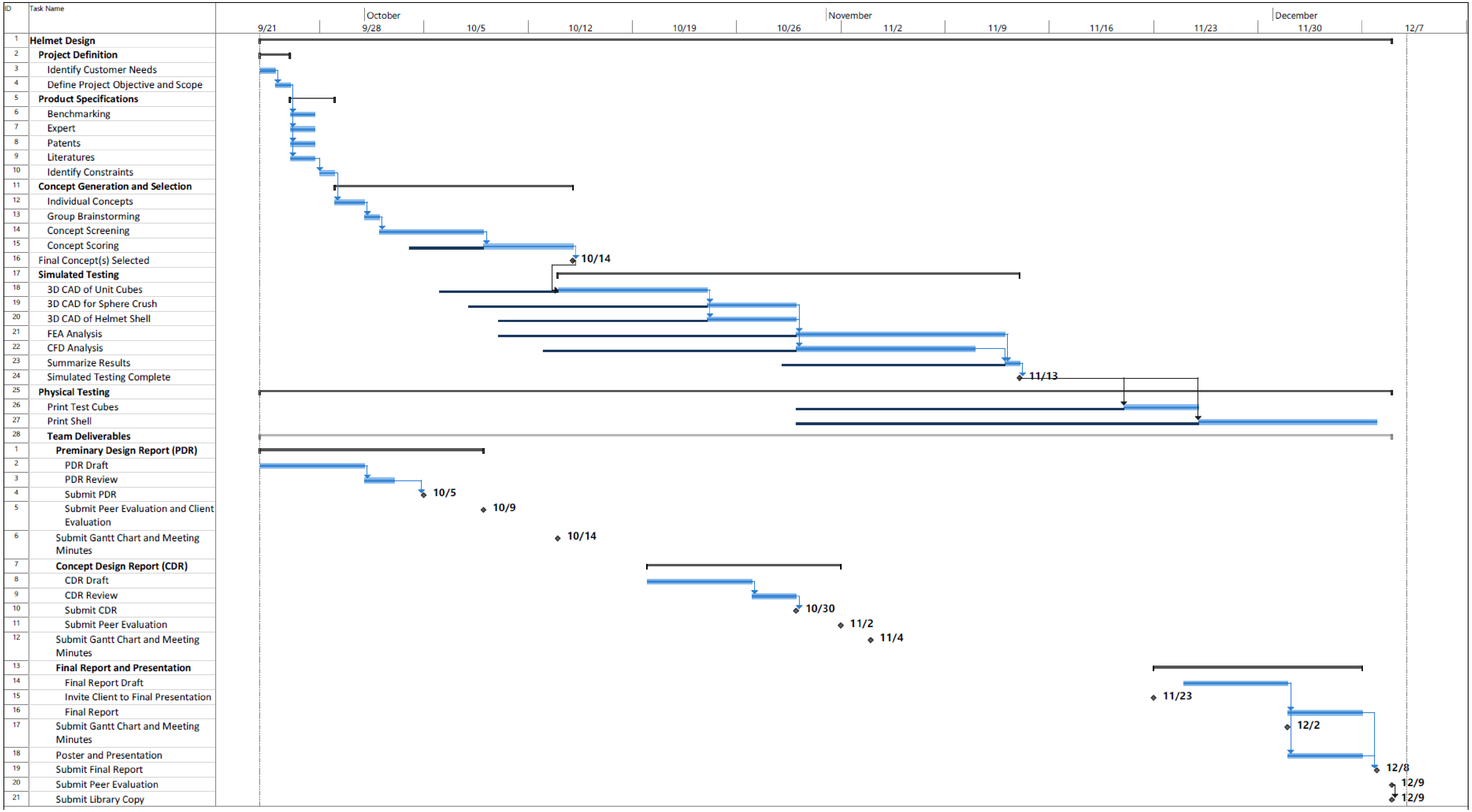

Figure 9: Final Gantt chart for project schedule

Appendix D: **SolidWorks FEA for Concept Screening**

Seventeen concepts were considered for the lattice structure of the bicycle helmet. The screening process for the concepts included assigning values of 1 to 5 for two categories: simplicity and energy absorption ability. The top five concepts were considered for further concept scoring. To aid in the visualization of how the lattice structure responds to an applied load, rectangular finite element analysis (FEA) models were designed using SolidWorks. Concepts with 8x8x3 cm dimensions were modelled and static FEA was performed. To standardize the FEA process, a static load of 300 N was applied with a semi-fine mesh. Acrylonitrile butadiene styrene (ABS) used as the material. The samples were also made to have a weight of 50 +/- 1g. The stress and displacement plots were then collected and aided in the concept screening. The stress and displacement plots are summarized in TABLE VIII.

TABLE VIII: STRESS AND DISPLACEMENT PLOTS FOR CONCEPT SCREENING

<table>
<tr><th colspan="2">Concept 1 – Offset Boxes</th></tr>
<tr><td>Stress Plot</td><td>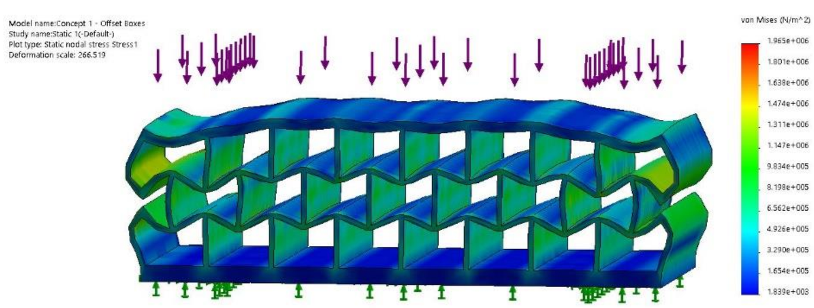
</td></tr>
<tr><td>Displacement Plot</td><td>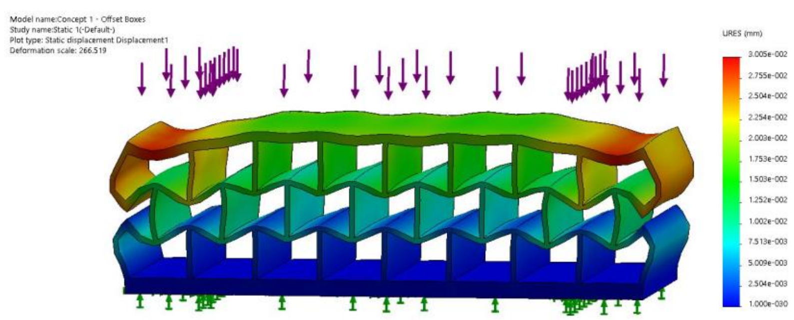
</td></tr>
</table>

Concept 2 – Aligned Boxes

Stress Plot

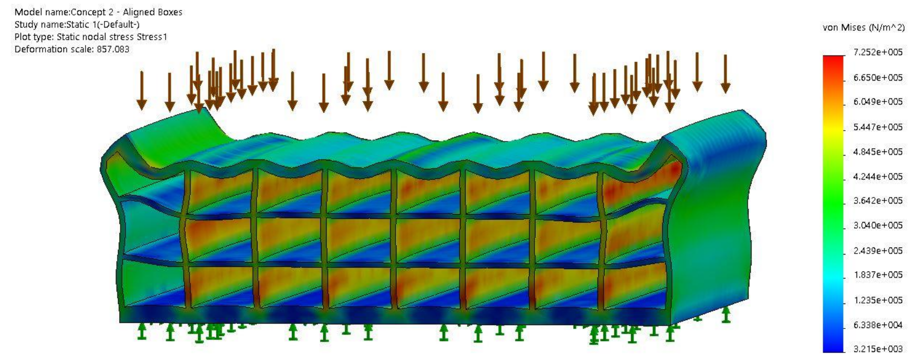

Displacement Plot

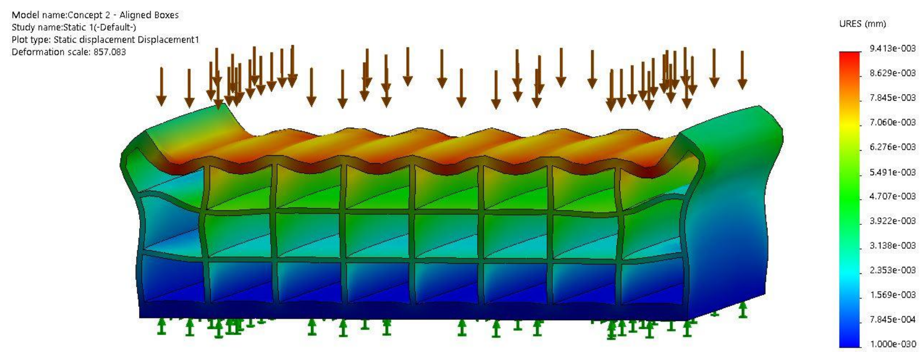

Concept 3 – Offset Triangles

Stress Plot

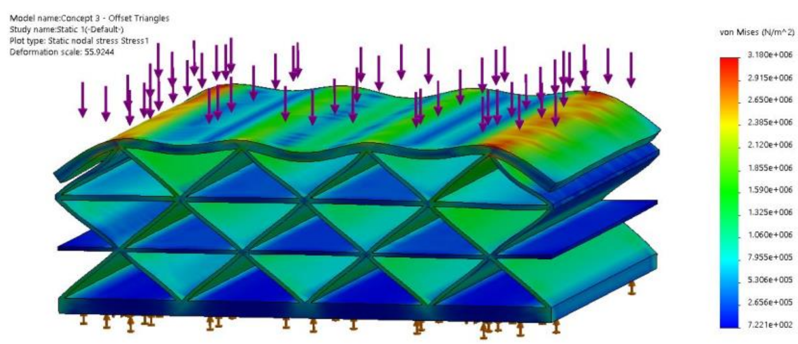

Displacement Plot	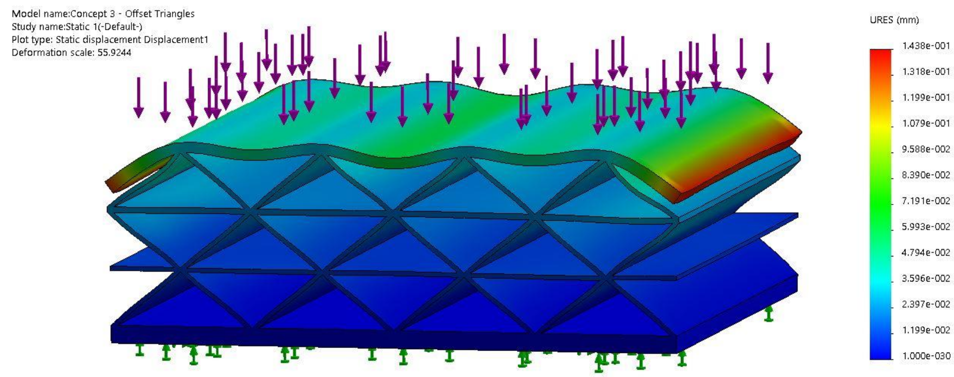
Concept 4 – Aligned Triangles	
Stress Plot	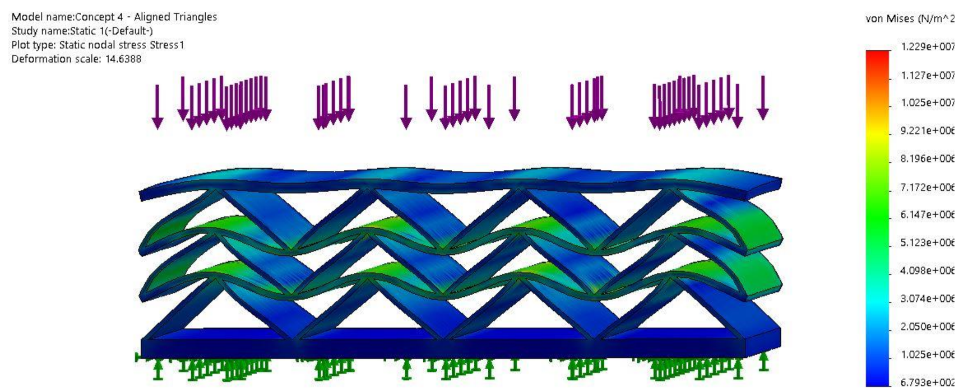
Displacement Plot	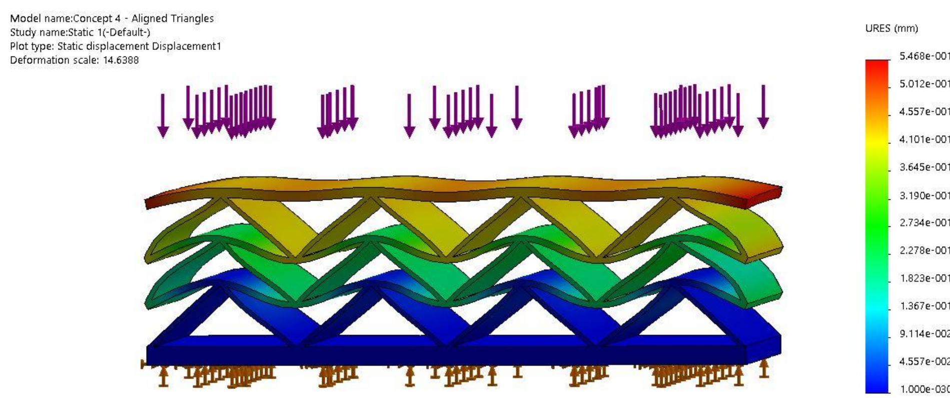

Concept 5 – Offset Circles	
Stress Plot	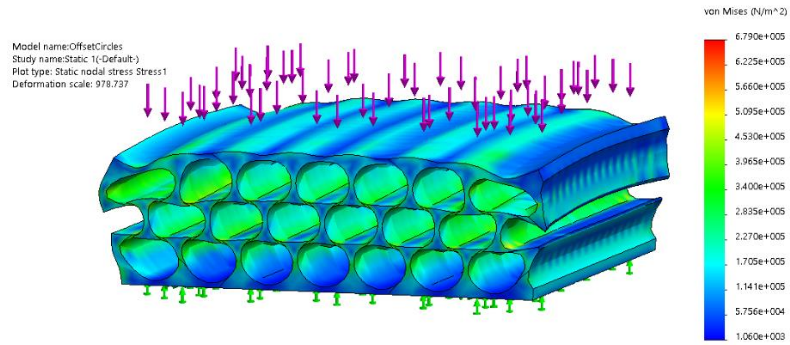
Displacement Plot	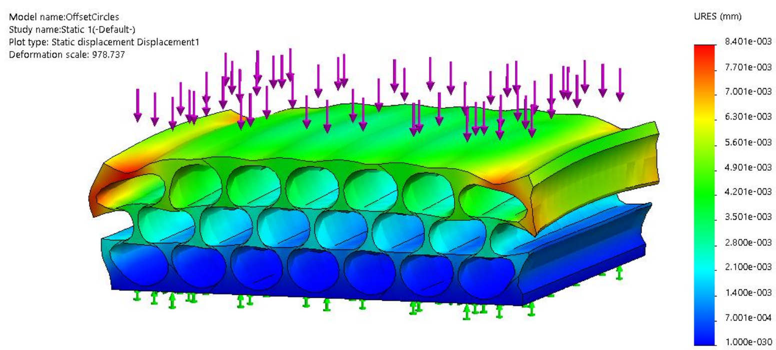

Concept 6 – Aligned Circles	
Stress Plot	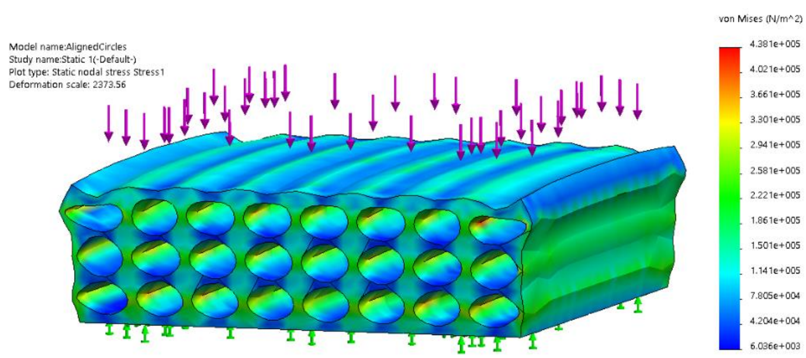

Displacement Plot	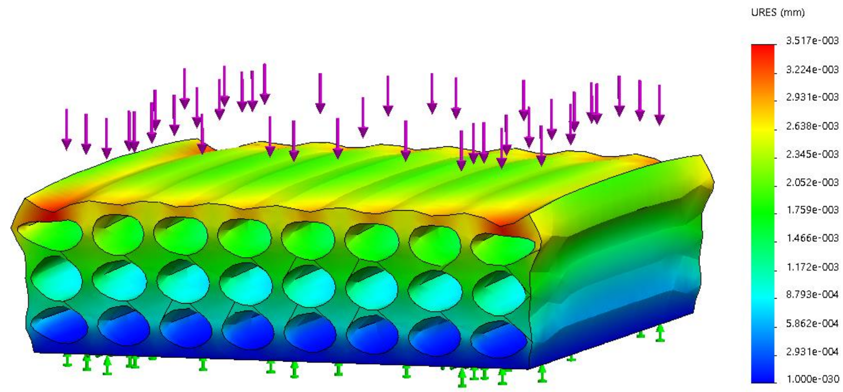
Concept 7 – Aligned Hexagons	
Stress Plot	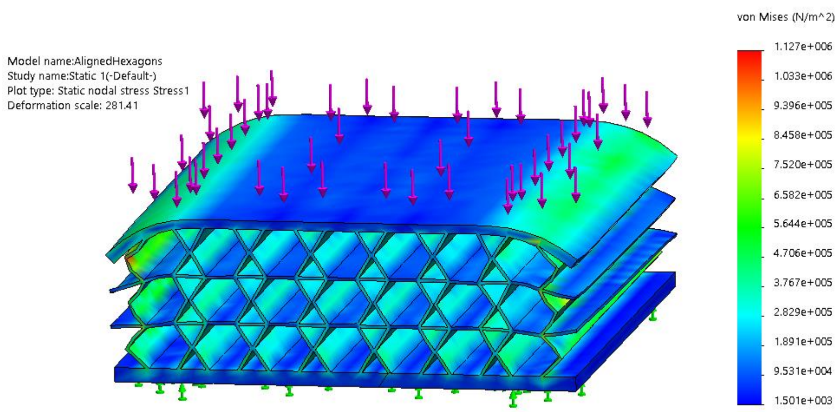
Displacement Plot	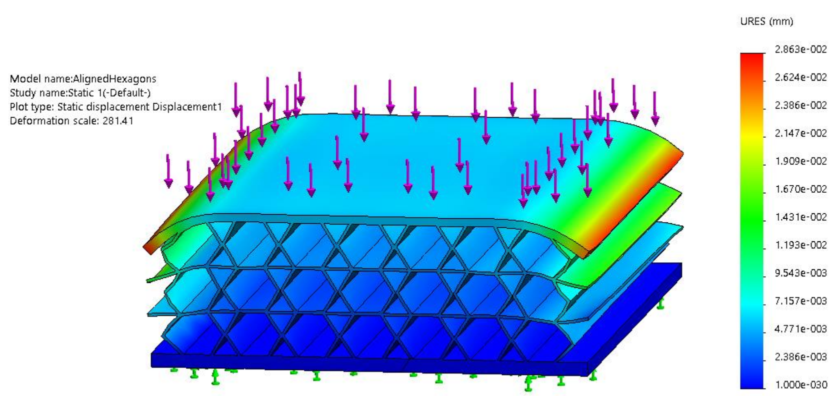

Concept 8 – Spaced Hexagons

Stress Plot

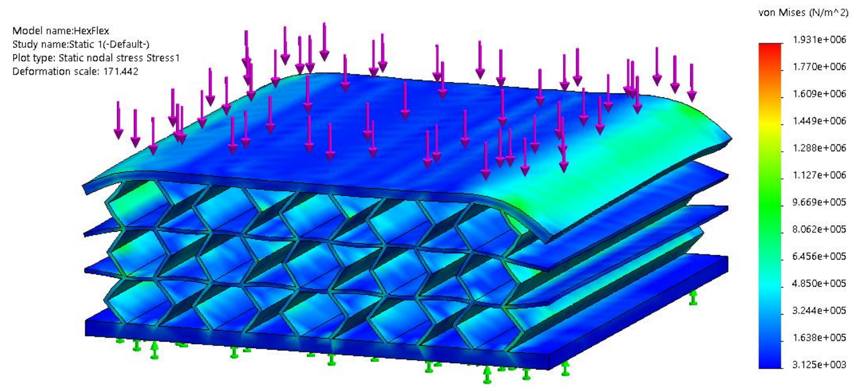

Displacement Plot

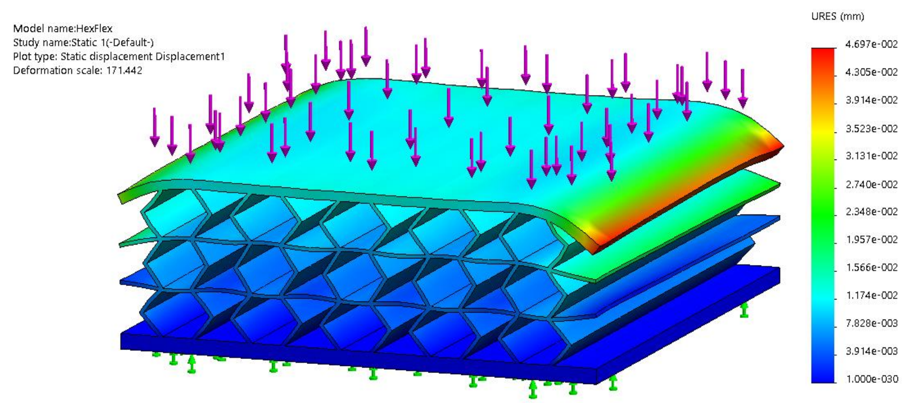

Concept 9 - Honeycomb

Stress Plot

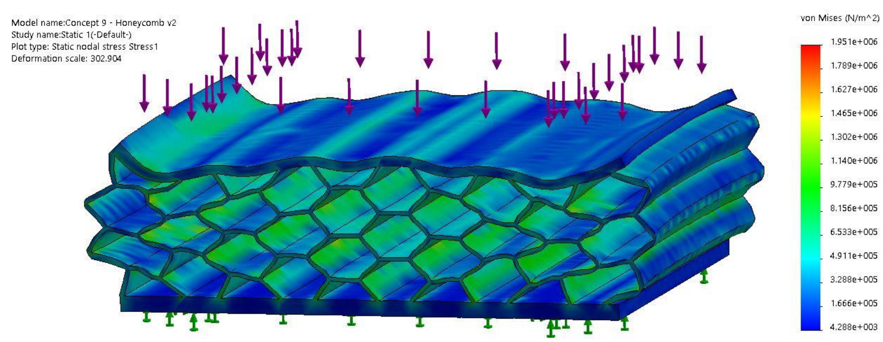

Displacement Plot	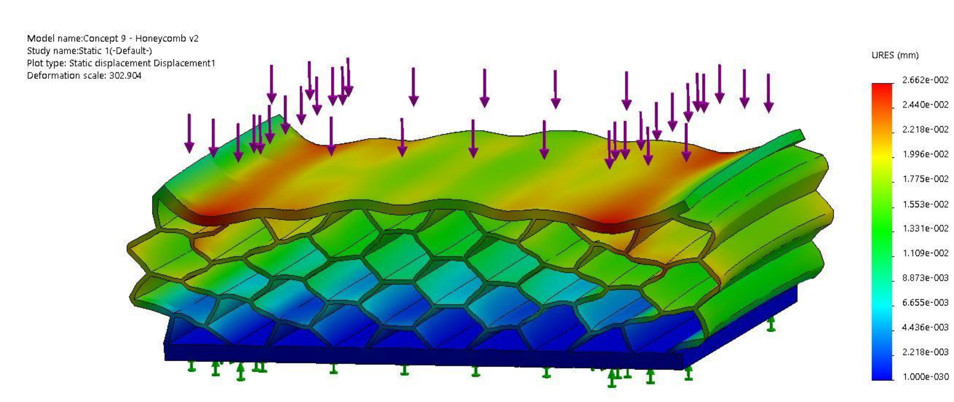
Concept 10 – Octet Truss	
Stress Plot	Unable to mesh
Displacement Plot	Unable to mesh
Concept 11 – 3D Kagome Structure	
Stress Plot	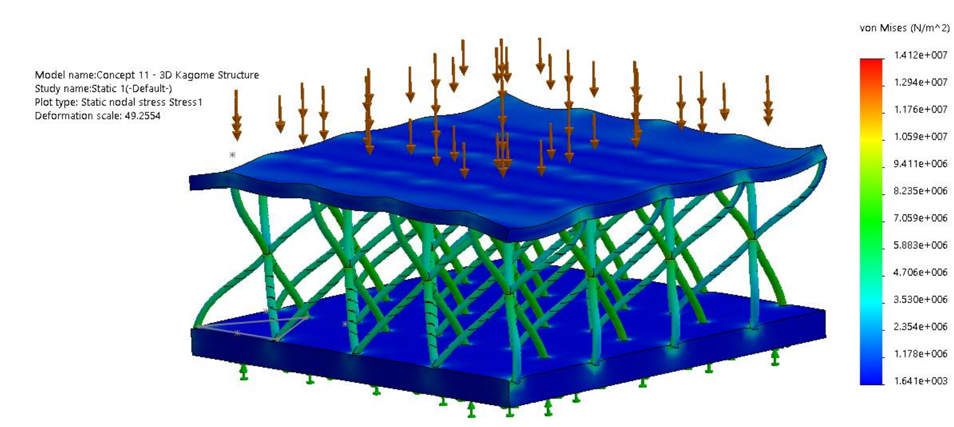

Displacement Plot	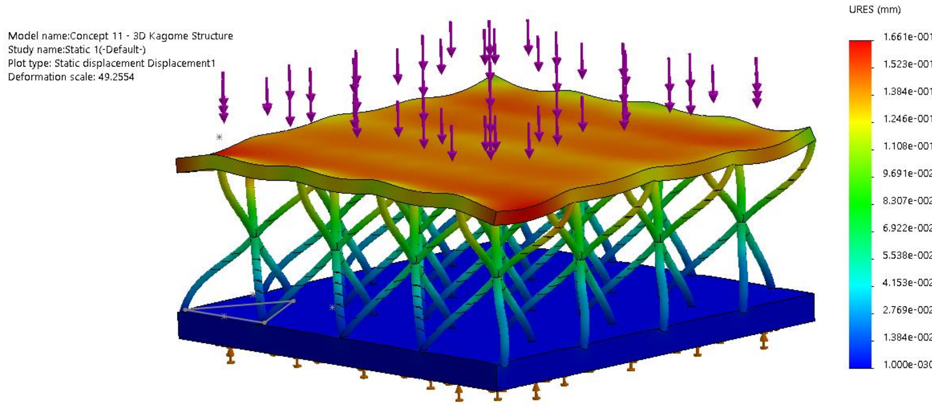
Concept 12 – Cubic Nodal Lattice	
Stress Plot	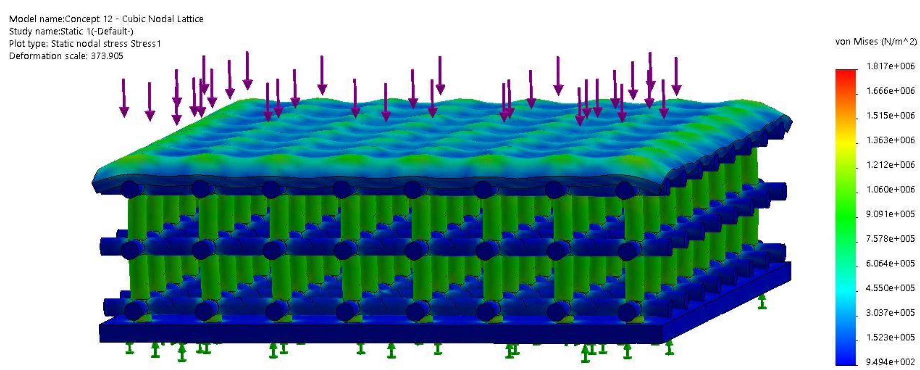
Displacement Plot	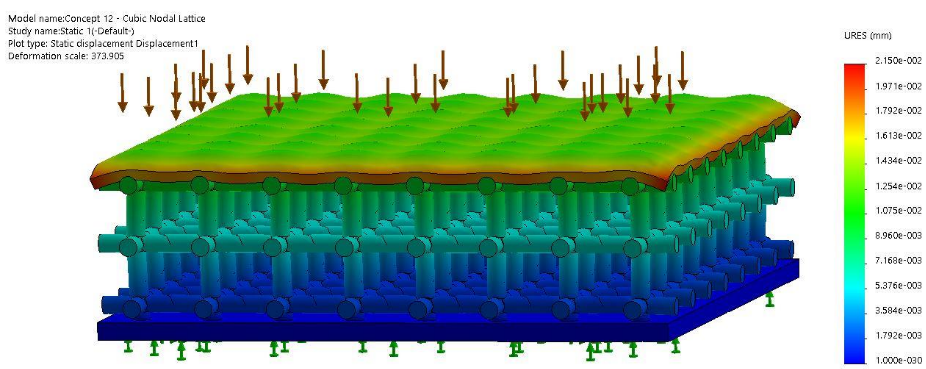

Concept 13 - Pillars	
Stress Plot	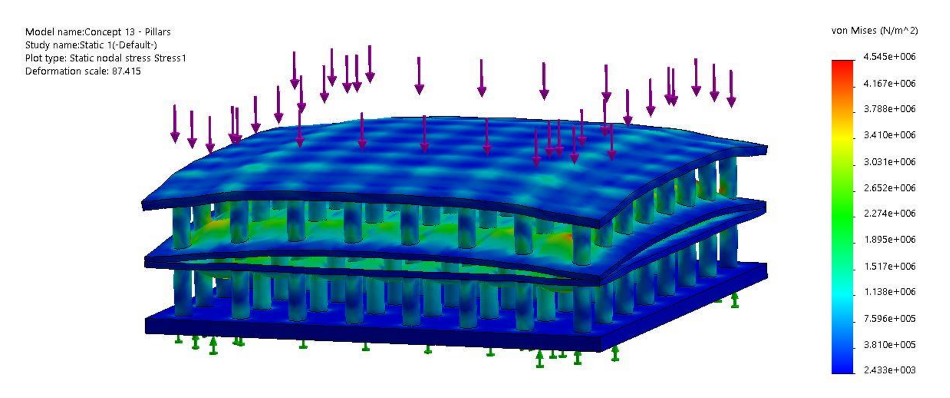
Displacement Plot	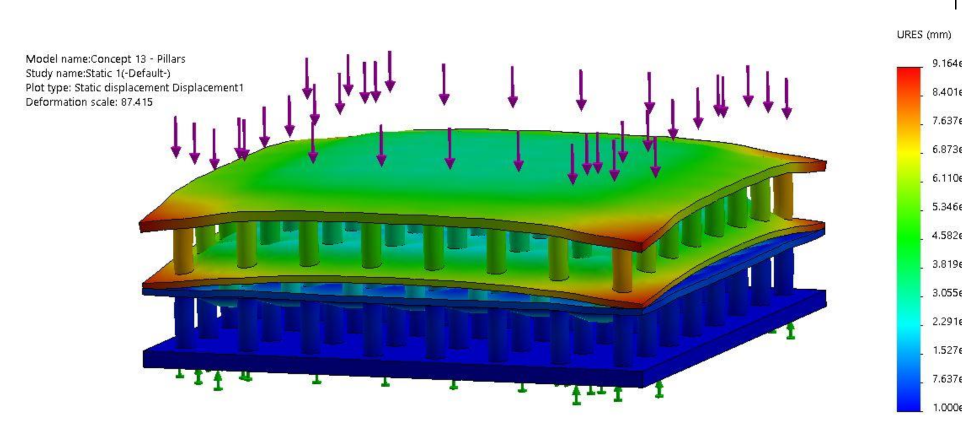
Concept 14 Lateral Voids	
Stress Plot	Not Designed
Displacement Plot	Not Designed

Concept 15 – Asterisk Lattice	
Stress Plot	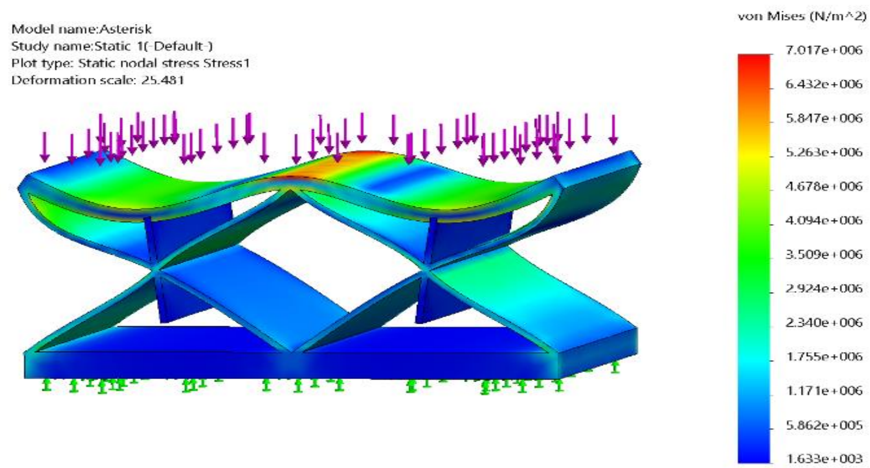
Displacement Plot	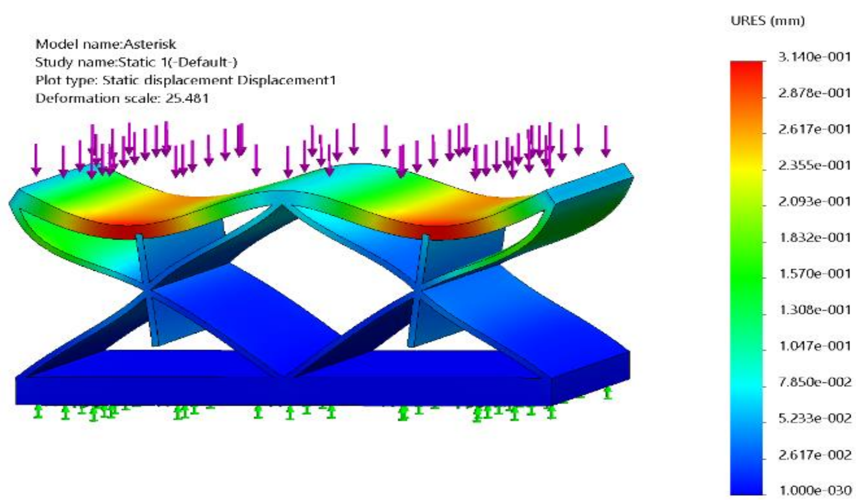

Appendix E: Generated Mesh for Concept Impact FEA

A tetrahedral mesh was automatically generated for each concept FEA model. A seed size of 0.0023 meters was used. The generated mesh for concepts 1, 4, 8, 9, and 13 are shown in Figure 10 to Figure 14.

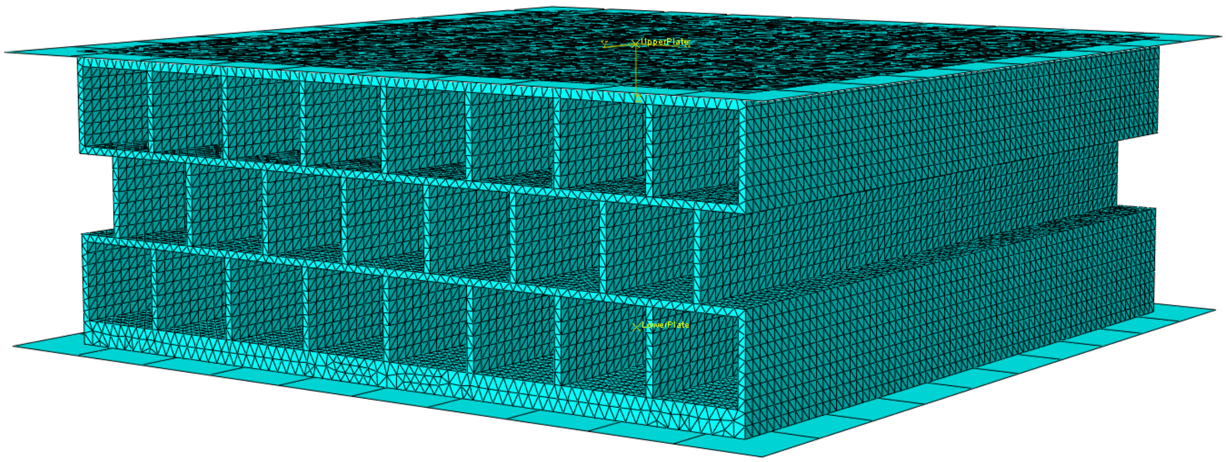

Figure 10: Generated Tetrahedral Solid Mesh of Concept 1 with a 0.0023 meter Seed Size

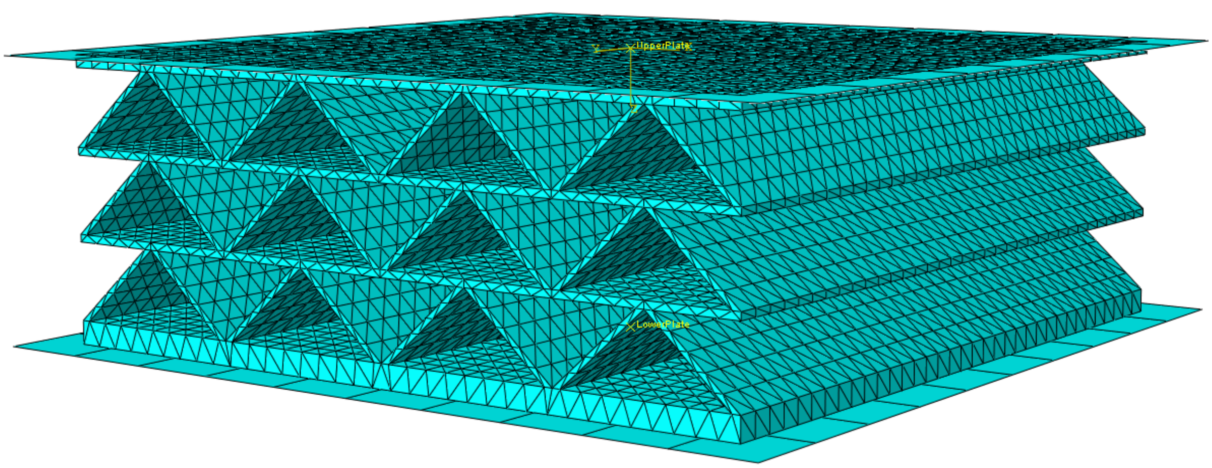

Figure 11: Generated Tetrahedral Solid Mesh of Concept 4 with a 0.0023 meter Seed Size

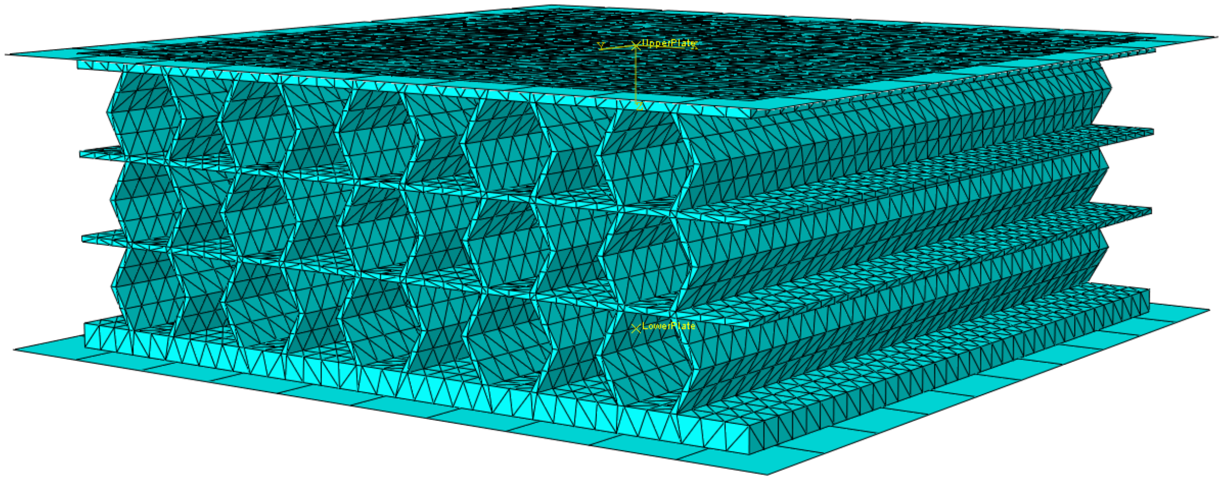

Figure 12: Generated Tetrahedral Solid Mesh of Concept 8 with a 0.0023 meter Seed Size

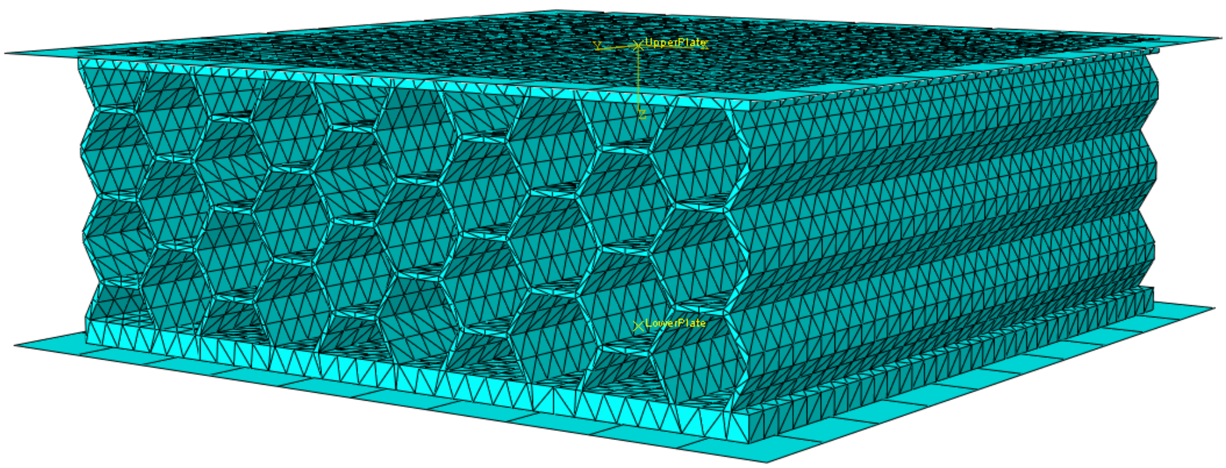

Figure 13: Generated Tetrahedral Solid Mesh of Concept 9 with a 0.0023 meter Seed Size

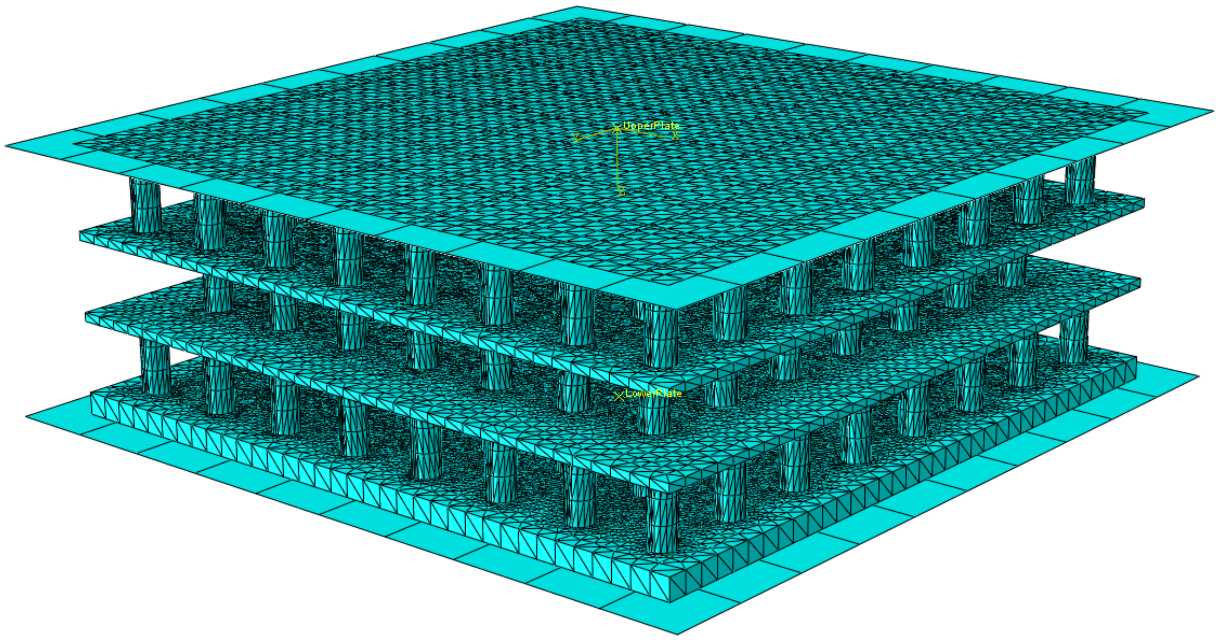

Figure 14: Generated Tetrahedral Solid Mesh of Concept 13 with a 0.0023 meter Seed Size

Appendix F: **Technical Drawings for Helmet**

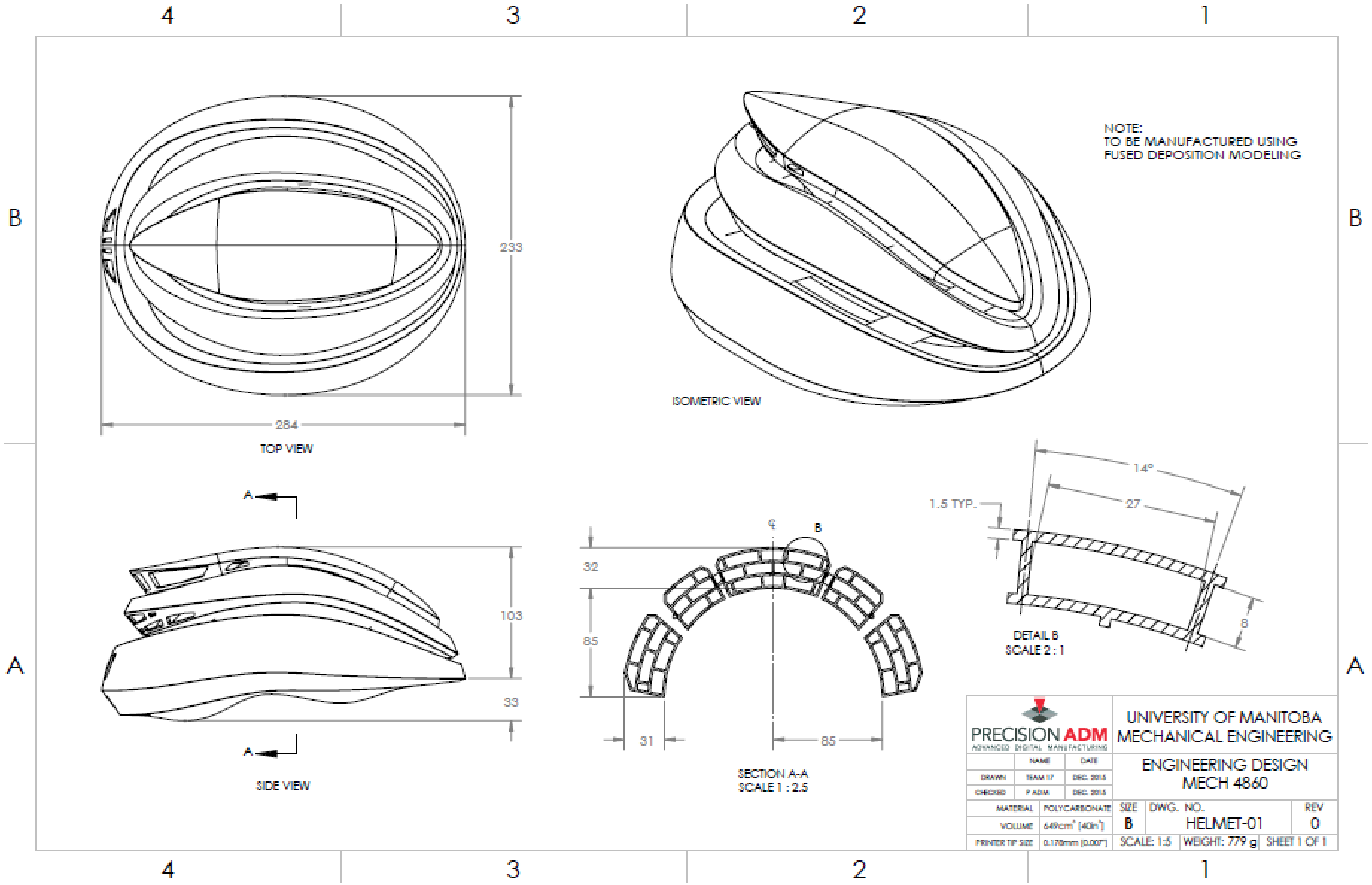

Appendix G: **References**

[1] S. K. Moon, Y. E. Tan, J. Hwang and Y.-J. Yoon, "*Application of 3D Printing Technology for Designing Light-weight Unmanned Aerial Vehicle Wing Structure*," *International Journal of Precsision Engineering and Manufacturing-Green Technology,* vol. 1, no. 3, pp. 223-228, 2014.

[2] S. Soe, P. Martin, M. Jones, M. Robinson and P. Theobald, "*Feasibility of optimising bicycle helmet design safety through the use of additive manufacturing TPE cellular structures*," *International Journal of Advance Manufacturing Technology,* no. 79, pp. 1975-1982, 2015.

[3] D. B. R. W. a. R. H. J Brennan-Craddock, "*The design of impact absorbing structures for additive manufacture*," *Journal of Physics,* vol. 382, p. 7, 2012.

[4] F. Alam, A. Subic and A. Akbarzadeh, "*Aerodynamics of Bicycle Helmets (P68)*," in *The Engineering of Sport 7*, Paris, Springer, 2008, pp. 337-344.

[5] Stratasys, "*FORTUS PC (Polycarbonate) Characterization of Material Properties*," Stratasys, Eden Prairie, 2013.

[6] Stratasys, "*FORTUS ABS-M30 Characterization of Material Properties*," Stratsys, Eden Prairie, 2013.

[7] H. Chowdhury and F. Alam, "*An experimental study on aerodynamic performance of time trial bicycle helmets*," *Sports Engineering,* vol. 17, pp. 165-170, 2014.

[8] stratasys.com, "*FDM Thermoplastics*," Stratasys, 2015. [Online]. Available: http://www.stratasys.com/materials/fdm. [27 September 2015].